Deliverable 2.1: Initial State of the Art on the assessment of the chemical evolution of ILW and HLW disposal cells

Work Package 2

This project has received funding from the European Union's Horizon 2020 research and innovation programme 2014-2018 under grant agreement N°847593.

Document information

Project Acronym	**EURAD**
Project Title	**European Joint Programme on Radioactive Waste Management**
Project Type	**European Joint Programme (EJP)**
EC grant agreement No.	**847593**
Project starting / end date	**1st June 2019 – 30 May 2024**
Work Package No.	**2**
Work Package Title	**Assessment of Chemical Evolution of ILW and HLW disposal cells**
Work Package Acronym	**ACED**
Deliverable No.	**2.1**
Deliverable Title	**Initial State of the Art on the assessment of the chemical evolution of ILW and HLW disposal cells**
Lead Beneficiary	**COVRA**
Contractual Delivery Date	**01 December 2019**
Actual Delivery Date	**30 June 2022**
Type	**Report**
Dissemination level	**PU**
Authors	**Erika Neeft (COVRA), Diederik Jacques (SCK•CEN), Guido Deissmann (FZJ)**

To be cited as:

Neeft E., Jacques D., Deissmann G., (2022): Initial State of the Art on the assessment of the chemical evolution of ILW and HLW disposal cells. D 2.1 of the HORIZON 2020 project EURAD. EC Grant agreement no: 847593.

Disclaimer

Acknowledgement

This document is a deliverable of the European Joint Programme on Radioactive Waste Management (EURAD). EURAD has received funding from the European Union's Horizon 2020 research and innovation programme under grant agreement No 847593.

Status of deliverable		
	By	Date
Delivered (Lead Beneficiary)	E. Neeft (COVRA)	25 Feb 2022 (draft)
Verified (WP Leader)	D. Jacques (SCK CEN)	25 Feb 2022
Reviewed (Reviewers)	M. Leivo (VTT) C. Wittebroodt (IRSN) G. Kosakowski & B. Ma (PSI)	7 Apr 2022 11 Apr 2022 28 Apr 2022
Revised (Lead Beneficiary)	E. Neeft (COVRA)	22 June 2022
Verified (WP Leader)	D. Jacques (SCK CEN)	30 June 2022
Approved (PMO)	L. Théodon (ANDRA)	30 June 2022
Submitted to EC (Coordinator)	ANDRA	30 June 2022

Executive Summary

Main features of the chemical evolution of disposal cells

The broader scope of the work package ACED is the assessment of the chemical evolution at the disposal cell scale involving interacting materials and thermal, hydraulic and/or chemical gradients by considering Intermediate Level Waste (ILW) and High Level Waste (HLW) disposal concepts. These concepts are representative for Europe. HLW and ILW disposal cells in granitic and clay host rocks are studied in ACED. Disposal of this waste is foreseen in geological disposal facilities at a sufficient large depth to minimize the impact of climate change on the chemical evolution of these disposal cells. The waste is removed from the immediate human and dynamic, natural surface environment and the stable geological deep environment provides predictable conditions for the chemical evolution of the materials within these disposal cells. A key feature in the chemical evolution of disposal cells in the post-closure phase is the availability of water. Construction and operation can have an important influence on this availability, especially for disposal cells in indurated clays.

Clay host rocks and granitic host rocks are frequently interfacing concrete in the disposal cells. Both rocks are alumina-silicate bearing rocks and this similarity is important for the identification of the key processes in these host rocks. The potential sequence of secondary mineral formation by interaction with alkaline fluids and alumina-silicate bearing rocks has been deduced from detailed investigation and understanding of the processes taking place in a natural analogue. The secondary mineral formation sequence in these host rocks is C-S-H phases, low in Ca C-S-H phases, C-A-S-H, low Si/Al zeolites and high Si/Al zeolites as a function of pH. The low permeability in clay host rocks ensures that the mineralogical alteration is minimal in a period of 100,000 till 1 million years. The secondary mineral formation takes place within the fractures of granitic host rocks. This mineral formation can close the fractures and thereby reduce the ingress of dissolved species into concrete.

The chemical alteration of concrete by gaseous carbonation takes place in the operational phase of the geological disposal facility. The extent of this alteration depends on the engineered quality of concrete and egress of water from the host rock. Gaseous carbonation may not be detrimental for the performance of concrete if the concrete has been well engineered as evidenced by the still functioning load-bearing structures from the Roman empire. Precipitation of calcite by gaseous carbonation reduces the porosity of concrete and can reduce the permeability of concrete and increase the strength of concrete, especially for concrete made with Ordinary Portland Cement; the impact of gaseous carbonation on concrete made with a blended cement with a high slag content is not so clear. A potential porosity reduction due to carbonation can lead to a decrease in radionuclide migration rates, but may have adverse effects with respect to gas pressure build-up.

There are many similarities in the pore water chemistries of clay host rocks and granitic host rocks and these similarities are important for the identification of the key processes in the alteration of concrete in the post-closure phase. These chemical alterations processes can also occur in the operational phase for granitic host rocks and poorly indurated clays. For indurated clays, these alteration processes may be limited during in-situ hardening of concrete in the operational phase, due to lack in diffusional pathways of dissolved species from this host rock towards concrete.

Dissolved species in the host rock pore water considered in the chemical alteration processes in concrete are bicarbonate, sulphate, chlorine, calcium, magnesium, potassium and sodium. Ingress of bicarbonate reacts with the hydroxyl ions and decalcifies cementitious minerals in concrete. These reactions reduce the porosity of concrete, produce water and eventually result in a reduction in the pH of concrete pore water. This wet carbonation may - like gaseous carbonation - not be detrimental to the durability of concrete.

Ingress of magnesium has been identified as one of the main contributors to deteriorate the strength of concrete if civil engineering codes have been followed for the manufacturing of concrete, i.e. sulphate attack (delayed ettringite formation) and alkali-silica reactions can be prevented. The permeability of concrete is increased by the reduction in strength due to this decalcification of cementitious minerals by

secondary magnesium mineral precipitation. This increase in permeability enhances the chemical evolution of concrete and the loss in strength allows the load from the host rock being transferred to the waste package.

Leaching of calcium from concrete towards host rocks can be another contributor that deteriorates the strength of concrete and increases the permeability of concrete due to increase in porosity. The poor calcium content in the host rock pore water chemistries for some countries makes this leaching process immediately possible. The still existing structures from the Roman empire that are exposed to the weathering waters shows that this leaching process can be very slow if well engineered. For other countries, the dissolved calcium concentration in the host rock pore water is larger than the initial dissolved calcium concentration in concrete pore water, which makes leaching as a key process less likely.

Specific vitrified HLW features

Vitrified HLW is investigated in ACED and this waste form arises from the reprocessing of spent fuel. The produced liquid waste with a high content of radionuclides is mixed with melted borosilicate glass and the mixtures are poured in stainless steel canisters. The thickness of these stainless steel canisters is too small to withstand the underground lithostatic load. The stainless steel canisters are therefore to be encapsulated in carbon steel overpacks in order to prevent contact between the waste form and pore water for a period of 500 years or about 1000 years, depending on the disposal concept. The carbon steel overpack is frequently surrounded by a low-permeable buffer made from bentonite or concrete. Radiation decomposes water molecules and the resulting recombined products are slightly oxidizing. This radiation induced oxidizing environment in the vicinity of steel increases the corrosion rate of steel. However, radiation enhanced corrosion of the carbon steel overpack is negligible compared to chemical corrosion in the proposed European disposal concepts after the envisaged cooling period in storage facilities.

Microbes require organic matter as a food source but also other nutrients to build their DNA and proteins, sufficient space, sufficient water activity, specified range in pH and specified range in temperature. Microbial activity is negligible by space restriction in virgin clay host rocks and low-permeable engineered materials if manufactured with an appropriate design limit and installed correctly.

The initial thermal load for vitrified HLW disposal cells dries the buffers, which limits the chemical interaction with the carbon steel overpack. The reduction in the thermal load due to decay of radionuclides in this waste increases the availability of water for chemical reactions. Entrapped oxygen available for corrosion can be minimized by manufacturing processes. Only anaerobic corrosion needs to be considered on the long-term. Archaeological analogues provide the evidence that a metal-oxide alteration layer on the steel and an iron-enriched alteration zone in the buffer will be formed at both the interfaces steel-clay and steel-concrete.

The long-term corrosion rates are steady states between the formation of a metal-oxide towards the virgin steel and dissolution of the metal-oxide towards the clay or concrete. In situ long-term corrosion rates can be measured for steel exposed to solutions by measuring the hydrogen flux from the solutions. In-situ corrosion rates are more difficult to measure for steel exposed to clay or to concrete, due to the delay in hydrogen arrival in these low-permeable materials. Weight loss and other techniques in which the corroded thickness is measured as a function of time may overestimate the corrosion rate, since these rates include the initial higher corrosion rates due to the formation of an metal-oxide layer. These initial rates are multiple orders larger than the steady state long-term corrosion rates. Sorption of dissolved iron increases the corrosion rate. This sorption of dissolved iron-hydroxide-complexes occurs by clay minerals but is less likely for dissolved iron-carbonate complexes. Whether this sorption of iron also occurs by cementitious minerals depends on the pH of the concrete pore water and pH dependent speciation of iron in the vicinity of the metal-oxide. The metal-oxide is usually assumed to be magnetite but the presence of calcium, especially in concrete pore water, might lead to another thermodynamic

stable passivating alteration layer. Maxima in long-term anaerobic corrosion rates are 10 µm per year for steel exposed to bentonite and 0.1 µm per year for steel exposed to concrete. The pH of concrete in the vicinity of steel eventually reaches neutral values and pH has been assumed to have an influence on the corrosion rate. However, also long-term corrosion rates for steel exposed to anaerobic granitic groundwater were smaller than 0.1 µm per year. Hydroxyl ions are released in the vicinity of steel in the corrosion process by which the pH is locally increased, i.e. the pH of the exposing medium to steel may not be the only reason for a high pH in the vicinity of steel.

The impact of the dissolved iron species migration onto the physical and chemical properties of bentonite is the transformation of swelling clay minerals into non-swelling sheet silicates in the iron-enriched bentonite zone at the steel-bentonite interface. The extent of this zone can also be modelled. This modelling helps to improve the design of the disposal concept. The impact of the iron-enriched zone in concrete is not so clear and no modelling studies have been found. The uptake of iron by concrete prevents the creation of a larger volume of iron corrosion products. The stress intensity at the steel-concrete interface can become too large by a too high increase in volume of corrosion products. Spallation of concrete occurs at high aerobic corrosion rates especially in carbonated concrete. Well-engineered reinforced concrete has a sufficient thick coverage around steel in order to prevent these neutral, oxidic environments in the vicinity of steel.

Eventually the non-corroded thickness of the carbon steel overpack becomes too small to sustain the load by the host rock and fracture of the carbon steel overpack and stainless steel canister ensures contact between the vitrified waste form and pore water. An alteration layer on the surface of glass is developed by this contact between the vitrified waste form and water. This alteration layer consists of a diffusion-gel layer and secondary mineral precipitates such as clay minerals and zeolites. The glass alteration rate slows down until a steady state between the formation of the diffusion-gel layer and dissolution of this diffusion-gel layer has been established. The formation of this diffusion-gel layer and secondary mineral precipitates closes small cracks in the bulk of the vitrified waste form. Higher alteration rates are present for glass in the vicinity of steel due to sorption of dissolved silicon on the iron corrosion products. The corrosion of steel also locally increases the pH by which the local solubility of silicon is increased, leading to higher alteration rates. Radionuclides dissolved as cationic complexes by the glass alteration process can be incorporated in secondary mineral precipitates. The glass alteration rate is therefore suggested to be only representative for the release rate of radionuclides dissolved as anionic complexes.

Specific cemented ILW features

Cemented metallic and organic ILW is investigated in ACED. The ILW disposal galleries are larger in size than the HLW disposal galleries. Also, more host rock damaging construction methodologies can be used for ILW disposal galleries than for HLW disposal galleries. Construction and operation can therefore have a higher impact on the chemical evolution in ILW disposal cells than in HLW disposal cells.

Metallic ILW has been identified from the national programmes as steel (carbon steel and stainless steel) and Zircaloy. Neutron irradiated Zircaloy are the hulls in spent nuclear power fuel. These hulls are compacted as a waste product from the reprocessing of spent nuclear power fuel. Neutron irradiated steel can be from spent nuclear fuel assemblies and other components used in nuclear reactors. Organic ILW has mainly been identified from these programmes as spent ion exchange resins. These resins purify the reactor waters by concentrating the radionuclides by exchange with non-radionuclide complexes. Examples of cellulosic waste are paper and clothing and therefore usually LLW, but in exceptional cases cellulosic waste can also be ILW.

The porosity in cementitious materials is controlled by their application. The processing of ILW with cementitious materials can have a higher porosity than the concrete buffer surrounding the metallic overpack in HLW disposal cells. A higher porosity reduces the possibility to limit microbial activity by

space restriction. The high alkalinity for cemented ILW, however, limits microbial activity. The pH of the concrete pore water eventually reduces by egress and ingress of dissolved species. This pH limiting factor is therefore reduced in the long-term. Microbial activity can then be a key parameter for disposal cells with organic ILW, if sufficient energy can be gained from the breakdown of the organic waste form. Insufficient energy can be gained from the breakdown of spent ion exchange resins but not for cellulosic waste.

The porosity, permeability, saturation degree of both concrete and host rock as well as the extent in the difference in the concentrations of dissolved species between concrete and host rock determine the chemical alteration rate of concrete and water available for anaerobic corrosion of metallic ILW. Steel releases hydrogen in this corrosion process to its surroundings but this hydrogen is taken up by Zircaloy. Zircaloy as ILW is only present in countries that also store vitrified HLW. The metallic surface exposed to concrete is for ILW disposal cells several times larger than HLW disposal cells. Specific research is devoted to the perturbation of hydrogen gas in clay host rocks since this perturbation can increase the migration rate of radionuclides within this host rock. However, hydrogen release rates from ILW disposal cells with steel require the transport of water in these cells in order to balance the consumption of water in the corrosion process. This transport of water combined with the water producing chemical processes such as carbonation have not yet been modelled to determine the hydrogen release rate.

Content

List of figures

List of Tables

Glossary

B	Binder
BFS	Blast Furnace Slag
CAST	Carbon-14 Source Term; EURATOM 7th framework programme project
Cebama	Cement-based materials, properties, evolution, barrier functions; Horizon 2020 framework programme project
CSD-v	Conteneur Standard de Déchets vitrifiés
DPL	Dense Product Layer
DZ	Damaged Zone
ECOCLAY	Effects of cement on clay barrier performance; EURATOM 5th framework programme project
EDZ	Excavated Damaged Zone
GLASTAB	Long-term behaviour of glass: improving the glass term and substantiating the basic hypothesis; EURATOM 5th framework programme
HLW	High Level Waste
ILW	Intermediate Level Waste
LLW	Low Level Waste
MIND	Microbiology in Nuclear Waste Disposal; Horizon 2020 project;
MOX	Mixed OXide of plutonium and uranium
NAnet	Network to review natural analogue studies and their applications to repository safety assessment and public communication; EURATOM 5th framework programme project
NF-PRO	Understanding and physical and numerical modelling of the key processes in the near field and their coupling to different host rocks and repository strategies; EURATOM 6th framework programme project
OPC	Ordinary Portland Cement
RED-IMPACT	Impact of partitioning, Transmutation and Waste Reduction Technologies on the Final Nuclear Waste Disposal; EURATOM 6th framework programme project
RTD(1990-1994)	4th framework programme (RTD) project; invited papers EUR 17543
S	Soil
SCM	supplementary cementitious material
SELFRAC	Fractures and self-healing within the Excavation Disturbed Zone in Clays; EURATOM 5th framework programme project Task 3 Characterization of radioactive waste forms. A series of final reports (1985-89), 3rd framework programme (RTD) project
TiMoDaz	Thermal Impact on the Damaged Zone around a radioactive waste disposal in clay host rocks; EURATOM 6th framework programme project
TM	Transformed Medium

1 Introduction

The most safe and sustainable option for the end point management of high-level (HLW) and intermediate-level (ILW) radioactive waste is to isolate the waste and contain the radionuclides in a system of engineered barriers and natural barriers. The waste packages are to be emplaced in a deep (several hundreds of meters) facility that is constructed in a stable geological formation (a natural barrier). After closure of this facility, the isolation of the waste and containment of radionuclides is controlled by natural processes, i.e. the waste is no longer managed. The depth of the disposal facility determines the vulnerability of the barriers for climate change. The impact of climate change on the natural chemical conditions of the host rock is assumed to be absent in ACED.

All EU countries need to have a national programme to deal with radioactive waste (EC 2011). In general terms, the engineered barrier system consists of a solidified waste form in a (backfilled) disposal container that is placed in a sometimes backfilled and/or lined disposal gallery. Several materials coexist in the engineered barrier system such as glass, cementitious materials or bitumen in the waste form, concrete and steel for containers, and cementitious materials or clay (bentonite) as buffer or backfill and concrete or steel as liner material. In addition, different types of host rocks, i.e. the stable geological formation, are envisaged with a clayey or a granitic type of rock being the most common host rock types in Europe. Figure 1-1 shows the general concept of engineered and natural barriers in which in this case a deep clay formation has been chosen with other rock formations on top of this clay formation. This geological environment provides isolation of the waste. Granitic rock is present with a larger thickness than clay formations by which a single granitic rock provides sufficient isolation.

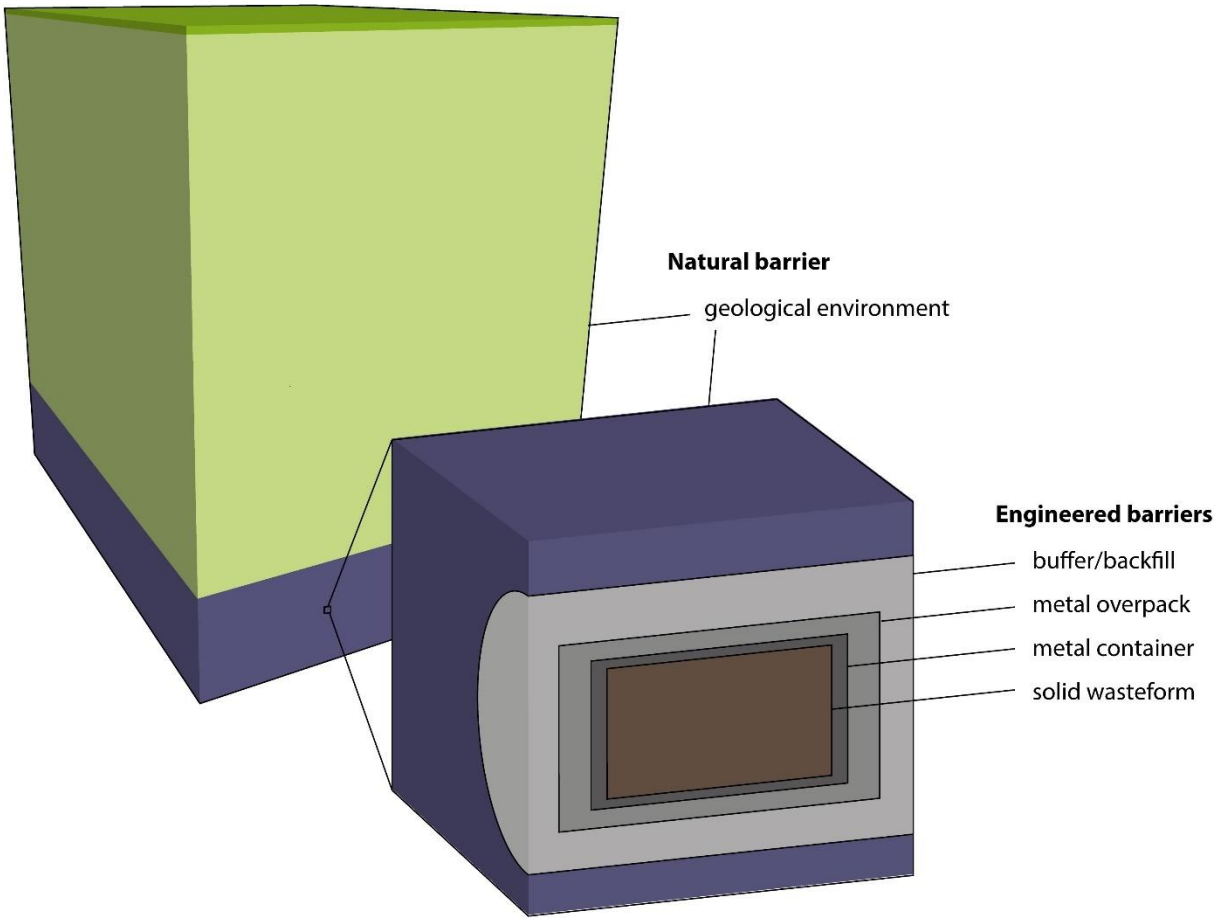

Figure 1-1: The general concept of the multiple barrier system for geological disposal or radioactive wastes (adapted from Chapman and Hooper, 2012)

The engineered barriers provide containment of the radionuclides in various functions:

- The solid waste form can have a very low solubility in order to limit the radionuclide release rate;
- The metal overpack – in which the solid waste form is to be encapsulated - prevents contact between the waste form and groundwater for thousands till hundreds of thousands years after closure of the disposal facility;
- The buffer or backfill can provide beneficial physical and chemical conditions to the overpack to limit corrosion of the metal overpack.

These functions are just a few examples of safety functions of the engineered barriers and described here in order to introduce the reader into the multiple barrier system. Each barrier can also have multiple functions that contribute to the containment of radionuclides (Chapman and Hooper, 2012). The engineered barriers to contain radionuclides can be different for ILW and HLW. Some safety functions can be time-dependent. The required time depends on the radiotoxicity of the waste. This radiotoxicity decreases by decay of radionuclides. Figure 1-2 shows that it takes about 25,000 years for vitrified HLW to achieve the same radiotoxicity as uranium ore. Uranium ore is a natural material that does not require management when the ore is not explored.

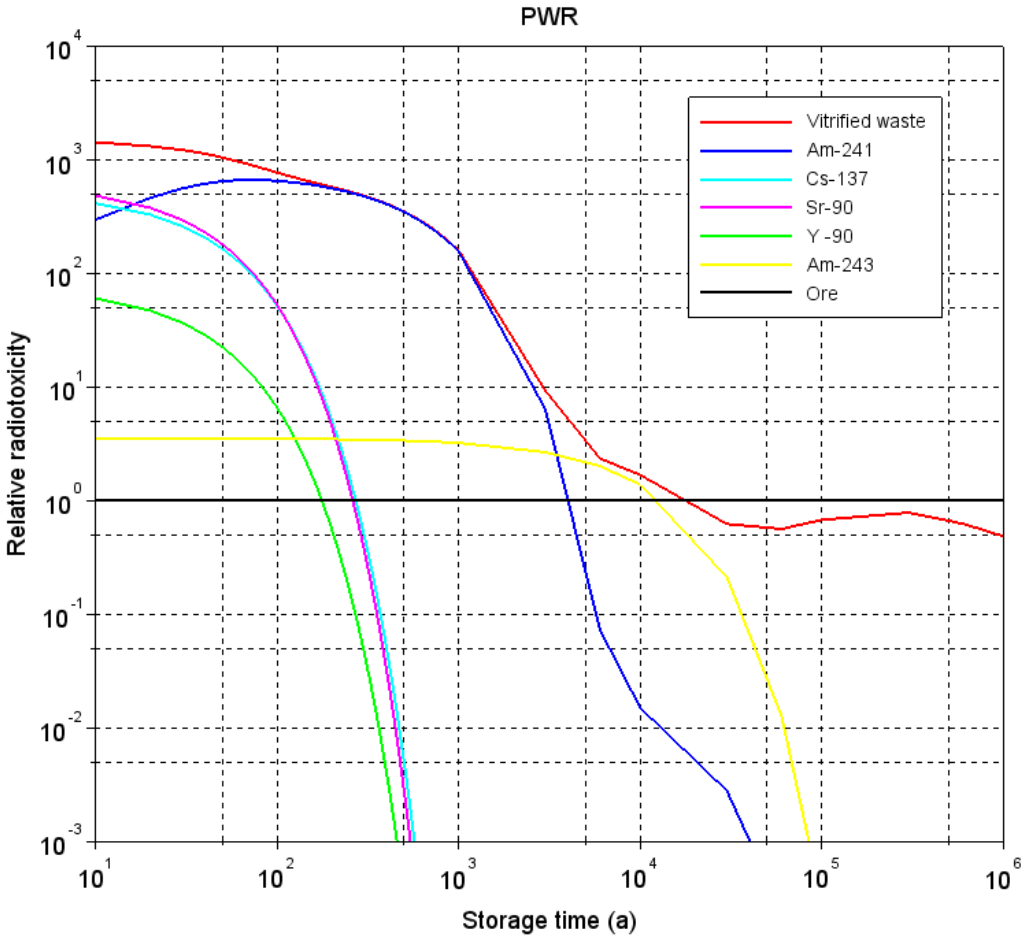

Figure 1-2: Radiotoxicity of vitrified HLW from recycling of spent nuclear power fuel from a pressurised water reactor (PWR). Calculations performed by Professor Jan Leen Kloosterman from Delft University of Technology in the Netherlands in 2017.

The americium isotopes are mainly responsible for the large period. Spent nuclear power fuel can also be regarded as HLW. Larger periods are required to achieve the same radiotoxicity since plutonium-isotopes have larger half-lives than americium isotopes. The ultimate goal of a geological disposal

system is long-term (post-closure) safety for people and the environment. To assess the long-term safety and performance, analyses at the disposal system scale as a whole including the engineered barriers, the host rock and the geological environment are required. To scientifically underpin such analysis, many additional aspects are studied experimentally and numerically, ranging from the repository scale (or disposal facility, including mainly engineered barriers) to more detailed scales (e.g. interfaces between materials).

A particular scale between repository scale and detailed scale is the scale that represents the waste container, the gallery and a few meters of the host rock around the gallery. This scale is called the **disposal cell scale** in this report. The disposal cell scale consists of several different types of materials with different geochemical properties. As such, all these materials will evolve geochemically and consequently also physical and mechanical properties will vary over long time scales. These alterations are driven by chemical gradients between the materials and disequilibrium with their environment. The performance of the engineered barriers will change during the lifetime by these chemical alterations. Ultimately, the prevailing geochemical, physical and mechanical conditions of the waste form, other engineered barriers and the host rock will influence radionuclide release, fate and transport.

1.1 Objective of this report

The challenges to assess the chemical evolution at the disposal cell scale are how scientific understanding and knowledge on individual materials or processes and the conceptual and mathematical models can be integrated at a disposal cell scale, and how these complex integrated models can be simplified to obtain model descriptions with a complexity appropriate for a given application in the safety and performance assessments. Crucial points are thus to:

- describe, which processes are influencing the chemical evolution at the disposal cell scale (narrative of chemical evolution);
- understand the chemical processes at the interface between materials;
- integrate the scientific knowledge into conceptual and mathematical models for simulating the long-term large-scale evolution;
- simplify – abstract these models to allow sensitivity and uncertainty calculations or optimisation.

This report concentrates mainly on the first two points mentioned above but also on information on the implementation in numerical models. It gives a generic description of the chemical evolution of ILW and HLW disposal cells and methods to assess the chemical evolution as a general basis for the EURAD ACED work package on the “Assessment of Chemical Evolution of ILW and HLW Disposal Cells”. After introducing ACED (this section), this report summarizes the most important characteristics of disposal cells in European programs (section 2.1). In line with the general methodology in ACED, the phenomenological processes at the interface scale are reviewed (section 2.2) leading to a narrative of the time-space evolution at the disposal cell scale (section 2.3). Chapter 3 reviews how information on the chemical evolution could be obtained based on archaeological or natural analogues (section 3.1), and dedicated experiments (section 3.2) or mathematical models to integrate the process knowledge (section 3.3). In chapter 4, a short description is given of the relevance of assessing the chemical evolution.

There may be current European practices why the chemical evolutions at disposal cell scale are included in safety assessments and how these chemical evolutions have been treated e.g. in safety cases. The conceptualisations of the chemical evolutions and which parts have been modelled in Europe have been collected in ACED (Neeft et al. 2019). Desk-based studies have been performed to provide a structured overview of existing (experimental data) on relevant processes at interfaces relevant for disposal of vitrified HLW and cemented ILW. The phenomenology, experimental evidence and modelling approaches of chemical interactions have been described at interfaces relevant for disposal cells with these type of wastes in clayey and granitic rock (Deissmann et al. 2021). The following interfaces have been selected:

- glass-steel,
- cement/mortar-granite,
- cement/concrete-clay,
- steel/iron-bentonite,
- steel/iron-cement/concrete, and
- steel/iron-granite

These two documents are an important basis for this initial state of the art on the assessment of the chemical evolutions of ILW and HLW disposal cells.

1.2 Assessment of the chemical evolution at the disposal cell scale (ACED)

1.2.1 Scope of ACED

The broader scope of ACED is the assessment of the chemical evolution at the disposal cell scale involving interacting components/materials and thermal, hydraulic and/or chemical gradients. The study of the disposal cell ranges from microscale processes at interfaces between different materials up to interactions of waste packages with their immediate surrounding near field environment and the host rock.

1.2.2 Objective of ACED

The main objective of ACED is to improve methodologies to obtain multi-scale quantitative models for the chemical model at cell disposal scale, based on experimental data and process knowledge, and to improve the description of the most relevant processes driving the chemical evolution into robust mathematical frameworks. Applications will lead to integrated process understanding at larger temporal and spatial scales compared to individual process scale studies. More specific objectives are:

- Compile and integrate the process level knowledge and description of reactivity at the interfaces between materials relevant for ILW and HLW disposal cells;

- Develop and evaluate methodologies to integrate available process-level knowledge and processes into a multi-process and multi-scale modelling framework for assessing chemical evolution at the disposal cell level;

- Propose and apply a step-wise scale-up process-based approach to identify (i) processes and features which control the chemical evolution for representative HLW and ILW disposal cells, and (ii) to which detail and complexity these processes should be incorporated in models for different type of safety and performance related studies. The information gained through the study of the more generic but representative European HLW and ILW disposal cells can later be used and adapted for more specific, national disposal cell designs.

1.2.3 General methodology of ACED

As processes and features on small scales may affect the chemical evolution at a cell disposal scale, a major step is to evaluate how to pass information from relatively isolated small-scale processes investigated on interface scale to more complex systems at waste package scale and further to full disposal cell scale.

The key features of these scales are:

- **Interface scale:** The focus of the interface scale is on two materials in contact with each other to obtain information on the geochemical evolution close to an interface in terms of chemical variables and alteration in solid phase composition at a detailed small scale.
- **Waste package scale:** The key feature of the waste package scale is that several materials are present in a specific configuration and are interacting with each other under chemical and possible other gradients. Typically, no interactions with host rock or other waste packages are considered. For HLW cells, in which the chemical evolution of the waste package is governed to a very high degree by the integrity of the canister, mainly the small-scale evolution of the system glass, iron corrosion products and part of adjacent backfill material (clay/cement) after canister breaching is of interest to assess the evolution of the glass and cement alteration zones when the materials are in contact via a permeable stainless steel barrier.
- **Disposal cell scale:** The disposal cell scale consists of waste packages and their immediate surrounding being other waste packages or other near field components.

Figure 1-3 shows a graphical representation of these three different scales.

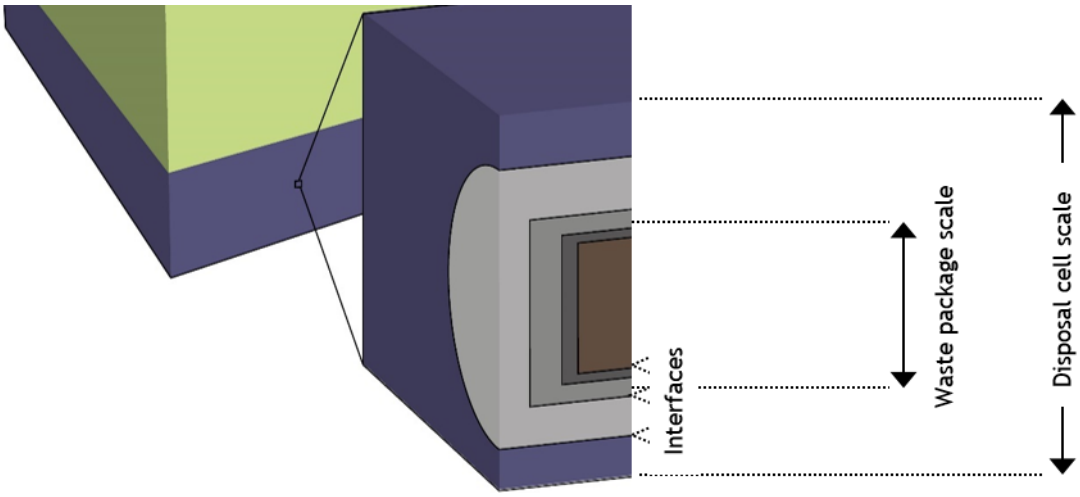

Figure 1-3: Investigations at ACED at different scales

To develop integrated models for assessing the chemical evolution at different scales, two main methodological routes will be evaluated being process integration and model abstraction:

- **Process integration:** This concerns the integration of scientific knowledge, conceptual and mathematical models on individual or selected processes into an integrated conceptual and mathematical model. The integration will increase the understanding of the system behaviour and evolution, helps identifying key processes or parameters, or enables transfer of information from a more detailed scale to a larger scale.
- **Systematic abstraction:** The aim is to reduce model complexity in a systematic way such that (i) an acceptable description of the chemical evolution is preserved during model abstraction, and/or (ii) differences in some key variables of the chemical evolution can be described qualitatively and/or quantitatively. This leads to a better representation of the expected evolution in safety or performance models, thus helping in reducing and quantifying conservatism and uncertainty and thus directly impacts the definition of safety margins.

1.2.4 Relevance of ACED

1.2.4.1 Within the joint programme EURAD

ACED addresses several research subjects relevant for the long term management of radioactive waste, in particular for the post-closure phase in geological disposal:

- **Radionuclide Release from Waste Forms other than Spent fuel:** The geochemical evolution influences degradation/corrosion of different waste immobilisation matrices (vitrified waste, cemented waste) and metallic wastes as function of the evolving conditions imposed by different materials and geometrical features. The release kinetics of radionuclides itself are not part of ACED, but the experimental and modelling studies concerning waste form alteration provide essential information on the mechanisms and kinetics of radionuclide release.
- **Waste Packages Interfaces:** The waste package and its interface is one of the central themes of ACED. Information will be collected and provided on the state-of-the-art of experimental studies, conceptual models and parameters for relevant interfaces in waste packages – summarized in Deissmann et al. (2021). This information will be integrated to obtain conceptual and mathematical models which assess the geochemical evolution at these interfaces at relevant temporal and spatial scales; first via narratives about the evolution, and next via conceptual model development and implementation into mathematical models. The impact of these geochemical transformations on the evolution of porosity (including clogging phenomena) will also be investigated, as porosity represents the primary affected physical variable determining radionuclide migration and fluid flow.
- **Metallic & Cementitious Chemical Perturbations - Bentonite and other Clay based Components:** Two interphases will be studied in more detail (cement-steel and clay-steel), using experimental and modelling approaches to describe the geochemical transformations at that interface.
- **HLW/ ILW Near-field Evolution:** Integration of process knowledge in models describing the chemical evolution between the waste form (glass, cemented waste) and the near field materials is crucial to assess the evolution of the buffer, container and waste matrix. Possible feedbacks between the transport of reactive species and/or other drivers for geochemical alterations are incorporated. Evaluation is made what (type of) processes are important for a representative estimation of the geochemical evolution.
- **THC evolution:** The work contributes to describing coupled Thermal-Hydraulic-Chemical (THC) processes (main emphasis on coupled C processes but not excluding T and H influences) at the disposal cell scale, i.e. waste packages in contact with other components of a repository system including other waste packages). The aim is to develop and evaluate approaches to integrate process knowledge (available at a given stage) to describe the integrated chemical evolution at the disposal cell scale. Analysis of the required level of model complexity and parameter sensitivity are used to identify key features, processes and parameters to describe the chemical evolution at the relevant space and time scales.

To be useful for the waste management programs in different European countries, the studies performed in ACED are done for generic but representative disposal cells that have the most important characteristics of the disposal cells.

1.2.4.2 Implementation, safety and science-technology

Assessment of the chemical evolution at the cell disposal scale will give input to identify critical features in the design of a disposal cell. The model capacity and benchmarked simplified models will help in the engineering and design of immediate surroundings of waste packages.

The methodological developments and applications for assessing the chemical evolution at the disposal cell scale will allow for better representation of interactive and complex processes, with emphasis on chemical processes, within ILW or HLW disposal cell systems. The chemical evolution forms the basis for the evolution and the assessment of many safety- and performance-related aspects, such as waste form degradation, material alteration, source term (radionuclide release), and radionuclide speciation, fate and transport. This better representation of expected evolutions will help:

- To assess and quantify the one of the two princpal objectives of the multiple barrier system to contain the radionuclides from the waste through various safety functions. The chemical conditions induce geochemical alteration of different barriers. These alterations may lead to changes in lifetime of a barrier, including the waste package container, and changes in the mobility of radionuclides, including both solubility and sorption. The methodologies developed and evaluated in this work package contribute to the assessment of the

containment of radionuclides as they will describe the change in chemical conditions over time, when different materials, waste packages and disposal cells interact with each other.

- To further reduce conservatism and uncertainty, and to quantify the safety margins.
- To define the requirements on materials, including the robustness of allowable tolerances. The specifications, including dimensioning, of the packages and disposal cell(s) can be influenced based on the calculations of the geochemical evolution. The geochemical evolution can be one of the factors for defining acceptance criteria for varying wastes and stabilization materials.

2 Chemical evolution in disposal cells

The conceptualisations of the chemical evolutions require the radiological, chemical, and physical properties of the engineered barriers and natural barriers and the potential microbial activity in these barriers. The radiological properties determine the classification of waste.

- HLW has a very high activity content and also generates heat in such amounts that special measures for sufficient heat dissipation need to be made during storage and disposal of this waste. Examples of HLW are vitrified waste forms from the recycling of spent nuclear fuel and spent nuclear fuel.
- HLW and ILW both require shielding during transportation of this waste, but no additional measures for heat dissipation need to be made for ILW. An example of ILW are the compacted metallic parts of spent fuel that arise during the recycling process of spent fuel. Also sources with alpha-emitting radionuclides with smaller half-lives than naturally occurring uranium isotopes such as plutonium and americium can be ILW.
- No shielding measures are required for LLW and lower level waste. Examples of these types of waste are the uranium tails produced during the fabrication of nuclear fuel, material that has been contact-handled by people during maintenance of a nuclear plant, and waste arisings after research has been performed.

Figure 2-1 shows the concept of waste classification as defined by IAEA.

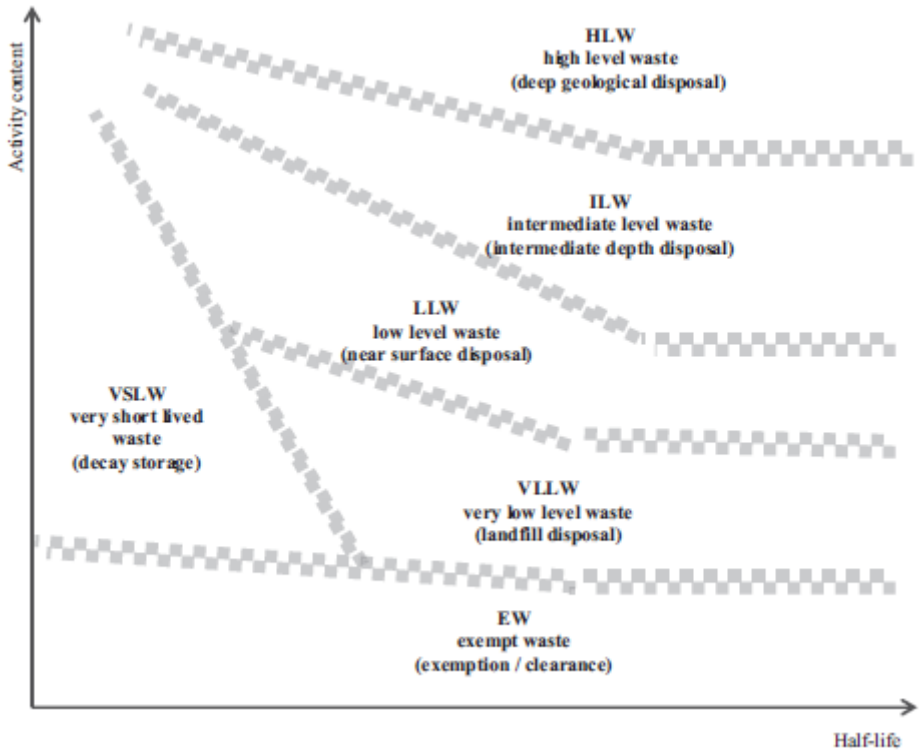

Figure 2-1: Concept of illustration of the waste classification scheme (IAEA 2009)

In ACED, disposal of HLW and ILW is investigated. Disposal of LLW is already taking place for decades for example in Finland, Sweden, France, Hungary, Bulgaria and Spain. The disposal facilities in these countries are also accepting short-lived ILW for example the SFR in Sweden. The radioactivity of the disposed waste in the SFR is dominated by short-lived radionuclides. A large fraction of the activity deposited in SFR will decay substantially during the operational phase. The total activity content at 100 years after closure is evaluated to be less than half its original value, and 2% remains after 1,000 years. The short-lived waste includes radionuclides with a half-life shorter than 31 years (Vahlund and Andersson, 2015).

The chemical properties of the engineered barriers and natural barriers are determined by the chosen materials and depth of the facility in the host rock. Usually, the depth of the disposal facility is so large that reducing chemical conditions are present in the virgin clayey and granitic host rock. The diversity in the chemical composition of the waste forms generally decreases with increasing radioactivity of the waste:

- HLW: Spent nuclear power fuel has currently always uranium oxide as a waste matrix and the HLW arising from recycling of this fuel result into a vitrified waste form. The chemical alteration rate of these waste forms is very small and generally well understood for example by studying natural analogues. These analogues do however not have complementary materials such as steel that might alter the chemical process on a small scale. Spent research reactor fuel has an aluminium or silicon matrix and the alteration rate at disposal conditions is envisaged to be faster than uranium oxide or glass.
- ILW: The chemical nature of the waste form can be metallic and organic. Radiation resistant resins (organic) are used to absorb radionuclides from water used in operation and maintenance of nuclear reactors. The volume of waste is reduced since the radionuclides are concentrated in these resins and the cleaned water can be re-used. Metallic waste can be compacted Zircaloy hulls from spent nuclear power fuel but also stainless steel that has been neutron irradiated in nuclear plants. There are several reasons why these metallic materials have been chosen and one of them is their high corrosion resistance. The chemical alteration rate associated to both resins and these metallic materials can also be very small but only for resins evidence from natural analogues is available.
- LLW: The chemical nature of the waste form can also be metallic and organic, but the diversity in organic material arising from nuclear power plants is generally larger for LLW than for ILW. Exceptions are the waste arisings from research and reprocessing plant dismantling operations; a similar diversity in the chemical nature of the waste forms may be for LLW and ILW. Everything that people use in ordinary life such as cloths, paper (tissues), rubber, steel, aluminium can also become contaminated with radionuclides and become waste. Substantiation of the chemical alteration process and the prediction of the chemical alteration rate of some specific waste forms is still investigated, since degradation of these waste forms can enhance the transport of radionuclides into our living environment.

The physical properties that have an impact on the chemical evolution are the porosity, the distribution in size of pores and the presence of cracks in the engineered materials and host rocks. These two properties and the water content in the pores and cracks of these materials determine the potential exchange of chemical species and microbial activity. The potential diffusional pathways of dissolved species in materials increase with increasing saturation degree. The interfacing materials are not in equilibrium and a new precipitated material between the interfacing materials may arise. This new material can also have physical properties that impacts the chemical evolution.

There is always presence of microbes but there is no microbial activity if these microbes are in a dormant phase. The microbial activity depends on various factors that can be generalized (see Figure 2-2). There are also very different types of microbes but the alteration of a material may require specific microbes. Microbes require organic matter as a food source but also other nutrients to build their DNA and proteins. Organic matter can be present in the waste forms of LLW and ILW but not in a HLW waste form.

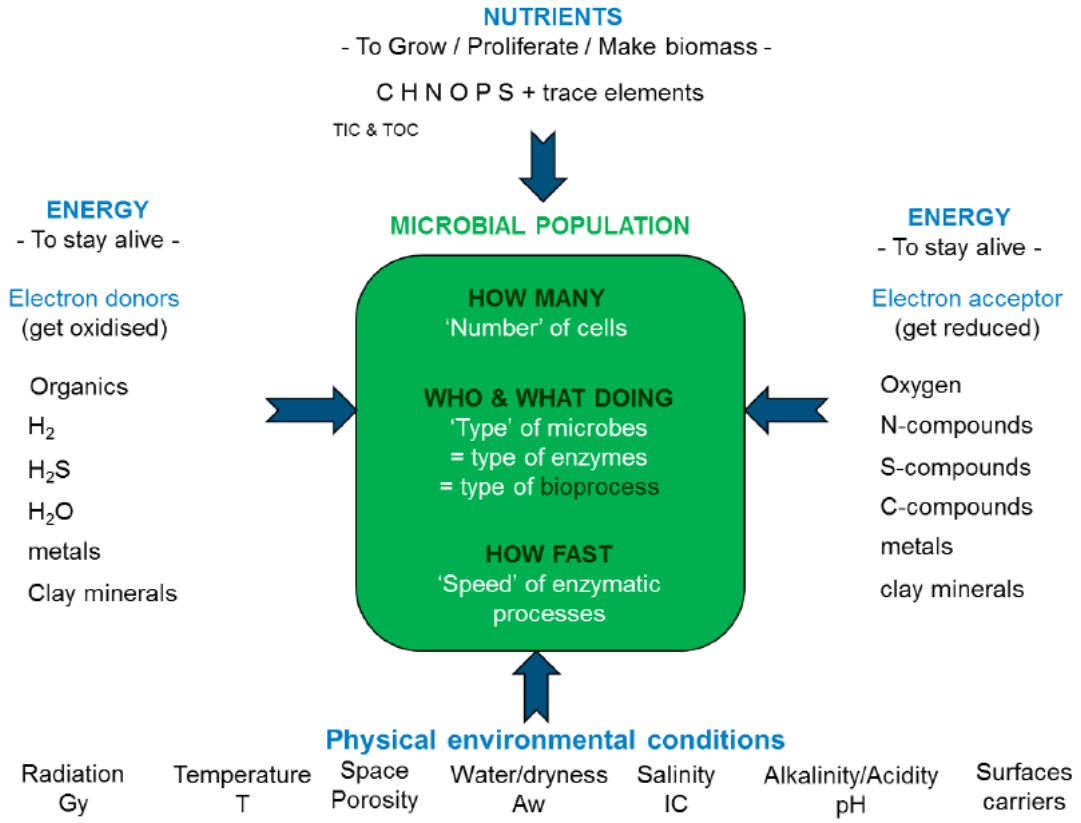

Figure 2-2: Generalized overview of restricting and enhancing parameters for microbial life (Wouters et al. 2016).

Radiation

There is a wide diversity of values considering the radiation resistance of microbes. It is the hydroxyl radical that is formed during irradiation of water and water containing media that is the most damaging agent since this radial oxidises DNA, RNA, proteins and lipids (Brown 2003). The upper limit of the radiation dose of microbes is 30 kGy (Wouters et al. 2016). For example, microbes that can enhance corrosion of steel and have been added to steel lose their activity after 100 days irradiation at dose rates of 2.1 Gy per hour, i.e. 5 kGy (Bruhn et al., 2009).

Temperature

The diversity in the denaturation resistance of microbes is large and can range from -20 °C till 122 °C (Wouters et al. 2016). The optimal activity of sulphate reducing bacteria[1], i.e. bacteria mainly responsible for microbial induced corrosion, is 28 to 30°C, but these bacteria can tolerate a temperature as high as 75 °C (Virpiranta et al. 2019).

Space/porosity

A microbial cell should have a certain minimal size in order to harbour all essential proteins and nucleic acids to maintain life. The range in diameters of microbes is between 0.2 µm and 2 µm. The connecting pore throats in clayey host rocks such as Boom Clay is smaller than 10 to 50 nm. The microbial activity

[1] The presence of FeS is attributed to the presence of sulphate reducing bacteria in soils and although these bacteria are regarded as harmful to steel, archaeological analogues do not confirm this behaviour (Dillmann et al., 2014).

is restricted in space in these clayey rocks not only because they are not mobile but also because the transport of electron donors and acceptors and carbon sources is very slow (Wouters et al. 2016). The best natural analogue to illustrate negligible microbial activity in clays is the Dunarobbe forest in Italy in which 2 million year old trees had been preserved in compacted clay. These trees were protected against microbial degradation and therefore had cellulose contents similar to present-day wood (Lombardi and Valentini, 1996), (De Putter et al., 1997). Manufactured concrete can also have pores with a maximum in diameter till 50 nm. A maximum in 100 nm (0.1 µm) is not uncommon for concrete by which it can also be assumed that the potential microbial activity is limited due to space restriction in concrete. Dormant microbes can become activated when cracks in clayey rock or concrete appear.

Water/dryness

Most microbes require water activities larger than 0.9 (Swanson et al., 2018), i.e. a relative humidity of 90%. However, there is also a wide diversity in the desiccation resistance of microbes. Sulphate reducing bacteria have been experimentally examined to require a minimum in water activity of 0.96 (Stroes-Gascoyne and West, 1997). Lower relative humidities can be present during storage of the waste, in the operational phase of the disposal facility and early in the post-closure phase for HLW disposal cells, when the waste emits heat and drying occurs.

Salinity

Salinity has a similar effect as drying, i.e. the water activity is reduced with increasing salinity. A water activity of 0.90 is equal to ≈ 2.7 M NaCl solution or ≈ 1.4 M $MgCl_2$ solution (Swanson et al., 2018).

pH

Microbial life in high pH environments requires a mechanism to keep a neutral cellular life and a proton motive force across the cell membrane to preserve proteins and produce adenosine triphosphate (ATP), a carrier of energy. The concentration of H^+ is very small at high pH and an upper limit of 12 is generally assumed, although also microbial communities have been described to grow up till a pH of 13.2 (Wouters et al., 2016). These microbes have been found in a lake in which steel slag had been dumped (Roadcap et al., 2006).

2.1 Main characteristics of European HLW & ILW disposal cells

The characterisations of disposal cells have been collected in ACED (Neeft et al. 2019). Although the HLW and ILW disposal cells have country or program-specific features and specifications, it is possible to group them into different classes with respect to the different components, structures, interfaces etc. This section describes this grouping and the main characteristics of the HLW and ILW disposal cells in European countries/programs. It serves as a basis for much of the work that will be done within ACED and guarantees that the studies performed and information obtained within ACED are relevant for European radioactive waste disposal programs. The section starts with the characteristics of the waste and the engineered barriers. Construction and operation of the disposal facility can have an impact on the clayey and granitic host rock and affect both ILW and HLW disposal cells and are described at the end of this section.

2.1.1 HLW disposal cells

2.1.1.1 Characteristics of vitrified HLW

The HLW investigated in ACED is vitrified HLW. This waste product results from the reprocessing of spent fuel in which uranium and plutonium have been extracted. The High-Level Liquid Waste (HLLW) has been poured with a melted glass frit into a stainless steel container. This waste processing ensures that the radionuclides are homogeneously distributed in a borosilicate glass matrix. This matrix contains

traces of plutonium and uranium, other actinides that have not been extracted such as americium and fission products. These vitrified waste products have been made in Sellafield (UK) and are still being made in La Hague (France). The largest amount comes from France and therefore frequently, the French abbreviation for this waste product is used: Conteneur Standard de Déchets vitrifiés, CSD-v. The vitrified waste product is made in two batches with each of 200 kg (Moncouyoux et al., 1991). For ACED, the dimensions of the canister, thermal power as a function of time and parameters to conduct the generated heat are needed. Figure 2-3 shows the dimensions of the matrix and canister. The thermal power as a function of time and other properties of a CSD-v with a high actinide content can be found in Appendix A.

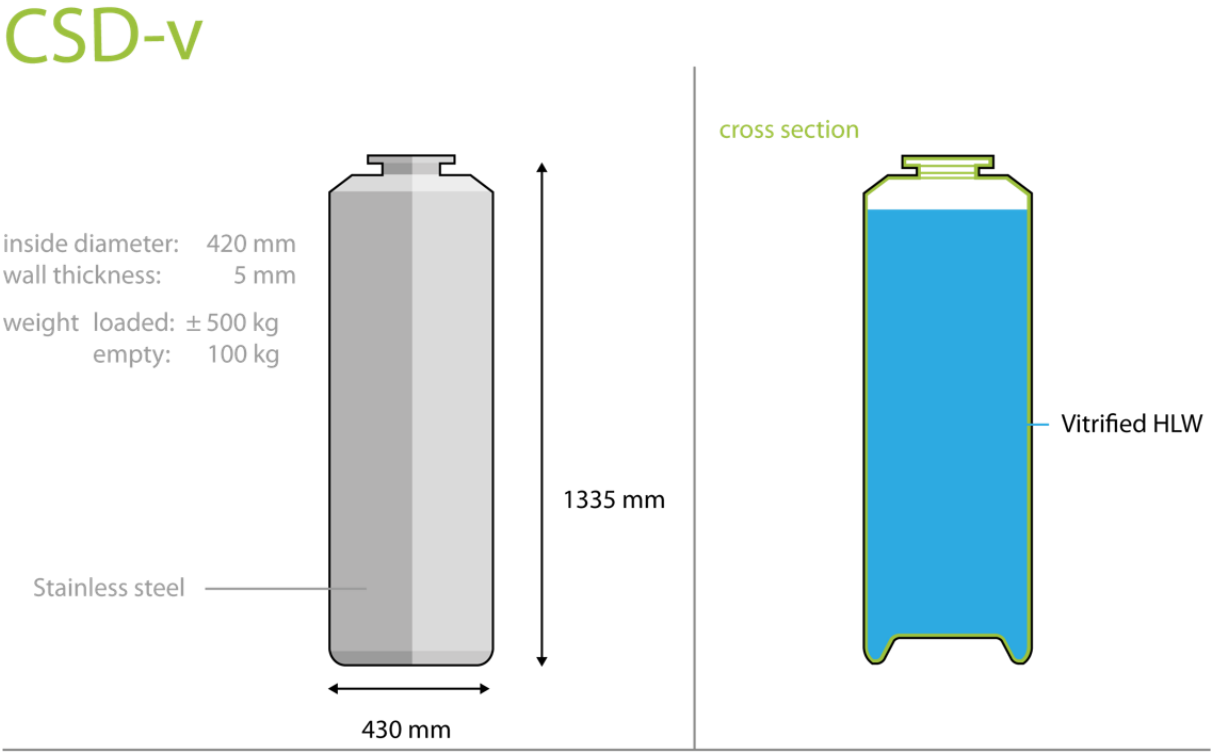

Figure 2-3: Schematics of CSD-v (AREVA 2007)

The number of cracks that are present within this waste form after pouring into the canister and subsequent cooling may be limited, but a tomographic or X-ray image of a canister with processed waste to deduce the cracks within the waste form has not been found. The experimental studies performed in the nineties for the 3rd framework (RTD) programme to characterize radioactive waste forms have demonstrated that it is possible to produce homogeneous glass blocks by applying appropriate cooling procedures even with non-radioactive simulate HLW, as has been observed with tomograms (Reimers, 1992). The full scale tests with non-radioactive simulant without appropriate cooling procedures show large glass shrinkage cavities (Moncouyoux et al., 1991) as the inner part solidifies last. Rapid cooling also generates a large number of circumferential cracks due to the stress associated with the large thermal gradient (Reimers, 1992). In reality, (passive) cooling systems are needed in order to store these vitrified waste forms. It can take 65 years in order to have a sufficient heat loss for disposal. The 'so-called' reference blocks with a controlled cooling rate of 2.8 °C per hour (Moncouyoux et al., 1991) may therefore provide the best estimate for the determination of a cracking factor. This factor is a parameter that is used in performance assessment studies to determine the alteration/dissolution rate of glass and radionuclide release rate. The outer surface of a glass block would be 1.781 m^2, assuming the surfaces at top and bottom to be flat. After the reference block of 391 kg was taken out of the canister, it was broken into 11 pieces: one weighing 250 kg, another 80 kg and nine pieces with a weight of less than 10 kg. The outer surface was 2.787 m^2 as measured by wrapping all the faces in aluminium foil

(Moncouyoux et al., 1991). The cracking factor then becomes 1.56. Please note that this cracking factor is smaller than average in cracking factor of 40 obtained from leaching experiments with another experiment with inactive glass blocks at full-scale. This factor is reduced during the leaching experiment until an average in cracking factor of 5 due to alteration of glass by which the small cracks were closed (Ribet et al., 2009).

The presence of radionuclides within glass has some beneficial characteristics to prevent or heal cracks. The thermal power source and the radioactivity work as glass network modifier by producing ionization rays. The α-decay of actinides present in waste diminishes slightly the glass density and its mechanical properties and appreciably improves, especially its resistance to cracking (Ribet et al. 2009). The evolving helium diffuses at such a high speed at room temperature that helium implantation below room temperature is necessary to make helium observations within glass using neutron activation analysis (Chamssedine et al., 2010). Consequently, defects generated by stopping the highly energetic alpha particles within the waste form are annealed at room temperature by which helium trapping by defects within the waste form glass does not occur at temperature conditions representative for storage and disposal.

2.1.1.2 Metal overpack

For disposal, the stainless steel canister with vitrified waste is envisaged to be put in a carbon steel overpack in many national programmes (Neeft et al., 2019). This steel has predictable corrosion kinetics; general corrosion is considered the predominant mechanism rather than localised corrosion processes. In all programmes, the safety function of the overpack is to prevent contact between the vitrified waste form and groundwater but the required periods for this physical containment are different. The difference in periods are caused by the used safety concept.

- In the French programme, there is no contact between pore water and vitrified waste until the temperature of the core of the vitrified waste form is lower than a certain temperature. This temperature is determined by the advances in knowledge about the behaviour of vitrified waste form and radionuclides in solution. The required period for containment is envisaged to be less than 500 years.
- The temperature of the host rock is considered as a criterion in other programmes for this physical containment for example in the Belgian and Dutch programme. The heat dissipation to the host rock should be negligible. If that is achieved, radionuclide migration data obtained in laboratory experiments performed at room temperature or the radionuclide migration data extracted from the site, can be used to calculate the transport of the released radionuclides in the clay formation. The required period for containment is envisaged to be more than 1000 years.

The disposal packages with a metal overpack are disposed in a low-carbon steel sleeve which is a casing for a micro-tunnel in the French programme (see Figure 2-4).

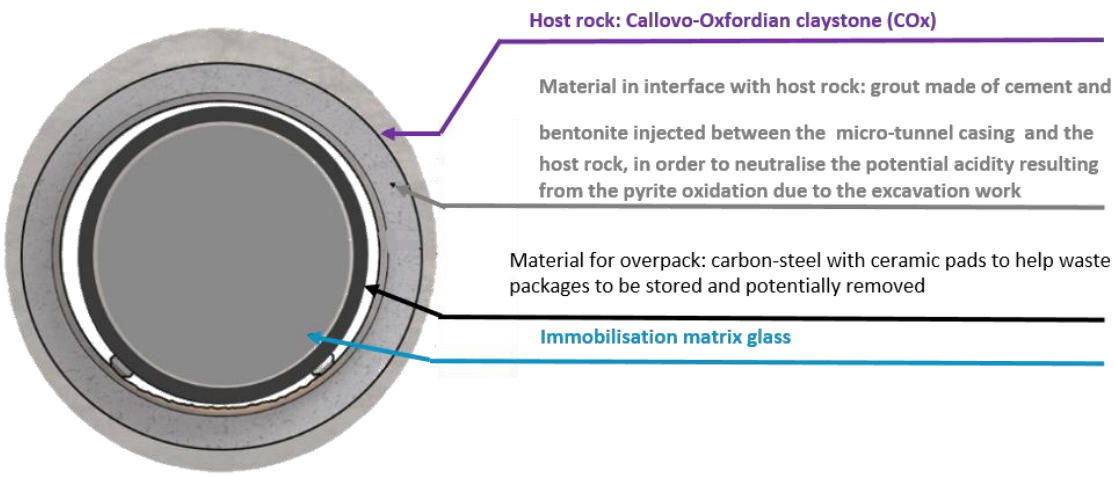

Figure 2-4: Section of a French HLW disposal cell with identification of the different materials (Cochepin et al., 2019)

The Czech and Spanish programmes do not consider vitrified HLW but they do consider these steel overpacks for physical containment of spent nuclear power fuel. This steel overpack is in contact with an engineered buffer in their programmes. Many other programmes also envisage an overpack interfacing an engineered buffer (Neeft et al., 2019).

2.1.1.3 Characteristics of disposal cells with buffer materials

Bentonite and concrete are envisaged as interfacing materials for the carbon steel overpack. Bentonite buffers are considered in the Czech, English, German, Spanish and Swiss programmes and concrete buffers are considered in Belgian and Dutch programmes. These engineered buffers are carefully designed to meet specific criteria.

2.1.1.3.1 Characteristics of bentonite buffer

Bentonite has a high smectite content of which montmorillonite is the most famous species. These minerals can swell and therefore induce a large impact on the distribution in size of pores, its consequent connecting pore throats and hydraulic conductivity. The smectite content can be 88 wt% as used in the Czech and 75 wt% in the Swiss programme, in which smectite is further specified as Na-montmorillonite in Wyoming MX-80 (Müller-Vonmoos and Kahr, 1983). Wyoming MX-80 bentonite is also used in the Swedish programme (Wanner et al., 1994). Please note that these clay contents are higher than the clay contents of around 60 wt% in any clay host rock considered in the national programmes (see Appendix B). The bentonite is compacted to an optimum in density and its resulting swelling pressure. The density and swelling pressure should be high enough to reduce microbial activity and resulting swelling pressure to prevent movement (sinking) of the overpack and limit advective transport (Hedin et al., 2011). There is much evidence indicating that microbial activity will not occur in compacted bentonite with a dry density exceeding 1600 kg/m^3, either because of low water activity or because of the effect of swelling pressures in excess of 2 MPa on the physiology of the microbes (Johnson and King, 2008). There are a number of interface locations such as placement gaps, contact regions with materials of different densities and contact points with water carrying fractures in the rock by which the dry density can become smaller than 1600 kg/m^3 upon expansion of compacted bentonite into a void. The reduction in dry density can stimulate or restore the cultivability of indigenous microbes which would increase the possibility for in-situ microbial activity. Reductions in dry density should therefore be minimized or eliminated by adequate design (Stroes-Gascoyne et al., 2011). The density and resulting swelling

pressure should also be low enough to prevent damage to the metal overpack and host rock (Hedin et al., 2011).

Bentonite buffers are usually 'dry' emplaced. Dry can mean for bentonite buffers a water content of 17 wt% (e.g. Johannesson et al., 2020) or 10% (e.g. Atabek et al., 1991). The saturation of these dry blocks with which the buffer is constructed is between 50-60% (Johnson and King, 2008). The pore water chemistry of this engineered barrier is therefore determined by the inflow of host rock water and establishment of equilibria between dissolved species present in this host rock water and minerals present in bentonite, i.e. there is no initial pore water chemistry as in concrete.

2.1.1.3.2 Characteristics of concrete

The required strength of concrete, environmental class, fluidity during pouring and distribution in size of aggregates have all been defined before fabrication of any cementitious material. The strength of concrete is determined by the strength of aggregates and the attachment of the aggregates with the cementitious phase in concrete. Choices in concrete recipe and type of mixing of ingredients follow from these requirements and available knowledge. This available knowledge is integrated in standards for civil engineering. These standards are regularly updated. The European standard EN 206 divides the potential degradation of concrete or the reinforcement inside the concrete into 18 exposure classes. There are three exposure classes for ranges in dissolved sulphate content, pH, amount of dissolved CO_2, dissolved ammonium and magnesium content. All these complexes are also present in the pore water of clay and crystalline host rock except for dissolved ammonium, which is characteristic for polluted groundwater. Polluted groundwater may not be relevant for disposal studies. The pH of concrete pore water is high after fabrication of concrete, around 13 (see Appendix B). The ingress of CO_2 can lower the pH of the concrete pore water, which can be detrimental to the steel used for the reinforcement, i.e. ingress of CO_2 may not be detrimental to concrete itself. The resulting calcite precipitation within concrete results in a porosity reduction that can decrease the permeability of concrete. The environmental class determines many requirements. For example, concrete being exposed to the highest magnesium concentration (XA3) requires:

- the smallest water to cement ratio since this ratio has an impact on the permeability of concrete and thereby ingress rate of dissolved magnesium. A small permeability is characteristic for a concrete with a high strength and has the smallest ratio in water to cement;
- the largest cement content in order to buffer the ingress of magnesium;

Superplasticisers are used to achieve a well mixing and processability of cementitious fluid with a reduced water content. There are chemical alterations in which the mechanical strength of fabricated concrete is too early too much decreased in the operational phase of the disposal facility or in the post-closure phase of the disposal system. These alterations can be prevented with a proper choice in cement, content of cement in concrete and a proper choice in combination of cement and aggregates and are therefore not studied within ACED. For example, sulphate resistant cement is used to prevent Delayed Ettringite Formation (DEF). DEF can be caused by:

- an internal sulphate attack, when the temperate during hydration is too high t;
- an external sulphate attack by ingress of dissolved sulphate species reacting with tri calcium aluminate (C_3A).

The hardened cement between the aggregates is cracked when DEF occurs. Both cases of DEF can be prevented by limiting the C_3A concentration. A Portland cement blended with microsilica, fly ash or slag also reduces the temperature for hydration by which internal sulphate attack is prevented. These blended cements can be called sulphate resistant cements for example CEM III/B.

Another example of a proper choice to prevent chemical alteration in which the mechanical strength of fabricated concrete is too early too much decreased is using calcite or quartz aggregates instead of aggregates with silica polymorphs. For example, chalcedony, a siliceous mineral, reacts with the alkalis

in the concrete pore water into the formation of silica gels; cracks become present through the reactive siliceous aggregates. The use of blended cements also reduces the probability of the alkali silica reaction (ASR) due its low permeability at an ordinary engineering time scale of about 100 years. Concrete made with blended cements are called low-permeability concretes, due to their more refined pore structure compared to concrete made with Portland cement (Atkins et al., 1991; Atabek et al., 1991; Jackson et al., 2017). A porosity between 10 to 15 vol% is a good estimate for the concrete buffer.

2.1.1.3.3 Characteristics of the bentonite buffer and concrete buffer

Both bentonite and concrete buffers have small connecting pore throats by which two beneficial physical conditions are provided for the durability of the carbon steel overpack:

- the transport of dissolved chemical species is dominated by predictable slow diffusional processes;
- microbial activity is limited.

The corrosion of many metals is determined by the solubility of the metal-oxide that is formed, the diffusion of species through this metal-oxide and the concentration of dissolved species near this metal-oxide. These dissolved species have a larger diffusional speed in stagnant groundwater than in these buffer materials, by which the removal speed of these dissolved species is larger. The concentration of dissolved species near the metal-oxide can however also be reduced, if the buffer adsorbs the dissolved species. The microbial corrosion rate is usually larger than the chemical corrosion rate, but the initiation of microbial corrosion does not take place when the microbial activity is absent. This absence may be possible by space restriction in both buffers. The high pH for the concrete buffers is also limiting the microbial activity.

Both buffers have a temperature limit of 100 °C in many disposal programmes. The reason for this temperature constraint is to limit degradation or mineral alteration of the bentonite buffer for bounding the uncertainty in the long-term predictability of this buffer. For the concrete buffer, this temperature constraint has been set to limit the formation of a gaseous phase.

Figure 2-5 shows an abstraction of the disposal cells considered in Europe for the following host rocks: granite (e.g. Czech Republic[2]), poorly indurated clay (e.g. Belgium) and indurated clay (e.g. Switzerland). The disposal concept of compacted clay buffer bricks surrounding vitrified waste in granitic host rocks has been studied earlier in Europe (e.g. Atabek et al., 1991) but these studies were without a carbon steel overpack. Please note that the thickness of the carbon steel overpack considered for concrete buffer is thinner (about 3 cm (Neeft et al., 2019)) than considered for this overpack for bentonite buffers (about 14 cm, e.g. in the Swiss programme (Leupin et al., 2016). The reason for this difference in thickness is the higher corrosion rate foreseen for steel interfacing bentonite compared to concrete.

[2] Spent fuel is not reprocessed in the Czech and Spanish programmes; thus, there is no vitrified HLW to be disposed of in Spain and Czech Republic. The HLW disposal cell does have the steel/iron-bentonite and steel/iron-granite interfaces investigated within ACED. The available knowledge from these programmes is therefore relevant for ACED until there is contact between the pore water and the waste form.

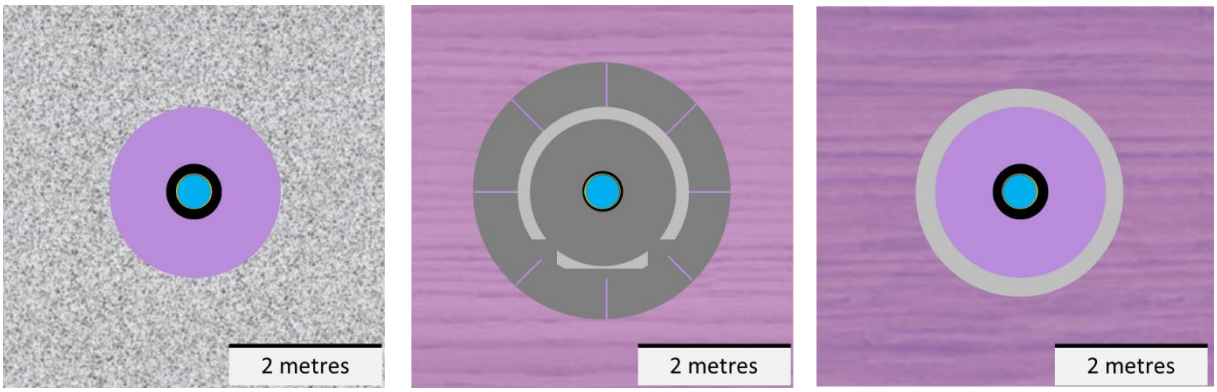

Figure 2-5: Abstracted disposal cells containing vitrified HLW considered in Europe for the host rocks: granite, poorly indurated clay and indurated clay. Blue = vitrified HLW, black = steel overpack, bentonite (purple) or concrete buffer (grey) surrounds the overpack and grout = light grey.

Lining material to support the rock is not needed and used for the granitic rock. Pre-fabricated concrete segments are needed to construct a disposal gallery in poorly indurated clay. These hardened segments need to be directly applied against the fast convergence of this clay. There is more time to apply a lining in indurated clay for example when excavation has been finished. The lining is made by in-situ curing of shotcrete (grout). Grouts are sprayed against the surface of excavated rock in a disposal gallery for indurated clays. Chemical interactions between the cementitious fluid and clay host rock take place before hardening. Reaction rims between shotcrete and clay may have been formed in order to enhance the bonding of the shotcrete with the clay host rock.

The porosity of the pre-fabricated concrete segments is similar to the concrete buffer, i.e. between 10 to 15 vol%. The porosity for the backfill grout and shotcrete is larger between 25 to 35 vol%.

2.1.2 ILW disposal cells

2.1.2.1 Characteristics of ILW

2.1.2.1.1 Metallic ILW

If further specified, the metallic ILW was Zircaloy, stainless steel and carbon steel (Neeft et al., 2019). Metallic radioactive waste is mainly generated by reaction with neutrons and elements within these metals.

Stainless steel and carbon steel arise from the maintenance and dismantling of nuclear reactors. Metallic waste also arises from reprocessing spent fuel from nuclear plants: Compacted waste Standard Residues (Collis Standard de Déchets Compatés: CSD-c). It comprises metal parts from the spent fuel assemblies that have been cut off to extract the spent fuel, then rinsed and dried. A canister of about 170 litres internal volume is filled with either hulls or end pieces. The hulls are made of Zircaloy; other metal parts are usually made of Inconel. End pieces are solid stainless steel sections. Drums with other waste arising from reprocessing fuels, such as pumps, stirrers and filters, are primarily made of stainless steel. All drums are compacted to produce pucks that are loaded into CSD-c canisters with similar outer dimensions to those used for vitrified waste, which are welded closed. The void space is about 20% in the canisters. Figure 2-6 shows the schematics for this waste.

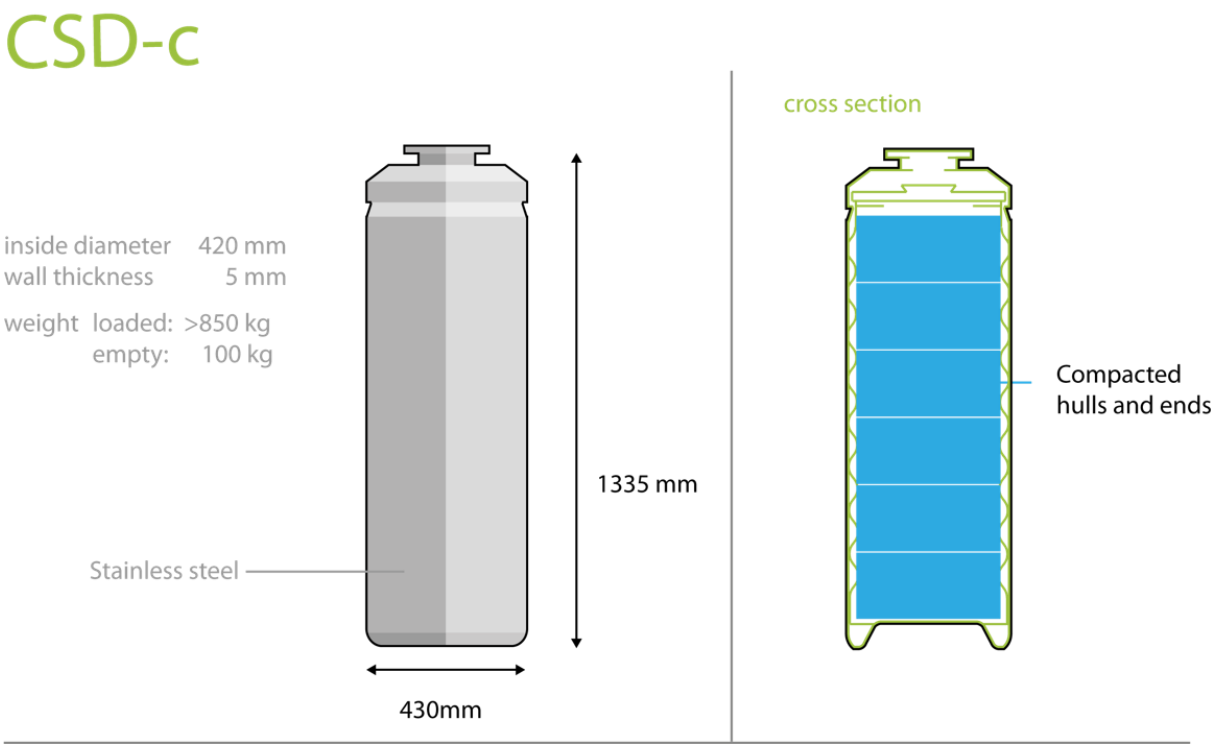

Figure 2-6: Schematics of CSD-c with 6 pucks (compacted drums); dimensions in millimetres (COGEMA, 2001)

CSD-c canisters can later be encapsulated in concrete containers (see Figure 2-8). Another example of pure metallic ILW is activated steel (e.g., Stein 2014). Frequently, however, radioactive steel is processed with organic ILW (e.g., Uras 2021).

2.1.2.1.2 Organic ILW

If further specified, the organic ILW in ACED were spent resins, but the French programme noted a special interest in PVC and cellulose since degradation of both polymers lead to complexing agents for radionuclides (Neeft et al. 2019). The amount of cellulose based material identified in the ILW inventory in the French programme is 25 wt% (Altmaier et al. 2021).

Resins purify reactor coolant water and other types of water used during operation and maintenance of the nuclear reactor. The most common form of synthetic ion exchange resins is polystyrene divinylbenzene in powdered form with diameters from 5-150 µm or in beads from 0.5-2 mm. The resins have functional groups that are to be exchanged with a radionuclide in cationic form such as $^{60}CoOH^{+}$ or in anionic form such as $H^{14}CO_3^{-}$. Spent resins are mixed with a waste matrix that can be a cementitious matrix. Figure 2-7 shows the schematics of this waste with an example showing a detail with the embedding of resin beads in a cementitious matrix (blue). This matrix is fabricated without siliceous aggregates. This type of waste is a so-called homogeneously mixed cemented waste (Uras, 2021).

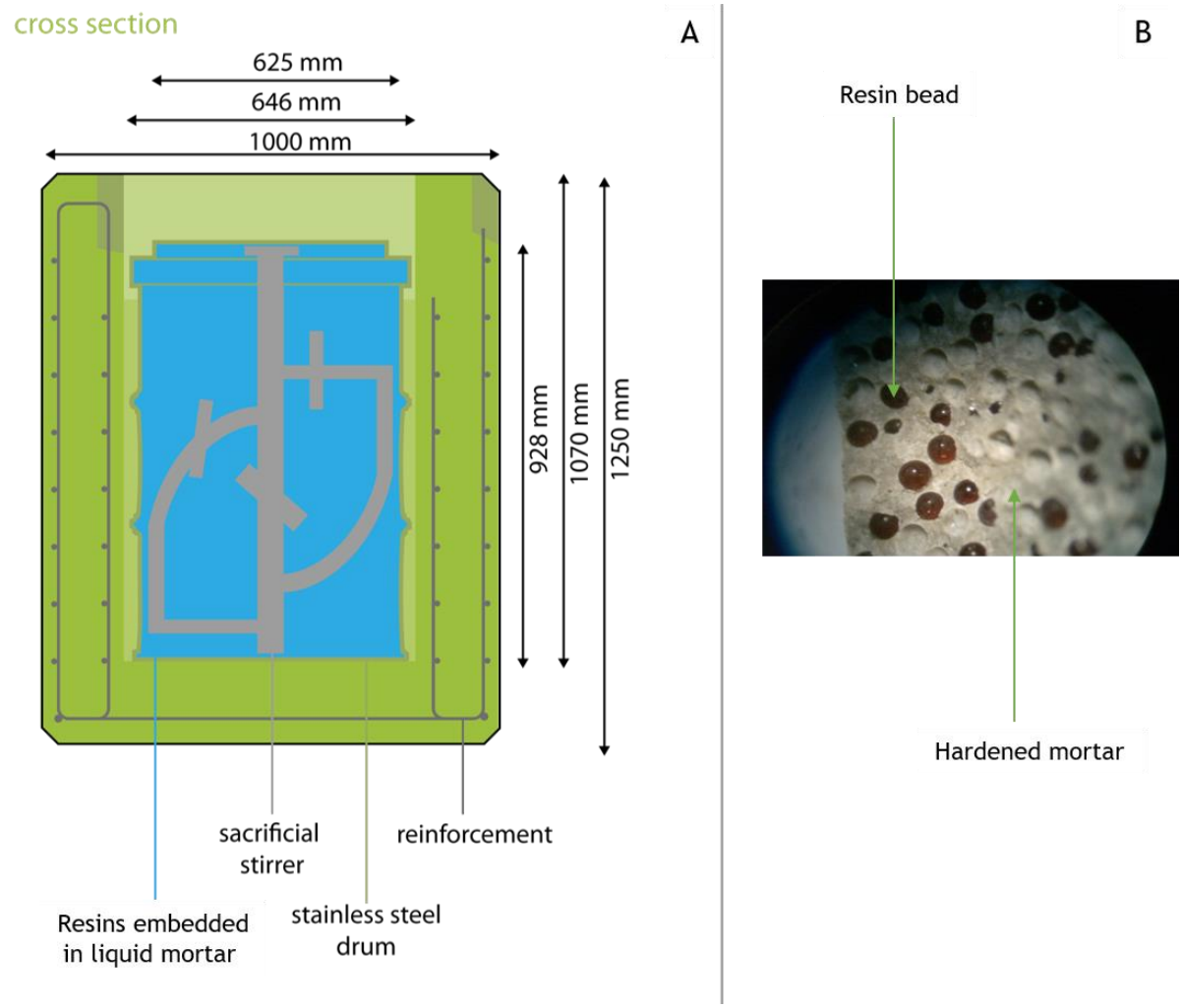

Figure 2-7: A: Schematics of processed resins (adapted from (Verhoef et al. 2016)). Magnetite aggregates are used for the fabrication of the concrete in reinforced concrete container in order to contribute to shielding. B: Detail with the resin beads embedded in a cementitious matrix.

An image of a heterogeneously cemented waste is compacted plutonium contaminated material generated at the Sellafield site in the United Kingdom that contains halogenated plastics (PVC) and non-halogenated plastics, are available in the MIND project from the Horizon 2020 programme. These compacted plastics have been enclosed in an annulus of cement grout (Abrahamsen et al., 2015).

2.1.2.2 Characteristics of ILW disposal cells

Cementitious materials are used to condition the ILW but can also be used as a backfill. The dimensions of a disposal gallery for ILW are usually larger than those of galleries constructed for disposal of HLW. Figure 2-8 shows an abstraction of the ILW disposal cells considered in Europe for the following host rocks: granite (e.g. Sweden) and poorly indurated clay (e.g. Belgium). The ILW disposal cells in granitic rock consist of vaults that are lined with shotcrete to stabilise the rock in the operational phase and caissons in which the waste containers are emplaced.

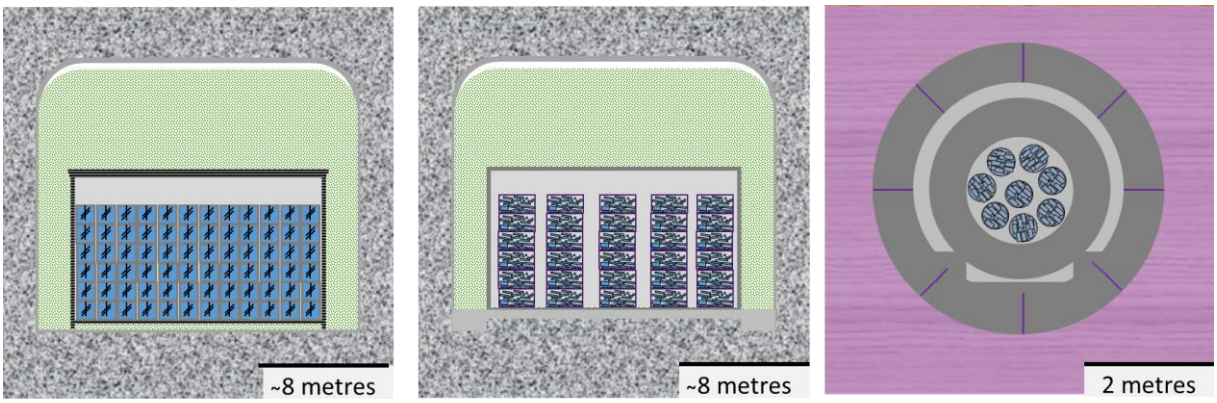

Figure 2-8: Abstracted disposal cells containing cemented ILW considered in Europe for the host rocks: granite and poorly indurated clay. Blue = ILW or cemented ILW, black = steel, green = crushed granitic rocks, grey = concrete and light grey = mortar or shotcrete.

The types of waste drawn in Figure 2-8 are processed spent ion exchange resins with a sacrificial stirrer for each package and metallic waste arising from the maintenance of a nuclear reactor and being mostly steel (both disposed in granitic rock). As an example, processed resins have been drawn within reinforced concrete caisson and metallic waste in unreinforced concrete caisson. The coverage of concrete in well-engineered reinforced concrete depends on the environmental class for example 40 mm for the highest environmental class XA3 in the European standard EN 206. For reinforced concrete, the attachment between steel and the cementitious phase is important. Steel rebars have usually ribbons and are commonly oxidised in air before concrete pouring in order to obtain a good attachment between concrete and steel. Gaps between steel and the cementitious phase of concrete may arise due to shrinkage of the cementitious phase during hardening, when polished and smoothend steel is used. Oxygen in air can increase the corrosion rate of steel. The corrosion rate of steel is minimized if steel is exposed to reducing, alkaline conditions, since a passivation layer on the steel surface that limits corrosion is stable at these chemical conditions. Consumption of oxygen by corrosion of steel can deplete oxygen in the vicinity of the steel bar by which aerobic corrosion is followed by a lower anaerobic corrosion rate. High aerobic corrosion rates caused by the insufficient coverage of the steel bar by concrete may result into the spallation of concrete during the operational phase of the disposal facility. Especially if carbonation of the concrete cover has occurred by which the alkaline environment is no longer provided. So far, only cracking of concrete by aerobic corrosion of rebars has been known with characteristic orange-brown corrosion products with minerals such as hematite and lepidocrocite (Argo, 1981). Anaerobic corrosion of rebars is characterised by dark-brown to black corrosion products with minerals such as magnetite (Argo, 1981).

For granitic rocks, also shotcrete or a grout can be applied sometime after excavation as previously explained for the HLW disposal cells constructed in indurated clay. The caissons are backfilled with cementitious grout after completion of emplacement of waste packages. The empty volume between the caissons and shotcrete is backfilled with crushed granitic rock to control the waterflow in the disposal gallery. Granitic rock is easily available from the excavation activities.

Hardened concrete segments need to be immediately applied after excavation of poorly indurated clay as previously explained for the HLW disposal cells constructed in poorly indurated clay. A cylindrical concrete disposal package containing eight canisters CSD-c is envisaged to be emplaced in this disposal gallery. This gallery is backfilled with mortar.

2.1.3 Characteristics of host rocks

Usually the depth of the disposal facility is so large that reducing conditions are dominant for clayey and granitic host rocks. Determination of the chemistry of the porewater is not always possible by measurements, modelling needs to be used especially for clayey host rocks. The pore water chemistry of the virgin host rock and how this chemistry has been determined and the mineralogy and its impact on the pore water chemistry are described in Appendix B.

The properties of the host rock in the vicinity of the engineered materials changes during excavation of the host rock and may change during the operation of the facility. There will be some fractures generated in the host rock and the size and density of the cracks depends on the excavation technique, size of excavated volume and type of host rock. The disposal galleries to emplace HLW packages are usually smaller in diameter than the disposal galleries to emplace packages containing ILW and the excavation procedure can be different. The outcome of both features is that the Excavation Damaged Zone (EDZ) is smaller for galleries to dispose HLW than for galleries to dispose ILW. The required time to heal or seal these fractures is host-rock dependent.

2.1.3.1 Granitic host rocks

2.1.3.1.1 Construction

Crystalline rock specific excavation procedures have been defined in Finland and Sweden to make galleries to dispose HLW with an acceptable limited water inflow through fractures to emplace the engineered material bentonite in the operational phase (e.g. Baxter et al., 2018). The water flow from the host rock into the disposal cells needs also to be limited for the post-closure phase to limit ingress of species from shallow and deep ground water (Vieno et al. 2003) and bentonite erosion (Baxter et al., 2018). Excavation of rock to construct disposal galleries for short-lived ILW (and LLW) is performed by drilling and blasting. Rock support are bolts and shotcrete; the density of applied bolts as well as non-reinforced or reinforced shotcrete is determined by the fracture extent of the rock (e.g. Carlsson and Christiansson 2007). Shotcrete hardens in-situ and chemical interactions between the cementitious fluid and granitic host rock can take place before hardening. Reaction rims between shotcrete and granite may have been formed in order to enhance the bonding of shotcrete with the granitic host rock.

2.1.3.1.2 Operation

Decades of experience is available for operating a disposal facility for LLW and short lived ILW. Pumps are needed to keep the disposal facility dry. The main inflow of water into this facility is however the access tunnels and not the disposal galleries (Carlsson and Christiansson 2007; Vahlund and Andersson, 2015). The permeability of the shotcrete lining is smaller than the permeability of the crystalline rock. The same accounts for the bentonite buffer that is emplaced in HLW disposal cells. Consequently, the concrete lining and bentonite buffer acts as a barrier for further transport of water into the facility by which sufficient access of water is present in the operational phase to heal the cracks in the rocks. Sealing of fractures can take place by precipitation of minerals, e.g. calcite, chlorite and clay minerals (Drake et al. 2006).

Also the ingress of dissolved species from the host rock pore water that can alter the cement mineralogy of the lining in ILW disposal cells starts in the operational phase. The shotcrete used for disposal cells in granitic rock can become atmospherically carbonated due to ventilation air. The fractures in granitic rock give a heterogeneous influx of granitic pore water into the shotcrete. The ingress of bicarbonate, sulphate and dissolved magnesium (depending on the host rock geochemistry) may precipitate into minerals that replace the calcium-containing cement minerals. There can therefore be a loss in strength of shotcrete liner in the operational phase since the calcium-containing minerals provide the binding and strength of the shotcrete.

2.1.3.2 Poorly indurated clay

2.1.3.2.1 Construction

Special tunnel boring machines are used to construct galleries in poorly indurated clays. Concrete segments are immediately applied after excavation of the clay with these machines. The stability of the lining is caused by the use of a wedge block. The block is emplaced between concrete segments. Concrete interfacing clay in the HLW and ILW disposal cells (Figure 2-5 and Figure 2-8) is the external diameter of the gallery. The diameter of the excavated clay is slightly larger than the envisaged external diameter of the gallery. This so-called overcut is needed in order to able to emplace the concrete segments. So far, the EDZ has been measured by the larger hydraulic conductivity compared to virgin clay. The larger hydraulic conductivity is attributed to the presence of cracks. The hydraulic conductivity of clay interfacing the concrete liner is the largest measured hydraulic conductivity. Further away from this interface, the hydraulic conductivity diminishes and approaches the virgin hydraulic conductivity.

The cracks induced by excavation revoke the limitations for microbial activity that were initially present in the virgin host rock. Active microbial communities present in various boreholes demonstrate that only providing space is sufficient to initiate the establishment of an active microbial community (Wouters et al., 2013; Mijnendonckx et al., 2019). The smectite content of poorly indurated clay is more than 20 wt% (see Appendix C). The dominant process for closure of cracks is self-healing by swelling clay minerals. The decrease in hydraulic conductivity by self-healing of cracks will limit the transport of cells and nutrients. This excavation induced microbial activity is therefore envisaged to be only temporarily present.

2.1.3.2.2 Operation

The concrete segments are usually manufactured with a so-called engineered impermeability; envisaged porosities are between 10 and 15%. This limits the diffusional exchange between the dissolved species in the concrete segments and clay but also dehydration of the clay; the Boom Clay surface - at emplaced concrete segments that had been removed for experimental reasons - felt wet. The flow of water into the disposal facility is so small that ventilation is sufficient to keep the facility dry. The salts that have been deposited at the intrados of the concrete liner especially at joints between concrete segments indicate the preferential flow of clay pore water (Levasseur et al., 2021). The concrete lining acts as a barrier for further transport of water into the facility by which sufficient access of water is present in the operational phase to seal the fractures. The sealing of these cracks takes place by swelling of clay minerals such as smectite. This process can be very fast. No difference in hydraulic conductivity has been found for galleries constructed with an external diameter of 2.5 metre (Dizier et al., 2017). The overcut during the construction of the gallery was minimized. In the SELFRAC project from the FP5 programme, the hydraulic conductivity in clay surrounding a gallery with an external diameter of 4.6 metre was studied. This gallery was constructed with a larger overcut. After a few months, the hydraulic conductivity at 1.5 metre from the interface with concrete was measured to be 3 times larger than the virgin hydraulic conductivity (Bernier et al., 2007) and two times this hydraulic conductivity after 8 years (NIROND, 2013). The virgin vertical hydraulic conductivity is about 1.7×10^{-12} m/s for Boom Clay, i.e. a poorly indurated clay (Levasseur et al., 2021).

Atmospheric carbonation of the concrete segments from the intrados towards the extrados is expected but the small porosity and the engineered water tightness of the concrete segments prevents carbonation. Carbonation of well-engineered buildings at the surface exposed to the atmosphere for more than 100 years have measured carbonation depths smaller than 1 cm (Mallinson and Davies, 1987). This carbonation depth is very small. Above all, carbonation may not necessarily be a problem for the performance of unreinforced concrete. Spallation of concrete from reinforced concrete can occur especially if sufficient ingress of oxygen takes place for aerobic corrosion of the rebars.

The thermal impact on the damaged zone in poorly indurated (and indurated clays) has been investigated in the 6th framework programme TiMoDaz. There will be an increase in temperature in the host rock due to the conduction of the emitted heat by HLW for the HLW disposal cells. This 6th framework programme provided the evidence that the thermal-induced plasticity, swelling and creep of clay are likely beneficial for the sealing of fractures and recovery of the permeability of the EDZ to the original state of the clay host rock (Li et al., 2010).

2.1.3.3 Indurated clay

2.1.3.3.1 Construction

Road headers and tunnel boring machines are used to construct the excavation rooms in indurated clay. The lining does not need to be applied immediately. The virgin vertical hydraulic conductivity for indurated clay can be more than 10 times smaller than in poorly indurated clays, for example 1×10^{-13} m/s for Callovo-Oxfordian clay and 10^{-14} m/s for Opalinus Clay (Levasseur et al., 2021). The excavation has a higher impact on the transport properties of indurated clay surrounding the lining than for poorly indurated clay. The fractures generated in clay host rocks are believed to have an atmospheric pressure immediately after excavation. The driving forces to close these cracks are compressive load or confining pressure and access to water. The smectite content of indurated clays can be less than 2 wt% (see Appendix C). The dominant process for closure of fractures is cementation, i.e. precipitation of minerals (self-sealing). This precipitated phase has a smaller tensile strength than the surrounding restored clay host rock. The closure of cracks can be measured as the increase in pore water pressure; equilibrium is achieved when the formation pressure is achieved (Alcolea et al., 2014). The EDZ is characterised in clay host rocks as a zone with a larger porosity and permeability than the virgin host rock. The values for hydraulic conductivity or permeability are largest near the interface between concrete and clay. These values asymptotically decrease as a function of the radial distance till the values measured for the virgin host rock after about 6 metres from this interface.

2.1.3.3.2 Operation

The necessary ventilation in the operational phase may have an impact on the clay host rock at the start of the post-closure phase. The lining of a facility built in indurated clay decreases further drying by ventilation; the associated formation of drying shrinkage cracks of this clay host rock is limited but the porosity of the shotcrete is larger than that of clay, so further drying cannot be prevented. The formation pressure is therefore expected to be achieved in the post-closure phase and not in the operational phase. After recovery of the formation pressure, the modelled variation in hydraulic conductivity has decreased by less than 2 orders in magnitude (Alcolea et al., 2014).

After the concrete of the lining has been hardened (in the case of a lining made with in-situ curing), the clay may be too dry for dissolved species in the clay pore water to enter the lining in the operational phase. Any chemical alteration of the lining before emplacement of the waste is expected to be mainly caused by ingress of carbon dioxide from the ventilation air.

2.2 Phenomenological description of processes at interfaces

The long-term safety of the geological disposal of radioactive wastes is based on a multi-barrier concept combining man-made engineered barriers (such as waste form, waste canister, backfill and sealing materials) with a suitable geological barrier (i.e., the host rock). The prediction of the evolution of the waste matrices, the waste canisters and overpacks, the engineered barriers (e.g., bentonite or cementitious backfill) with time in response to physical and chemical perturbations is an important aspect with respect to the performance and long-term safety of a repository. The introduction of "foreign materials" such as borosilicate glasses, metallic canisters, and cementitious materials will induce chemical gradients across the repository components, which can induce perturbations such as pH and redox changes, or changes in mineralogy and microstructure that may alter the performance of the barriers over time (e.g., NAGRA, 2002). Dissolution and precipitation processes occurring in this context can be associated with modification of porosity and pore architecture, thus affecting permeability and diffusivity of porous media and consequently transport of solutes or transfer of gases. Predicting the interactions between the different materials entails understanding and evaluating the pertinent coupled thermal, hydraulical, mechanical, and (radio and/or bio)geochemical processes. A number of studies on deep geological disposal of nuclear wastes showed that chemical and physical interactions will be focused on interfaces between the different barrier materials, due to the prevailing chemical gradients (e.g., Claret et al., 2018;, Bildstein et al., 2019). In this context, the nature and the extent of the alteration within the different materials, the progress of the perturbations with time and the evolution of the material properties are essential to evaluate the impact on the overall performance of the disposal system.

Within ACED, we start from the knowledge available at the scale of interfaces between two materials in order to build models for assessing the chemical evolution at the cell disposal scale. This section describes the state-of-the-art on the phenomenological chemical processes occurring at the interface between two materials for the combinations relevant for European repository concepts (cf. section 2.1; see also Neeft et al., 2019). For each interface, a short description of the phenomenology is given together with references to studies that give evidence for these processes. A comprehensive and structured overview of existing information and data on relevant processes occurring at the interfaces, including natural/archaeological analogues that may provide insight/data for long-term processes relevant to the chemical evolution of the disposal cells, as well as on conceptual and numerical models used to describe the processes at the interfaces has been compiled in Deissmann et al. (2021).

2.2.1 Interface "glass – steel

This interface is related in particular to the disposal of vitrified HLW and has been investigated in the context of the disposal concepts of countries where spent nuclear fuels have been or are reprocessed, as, e.g., in France, Belgium, Russia, Japan, Germany, the Netherlands, the UK or the USA (Gin et al. 2013). The glasses developed for this purpose (i.e., in particular borosilicate glasses) are contained in stainless steel canisters, which are placed usually in carbon steel overpacks prior to disposal (cf. section 2.1.1). However, it should be noted that in recent years some preliminary studies conducted, e.g., within the frame of the European collaborative project THERAMIN, investigated also vitrification of ILW (e.g., Scourfield et al., 2020; Clarke et al., 2020), where the treated product may also be packed in steel containers.

The physico-chemical interactions at the glass-steel interface will start once the overpack and the canister are breached due to corrosion and/or lithostatic pressure and water can enter the canister. Thus, besides metallic iron/steel, corrosion products from the metal containers will also be present as surrounding materials close to the glass-steel interface. Corrosion products formed during anaerobic corrosion of low-alloy steel disposal containers are mainly composed of iron oxides such as magnetite (Fe_3O_4), or iron carbonates such as siderite ($FeCO_3$) or chukanovite ($Fe_2(OH)_2CO_3$) (e.g., Honda et al., 1991; Taniguchi et al., 2004). Localised variations in pH and in concentrations of carbonates may favour the formation of the one or other corrosion products (Michelin et al., 2015). In some cases, FeIII oxy-

hydroxides were detected; they may have formed during the initial period of the corrosion test with remaining traces of oxygen. Iron corrosion products formed in situ in the presence of claystone are typically iron silicates and carbonates and, more rarely, iron sulphides (De Combarieu et al., 2007; Schlegel et al., 2014, 2016).

A distinction needs to be made with respect to corrosion products formed in a first phase, in which the steel container or overpack corrodes in the groundwater until its failure, where the corrosion products formed are characteristic of corrosion in the host rock medium and some residual metallic iron remains in the system. In a subsequent phase, the disposal container continues to corrode in parallel to the alteration of the glass, i.e., the nature of the corrosion products forming may then be influenced by the solution chemistry at the glass/iron interface, including elements released by the glass.

The alteration and dissolution of nuclear waste glass in contact with water is controlled by several inter-related processes at the glass surface. Based on extensive studies on the dissolution of nuclear waste glasses and in particular simulated HLW borosilicate glasses, a general picture on the typical dissolution behaviour of HLW borosilicate glasses under conditions representative for geological disposal environments has been established (Figure 2-9, cf. van Iseghem et al., 2006; Gin et al., 2013; Gin, 2014).

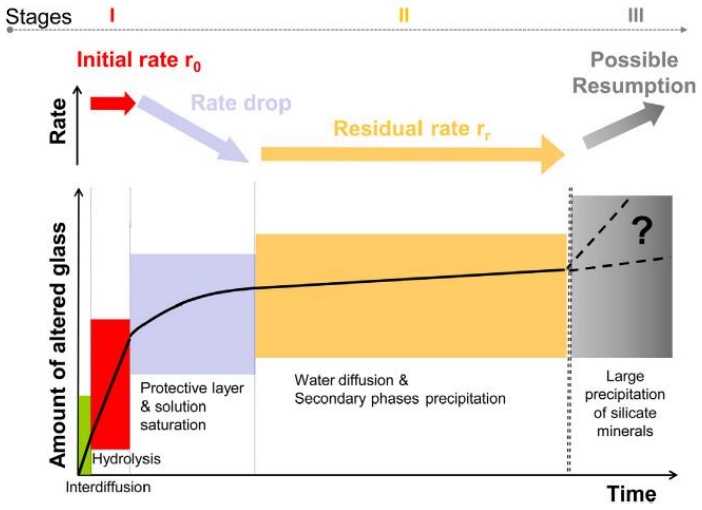

Figure 2-9: Stages of nuclear glass corrosion and related potential rate-limiting mechanisms (Gin et al., 2013).

Understanding the glass/steel interactions and their consequences on the long-term behaviour of nuclear waste glasses requires knowledge regarding the main processes controlling the aqueous alteration of glass. According to Vienna (2013) and Gin et al. (2015), glass alteration is due to the formation and dissolution of an alteration film layer, which is likely to incorporate chemical elements from the solution and acts as a diffusion barrier for reactive species. The effectivity of this barrier depends primarily on the concentration of silicon in solution in the vicinity of the glass, with glass dissolution rates increasing when the saturation state of the aqueous medium with respect to silica decreases. Other parameters affecting the glass alteration and its rate are (local) solution pH and solution composition, since some elements may stabilise (e.g., calcium (Paul, 1977; Gin et al., 2012)) or destabilise (e.g., magnesium (Aréna et al., 2016)) the hydrated glass layer.

Generally, the presence of iron and iron corrosion products has been found to increase glass alteration by maintaining high alteration rates over longer periods than in the same leaching solution without iron or corrosion products (cf. Martin, 2021). However, this impact is only perceptible at local scale, and seems to be significantly attenuated as the distance between glass and the iron source increases. There are four possible mechanisms that are discussed in literature to explain the increase in glass alteration rates due to the presence of iron or iron corrosion products (Rébiscoul et al., 2015):

- silicon sorption at surface sites of corrosion products, or silica precipitation at the iron source;
- formation of iron silicates;
- retention of iron in the gel layer, which could modify its structure and its protective properties;
- increase in pH due to iron corrosion.

The first two mechanisms both lead to the consumption of cross-linking elements, in particular silicon, leading to either (i) a depletion of the concentration of silicon in solution, which increases glass dissolution rates, or (ii) the formation of a gel depleted in silicon which is, therefore, less protective (cf. Lemmens, 2001). These effects both hinder the formation of a protective layer, delaying saturation of the aqueous solution needed for its formation. In the first case, the effect works by making the initial rate phase (r_0) last longer, and, in the second case, by slowing down the rate drop (cf. Figure 2-9).

2.2.1.1 Sorption of silicon on corrosion products

The sorption of species like silicon produced by glass alteration on steel corrosion products close to the glass/steel interface can delay the beginning of a rate drop. This effect has been demonstrated in the presence of steel corrosion products such as magnetite (Grambow, 1987; Grambow et al., 1987; Bart et al., 1987), goethite (Bart et al., 1987; Grambow ,1987; Grambow et al., 1987), and siderite (Michelin et al. 2013a). Since the number of surface sites on the corrosion products available for sorption is finite, the effect of silicon sorption on glass alteration lasts for a period that is proportional to the sorption capacity of the corrosion products. The higher the sorption capacity of the corrosion products, which is dependent on their amounts and their specific surface, the longer it takes to reach silicon saturation in solution, which in consequence delays the rate drop. However, the results from different glass alteration experiments carried out in the presence of corrosion products seems to indicate that the sorption of silicon to corrosion products does not prevent a slowing of the alteration rate over time. Studies on silicon sorption on steel corrosion products (magnetite, siderite, goethite) indicate (i) that the maximum sorption occurs at pH values between 6 and 9 and decreases, both under more acidic and alkaline conditions, and (ii) that silicon sorption by steel corrosion products will be maintained for a relative short period of time compared to the time scales relevant for geological disposal (Philippini et al., 2006, 2007).

2.2.1.2 Precipitation of iron silicates

Sorption of silicon on corrosion products alone seems not to be sufficient to explain the quantities of altered glass in experimental tests since even after saturation of the sorption sites, glass alteration rates in the presence of steel and corrosion products remained higher than the residual rate (r_r) observed in the absence of steel and corrosion products over longer periods. Thus, other mechanisms such as the formation of silicates may prolong the consumption of silicon in the longer-term. Most studies performed in this context suggest the formation of various ferrosilicates (e.g., Grambow, 1987; Grambow et al., 1987; Werme et al., 1990; McVay and Buckwalter, 1983; Shade et al., 1983; Shanggeng et al., 1995; Kim et al., 1997; Björner et al., 1989; Godon et al., 2013; Michelin et al., 2013a; Dillmann et al., 2016), sometimes in nano-colloidal form. The precipitates formed may incorporate other elements in addition to iron, such as magnesium, aluminium, sodium and calcium (e.g., Burger et al., 2013). The silicates formed in this context may include trioctahedral serpentines (e.g., greenalite, berthierine, cronstedite), trioctahedral smectites (e.g., hectorite, saponite) or dioctahedral smectites (e.g., nontronite). The (Fe+Mg)/Si ratio of the silicates formed can vary, especially depending on the distance from the iron source. Moreover, the nature of the precipitated silicates highly depends (i) on temperature (e.g., favouring the formation of serpentines at higher temperature), and (ii) on local pH, since iron/magnesium silicates can only be precipitated above a certain pH, which is a function of the silicon activity imposed by glass alteration.

Experimental observations indicate that the formation of ferrosilicates is limited in the presence of steel corrosion products alone (e.g., Björner et al., 1989) but significantly higher in the presence of metallic iron in which iron silicates may form from the start of alteration. Therefore, the formation of corrosion products in situ at the same time as glass alteration seems to modify the predominant mechanisms and causes more precipitation of secondary silicate phases. This may be explained by a more or less significant iron flux induced by iron corrosion or the solubility of the corrosion products (Dillmann et al., 2016). The formation of iron silicates correlates to more extensive glass alteration; these ferrosilicates thus have the same effect on glass alteration as other secondary phases, such as zeolites, which consume silicon and inhibit the effects of solution saturation, except that in this case their formation is conditioned by the flux of iron released by the corroding steel. Thus, the formation of ferrosilicates and their impact on glass alteration depends on the quantity of metallic iron remaining, its corrosion rate, and on the solubility of iron in solution.

2.2.1.3 The influence of iron on the morphology and structure of the gel layer

The interactions between silicon and steel corrosion products, playing the role of "silicon sink", could be detrimental to the protective properties of the gel layer on the glass surface. During glass alteration in the presence of corroding iron or iron corrosion products, a large quantity of iron is dissolved, from the first stage of hydrolysis at r_0 (Figure 2-9). In this case, the gel layer on the glass becomes depleted in silicon (relative to pristine glass) and enriched in iron (Rébiscoul et al., 2015; Reiser et al., 2017; De Echave et al., 2019), though, according to Reiser et al. (2017), this enrichment may only affect parts of the gel layer. De Combarieu et al. (2011) suggested that the increased alteration of glass in the presence of iron is due to a higher porosity of the (iron-enriched) gel layer, depleted in cross-linking elements (e.g., silicon, aluminium, etc.), thus reducing its protective nature. Dillmann et al., (2016) related the iron enrichment of the gel formed during glass alteration in the presence of iron or corrosion products to the presence of structural nano-crystals similar to greenalite ($Fe_{2\text{-}3}Si_2O_5(OH)_4$), possibly precipitated due to the highly porous structure of the amorphous gel layer (cf. Burger et al., 2013). The impact that these nano-crystalline phases may have on the properties of the gel has not yet been clearly assessed. The presence of iron changes the equilibrium between the glass and the solution and alters the stoichiometry of the gel. Furthermore, the iron precipitating in the form of ferrosilicates may influence the depolymerisation of the silicate network. Burger et al. (2013) suggest a possible clogging of porosity and, as a result, a decrease in the diffusion coefficient of the reactive species.

2.2.1.4 Impact of iron corrosion on pH

In addition to the consumption of silicon, iron corrosion also affects the pH of the solution. The corrosion of metallic iron and the formation of corrosion products occurring at the same time as glass alteration, tends to raise the pH (Bildstein et al., 2007), thereby favouring glass alteration (e.g., Corkhill et al., 2013, Utton et al., 2012, 2013) and the formation of magnesium silicates, which, concomitantly affects glass alteration due to consumption of silicon. The pH values during glass alteration in aqueous media in the absence of corroding iron (i.e., governed by the presence of the glass) are generally neutral to slightly alkaline (e.g., between 7.5 and 8.7 in clay water) have been found to increase up to 9.7 in the presence of metallic iron (cf. Martin, 2021). This increase in the pH is due to the formation of hydroxyl ions (OH^-) during anoxic corrosion of iron in an aqueous medium according to:

$$Fe + 2H_2O \rightarrow 2OH^- + H_2 + Fe^{2+}$$

Moreover, also in the presence of corrosion products like magnetite the solution pH during glass alteration was found to be higher than in leaching tests on glass alone (Rébiscoul et al., 2015). Here, the increase in pH is the result of a larger quantity of altered glass, i.e., of a higher quantity of alkaline species (e.g., Ca, Na) being released into solution.

2.2.1.5 Concluding perspective

The physico-chemical interactions at or close to the interface glass/steel lead generally to an increase in glass alteration rates compared to the absence of metallic iron and/or corrosion products. The main phenomenon related to this is the consumption of silicon delaying the formation of a passivating gel. This impact on glass alteration is conditioned by the geometry of the system and the transport and fluxes of dissolve iron and silicon in solution and seems to be significantly weaker when the glass is far from the iron source (e.g., corrosion products or metallic iron). Assessing the processes at the interface on glass alteration requires an understanding of the nature of the corrosion products, their position in relation to the glass, and the transport conditions within the system investigated, bearing in mind the influence of physical and chemical conditions (properties of the host rock, composition of the porewater, redox conditions, pH) and hydrodynamics on glass alteration processes. Glass/iron interactions occur as a result of very localised conditions which depend on the dissolution rates of iron and glass, and on the transport of different elements in solution. In spite of the importance of understanding the coupling of transport processes and geochemical reactions in the evaluation of interactions occurring at the glass/steel interface with respect to nuclear waste disposal, coupled reactive transport simulations addressing this glass/steel/(clay) interactions are scarce to date (cf. Bildstein et al., 2007, 2012, 2019; Claret et al., 2018).

2.2.2 Interface “steel – concrete”

An interface between steel and cement-based materials is present in many disposal concepts for geological disposal of radioactive wastes in Europe (cf. chapter 2.1 and Neeft et al., 2019). The interface between steel and cementitious materials may occur at different locations and with different functions/roles. In some disposal systems, reinforced concrete is used with carbon steel, for example for the container of ILW waste packages. In this case, the carbon steel / concrete interface is typically located at a few centimetres from the boundary of the concrete component. In some HLW disposal concepts, carbon steel is used as overpack of the vitrified waste package. In some countries like Belgium and the Netherlands, a cement-based buffer is placed around the carbon steel overpack to ensure high pH conditions and thus lower corrosion rates for a long period of time (so-called supercontainer concept, e.g., Bel et al., 2006). Here, the concrete cover is typically several decimetres thick. In the management of ILW, waste packages may contain also stainless steel or waste canisters are made of stainless steel (e.g., CSD-C canisters). The latter are often immobilized inside a concrete or steel container with cement-based materials such as mortar or grouts. In the following sections, the focus is on the interface between carbon steel and cementitious materials, since these interfaces are more relevant for the long-term performance and safety of the disposal cells. There exists a significant amount of literature of processes at the steel-concrete interface under aerobic conditions, which is relevant for many civil structures. However, most of the discussion here is limited to anoxic conditions, as the oxic period in a geological disposal facility, even if it lasts several hundreds of years, will most probably occur under conditions of high pH (buffered by the cementitious material) with low passive steel corrosion rates.

2.2.2.1 Steel corrosion in anoxic cementitious environments

In a deep geological repository in saturated conditions, oxygen is assumed to be depleted relatively quickly, so that anoxic conditions will be established soon after repository backfilling and closure. Oxic conditions then mainly prevail during the operational phase and when the disposal cell is not completely saturated. However, many different processes in an ILW or HLW disposal cell compete for oxygen (corrosion, oxidation of minerals, microbial respiration). In addition, the steel interface is embedded in mortar or concrete materials (reinforced concrete in HLW and ILW disposal cells, overpack in HLW disposal cells, waste containers and waste in ILW disposal cells) which pose diffusion-limited oxygen availability at the interface and induce a passivating protective layer at the steel-concrete interface (e.g., Smart et al., 2019). In addition, also the cement used to produce the mortar or concrete can contribute

to an anoxic environment. Concrete made from pure OPC cement or OPC cement blended with micro silica are slightly oxidizing since they lack redox sensitive species. Blended cements can contain fly ash, which is a by-product from coal-firing power plants or blast furnace slag, which is a by-product from steel production, besides OPC. In the first case, the concrete also lacks redox sensitive species and is therefore slightly oxidising. However, the second case, the concrete contains pyrite and is therefore reducing after fabrication.

Several studies show that the formation of a passivating film on the steel occurs relatively fast (L'Hostis et al., 2001; Chomat et al., 2017). For a HLW disposal cell, a transition phase is sometimes thought to exist due radiolysis of water producing, inter alia, hydrogen, oxygen, hydrogen peroxide and reactive radicals, which might temporarily sustain relatively constant, mildly oxidising conditions (Kursten et al., 2011) although some experiments indicated a decrease in redox potential under gamma irradiation (Smart et al., 2019).

Oxic corrosion of iron is described by the following global reaction:

$4Fe + 6\ H_2O + 3O_2 \rightarrow Fe^{3+} + 12\ OH^-$

Corrosion products under oxic conditions are for example goethite (alpha-FeOOH), ferrihydrite ($Fe(OH)_3$) and lepidocrocite (gamma-FeOOH) (L'Hostis et al., 2011). Anaerobic corrosion of iron is associated with the generation of hydrogen through the following global reaction:

$Fe + 2\ H_2O \rightarrow Fe(OH)_2 + H_2$

or, if the Schikorr reaction occurs, by the reaction:

$3\ Fe + 4\ H_2O \rightarrow Fe_3O_4 + 4\ H_2$

The rate of hydrogen generation can be monitored and is often used in experimental programmes to estimate corrosion rate assuming either iron(II)hydroxide (1 mol hydrogen generated per mol iron corroded) or magnetite (1.33 mol hydrogen per mol iron) as main corrosion product. Under anoxic conditions, corrosion products as magnetite (Fe_3O_4) and hematite (Fe_2O_3) are formed (L'Hostis et al., 2011).

Corrosion processes may be subdivided into a uniform passive corrosion mechanism and localised corrosion mechanisms (e.g., pitting corrosion, crevice corrosion, and stress corrosion cracking). In a concrete-based geological disposal concept, the followed strategy is usually to demonstrate that localised corrosion phenomena cannot occur in highly alkaline disposal conditions. Therefore, the focus of the experimental studies with respect to this interface is on rate measurements of uniform passive corrosion through different methods and techniques (for details see Kursten et al., 2021). Thus, for the interface between carbon steel and cementitious materials, mainly uniform corrosion processes and coupled processes are relevant, so that in geological disposal conditions, the main corrosion process would be passive corrosion of steel/iron in anoxic, alkaline conditions. Due to the formation of a passivating oxide film on the steel surface in these conditions, the measured initial corrosion rates (up to some tens of µm yr^{-1}) decrease over time towards constant (steady state) and very low values. Long-term corrosion rates (exposure times > 365 days) in the range of 0.1 µm yr^{-1} or lower have been reported for temperatures up to 80 °C in chloride-free solutions with a pH between 11.8 and 13.5 (cf. compilation in Kursten et al., 2021).

However, depending on the steel type and the evolution of the environment, the corrosion processes can be influenced by several factors such as temperature, degree of water saturation, radiation gradients, the composition of the near-field water with respect to pH and the content of potentially aggressive species (e.g., chloride, sulphate, thiosulphate), and the presence of microbial activity. The steel corrosion products may take a volume that is larger than the bare material, leading in turn to stress and (local) alteration of the pore structure at the interface and consequently to changes in transport properties. Spallation of concrete has so far only been observed for oxic corrosion of steel. The volume of bare material is reduced if the corrosion rate equals the iron dissolution rate from the corrosion product as measured for anoxic corrosion of (stainless) steel in the FP7 CAST project (Mibus et al., 2018). The

thickness of the layer of corrosion products does not increase in such a case by which the induced stress in concrete is too limited to cause fractures. The corrosion process is bounded to equilibrium between diffusion of water through the oxide layer and dissolution at the solid-liquid interface.

2.2.2.2 Factors influencing corrosion rates

Temperature can play an important role in the corrosion of steel in concrete in many different ways because all processes and many parameters involved can be influenced by changes in temperature, such as:

- kinetic parameters of the corrosion reaction;
- rate of diffusion of O_2 and aggressive ions into the concrete;
- solubility of oxygen;
- pore solution chemistry of concrete.

The corrosion of steel reinforcement is an electrochemical reaction; its rate can be greatly affected by temperature. Generally, the (initial) corrosion rate increases significantly as temperature increases (e.g., Smart et al., 2004; Fujisawa et al., 1997; Fujisawa et al., 1999; for details see also Kursten et al., 2021). On the other hand, the solubility of oxygen in water is known to decrease with increasing temperature, which results in a significant decrease of the concentration of dissolved oxygen as reactant for the process of steel corrosion, thereby lowering the corrosion rate (Davis, 2000; Živica, 2002). However, this effect might be more relevant under oxic conditions. Other physicochemical properties affected by temperature are the viscosity and the conductivity of the concrete pore solution. The viscosity will decrease with increasing temperature, which will aid oxygen diffusion. Ionic mobility will also increase with temperature, increasing the overall conductivity of the electrolyte. Moreover, the chloride binding capacity of cementitious materials can be reduced at elevated temperatures, leading to an increase in chloride concentrations of the pore water of the cementitious material (Hussain and Rasheeduzaffar, 1993; Hussain et al., 1996; Maslehuddin, 1994; Maslehuddin et al., 1996), which has been attributed to the decomposition of Friedel's salt (i.e., a chloride containing AFm phase) at elevated temperatures. However, data on long term (i.e., > 365 days) corrosion rates for carbon steel in anoxic alkaline environments for different temperatures reported in the literature show that at the later stages of the corrosion process (i.e., when steady state conditions prevail), temperature no longer has an effect on the uniform corrosion rate (Kursten et al., 2021).

Corrosion of steel in concrete strongly depends on the moisture condition of the concrete. This is due to the fact that moisture affects both the resistivity of the concrete and the diffusion rate of oxygen. In dry concrete, which is characterized by a high resistivity, oxygen diffusion can take place unhindered. The resistivity in water saturated concrete is low but, on the other hand, the diffusion rate of oxygen is slow compared to the diffusion rate in dry concrete. This means that the corrosion rate is slow and that the corrosion is under diffusion control (Bertolini et al., 2004). According to Tuutti (1982) steel corrosion rates in concrete reach a maximum for a moisture content equivalent to the equilibrium with a relative atmospheric humidity of about 95%; moving away from these values of humidity in either direction, the corrosion rate decreases (Bertolini et al., 2004). On the other hand, ionic mobility will increase with increasing saturation degree, thereby facilitating transport of aggressive species (e.g., chlorides) towards the overpack surface. However, Michel et al. (2013) showed that when steel in concrete is in a passive state, the corrosion rate is not affected by the moisture conditions of the concrete.

The pH of the pore solution in cementitious material has a distinct effect on the corrosion of steel at the interface, since the protective oxide film is believed to remain stable only as long as the pH stays higher than a threshold value (~9 < pH < ~11.5). If the pH should drop below this threshold value (e.g., due to leaching of alkalis and complete removal of portlandite from the cementitious material in the long-term, cf. section 2.6), depassivation of the steel surface can take place and the protection is lost, leading in turn to an increase in the rates of uniform corrosion. Moreover, a decrease in pH can also increase the susceptibility to localized corrosion, though this effect is coupled to the exceedance of a threshold

concentration of chloride ions in the pore water. Although this assumption has been generally accepted, there is little agreement concerning the quantitative function relating the two (cf. Kursten et al., 2021).

The corrosion rates of (carbon) steel can be distinctively enhanced due to the presence of aggressive species, in particular chloride ions, in the contacting solution. A huge amount of information is available in the literature on the effect of chloride on the corrosion rates of carbon steel in concrete under aerobic conditions (e.g., Goñi and Andrade, 1990; Deshpande et al., 2000; Zhang et al., 2009), where a general trend of increasing corrosion rates with increasing chloride concentration could be observed. Studies on the effect of the chloride concentration on carbon steel corrosion under anoxic and highly alkaline conditions have been performed in particular within the context of various national nuclear waste management programmes (e.g., L'Hostis et al., 2011; Smart et al., 2004; Smart, 2009; Fujiwara et al., 2001; Mihara et al., 2002). Corrosion rate data reported in the literature for mild steel in anoxic and alkaline solutions containing elevated chloride concentrations indicate that the measured (initial) corrosion rates decrease with increasing exposure time even in the presence of chloride ions. From comparison with data obtained in chloride-free solutions, it can be concluded that the presence of chloride (up to 20,000 mg L^{-1}) has no discernible effect on the long-term corrosion rate of carbon steel in anaerobic high pH media (Kursten et al., 2021). However, it is important to note that high chloride concentrations, combined with the potential risk of the passive film being destroyed locally, may result in a significant increased susceptibility to localized corrosion phenomena such as pitting corrosion, crevice corrosion, and/or stress corrosion cracking.

2.2.2.3 Consequences of steel corrosion on concrete properties

During the corrosion of steel embedded in a concrete structure, a layer of corrosion products is formed on the surface of the steel. The volume of these corrosion products can be much larger than that of the initial bare metal (e.g., McCafferty 2010; Broomfield, 2007; Caré et al., 2008). The corrosion products will first fill the available pore space near the interface, which depends on the chemical state of the concrete and the process that initiated the faster corrosion. With the ingress of aggressive species, initiation of active corrosion may occur without significantly changing the microstructural properties of the concrete and thus the available pore space is close to the initial porosity of the concrete. However, when active corrosion occurs as a consequence of a pH decrease due to chemical degradation of concrete, the available pore space might be smaller or larger depending whether carbonation (resulting typically in a porosity decrease) or decalcification, i.e. dissolution of portlandite and incongruent dissolution of C-S-H (resulting typically in a porosity increase) is the dominant degradation process (cf. section 2.2.6 and, e.g., Glasser et al. (2008) for a description of these processes). After filling of the available pore space, the corrosion products will gradually increase the mechanical stress in the concrete. Fracture formation is initiated when the mechanical stress exceeds the tensile strength (Höglund, 2014) but the time for the first appearance of fractures depends on different factors such as thickness of concrete cover, quality and strength of the concrete, and corrosion rate (Andrade et al,. 2011). Note that creep of concrete can accommodate partly the effects caused by the corrosion products retarding to a given extent the initiation of fracture formation. Also, the anoxic corrosion rate can become equal to the iron dissolution rate from corrosion products. At that stage, there is no longer a volume increase.

The aerobic corrosion rate can be so fast that there is a volume increase. The fractures initiated by the corrosion products may influence the geochemical evolution of the concrete near the interface, especially when they are penetrating from the steel/concrete interface to the outside boundary of the concrete (e.g., an interface with host rock)). From these fractures, alteration fronts may develop within the concrete matrix and potentially creating larger regions of degraded concrete. Degradation fronts in fracture-matrix concrete systems can be described with approximated analytical models (e.g., Höglund, 2014), or with coupled reactive transport models (e.g., Perko et al., 2010; Perko et al., 2015).

Studies performed by L'Hostis et al. (2011) and Chomat et al. (2014, 2017) revealed the formation of an Fe-enriched layer in the cementitious material close to the interface. In this region Fe interacts with the

cement hydration phases and may form Fe-containing hydration phases. In addition, the cementitious material may also alter the composition of the corrosion product layer with an enrichment of calcium closer to the interface of the corrosion product layer and the cement/concrete (cf. L'Hostis et al., 2011).

2.2.2.4 Concluding perspective

Under the anoxic conditions prevailing in a geological disposal facility in the long-term, the corrosion of steel in a highly alkaline, cementitious environment is governed by passive uniform corrosion due to the formation of a passivating oxide film, leading to very low corrosion rates. Thus, in a concrete-based geological disposal concept, one focus is on the demonstration that localised corrosion phenomena cannot occur in the highly alkaline disposal conditions. Corrosion products, that have a higher molar volume than that of the metal, may reduce porosity, leading to clogging and gradually increase the mechanical stress in the concrete and may lead to fracture formation. However, the thickness of the corrosion layer is not increased over time when the corrosion rate is equal to the dissolution rate of iron from corrosion products. Furthermore, there are indications that a Fe-enriched layer will form in the cementitious material close to the interface, leading eventually to the formation of Fe-containing cement hydration phases.

Existing thermodynamic modelling studies of the solution chemistry in the context of iron/steel corrosion (e.g., calculating saturation indices of ferrous and ferric minerals), focus so far mainly either on steel corrosion in alkaline conditions (with a substantial knowledge base on reinforcement corrosion in concrete structures) or on corrosion in anoxic environments. However, only few examples have been found for thermodynamic modelling related to iron/steel corrosion in both anoxic and alkaline conditions, i.e., relevant for the disposal environment (e.g., Ma et al., 2018; Furcas et al., 2022).

Although a number of experimental studies on iron corrosion in concrete have been performed in the context of nuclear waste disposal, no reactive transport modelling studies addressing the interface steel/concrete in the context of a deep geological repository are available so far (cf. Bildstein et al., 2019). However, similar tools as for other interfaces, in particular the steel/clay interface might be used. Since electrochemical models for corrosion (e.g., Bataillon et al., 2010; Macdonald et al. 2011) are a pivotal issue of this problematic, the coupling of such models to reactive transport models could result in significant advances in modelling the steel/concrete interface (cf. Bildstein et al., 2019).

2.2.3 Interface "steel – clay"

Carbon steel canisters have been proposed for the storage and disposal of high-level radioactive wastes (HLRW) in deep geological repositories (DGR) in countries like Switzerland, France, Belgium, Germany, United Kingdom, Czech Republic, and Spain (cf. Neeft et al., 2019). The host rock and the design of the repository differ in each country but in many cases the canister will be in contact with compacted bentonite blocks or pellets. The main perturbations at the steel – clay/bentonite interface are canister failure due to corrosion and the interaction of corrosion products with the bentonite/clay, which could potentially result in the formation of new iron-rich minerals that alter some of its basic properties, such as hydraulic conductivity, diffusion coefficient and capacity to swell or retain radionuclides.

Canisters are estimated to provide containment for at least 1,000 years, although results from experiments, analogues and models indicate that failure is unlikely in less than 10,000 years. It depends, among others, of its thickness and chemical reliability. This section has to do with what it is known so far on the evolution of the DGR environment (thermal, hydraulic and/or chemical gradients - redox, pH and dissolved species - from the initial post-closure stage until the system reaches equilibrium) and its impact on the chemical evolution of the steel/iron-bentonite interface.

There are a number of papers about the corrosion of metals that provide results coming from laboratory experiments under a variety of conditions (e.g., Marsh et al., 1987, 1989; Gdowski and Bullen, 1988;

Blackwood et al., 2002; Azcárate et al., 2004; Kursten et al., 2004a,b; King 2008, 2014; Necib et al., 2016, 2017a,b). Padovani et al., (2017) made an analysis of the expected corrosion behaviour of candidate container materials and future R&D work. Results of corrosion rates and products obtained from the study of archaeological objects can be found in Qin et al. (2004), Smart and Adams (2006), Neff et al. (2006, 2010), Yoshikawa et al. (2008) and Michelin et al. (2013b), amongst others.

The interaction of corrosion products with bentonite has been reviewed in Marcos (2003), Landolt et al. (2009), Bradbury et al. (2014), Wilson et al. (2015) and Wilson (2017), among others. There are also various papers and reports from European projects NF-PRO, PEBS, TBT, and activities in underground research laboratories (e.g. FEBEX experiments at Mt. Terri) presenting the results from both laboratory and in situ experiments in URLs designed to advance in the understanding of iron-bentonite (and clay rock) interaction (e.g., Guillaume et al., 2004; Charpentier et al., 2006; Wilson et al., 2006a, b; Carlson et al., 2007; Hunter et al., 2007; Smart et al., 2008a; Milodowski et al., 2009; Fukushi et al., 2010; Osaky et al., 2010; 2013; Torres, 2011; Lanson et al., 2012; Schlegel et al., 2014, 2016; Torres et al., 2014; Cuevas et al., 2016; Wersin and Kober, 2017; Hadi et al., 2019). Some authors focused on the study of natural analogues from which obtaining information about influence of iron on the transformation of bentonite to iron-rich clays (e.g., Smart and Adams 2006; Pelayo et al. 2011).

The changing environmental conditions during the life of the repository influence the corrosion processes and products, the interaction of corrosion products with bentonite and finally, the integrity of both, the steel/iron and the bentonite. In the following, two phases are distinguished: i) a first phase with initially aerobic conditions at elevated temperatures (> 90 ºC) before repository closure, including a transient phase with progressively anaerobic conditions, encompassing a time scale of in total about 100 years, and ii) a second (long-term) phase with anaerobic conditions at temperatures < 90 ºC, which will decrease to ambient temperatures with time.

At the initial stages (≈emplacement to 20(50) years) water vapor and dissolved oxygen act as the oxidizing agents. Low steel corrosion rates and general corrosion occur and no changes are expected in the bentonite properties (cf. Turrero et al., 2021).

- Oxidizing conditions will prevail before closure of the repository and in the early post-closure stage. Oxygen trapped in the buffer and backfill materials will be consumed in several ways: corrosion of metallic elements, oxidation of pyrite (both in certain bentonites (e.g., FEBEX) and in host rock (e.g., Opalinus Clay and Callovo-Oxfordian formation). The high initial thermal load imposed by the vitrified HLW will probably impede biofilm formation on the surface of the canisters.
- Following the emplacement, the canister surface will be subjected to temperatures >90 ºC and thermally-induced drying at the canister surface/bentonite interface occurs (dry-out stage). Water activity will be low and under those conditions, low corrosion rates and general corrosion processes occur, which do not endanger the performance of the metallic canister (Turrero et al., 2021).
- Aerobic corrosion under oxidizing/unsaturated conditions can produce multi-layered corrosion products, which in order of proximity to the metal surface can be magnetite/maghemite, hematite, goethite and lepidocrocite. Green rust may form as an intermediate product transforming later into hematite or magnetite. (cf. Torres et al., 2009, 2014; Torres, 2011; Majzlan et al., 2013).
- At this phase, changes in the bentonite properties due to iron/clay interaction are not expected since there is no water to mobilize iron (Torres et al., 2014; Turrero et al., 2021).

During a transient phase to anaerobic conditions (≈ 20(50) to 100 years), temperature and hydration gradients induce an increase in the corrosion rate and localized corrosion. The mineralogy of the bentonite can be altered to non-swelling Fe-rich phyllosilicates.

- In this stage corrosion will occur mainly under unsaturated condition, but as system hydrates relative humidity will increase and a moisture film will form on the metal surface. The temperature at the canister/bentonite interface will be around 90 ºC or higher, which have to be taken into account, as corrosion rate increase with that higher humidity and high temperature. The time leading from aerobic to anaerobic conditions will depend primarily on the (advective-)diffusive transport of

oxygen, either in the gas or liquid phase, in the unsaturated compacted bentonite, and on the corrosion rate of iron and accessory minerals (e.g., pyrite) as well, as corrosion progressively consumes the oxygen of the system.

- The aqueous chemistry at the interface will depend on the interaction between the groundwater (fresh or saline) and the bentonite, which contains salts (e.g., NaCl and $CaSO_4$). At this stage temperature is still high; the saturation of the system progresses and the bentonite at the interface remains unsaturated although relative humidity increases. Under these conditions, geochemical evolution of the bentonite barrier can result in the formation of saline fronts in the vicinity of the canister (e.g., Cuevas et al., 2002), which can affect the corrosion rate and promote localised corrosion (e.g., Druyts et al., 2001; Bradbury et al., 2014). The existence of hygroscopic salts can decrease the value of critical relative humidity (CRH) and significantly enhance corrosion processes at relative humidity quite lower than 100%. Hygroscopic salts sorb moisture and form concentrated brines that promote the electrochemical corrosion of steel and the nucleation of pits on the metal surface leading to localized corrosion. The nucleation time for pits depends on factors such as the oxidizing character of the environment, the concentration of aggressive ions such as chlorides, pH and the alloy composition of the metal. Sulphates could also be relevant in the presence of microorganisms because sulphate reducing bacteria that are primarily responsible for microbial induced corrosion.
- As saturation advances, the chemical composition of bentonite porewater will homogenize along the clay barrier due to diffusion and the generated saline fronts will disappear. When the residual oxygen is consumed other mechanism could be responsible for localized corrosion, for example the reductive dissolution of Fe(III) corrosion products coupled to Fe dissolution of the inner layers (electrochemical corrosion). Once oxygen has been depleted and anaerobic conditions are reached, corrosion will turn general and uniform. Green Rust (GR), a group of mixed Fe(II)/Fe(III) hydroxides will be the prevailing corrosion product in moderately reducing environments and circumneutral pH as those expected in this phase (e.g.; Torres et al., 2007; Turrero et al., 2021).
- As canister corrosion progresses and relative humidity increases alteration in the bentonite mineralogy can occur, in terms of precipitation of iron corrosion products in the surroundings of the interface, destabilization of montmorillonite and replacement by Fe-rich smectites or by non-swelling Fe-rich phyllosilicates (e.g., chlorite, berthierite, cronstedite, serpentine) and cementation due to precipitation of iron corrosion products or of SiO_2 resulting from montmorillonite transformation (e.g. Guillaume et al., 2003, 2004; Wilson et al., 2006a; Charpentier et al., 2006; Mosser-Ruck et al,. 2010; Torres, 2011; Jodin-Caumon et al., 2012).

The radiation fields in the vicinity of the steel/bentonite interface may cause water to decompose into a range of redox-active species which can significantly influence corrosion kinetics. Then, an increase of the corrosion rate of the steel may occur (cf. Kursten et al., 2004b; Padovani et al., 2017). Over a certain dose of γ-radiation (>10-20 Gy h^{-1}) the bentonite properties might be affected as well, mainly decreasing cation sorption capacity, what indeed affect the swelling potential of clay, and inducing changes in the redox reactivity of the material (through changes in the Fe(II)/Fe(III) ratio) (cf. Allard et al., 2012; Holmboe et al., 2012; Lainé et al., 2017). During first stages of the repository life, radiation could also have an impact on the decreasing of microbial activity at the steel-bentonite interface.

After the transient stage (i.e., after about 100 years), conditions are expected to be anaerobic and with decreasing temperatures long-term conditions will be approached. At this stage the chemical environment at the interface between steel and bentonite/clay is anoxic and the pH is close to neutral. The saturation of the clay, decreasing of temperature and reducing conditions will favour uniform corrosion. Anaerobic corrosion of steel will lead to the generation of H_2–gas at this stage. Microbially-mediated corrosion might also occur. However, in compacted bentonite there may be too limited space for microbial activity.

- As time advances, average temperature in the steel surface will decrease at 50 or 60 °C, enhancing saturation and swelling of the bentonite at the contact. As relative humidity increases, canister surface will become uniformly wetted. In this phase, it is foreseen that residual oxygen has totally been depleted and reducing conditions are achieved. Then,

anaerobic corrosion of the steel canister will occur and corrosion will become uniform (Turrero et al., 2021).

- Anaerobic corrosion of steel consumes water and involves the generation of gas (H_2) (see section 2.2.2). Hydrogen produced could alter physical properties of the bentonite (e.g., formation of microfractures or preferential pathways). However, the expected corrosion rates will be extremely low. Therefore, gas generation is expected to be low as well. Hydrogen pressure is unlikely to exceed the breakthrough pressure of compacted bentonite. In the case of exceeding it, microfractures can be formed. However, bentonite is expected to be able to self-seal these fractures under saturated conditions.
- Microbial activity, in particular sulphate reducing bacteria may be important during this period by modulating redox conditions and transformation of iron phases (e.g., Smart et al., 2017b); However, temperature, low porosity and swelling pressure of saturated bentonite is expected to act as a protective film against microbially-influenced corrosion (MIC) (e.g., Stroes-Gascoyne et al., 2007, 2010).
- Corrosion rates will be below 10 µm yr^{-1} and corrosion products will be largely tied to site-specific conditions (e.g., Kursten et al., 2004a; Smart et al., 2017a). Magnetite, siderite and iron sulphides will be mainly formed, depending on the clay and the chemistry of solution (e.g., carbonate, chloride and sulphide concentration), pH and redox potential (e.g., Wersin et al., 2003; Smart et al., 2004; Torres et al., 2007; Necib et al., 2019). Green rust may occur as a metastable intermediate phase.
- Sorption sites on the clay can be filled by ferrous ions (e.g., Charlet and Tournassat, 2005; Géhin et al., 2007), which may compete with radionuclides or may act as a precursor of new Fe-Si phases. Also, reduction of structural Fe(III) can occur increasing the cation exchange capacity. Bentonite can be transformed into Fe-rich non-swelling silicates such as berthierine, cronstedtite or chlorite (e.g., Montes et al., 2005; Lantenois et al., 2005; Bildstein et al., 2006; Wilson et al. ,2006a; Schlegel et al., 2008; Lanson et al., 2012). This could jeopardize the long-term performance of the clay barrier by decreasing the swelling capacity, enhancing the hydraulic conductivity and increasing brittle failure.
- The formation of secondary minerals at the interface steel-bentonite/clay can affect physical properties such as porosity and microstructure of the bentonite, which in turn would have an impact on the transport properties for solutes or gases at the interface.

2.2.3.1 Concluding perspective

The evolution of the repository environment (thermal, hydraulic and/or chemical gradients - redox, pH and dissolved species - from the initial post-closure stage until the system reaches long-term conditions will impact on the chemical evolution of the steel/iron-bentonite interface. Laboratory and in situ experiments, as well as investigations on analogues, evidence that many of the processes and mechanisms occurring at the steel canister/bentonite interface are reproducible under similar conditions and are well understood under a broad range of temperature and physico-chemical conditions. Results show that corrosion rates and products are well established and can be predicted by reactive transport models, if a number of variables such as humidity, pH, concentrations of dissolved salts, organic carbon and oxygen concentration are known in each stage of the repository. However, to do that is necessary to establish clearly the evolution of the system from the dry-out stage up to system get equilibrium conditions, which is a difficult issue since is highly dependent not only on in situ conditions at each stage, but also on variables still not well known, such as the role of gamma-radiation in the corrosion rate during first stages of the repository and also the role of microbial activity along the lifetime of the repository. The results of laboratory and in situ experiments, as well as from archaeological or natural analogues highlight the ability of the clay to absorb or react with Fe(II) when anaerobic corrosion occurs. Swelling capacity of the smectite may decrease as a consequence of the formation of Fe-rich non-swelling clays (e.g., berthierine, cronstedtite and chlorite). Also, sorption sites on the clay can be filled by ferrous ions that can compete with radionuclides. The understanding of the interactions at the interface between steel and bentonite/clay is continuously increasing on the basis of laboratory experiments, field experiments in underground research laboratories and modelling studies. Extensive numerical reactive transport modelling studies of the interactions occurring at the steel-bentonite/clay interface under typical repository conditions and the effects of corrosion products on the bentonite have been performed

in the last two decades (cf. Bildstein and Claret, 2015; Claret et al., 2018; Bildstein et al., 2019 and references therein). Although the numerical studies often differ on the precise nature of the main secondary minerals, the extent of the perturbation is always predicted to be limited to a few centimetres (< 20 cm) into the clay barrier in the long term. Further improvements of reactive transport simulations of steel-clay interfaces are expected by the coupling of electrochemical corrosion models that calculate the steel corrosion rates as function of geochemical conditions (e.g., Bataillon et al., 2010; King et al., 2014) to reactive transport modelling codes (cf. Bildstein et al., 2019).

2.2.4 Interface “steel – granite”

In general, a direct interface steel-granite does not exist in repository concepts since there is always cementitious backfill or bentonite between the steel containers and the crystalline bedrock (cf. Neeft et al., 2019). For example, in Finland at the Olkiluoto site, parts of the low and intermediate level waste (containing both, carbon steel and stainless steels) are packed into carbon steel containers that are buried into concrete layered silos located 60 to 100 m under the sea level in crystalline bedrocks (cf. Somervuori and Carpen, 2021). Thus, the main interaction between steel (e.g., in waste containers) and granite can occur via granitic ground water. In case of a cementitious backfill, the evolution at the surface of the steel would be similar to those described in section 2.2.2, until the cementitious material is nearly completely degraded and the pH and composition of the pore water approaches the one of the bedrock groundwater.

In the following paragraphs, only the interactions of steel with bedrock groundwater in a crystalline repository environment are considered, since the granitic host rock is deemed not to be affected by the presence or corrosion of steel (cf. Somervuori and Carpen, 2021). In contact with (granitic) groundwater, corrosion of steel is affected by pH, temperature, oxygen content (redox), ground water composition, radiation, and the presence of microbial activity. Generally, groundwaters in granitic rocks can exhibit a wide range of hydrogeochemical characteristics, ranging from lowly mineralised waters (representing, e.g., also glacial meltwater) to higher saline brackish or marine waters, or basement brines, depending on repository site and depth.

The pH conditions in bedrock groundwater in granitic rocks are usually close to neutral (about 8). In anoxic conditions, corrosion rates of carbon steels are very low unless the groundwater is highly acidic or microbial activity is high. In neutral anoxic and abiotic environments, corrosion rates of carbon steel were found to be about 1 µm yr^{-1} or below (e.g., Smart et al., 2001). Under these conditions, formation of a magnetite (Fe_3O_4) film on carbon steel retards the rate of corrosion in groundwater environments (Smart et al., 2001).

Temperature is an important factor in corrosion of steel because a higher temperature usually means accelerated corrosion rates. In the bedrock, the temperature depends on the depth from the surface and the geothermal gradient and therefore on repository site and concept. Moreover, disposal of high-level waste can lead to elevated temperatures in the repository near field for several hundreds of years, depending on the heat output of the waste and the repository lay-out. Smart et al. (2001) found a large increase in the initial corrosion rates of carbon steel (1 to 2 orders of magnitude compared to ambient conditions) at elevated temperatures (up to 85 °C) in anaerobic granitic groundwater. The initial corrosion rates were at the level of 10 to 30 µm yr^{-1} but dropped to less than 0.1 µm yr^{-1} after an oxide film had formed on the steel surface. This suggests that the diffusion of various (aggressive) species through the film becomes more determinative for the corrosion process and the corrosion becomes less sensitive to temperature over time (cf. section 2.2.2).

The redox environment is very important in metal corrosion since many corrosion reactions need oxygen. In oxygen containing aqueous environments, the corrosion rates of iron and carbon steel are typically in the range from 0.05 to 0.15 mm yr^{-1}, i.e., several orders of magnitude higher than under anoxic conditions (Tunturi, 1988). In oxygen free (anoxic) water, the corrosion of carbon steel is very low unless the water is acidic or there is microbiological activity on the surfaces (e.g., due to the

presence of biofilms), due to the formation of a passivating magnetite film on carbon steel surface. In the anoxic abiotic Finnish bedrock groundwaters the average corrosion rate of carbon steel was between 1.1 µm yr^{-1} and 0.4 µm yr^{-1}, which was higher than the recorded values for corrosion rates of stainless steels (e.g., Carpén et al., 2018).

The groundwater composition in granitic bedrocks can exhibit a wide range of compositions and salinities, depending, inter alia, on the source of the groundwaters (e.g., fossil seawater, glacial meltwaters, near-surface groundwater, basement brines), ground water age and the extent of water-rock interaction. From the viewpoint of steel corrosion, in particular the concentration of chlorides and sulphates are of interest, since they are known to increase the steel corrosion rates at elevated concentrations and promote pitting corrosion (cf. section 2.2.2).

The effect of the radiation fields in a nuclear waste repository on the corrosion of steel is not clear and experimental results have been found to be inconclusive. Whereas some authors found no significant effects of gamma irradiation on the uniform corrosion of low-carbon steel aside from some pitting corrosion and an increase in hydrogen generation (e.g., Ahn and Soon, 1995), Liu et al. (2017) reported an increase in the corrosion rate of a carbon steel intended as canister material for high-level waste by 33 % due to gamma irradiation with a rate of 2.98 kGy per hour. This radiation rate is not expected for vitrified HLW disposal cells (see Figure 2-13).

The corrosion of carbon steel in anoxic groundwater is strongly affected by microbial biofilms and their metabolic activity, since microbiological activity on the steel surface accelerates the corrosion rate in oxygen free water (i.e., under anoxic conditions), e.g., due to decrease in the local pH (Small et al., 2008). Corrosion induced by microorganisms is mainly localized corrosion (Rajala ,2017). In the presence of carbon steel, the microbial community in anaerobic groundwater was found to be more diverse and abundant than in the same environment without carbon steel (Rajala et al., 2015). Černoušek et al. (2019) found that in natural granitic water in anaerobic conditions, the corrosion rate of carbon steel was accelerated due to biofilm formation. However, the formation of a biofilm, which was dominated by sulphate-reducing bacteria inhibited the corrosion rate at slightly elevated temperatures.

2.2.4.1 Concluding perspective

A direct interface between steel and granite does not exist in geological repository concepts for nuclear wastes (except, e.g., for the use of rock bolts), since there is always cementitious backfill or bentonite between the steel containers and the crystalline bedrock (cf. sections 2.2.2 and 2.2.3). Thus, only an indirect interaction via the granitic groundwater occurs, which, however, is modified by the presence and nature of the backfill material. Corrosion of steel/iron in contact with granitic water is affected by many factors including pH, redox and composition of water. High pH tends to decrease corrosion rates of steel whereas high chloride and sulphide contents in groundwater induce localized corrosion. The role of microbes on the corrosion of steel in anaerobic conditions is important and has to be taken into account in granitic bedrock environments. The effect of radiation on the corrosion of steel is not resolved yet. The effect of steel corrosion on the granitic bedrock is deemed to be negligible.

2.2.5 Interface “concrete – clay”

In many disposal concepts for radioactive wastes, significant use is made of cementitious materials, for example as structural support material for access galleries and disposal drifts or cells (e.g., concrete/shotcrete), as well as grouts/mortars used as containment material for low and intermediate level wastes (cf. section 2.1 and Neeft et al., 2019). Thus, these cementitious materials can be in contact with both, the host rock clay formation and bentonite barriers (cf. NEA, 2012; Sellin and Leupin, 2013; Neeft et al., 2019). Due to the contrasting chemical and mineralogical properties of cementitious materials and clays, interactions will occur at the cement-clay interface as a result of the chemical gradients. For example, the pH of pore waters in either clay formations (e.g., Opalinus clay, Callovo

Oxfordian clay, or Boom clay) and bentonite is typically in the range of pH 7 to 8.5. In contrast, the progressive degradation of cementitious materials after resaturation of the repository leads to a pH in the cement pore fluids ranging over time from 13.5 (for systems based on Ordinary Portland Cement, OPC) to 10 (for details see section 2.2.6), slowly approaching the pH of the surrounding ground water in the long-term (cf. Berner, 1992; Glasser, 2011; Beattie and Williams, 2012; Hoch et al., 2012; Drace and Ojovan, 2013). Even in so-called low-pH cementitious materials the initial pH of the young pore water can often be above pH 12 (e.g., Vehmas et al., 2020). The term low-pH cementitious material is used here for cementitious materials/concrete where significant amounts of OPC in the binder is replaced by siliceous supplementary cementing materials, in particular silica fume, ground granulated blast furnace slag, or fly ashes.

Within the context of deep geological disposal of nuclear waste disposal, cement/clay interactions have been investigated for more than three decades by means of laboratory and in situ experiments, studies on natural and industrial analogues, and reactive transport modelling. Comprehensive reviews on various aspects of cement/clay interactions have already been published in the past decades (e.g., Metcalfe and Walker, 2004; Michau, 2005; Gaucher and Blanc, 2006; Savage et al., 2007; Savage, 2009, 2011; Sidborn et al., 2014; Bildstein and Claret, 2015; Dauzères 2016; Claret et al., 2018; Savage and Cloet, 2018; Bildstein et al., 2019).

Short term laboratory (e.g., Adler et al., 1999; Adler, 2001; Dauzères et al., 2010, 2014; Fernández et al. 2016; Balmer et al. 2017) and longer-term in situ experiments (up to about 20 years) at different underground research laboratories like HADES, Mol, Belgium (Read et al. 2001), Mont Terri, Switzerland (e.g., Jenni et al. 2014; Dauzères et al., 2016; Lerouge et al., 2017; Mäder et al., 2017), Bure, Department Meuse/Haute Marne, France (e.g., Gaboreau et al., 2011, 2012; Dauzères et al., 2016), or at the Tournemire site in France (e.g., Tinseau et al., 2006; Techer et al. 2012a,b; Bartier et al., 2013; Lalan et al., 2016), as well as the FEBEX experiment in the Grimsel test site in Switzerland (e.g., Alonso et al., 2017; Fernández et al. 2017; Turrero and Cloet 2017) have demonstrated that at the cement/clay interface, alteration of both cement paste and clay material take place, leading to mineralogical changes that modify the microstructure of the altered region, which may influence transport relevant properties such as porosity and permeability, or the radionuclide retention behaviour of the materials.

2.2.5.1 Processes at the interface

Due to the contrasting chemical and mineralogical properties of cementitious materials and clay rocks or bentonite, reaction zones will develop, with diffusive transport of aqueous species across the material interface in response to chemical gradients. These gradients develop typically from the higher concentrations (activities) of species such as OH^-, K^+, and Ca^{2+} in the cementitious materials, thus tending to diffuse towards the clay materials[3]. In contrast, the concentrations of species such as Mg^{2+}, $SiO_2(aq)$ and HCO_3^-, are often higher in the pore water of the clay formation/bentonite, thus tending to diffuse into the cementitious materials. Based on the existing literature the following key processes have to be considered at cement/clay interfaces, as observed in laboratory and in situ experiments, and/or as inferred from natural analogue studies, performed in Maqarin (Jordan), Cyprus or the Philippines (e.g., Alexander et al., 1992, 2008; Smellie, 1998; Alexander and Smellie, 1998; Crossland, 2006; Savage, 2006; Alexander and Milodowski, 2011; Reijonen and Alexander, 2015; Milodowski et al., 2015, 2016) and various modelling studies:

- Diffusion of hydroxyl anions from the cement into the clay will destabilize silicate/aluminosilicate minerals, leading to slow hydrolysis of montmorillonite and other aluminosilicate minerals present (e.g., Cuevas et al., 2006; Yamaguchi et al., 2007),

[3] In more saline clay host rocks i.e. in France, Switzerland and the Netherlands, the dissolved Ca2+ concentration can be higher than this concentration in concrete pore water (see Appendix B)

consuming OH- ions and neutralising the high pH fluids, but leading to a decrease in swelling pressure of smectitic clays.

- Replacement of clay minerals by calcium silicate hydrates (C-S-H), sheet silicates, and/ or zeolites, with the secondary minerals forming in a zonal fashion (cf. Figure 2-10) (e.g., Gaucher and Blanc, 2006, Cuevas et al., 2006; Savage et al., 2007), potentially leading to an overall decrease in porosity (due to differences in molar volumes) and changes in the rheological properties of the clay (e.g., Jefferies et al., 1988).
- Decalcification due to dissolution of portlandite ($Ca(OH)_2$) and C-S-H, thus reducing its Ca/Si-ratio, in the cementitious material accompanied by rapid precipitation of Ca-carbonates, such as aragonite and calcite, directly at the interface, due to steep gradients in hydroxyl ion concentrations (higher on the cementitious material) and the partial pressure of carbon dioxide ($pCO_2(g)$, higher in the clay rock formation) across the cement/clay-interface; these reactions lead to an increase in porosity in the cementitious material and a porosity decrease in the clay in the longer term. In low-pH cementitious materials, where portlandite may be lacking, the decalcification of the C-(A)-S-H can proceed directly, leading to an earlier formation of amorphous silica as residue. However, low-pH cementitious formulations with slag and micro silica have a more refined pore structure leading to lower diffusivity and thus lower rates of mineral alteration.
- Formation of calcium aluminium silicate hydrates (C-A-S-H) and (amorphous) magnesium silicate hydrates (M-S-H) at the interface, affecting porosity and transport properties at the interface (e.g., Dauzères et al., 2016), and replacement of portlandite, C-S-H gel and monosulphoaluminate by ettringite (e.g., Savage, 2014). Note that in low pH formulations, C-A-S-H can be present already as initial hydration phase.
- Redistribution of sulphate towards the unaltered cementitious matrix due to the decrease in pH close to the interface, destabilizing earlier formed Ca-Al-sulphates (ettringite, monosulphate (AFm)) that re-precipitate in the higher pH regions (e.g., Mäder et al., 2017).
- Fast exchange of cations in interlayer sites in montmorillonite, due to diffusion of K^+, Na^+ and Ca^{2+} from the cementitious material into the clay, leading to a decrease of swelling pressure.
- Fast protonation-deprotonation reactions at clay edge sites, retarding the diffusive migration of hydroxyl ions due to reversible sorption processes.
- Slow hydrolysis of montmorillonite and other minerals present, either as additives (e.g. quartz sand), or as accessory minerals reactions consuming hydroxyl ions, thus chemically neutralizing the advancing cementitious porewater, leading to an increase in porosity and a decrease in clay swelling properties.

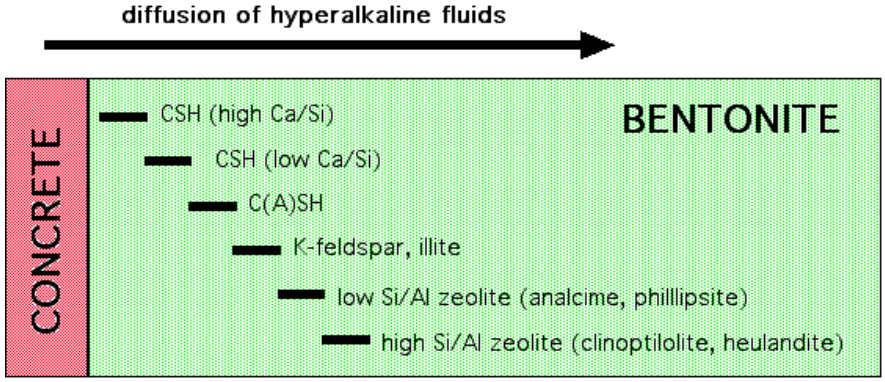

Figure 2-10: Schematic diagram of the potential sequence of secondary mineral forming as consequence of the migration of hyperalkaline pore fluids through bentonite (Savage and Benbow, 2007; Bamforth et al., 2012). Na/K phases may be replaced by more Ca-rich ones as the composition of cementitious pore fluids evolves with time.

The studies performed have shown that there is a strong coupling between fluid and solute transport, dissolution of solids and precipitation of secondary phases, ion exchange and edge site sorption on

clays, and the consequential changes in physical properties of the materials (i.e., porosity, permeability, swelling pressure of clay) (cf. Savage and Cloet, 2018). Depending on the extent of porosity/permeability changes (e.g., pore clogging), changes in hydraulic conductivity, diffusivity, and gas permeability may occur. Moreover, the potential dissolution and replacement of clay minerals may alter the safety-relevant swelling properties and sorption capacity of the clay materials. However, the extent of alkaline disturbance in the clay host rocks is limited to a few meters in the long term. The processes occurring at the cement/clay interface as well as their kinetics will depend to a large extent on the initial properties of the materials, such as the nature of the cementitious binder (OPC or low pH binder), the mineralogy and pore water composition of the clay material, and their initial transport properties (e.g., porosity, diffusivity, incl. water saturation) and thus on repository concept and site. Thus, the extent and significance of these processes will need to be assessed on a site-specific basis (cf. NDA, 2016). Due to this complexity and diversity, it is difficult to establish a general sequence of secondary minerals forming in the cement domain due to the impact of the clay pore water. Details on experimental observations with respect to secondary phases formed at the interfaces between various cementitious materials and clays, clay rocks or bentonite have been compiled e.g., by Dauzères (2016) and Deissmann and Ait Mouheb (2021).

The (long-term) interaction of cementitious materials with clays, clay rocks and bentonites have been subject to a large number of reactive transport modelling studies (cf. reviews in Bildstein and Claret, 2015; Claret et al., 2018; Bildstein et al., 2019; Deissmann and Ait Mouheb, 2021). In these simulations, cement-clay interactions have been mainly modelled as coupled Thermal-hydraulical-mechanical-chemical (THMC) processes in continuum scale reactive transport simulations, based on thermodynamic equilibria sometimes with the inclusion of kinetic data and diffusive transport, with various degrees of complexity. Most simulations addressed the interactions between cementitious materials and natural clay rocks, whereas relatively fewer studies investigated the interaction with bentonites. In the majority of the cases, OPC-based high-pH cementitious materials were addressed (CEM I); only recently, interface processes between low pH cementitious materials have been addressed in reactive transport modelling studies at different time and length scales (e.g., Berner et al., 2013; Dauzères et al., 2016; Idiart et al., 2020). With respect to the simulation of laboratory and in situ experiments, it can generally be concluded that reactive transport modelling shows a great capability for reproducing the experiments, e.g., regarding mineralogical transformation pathways and net porosity evolution (cf. Bildstein et al., 2019). Despite the differences in the approaches of long-term simulations of cement-clay interactions, there are general similarities in terms of the predicted thickness of the altered zones in the clay and cement domain, the types of secondary solid products and changes in porosity. Simulations of the long-term evolution of the interface revealed a narrow zone (mainly in the order of cm to dm) of perturbed mineral and fluid chemistry located close to the interface, for timescales up to and beyond 100,000 years (cf. Savage and Cloet, 2018; Bildstein et al., 2019). Regarding the predicted mineral transformations there are recurring results, such as decalcification of cementitious materials (i.e., portlandite dissolution, decrease of the Ca/Si ratio in C-S-H), precipitation of ettringite in the presence of sulphates, and/or carbonation and smectite dissolution, dedolomitisation, as well as formation of C-(A)-S-H solids, clay minerals (illite, saponite), zeolites and carbonates in the clay domain. Critical parameters identified in the various studies comprise dissolution/precipitation kinetics and the description of evolving reactive surface areas that can play an important role in sequential minerals' appearance or disappearance, the localization of porosity reduction and increase, the kinetics and the laws controlling the porosity/permeability and porosity/diffusivity feedback, and the inclusion of certain secondary phases (e.g., zeolites) and their thermodynamic/kinetic parameters.

2.2.5.2 Concluding perspective

The evolution of the interface between cementitious materials and clays (incl. poorly indurated clays, clay rocks, or bentonites) within the context of nuclear waste disposal has received widespread attention in the last decades. Substantial progress has been made in the characterization of the mineralogical and microstructural changes over relatively long time periods in the frame of experimental studies and

by investigation of natural analogues. Additionally, reactive transport modelling appears to predict well the chemical evolution occurring at the interface between cementitious and clay materials. The inclusion of new thermodynamic data on relevant phases (e.g., M-S-H, C-A-S-H, zeolites) that were made available recently (e.g., Roosz et al., 2018; Lothenbach et al. ,2019; Ma and Lothenbach ,2020, 2021) will probably lead to a further improvement of long-term predictions and the understanding of the interactions of cementitious materials with clays in the context of the evaluation of repository safety.

2.2.6 Interface “concrete – granite”

Cementitious materials are employed for various purposes also in waste repositories in crystalline (granitic) rocks (cf. Neeft et al., 2019). For example, the disposal tunnels are sealed with concrete end plugs to ensure mechanical and hydrological isolation of different compartments. In the Finnish final repository for HLW (i.e., spent nuclear fuel), several thousand tons of Ordinary Portland Cement (OPC)–based grouts, shotcrete and rock bolt mortars will be present in structural applications and for sealing of fractures. Also, in the LLW repository in Finland, isolation is achieved by a combination of cementitious barriers and the granitic host rock (cf. Leivo, 2021). Processes occurring at the interface of cement/mortar/concrete and granite can change both the properties of the cementitious material and the granite properties at the interface.

2.2.6.1 Processes in concrete

In general, cement-based materials used in the groundwater environment are fundamentally unstable in a long-term perspective, due to thermodynamic disequilibrium with their environment. Thus, concretes and cementitious materials/barriers used in geological disposal facilities in crystalline rocks (or clay rocks) will inevitably change their mineralogical, chemical and physical properties in the long-term, both as a consequence of recrystallisation and chemical interactions with their environment. With respect to the long-term evolution of cementitious materials at the interface to granitic/crystalline rock, interactions are mainly related to the contact with the groundwater present in the bedrock. Generally, groundwaters in granitic rocks can exhibit a wide range of chemical characteristics ranging from lowly mineralised waters (representing, e.g., also glacial meltwater) to higher saline brackish or marine waters, or basement brines, depending on repository site and depth. The processes occurring in the cementitious materials in a repository due to the contact with granitic groundwaters depend on the local environmental conditions (in particular the groundwater composition) and comprise the typical processes described in detail in the respective literature in the context of the performance and degradation of cementitious construction materials in the subsurface (e.g., Taylor, 1997; Hewlett, 1998). These processes include in particular

- removal of alkalis and decalcification,
- carbonation,
- attack by aggressive species (e.g., magnesium, sulphate, chloride), and
- alkali-aggregate reactions

Leaching of alkalis and decalcification causes changes of many physical and mechanical properties of cement-based materials such as porosity, elastic modulus, compressive strength, internal friction angle and creep. Leaching of concrete by percolating or flowing water can cause severe damage, e.g., in dams, pipes or conduits, and is potentially important for the long-term evolution of repository systems for nuclear wastes. These processes are expected to remove alkali hydroxides, dissolve portlandite ($Ca(OH)_2$) and decompose the hydrated silicate (i.e., calcium silicate hydrates, C-S-H) and aluminate phases (AFm/AFt), leading to a concomitant decrease of the pH of the pore solution in the cementitious materials. Initially, dissolution of KOH and NaOH within the cement will form a pore water with pH ~13. The pore water pH will then decrease to ~12.5 where it will be buffered by equilibration with portlandite. This pH will remain until all portlandite has dissolved, after which, pH will be controlled by equilibrium with the incongruent dissolution of the C-S-H gel and will decrease to ~10.5. The ultimate residue will

consist essentially of hydrous forms of silica, alumina and iron oxide, while all CaO will be lost. By this stage, the cement paste will be disintegrated. The schematic evolution of pore solution pH during degradation of OPC based cementitious materials by pure, demineralised water is shown in Figure 2-11. Removal of alkalis and decalcification generally lead to an increase in porosity/permeability and diffusivity in cementitious materials.

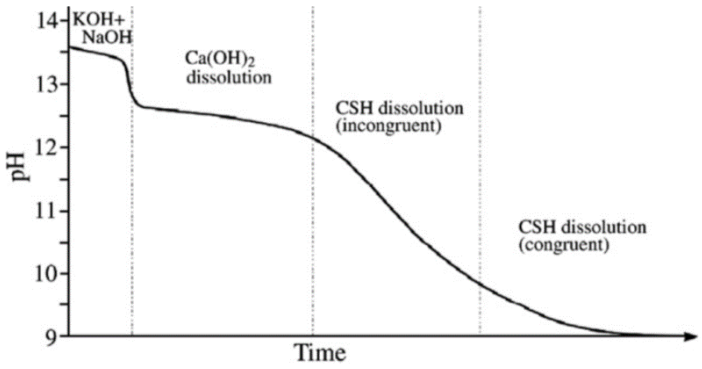

Figure 2-11: Schematic evolution of pore solution pH during leaching of Portland cement-based materials by pure water (Atkinson et al., 1985; Berner, 1992; Snelman and Vieno, 2005; Cau Dit Coumes et.al., 2006).

Carbonation occurs when carbon dioxide dissolves in the pore solution of cement paste, producing CO_3^{2-} ions, which will react with Ca^{2+} and produce $CaCO_3$ (calcite) on the expense of portlandite. Later, when portlandite is consumed, C-S-H is first decalcified and later decomposed. The AFm and AFt phases react with the carbonate anions and can form special carbonate phases (e.g., thaumasite, $Ca_3Si(OH)_6SO_4CO_3{\cdot}12H_2O$). If pH is lowered further by addition of more carbon dioxide, these initially formed carbonate species will decompose. The residues from complete carbonation of cementitious materials are calcite, amorphous silica, hydrocarboaluminates and different Al- and Fe-hydroxides. The pH value of the carbonated cement paste first drops to around 10 when all portlandite is consumed and later to a pH around 8, when the other phases are decomposed. These carbonation reactions are mostly happening at a slow rate and are especially pronounced during the operational phase of the repository, when the cementitious materials are in contact with gaseous CO_2 from the ventilated tunnels, and, in later stages, due to CO_2 production from degrading organic wastes, or due to interaction with carbonate-rich groundwaters. Due to microstructural changes, carbonation is often accompanied by a reduction of permeability and diffusivity of cementitious materials.

Sulphate attack in concrete originates mainly from interaction with sulphate rich groundwaters. The damage to concrete structures resulting from external sulphate attack is related to the chemical reactions between sulphate ions and the solid cement hydration products, leading in particular to the formation of ettringite ($Ca_6(Al,Fe)_2(OH)_{12}(SO_4)_3{\cdot}26H_2O$) and gypsum ($CaSO_4{\cdot}2H_2O$), which occupy a larger volume than their educts. This can lead to the generation of stress in the interior of the concrete as a result of the formation of the expansive products, which in consequence results in a mechanical response of the bulk material, such as cracking. However, the potential effects of sulphate attack in cementitious repository materials can be minimized by the utilisation of sulphate resistant cements.

The attack by magnesium ions present in groundwaters can be particularly deteriorating for concrete structures, as it can cause a complete disintegration of the C-S-H phases in the long term. In contact with magnesium rich groundwaters, the magnesium replaces the calcium in the hydration phases leading to the formation of amorphous $Mg(OH)_2$, magnesium silicate hydrates (M-S-H) as well as Mg-containing SiO_2 gel, accompanied with a drop in pH to approx. 10.5 (e.g., Taylor, 1997, Eglinton, 1998).

Deterioration of materials properties due to chloride ingress is one of the main causes of concrete degradation worldwide. Concrete itself is generally not adversely affected by chloride ingress, though

the formation of some new chloride-bearing phases such as Friedel's salt ($Ca_4(Al,Fe)_2(OH)_{12}Cl_2 \cdot nH_2O$) at the expense of other AFm/AFt phases is possible. However, the steel reinforcement and other steel materials inside concrete can be corroded at elevated chloride concentrations, which may lead to the formation of (expansive) corrosion products accompanied by crack formation due to mechanical stress. However, this is deemed to be more relevant under oxic conditions that may occur in concrete-granite systems when an insufficient concrete cover has been used or in the presence of glacial meltwaters. The transport and distribution of chlorides in a concrete structure are very much a function of the environmental exposure, i.e., chloride concentration and duration of exposure to solutions in contact with the concrete surface.

Alkali-aggregate reactions (AAR), also termed alkali-silica-reactions (ASR), are chemical reactions occurring between minerals present in certain types of aggregate, and alkali (Na^+ and K^+) and hydroxyl (OH^-) ions present in the pore solution of the cement paste in concrete. These dissolution reactions occur due to the high solubility of certain amorphous, disordered or poorly crystalline forms of silica (SiO_2) in highly alkaline solutions leading to formation of a hygroscopic alkaline gel. In general, these reactions are expansive in nature, resulting in internal stresses in concrete and consequently cracking. It is often accompanied by the appearance of efflorescence and exudations on the surface of the concrete. They can significantly decrease the durability of concrete as a result of cracking favouring other processes of deterioration, particularly in the cases of carbonation or chloride penetration resulting in reinforcement corrosion. However, ASR can be prevented in cementitious materials in the repository environment by using either non-siliceous aggregates, e.g. carbonates or using cements with a low alkali content (e.g. blended low-pH cements). The absence of ASR with the use of quartz aggregates and low-alkali binders has such extensive demonstrated experience that this combination has turned into a best practice for civil engineering. Different time frames are active for geological disposal of waste and ASR can thermodynamically not be excluded. Kinetically, ASR can be minimised through the reaction rims (see section 3.1.4.1.2). The extent of this minimization determines whether ASR has an impact on the chemical evolution of disposal cells.

2.2.6.2 Processes in granite

The production of alkaline leachates (high-pH plume, cf. Figure 2-12) developing at the concrete/granite interfaces from alteration of concrete may cause degradation of silicate minerals (e.g., feldspars) in the crystalline bedrock around the repository and precipitation of secondary phases further along fractures, where more neutral pH conditions prevail (Baker et al., 2002). These interactions between the cement leachate and the rock are a potentially important factor for altering flow in the near-field rock, due to clogging of fractures by formation of secondary minerals (e.g., Mäder et al., 2006; Alexander, 2012). However, there are still a number of uncertainties associated with this sealing of fractures due to the formation of secondary minerals (Savage, 2018). It has been stated that the beneficial effect of fracture sealing due to cement-host rock interaction cannot be taken into account in the safety case because they cannot be quantified (e.g., Pastina et al., 2012; Koskinen, 2014).

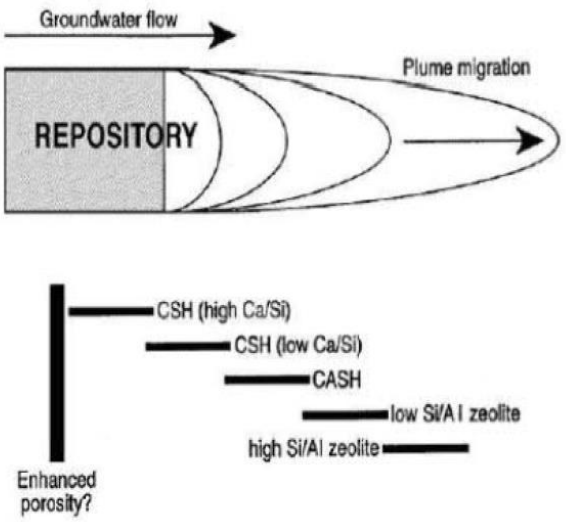

Figure 2-12: Effects of an alkaline plume in granitic host rocks (POSIVA 2012).

In the last two decades, a number of laboratory studies and experiments in underground research laboratories (e.g., at the Grimsel Test Site in Switzerland) have been performed addressing the interaction of cement leachates with crystalline granitic rocks (e.g., Bateman et al., 1999, Mäder et al., 2006, Pfingsten et al., 2006; Moyce et al., 2014, Lanyon, 2015, Watson et al., 2017), complemented by respective reactive transport simulations (e.g., Sole,r 2012; Soler et al., 2006, 2011; Soler and Mäder, 2007, 2010; Watson et al., 2017; Chapparo et al., 2017). There is a general agreement that the dissolution of the primary silicate minerals in granitic rocks by cementitious leachates is followed by the precipitation of secondary phases such as C-S-H, Ca-Al-Si-hydrates (C-A-S-H), magnesium-silicate-hydrates (M-S-H), calcite, clays and zeolites, mainly on fractures. Subsequent transformation of C–S–H to feldspars and zeolites can occur in the longer-term. In general, these reactions are very slow and highly dependent on pH, temperature and groundwater composition.

Recently, Szabó-Krausz et al. (2021) evaluated the geochemical interactions occurring at the granite-concrete interface in the operating LLW/ILW repository at Bátaapáti, Hungary. The main secondary phases observed at the interface after 1 to 15 months of reaction were the Ca-carbonates calcite and vaterite. Calcite veins occurred along the granite-concrete contact while vaterite precipitated in the pores of the concrete near the interface. This carbonation was explained by Szabó-Krausz et al. (2021) by reaction of Ca released by the dissolution of the cementitious material and HCO_3^- from the local granitic pore water. The carbonation process was found to reduce the porosity and permeability in the contact zone, avoiding or slowing down further interaction of the materials. Moreover, a frequent occurrence of titanite along or near the granite-concrete interface, but always on the side of the granite was observed. It was concluded by Szabó-Krausz et al. (2021) that titanite formed where i) the Ca concentration was not high enough to form carbonates, and ii) sufficient dissolved SiO_2 was in the solution, with the granite serving as a source of TiO_2. The observation of neighbouring calcite and titanite precipitation was seen as indicator for distinctively changing geochemical conditions within short distance of the interface.

2.2.6.3 Concluding perspective

The physico-chemical processes occurring at the interface between cementitious materials and crystalline, granitic rocks in a deep geological repository can change the mineralogical, geochemical and solute transport properties of both materials. However, compared to the interface between cementitious materials and clays or clay rocks, the interface with granitic/crystalline rocks has received less attention so far. Changes on the concrete side are related to the contact with the groundwater

present in the crystalline bedrock and comprise typical alteration phenomena observed in subsurface construction materials, which depend in particular on the composition and pH of the contacting water. The alkaline plume caused by the leaching of concrete due to interaction with the bedrock groundwater will have an influence on the granite by dissolving primary silicate minerals and the precipitation of secondary phases at the interface and on fractures, which may result in changes in the flow regime in the repository near field. In general, the chemical alteration processes at the concrete/granite interface in underground repositories are expected to be rather slow.

2.3 Narrative time-space evolution at disposal cell scale

An important step in the quantitative assessment of the chemical evolution at the disposal cell scale is the integration of individual studies in an integrated phenomenological description of the time-space evolution at the disposal cell scale. This section presents narrative evolutions for disposal cells defined using the main characteristics of the HLW and ILW disposal cells in European programmes, based on the information from the individual interfaces (Deissmann et al., 2021) and from the current handling of chemical evolution in European programmes (Neeft et al., 2019). The handling of the chemical evolution can be a compromise between ‘’what occurs’’, for example, what are the most relevant processes, and ‘’what can be modelled’. ‘What occurs’ is an understanding of the processes taking place in the chemical evolution and those process are included in this section. The ‘what occurs’ includes assumptions that need to be substantiated. The contributors of the handling of the chemical evolution in European programmes have been asked to limit their efforts to a normal evolution scenario. This section therefore only includes this scenario with the most likely processes.

2.3.1 HLW disposal cells

ACED does not address radiological and microbiological processes but it needs to be assessed whether their consequences need to be included in the chemical evolution. The carbon steel overpack (see section 2.1.1.2 and 2.1.1.3) is considered as an example in order to show how such an assessment can look like. Radiation enhanced corrosion depends on the radiation rate and access to water. Radiolysis of water can generate O_2 by which a more oxidising environment becomes present in the vicinity of the metal overpack. Aerobic induced steel corrosion rates are larger than anaerobic corrosion rates of steel. The radiation rate can be determined by the activity of the radionuclides in the vitrified waste form and the penetrating power of gamma rays that are released upon decay of these radionuclides. Figure 1-2 shows that the radiotoxicity of the waste is initially dominated by ^{90}Sr and ^{137}Cs but only ^{137}Cs and its daughter release upon decay a sufficient high gamma energy to contribute to the radiation dose rate at the surface of the carbon steel overpack. The vitrified waste form has guaranteed maxima in activity content of these two radionuclides of 6600 TBq for ^{137}Cs and 4625 TBq for ^{90}Sr (AREVA, 2007). The maxima are assumed to be the activity of these radionuclide at time is 0 years in Figure 2-13. The vitrified waste form is not immediately emplaced in a disposal facility but is cooled for a couple of decades; for example, the French programme uses an age of 85 years and 70 years in their disposal concept (Cochepin et al., 2019). The half-lives of the radionuclides that initially dominate the radiotoxicity are 29 years for ^{90}Sr and 30 years for ^{137}Cs. Consequently, the radiation dose rate has been significantly reduced upon emplacement of vitrified HLW. The metal overpack has a high density of about 8000 kg/m^3 and can therefore provide shielding that also limits the radiation dose rate at the outside of the metal overpack. Two examples of thickness of carbon steel overpack have been calculated in Figure 2-13:

- A thickness of 3 cm, which is characteristic for a disposal package with a concrete buffer as used in the Belgian and Dutch disposal programmes (Neeft et al., 2019);
- A thickness of 14 cm, which is the thickness considered in the Swiss programme (Leupin et al., 2016; Levasseur et al., 2021).

Based on the research by Smart et al. (2017), Figure 2-13 shows that the thinner carbon steel overpack of 3 cm has a high enough radiation dose rate for radiation enhanced corrosion for a disposal package with a concrete buffer for vitrified HLW with an age of 60 years. If specified, all programmes consider older waste packages (Neeft et al., 2019). Consequently, radiation enhanced corrosion does not need to be included in the chemical evolution in this HLW disposal cell.

Relevant literature about the impact of radiation on steel interfacing bentonite has not been found but the values found for steel exposed to groundwater (Smart et al., 2008b) are considered as a minimum, since the process is attributed to the radiolysis of water and accessible amount of water. Figure 2-13 shows that the radiation dose rates for a thicker carbon steel overpack interfacing bentonite is too low

for radiation enhanced corrosion at any age of vitrified HLW. Also, the dose rates of 10-20 Gy per hour listed in section 2.2.3 to affect the properties of bentonite do not occur.

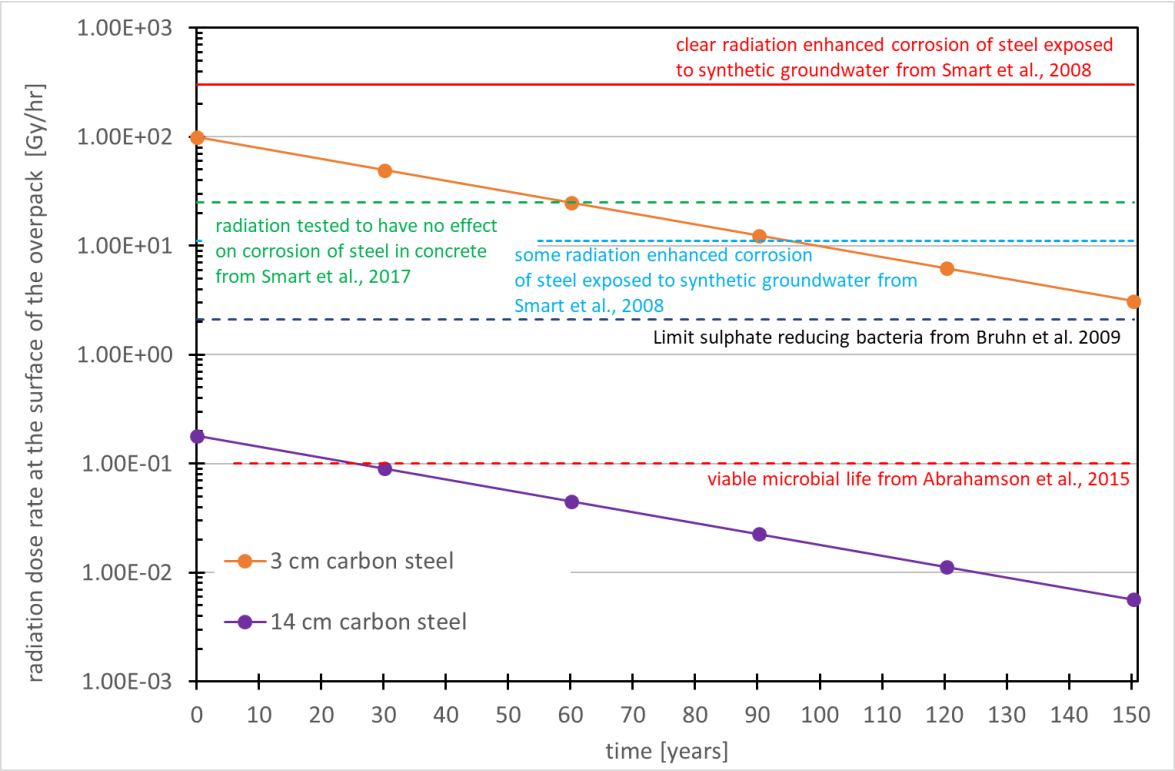

Figure 2-13: Radiation dose rate as a function of the time after CSD-v fabrication calculated with Microshield. Activity ^{137}Cs at 0 years is assumed to be 6600 TBq.

It can be deduced from the available literature that radiation enhanced corrosion and microbial induced corrosion can never occur at the same time, i.e. microbial activity requires lower radiation doses rates than required for radiation induced corrosion. Radiation has been known to kill microbes and this information is also used for health reasons such as sterilization of food. The decrease in the number of viable (i.e., culturable on a chosen medium) bacteria as a function of increasing total dose is determined and expressed as the D_{10} value, the total dose required to reduce the viable population by one order of magnitude or 90% (Abrahamsen et al., 2015). D_{10} values are additive; for a reduction of three orders in magnitude, a total dose equal to 3 times the D_{10} value is required. The D_{10} values for relevant bacteria ranged between 0.5 and 1.57 kGy (Stroes-Gascoyne and West, 1997). Consequently, sterilization can be achieved for any considered age of vitrified HLW since these doses are received multiple times. In research, usually sterilisation levels are achieved with high radiation dose rates, higher than representative for geological disposal. What lacks in the radiation sensitivity of microbes is the equilibrium between the reduction in viable population by radiation and increase in viable population by growth of this population by consumption of nutrients and electron acceptors and donors. Nevertheless, there are several other arguments by which microbial induced corrosion is highly unlikely, i.e. the high temperature load at the start of the post-closure phase, too small connecting pore throats that limit transport of food and energy sources, the drying of the buffers at the start of the post-closure phase by the heat emitted by the waste, and for the concrete buffer also the high pH of the concrete pore water. Microbial induced corrosion is therefore excluded in the narrative for HLW disposal cells, the only microbial activity considered possible is at the interface between bentonite and granitic rock and localised at the fractures in the rock. These microbial processes have negligible effects on the chemical evolution at disposal cell scale.

The chemical alterations of the engineered materials in HLW disposal cells in the post-closure phase are thus determined by:

1) the formation of an alteration layer between two interfacing materials. This alteration layer may have been formed already before or in the operational phase;
2) the diffusional exchange of species through this alteration layer and/or the thickness of the diffusional layer of dissolved species near the alteration layer. The maximum dissolved concentration in this diffusion layer is in equilibrium with the alteration layer. The thickness of this diffusion layer in the interfacing material depends on the speed of migration of the dissolved species in this material and sorption of dissolved species by minerals in this material.

2.3.1.1 From closure till about 1000 years

The heat generated by decay of the radionuclides in the vitrified HLW has initially an important effect on the chemical evolution of the engineered barriers. The temperature increase results into a decrease in saturation degree in the buffers by which the access to water needed to continue chemical corrosion is minimized. This effect has been modelled in the Spanish programme for the bentonite buffer in which saturation of the bentonite buffer was achieved within 20 years for HLW disposal cells in granite (Neeft et al., 2019). This short period is specific for granitic host rocks since there is sufficient access of water to saturate the buffer. There is less water available to saturate the bentonite buffer in indurated clay. A period between 100 and 1000 years is foreseen for saturation of HLW disposal cells with bentonite buffers in indurated clay (Leupin et al., 2016). The impact of this difference in access of water is visualized in Figure 2-14 with a smaller corroded part of the steel overpack for disposal cells in indurated clay compared to disposal cells in granitic rocks. Such modelling results for the saturation degree in the concrete buffers are available for poorly indurated clay (Weetjens et al., 2006; Poyet, 2006, 2007) and are foreseen to have a negligible effect on the chemical corrosion rate, since a temperature of 80 °C is achieved within a few decades (Neeft et al., 2019) and the same corrosion rate was measured at 25 °C and 80 °C (Smart et al., 2017c). After about 1000 years, a temperature below 50 °C is achieved at the steel overpack, and in disposal concepts in which the overpack is enclosed in a bentonite or concrete buffer, the host rock is almost no more heated by the waste (Neeft et al., 2019). Figure 2-14 shows that the chemical evolution at disposal cell scale after about 1000 years is envisaged to be small.

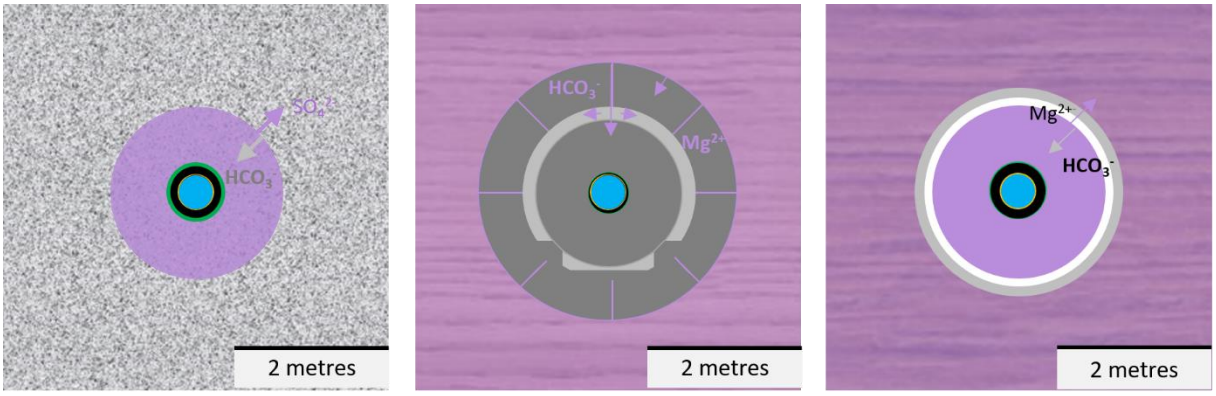

Figure 2-14: Chemically evolved disposal cells after about 1000 years containing vitrified HLW for the host rocks: granite, poorly indurated clay and indurated clay. Blue = vitrified HLW, black = left metallic substrate of steel overpack, green = corroded part of steel overpack, bentonite (purple),carbonated concrete (white), unaffected concrete (grey), grout (light grey). Ingress of ions are indicated e.g. Mg^{2+} and HCO_3^- from granitic / clay host rock into bentonite buffer / concrete segment.

There can be aerobic and anaerobic corrosion processes in this period from closure till about 1000 years. An alteration layer is formed during this corrosion process. There is thermodynamic data and software available to calculate the stability of alteration layers as a function of the pore water chemistry.

Figure 2-15 shows the Pourbaix diagrams with the available phases of calcium, iron-oxides with and without calcium and bicarbonate in the pore solution.

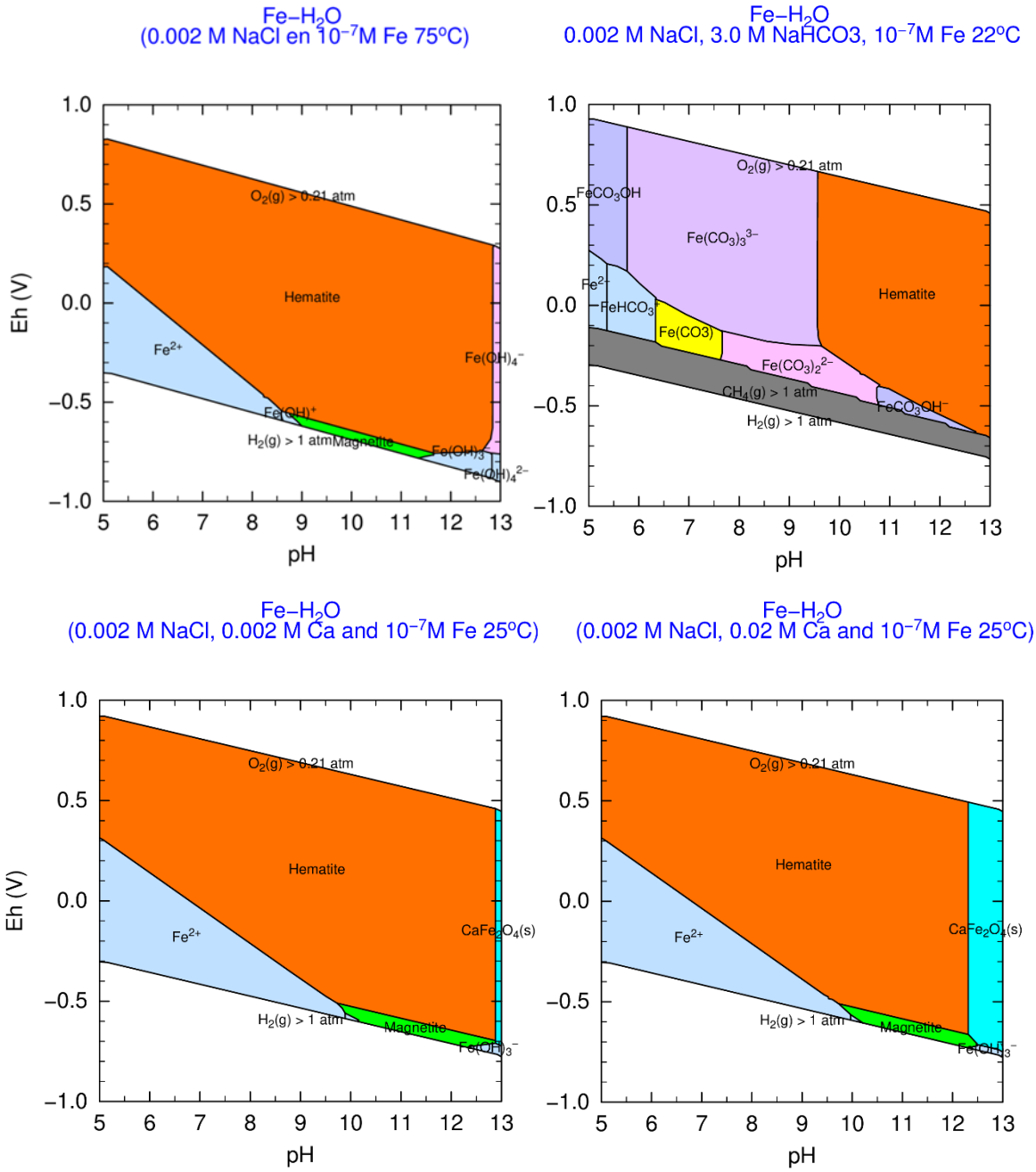

Figure 2-15: Pourbaix diagrams for the system Fe-H_2O with an activity of dissolved species of 10^{-7} M; 0.002 M Ca is a reasonable concentration for tap water and 0.02 M Ca is the maximum dissolved calcium concentration without alkalis (Berner, 1992) and (Vehmas and Itälä, 2019) and 3M HCO_3^- is the concentration found in Spanish and Czech granitic rocks and French indurated clay (see Appendix B) Magnetite (green) is Fe_3O_4(s) and Hematite (orange) is Fe_2O_3(s) and Siderite (yellow) $FeCO_3$ (s)[4].

[4] These figures have been made with Phreeplot (Kinniburg and Cooper 2018), a free available software programme that makes geochemical plots using Phreeqc (Parkhurst and Appelo 2013). The SIT database has been used as input for these calculations. This database corresponds to the PHREEQCi version of the ThermoChimie V.7.b, developed by Amphos 21, BRGM and HydAsa for ANDRA, the French National Radioactive Waste Management Agency.

Please note that supersaturated iron solutions have been used in the calculated Pourbaix diagrams; for example, the actual range in pH of the thermodynamically stable magnetite is smaller. The minimum in solubility has been calculated to be 10^{-9} M at 100 ºC and 10^{-10} M at 25 ºC (Hermansson, 2004).

2.3.1.1.1 Aerobic corrosion

Bentonite and concrete buffers contain entrapped oxygen as a result of the fabrication process. This oxygen is consumed by corrosion of steel or by reaction with traces of pyrite; these traces can be present in bentonite and in concrete that has been made with cement that is blended with blast furnace slag (BFS). The alteration layer formed during aerobic corrosion would be hematite as shown in Figure 2-15. The period in time for aerobic corrosion of the carbon steel overpack by this entrapped oxygen is expected to be smaller than a few years, but others consider a transient phase to anaerobic conditions lasting till 100 years (see section 2.2.3). Nevertheless, the available oxygen can be quantified for aerobic corrosion and conservative estimates predict a corroded thickness of 0.7 mm (Alexander and McKinley, 1999).

A period with aerobic corrosion can also be absent for example in the case of carbon steel interfacing a cementitious material that was a blend of Ordinary Portland Cement (OPC) and BFS (Naish et al., 1991) in which the rest potential is immediately achieved. Magnetite could only be measured on the carbon steel interfacing this cementitious material with BFS that was run for almost two years. This magnetite measurement using Raman spectroscopy and the electrochemical measurement provided the evidence that steel had become passivated. Other blends of OPC with fly ash and OPC showed no corrosion product on carbon steel, i.e. steels embedded in these cements still experienced active corrosion after two years. But like for clays, also for cementitious materials the available oxygen for aerobic corrosion can be quantified and a maximum in aerobic corroded thickness can be set. A maximum in air content in fabricated concrete is quality controlled through EN 12350-7.

2.3.1.1.2 Anaerobic corrosion

The anaerobic corrosion of steel uses water as an oxidant and magnetite is predicted in Figure 2-15. Passive corrosion of steel is achieved when the corrosion rate has become equal to the dissolution rate of the passive film (Grauer, 1988); the magnetite layer constitutes a barrier against transport of water towards steel and of dissolved iron species into solution. This passivation is expected to extend beyond the thermal phase for concrete buffers due to its high pH. However, the presence of magnetite is also assumed and measured for steel exposed to pore water with a lower pH. Precipitation of magnetite as a corrosion product in bentonite has been modelled at 25 ºC in the Czech and Spanish disposal programmes due to an increase of pH till 10 by iron corrosion at the vicinity of the bentonite-iron interface (Neeft et al., 2019). This rise in pH near the steel surface, which makes precipitation of magnetite thermodynamically possible, can be caused by insufficient dissipation of the generated hydroxyl ions in bentonite. This insufficient dissipation is also present in bentonite pore water by which the formation of magnetite was measured due to a local increase in pH of 10 (Kreis, 1991). The presence of bicarbonate in the pore water has an effect on the formation of the chemistry of the alteration layer. The ingress of bicarbonate into the bentonite buffers may result into a change of the alteration layer from magnetite to siderite as predicted in Figure 2-15.

The thickness of the steel overpack is at least three times smaller for countries considering a concrete buffer compared to countries that have chosen a bentonite buffer. The found long term corrosion rates, i.e. after an alteration layer has been formed, are also different in orders of magnitude. The long-term corrosion rates of carbon steel from section 2.2 are:

- below 10 µm per year, if this steel interfaces bentonite (see section 2.2.3);
- in the range of 0.1 µm per year or lower, if this steel interfaces concrete (see section 2.2.2);
- below 0.1 µm, if this steel interfaces granitic pore water (see section 2.2.6).

The higher corrosion rates for steel interfacing bentonite may be understood from the surface charge of minerals in the buffers. The zeta-potential of clay minerals in bentonite buffers is negative by which there is preferably sorption of cations. The speciation of dissolved iron is $Fe(OH)^+$ for pH<11 and $Fe(OH)_3^-$ for pH>11 as shown for the Pourbaix diagrams in Figure 2-15, as long as the bicarbonate content of the pore water is limited. The selective sorption of $Fe(OH)^+$ onto the clay minerals reduces the thickness in the diffusion double layer for the dissolved concentration of iron species. This reduction in thickness enhances the dissolution of the alteration layer and thereby corrosion. It is known that the tendency of the sorption of dissolved iron may increase the corrosion rate in clay (Johnson and King, 2008; Savage, 2014). This sorption induced corrosion may be different for porewaters enriched in bicarbonate, since the iron-(bi)carbonate dissolved species are negative at pH<6 according to Figure 2-15; i.e. selective sorption of these dissolved species by clay minerals would be absent. The corrosion rate would decrease if the removal of dissolved iron-(bi)carbonate species does not take place. An experimental comparison of carbon steel in bentonite with and without pore water containing bicarbonate is however unknown to the authors of this SOTA.

The zeta potential of cement minerals in concrete is positive at a pH>11.8 (Pointeau et al., 2008)[5]. There could also be sorption of dissolved iron species such as $Fe(OH)_3^-$.

Archaeological analogues (e.g. Dillmann et al., 2014) indicate that the chemical interaction between the buffers and steel remain in the vicinity of the interfaces. Cross section analysis from the metal or iron towards the porous materials - soils (e.g. argillaceous sediments) or cementitious materials - show similar patterns (Figure 2-16).

- The metallic substrate (M) in case of steel, and in case of iron, also some slag inclusions are present in this substrate;
- Product Layer (DPL) containing iron oxides and further towards these porous materials iron hydroxides. These phases are generally well crystallised and relatively compact;
- Transformed Medium (TM) a transition zone between DPL and the porous materials containing markers from the porous materials e.g. quartz grains;
- The binder (B) in cementitious materials or (S) soil where no corrosion products can be found.

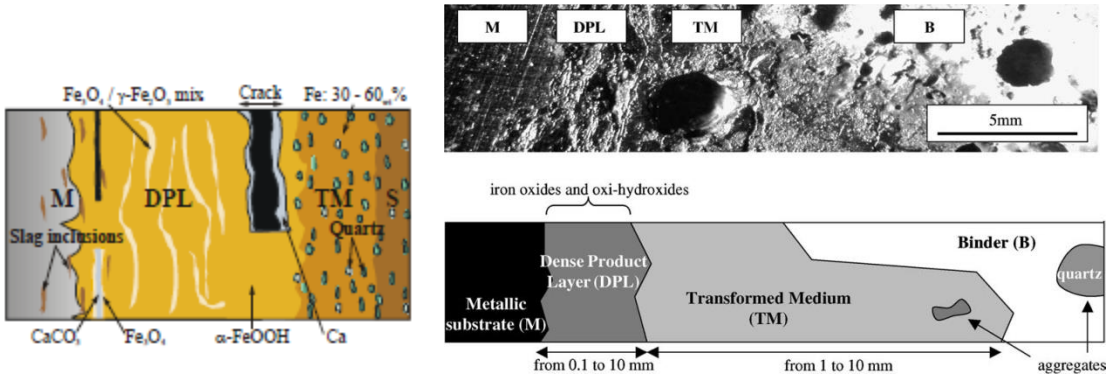

Figure 2-16: Main corrosion pattern observed on several metal-soil interfaces of several hundred years old (left) (Neff et al., 2004) and metal-binder interface of 350 years old (Chitty et al., 2005)[6]

[5] The surface charge as a function of the Ca/Si ratio of CSH-gel has been explored in Cebama (Grivé and Olmeda, 2015) since this Ca/Si ratio depends on pH (Berner, 1992). Indeed, CSH gels with a Ca/Si ratio of 1.4 show anionic exchange that has been proven with the MoO_4^{2-} uptake and CSH-gels with a Ca/Si ratio of 1.2 and 0.8 have lost this uptake (Grambow et al., 2015).

[6] Measurement of quartz and calcite for all binders by X-ray diffraction in Chitty's study indicates that all binders were fully carbonated and had a pH of 8. These pure lime binders harden by atmospheric carbonation.

2.3.1.1.3 Dense product layer / Inner Layer

The porosity of DPL has been measured to be 10 vol% (Chitty et al., 2005). The archaeological analogues are obtained at lower temperatures than envisaged at the steel overpack. The chemical interaction at the clay-iron interface at 90 °C shows however a similar result, expect that the DPL is further subdivided in an internal and external DPL (Figure 5-2[7] in Deissmann et al., 2021)). Other definitions of DPL and TM are a fairly dense Inner layer and an Outer layer (Atkins et al., 1991). The DPL is more or less the alteration layer magnetite or siderite as calculated in Figure 2-15. The impact of calcium on the formation of the alteration layer has not been included in the corrosion process in section 2.2 but dissolved calcium in clay and concrete seems to have a crucial role in the formation rate of the spinel-type passivation film (Kreis, 1991). At both the clay-steel interface (Neff et al., 2004) and the concrete-steel interfaces (Chitty, et al. 2005), the formed spinel corrosion product magnetite contains traces of calcium. Magnetite (Fe_3O_4) and $CaFe_2O_4$ are both spinels that cannot be distinguished by Raman spectroscopy; this technique is used to provide evidence that the steel has become passivated (e.g. Naish et al., 1991). Thermodynamically, it is possible to have a calcium-iron containing passivating film as calculated in Figure 2-15, especially at a pH>12.5, but so far it has not been identified as a passivating film[8]. The impact of calcium may therefore be important for understanding the corrosion process of the overpack enclosed in the concrete buffer. The chemical analysis of the surface films and difference in corroded thickness measured by weight loss and hydrogen generation monitoring also showed that another corrosion product than magnetite (Fe_3O_4) would have been formed on the surface of steel (Kaneko et al., 2004).

2.3.1.1.4 Transformed medium / Outer layer / Alteration zone

The transformed medium is a result of an interaction between the dissolved species from iron corrosion and clay or cement minerals. The quartz grains in concrete and sediment (soil) seem to remain unaffected in the analogues.

2.3.1.1.4.1 Zone in bentonite

The transformed medium can be the alteration zone of bentonite with a reduced porosity due to cementation of clay by precipitation of magnetite. The diffusion values in this zone may be smaller than in unaffected bentonite due this decrease in porosity. There can however also be an increase of diffusion values in this zone due to the reaction between dissolved iron and the swelling clay mineral montmorillonite into a non-swelling sheet silicate. The chemical characteristics of the transformed medium is quite well known for bentonite which is Fe-rich non-swelling silicates (see section 2.2.3). The work done by Savage (2014) includes some quantification of the processes at disposal cell scale by which the dominating processes can be elucidated. Figure 2-17 shows that the alteration of clay minerals in bentonite is strongly coupled to the iron corrosion process.

[7] Hematite instead of magnetite can be measured using Raman spectroscopy if the laser power heated the specimen beyond 400ºC (Neff et al., 2004). Only magnetite would be measured in deaerated soils (Dillmann et al., 2014)

[8] However, some experimental results support the hypothesis of a calcium-iron containing passivating film. Removal of dissolved calcium has been confirmed from batch sorption experiments with a fine powder of iron and cementitious pore water with a pH of 13.5. On the reacted iron particles - despite the calcium concentration being undersaturated - precipitation of $Ca(OH)_2$ had taken place as deduced from pair distribution function analysis. Interspersed $Ca(OH)_2$ within the iron-oxide layer is formed during the corrosion process, but co-precipitation into a solid solution between calcium and iron might also occur (Ma et al., 2018).

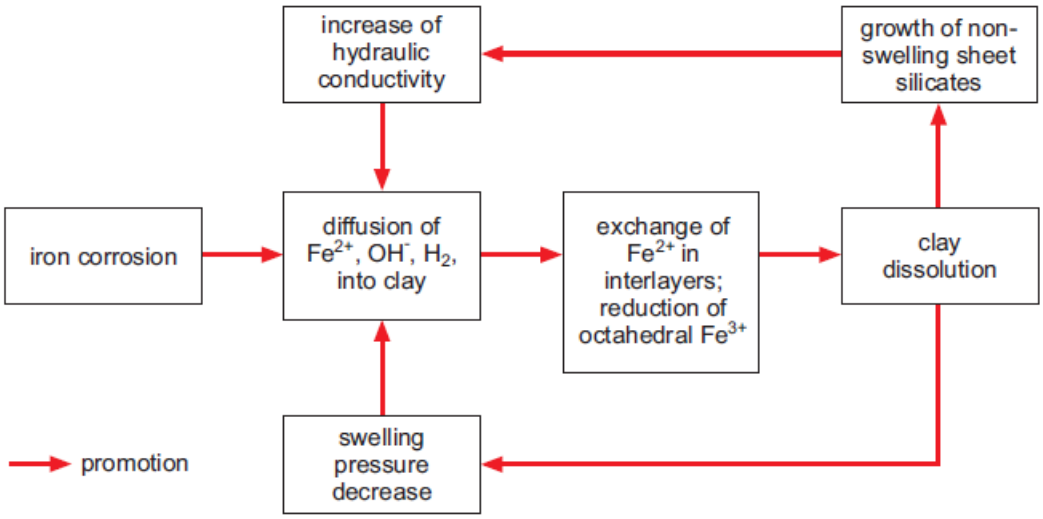

Figure 2-17: Impact of iron corrosion on clay minerals in bentonite (Savage, 2014)

As earlier explained, although the pH of the bentonite pore water is too low for magnetite, magnetite is formed by insufficient dissipation of hydroxyl ions. This local increase in pH due to steel corrosion determines the clay dissolution. This dissolution promotes the transformation of montmorillonite into non-swelling silicates. The slow dissolution rate of montmorillonite is considered the rate limiting step for the transformation of bentonite. The maximum in calculated thickness of the alteration zone in bentonite in simulations with the clay dissolution as the rate-limiting step was 0.1 m after 5000 years (Savage, 2014).

2.3.1.1.4.2 Zone in concrete

The transformed medium between DPL and binders also contains precipitated iron-hydroxides with a III+ valence that have resulted in a reduction in porosity of concrete near the DPL. (Chitty, et al. 2005; Atkins et al., 1991). For non-carbonated concrete with a concrete-steel interface lasting for 23 years, portlandite crystallites are also present in the outer layer. These crystallites had a distinctly different morphology than portlandite in the cementitious matrix and the transformed medium contained loosely bound material (Atkins et al., 1991). The observed loosely bound may indicate that the strength locally has diminished and that the hydraulic conductivity has increased.

Negatively charged dissolved iron species are expected at the pH of the concrete pore water. Sorption of these species by positively charged cement minerals is envisaged. An iron-enriched layer has been measured and it is assumed that iron (dissolved species) may form iron-containing cement hydration phases (see section 2.2.2.3). A mineralogical change of cement minerals with the coupling of processes - as identified for clay minerals (see Figure 2-17) - is not yet made, only a morphological change of portlandite crystallites indicating re-precipitation is known. Time-dependent mineralogical transformation of the cement minerals by sorption of iron is not yet performed although thermodynamic data about iron containing cement minerals are available (e.g. Höglund, 2014). Modelling the fate of dissolved iron species in the cementitious phase would help to provide some quantification of the expected thickness of the alteration zones as a function of time, as has been performed for the interface clay-steel.

2.3.1.1.5 Engineered barriers and materials interfacing host rocks

Chemical interaction that leads to an alteration zone in the bentonite buffer is not expected for bentonite buffer interfacing granitic rock. No alteration layers and zones have therefore been drawn in Figure 2-14. The exchange of dissolved species between the bentonite buffer and the pore water within fractures in

granitic rocks depends on the trace amounts of soluble salts that were present in bentonite and the pore water chemistry of the granitic pore water. Czech and Spanish granitic pore waters are not as saline as Swedish and Finnish granitic pore waters at suitable disposal depth, and the amount of soluble salts present in bentonite buffers can be chosen for particular site characteristics. For example, the bentonite buffer in the Czech programme also contains sodium bicarbonate as a soluble salt while this salt is not present in the Swedish bentonite.

Alteration zones are expected in both the bentonite buffer and the clay host rocks interfacing concrete support materials . The coupling of processes to determine the alteration of clay by concrete is reasonably well understood. Figure 2-18 shows that the alteration processes of bentonite by interfacing concrete are strongly coupled. The swelling clay minerals are transformed into secondary minerals. All these secondary minerals (see Figure 2-10) are non-swelling minerals.

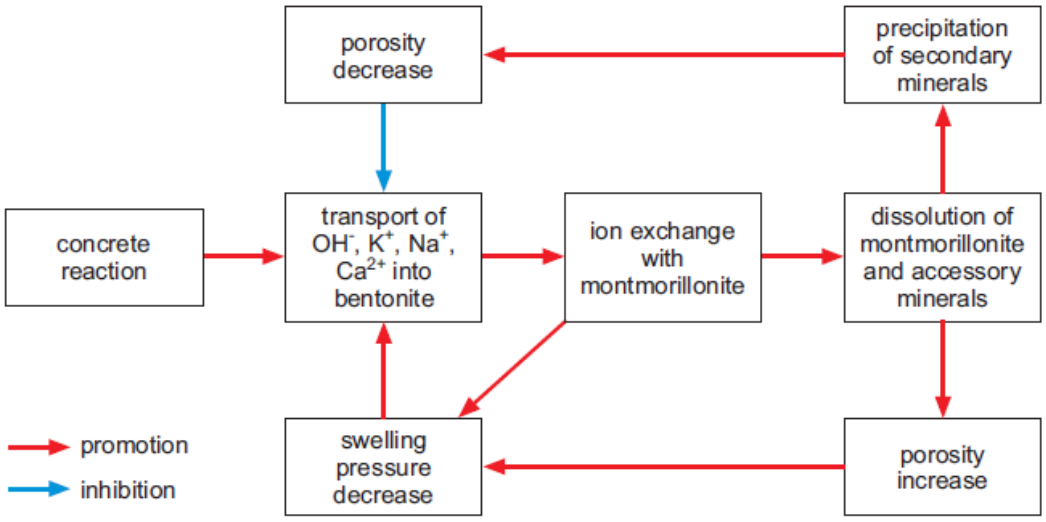

Figure 2-18: The coupling of processes for the determination of the alteration zone in bentonite by the cementitious pore fluid and bentonite interaction (Savage, 2014).

The overall impact of the transformation of swelling clay minerals into non swelling sheet silicates is a decrease in porosity, hydraulic conductivity and swelling pressure (Savage, 2014). Consequently, the primary safety function of clay to limit transport of radionuclides by the physical properties of clay may not have changed by this alteration. However, the mechanism for the closure of fractures changed from seal-healing of fractures into self-sealing of fractures. If fractures would have been induced, more time for their closure and the associated reduction in hydraulic conductivity would be required. Also, most of the formed secondary non-swelling minerals, e.g. CSH phases[9], illite and zeolites, also have sorption properties but their sorption capacities can be smaller than that of montmorillonite. The knowledge on the interaction of bentonite with cementitious pore fluids is sufficient to quantify the thickness of the alteration zone in clay. In many simulations, the overall reduction in porosity can achieve a porosity of 0% (Savage, 2014), by which the alteration is stopped. These calculations are performed with a uniform porosity. This thickness of the alteration zone has been predicted to be 0.02 m after 100,000 years. There will however always be some continuation since the distribution in size of pores in the sedimentary clay rock and bentonite buffer allows existing diffusional pathways. A ten times large thickness is

[9] Please note that the dissolved calcium and potassium in concrete pore water can be smaller than in clay pore water by which the necessary egress of calcium.

calculated after this period, i.e. 0.2 m, if no porosity reduction is assumed (Savage, 2014). Smaller alteration thickness is expected for clay interfacing concrete since:

- the egress of ions from concrete pore water takes place by limited diffusion due to the pore structure of concrete, and
- the transport of hydroxyl ions from concrete into clay is further decreased by the reduction in pH in concrete due to ingress of dissolved bicarbonate from the clay pore water.

Concrete may also have been gas carbonated in the operational phase by which no further alteration of the clay in the post-closure phase is expected, since the difference in pH between the pore waters of carbonated concrete and clay is negligible.

The initial porosity of bentonite and poorly indurated clay is about 40% (see Appendix C) which is larger than the so-called engineered impermeable concrete segments with an initial porosity between 10 and 15% (see section 2.1.3.2). The ingress of dissolved species from the clay host rock into these concrete segments is rather along the joints than within the concrete, as drawn in Figure 2-14. The shotcrete interfacing indurated clay may have been carbonated in the operational phase as explained in section 2.1.3.3. Consequently, the chemical and mineralogical alteration in the post-closure phase may be negligible for the carbonated shotcrete. The shotcrete is therefore envisaged to act as a permeable medium for the transfer of dissolved species from the clay host rock into the bentonite buffer.

2.3.1.2 From about 1000 years until fracture of the carbon steel overpack

The decay of radionuclides in vitrified waste has occurred till such an extent that temperature in all disposal cells has achieved the virgin temperature of the host rock.

2.3.1.2.1 Alteration layers and zones in bentonite

Anaerobic corrosion of the carbon steel overpack has continued and although the thickness of the DPL (alteration layer) may have slightly increased, the extent of corroded steel can be estimated from the affected bentonite, i.e. the alteration zone with non-swelling sheet silicates. The consumption of bicarbonate to form siderite results into an influx of bicarbonate from the granitic pore water into the bentonite. This influx of bicarbonate and water is smaller from disposal cells constructed in indurated clay due to the smaller diffusion value of bicarbonate in indurated clay compared to granitic host rocks. The envisaged alteration zone in bentonite is therefore drawn smaller in disposal cells in indurated clay compared to granitic host rocks in Figure 2-19. The size of the alteration zone is bounded by the thickness of carbon steel overpack and stainless steel container (Savage, 2014). With the geometry used in Figure 2-5, a thickness of iron-unaffected bentonite of at least 10 cm can be calculated by mass balance calculations.

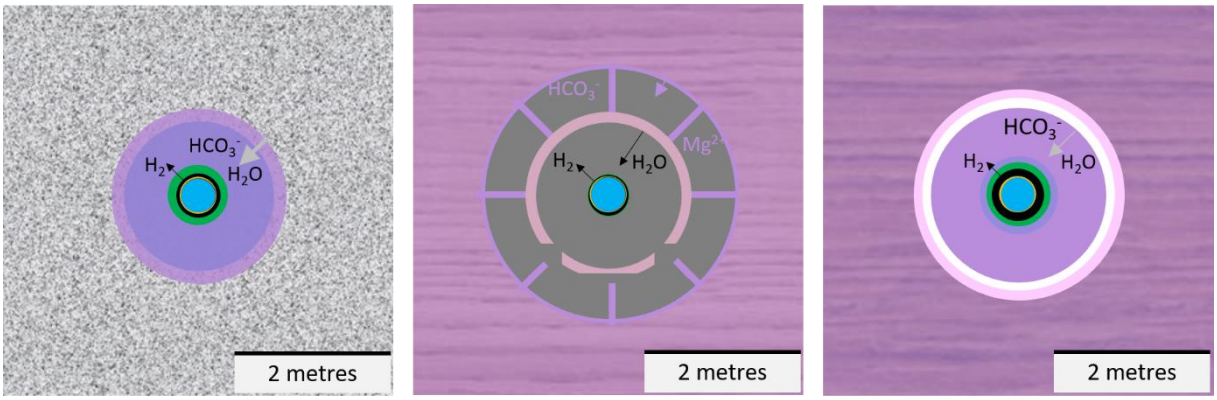

Figure 2-19: Chemically evolved disposal cells after about 10,000s years till 100,000s of years containing vitrified HLW for the host rocks: granite, poorly indurated clay and indurated clay. Blue =

vitrified HLW, black = left metallic substrate of steel overpack, green = corroded part of steel overpack, unaffected bentonite (purple), affected bentonite (blueish purple), carbonated concrete (white), unaffected concrete (grey), affected grout (lila).

In NF-PRO, a project in the 6th Framework programme, experimental work has been performed to investigate the interaction between bentonite and carbon steel canisters (NF-PRO, 2008). Pieces of bentonite in contact with iron were no longer plastic but became brittle, only crumbled pieces of bentonite could be removed (Carlson et al., 2008). For the narrative, it is therefore assumed that the buffer has become more brittle with much less possibilities for creep and more vulnerable to form cracks, due to the compressive load of granitic rock. The alteration zones in bentonite have a higher hydraulic conductivity than virgin bentonite, which may enhance the dissipation of hydrogen further into the bentonite buffer. The radial dissipation quadratically reduces the hydrogen concentration in the bentonite buffer, which reduces the probability for gas perturbation. Anaerobic corrosion of the steel overpack also occurs in the disposal cell with the concrete buffer. An alteration zone in concrete may not be yet visible, due to the smaller corrosion rates in concrete compared to bentonite. First alteration zones within concrete by ingress of dissolved species from clay pore water are envisaged to be visible at disposal cell scale.

2.3.1.2.2 Alteration zones in concrete

Figure 2-11 in section 2.2.6.1 shows the schematic evolution of pH of concrete pore water during the four different stages, since the stability of cement minerals is pH-dependent. The reduction in pH by leaching is however not foreseen but rather by the reactions with ingress of gaseous CO_2 in the operational phase from the ventilation air and bicarbonate ions from the clay pore water. The concrete buffer and concrete segments have a high mechanical strength, which prevents the lithostatic load of the underground host rock being transferred to the waste package. Ingress of bicarbonate reduces the pH of the concrete pore water but the calcite precipitation in this alteration zone may result into an increase in strength of the concrete buffer and segments. The carbon steel overpack cannot be cracked as long as the concrete buffer has not reduced in mechanical strength. The ingress of dissolved magnesium and the transformation from calcium containing cement phases into magnesium containing minerals are considered to decrease the strength of concrete (Atkinson et al., 1985). There is almost always magnesium enrichment in concrete since all clay pore waters have a larger magnesium concentration than the concrete pore water, except for the Belgian clay pore water (see Appendix B). It is assumed that the progressive increase of a magnesium front reduces the thickness of the buffer with strength. Figure 2-20 shows an estimated time scale for the evolution of the pH at room temperature in concrete with a cement content of 185 kg/m^{-3}, using a groundwater flux density of 10^{-10} m/s. Apart from changes in pH, also other processes take place (Atkinson et al., 1985), (Berner, 1992), (Grivé and Olmeda, 2015), (Pointeau et al., 2008), (Atkins et al., 1991), (Dauzerès, 2016):

- Concrete pore water with a pH > 12.5 controlled by dissolved alkalis. The dissolved calcium concentration of initially about 0.002 M increases to 0.02 M, when the dissolved alkalis and hydroxyl ions are dissipated to the surrounding media with a smaller pH. The cement minerals become more positively charged due to loss of the alkalis. The loss of hydroxyl ions in concrete pore water can also be caused by precipitation of brucite with ingress of magnesium from clay;
- Dissolution of portlandite controls concrete pore water at a pH of 12.5. The dissolved calcium concentration remains at 0.02 M until the cement matrix is exhausted in portlandite. The cement minerals remain positively charged. The dissolved calcium and bicarbonate from clay may result in precipitation of brucite and calcite. There can be ingress of sulphate from clay pore waters that are as saline as seawater or in which the sulphate concentration is in equilibrium with celestite leading to thaumasite formation;
- Decalcification of C-S-H-phases in the pH range between 10.5 and 12.5 causes a reduction in pH of the concrete pore water. The dissolved calcium concentration in equilibrium with C-S-H-phases is reduced from 0.02 M till 0.002 M, the cement minerals become less positively charged. At a pH < 11.8 and CaO/SiO_2 <1.4, the left cement minerals become negatively

charged and there can be uptake of dissolved alkalis by C-S-H-phases. Ettringite starts to dissolve and generates high dissolved sulphate concentrations that can precipitate with left dissolved calcium into gypsum but with the ingress of bicarbonate from clay there is also a potential to form thaumasite;

- Dissolution and decalcification of C-S-H-phases, the dissolved calcium concentration remains constant at around 0.002 M. The released calcium can react with ingress of bicarbonate into calcite or bicarbonate and sulphate into thaumasite; thaumasite can be later altered to calcite (Milodowski et al., 2015). C-S-H phases are replaced with magnesium silicate phases (M-S-H phases).

The ingress of sulphate leading to delayed ettringite formation can be prevented by a choice in cement (see section 2.1.1.3) and s therefore not included in Figure 2-20. The formation of thaumasite can be deleterious for the strength of concrete (Höglund, 2014). This thaumasite formation seems with the current available knowledge not been able to be prevented but is not always observed (see section 3.1.4.1). Initially formed ettringite that contributed to the fabricated strength of concrete is dissolved at a later stage.

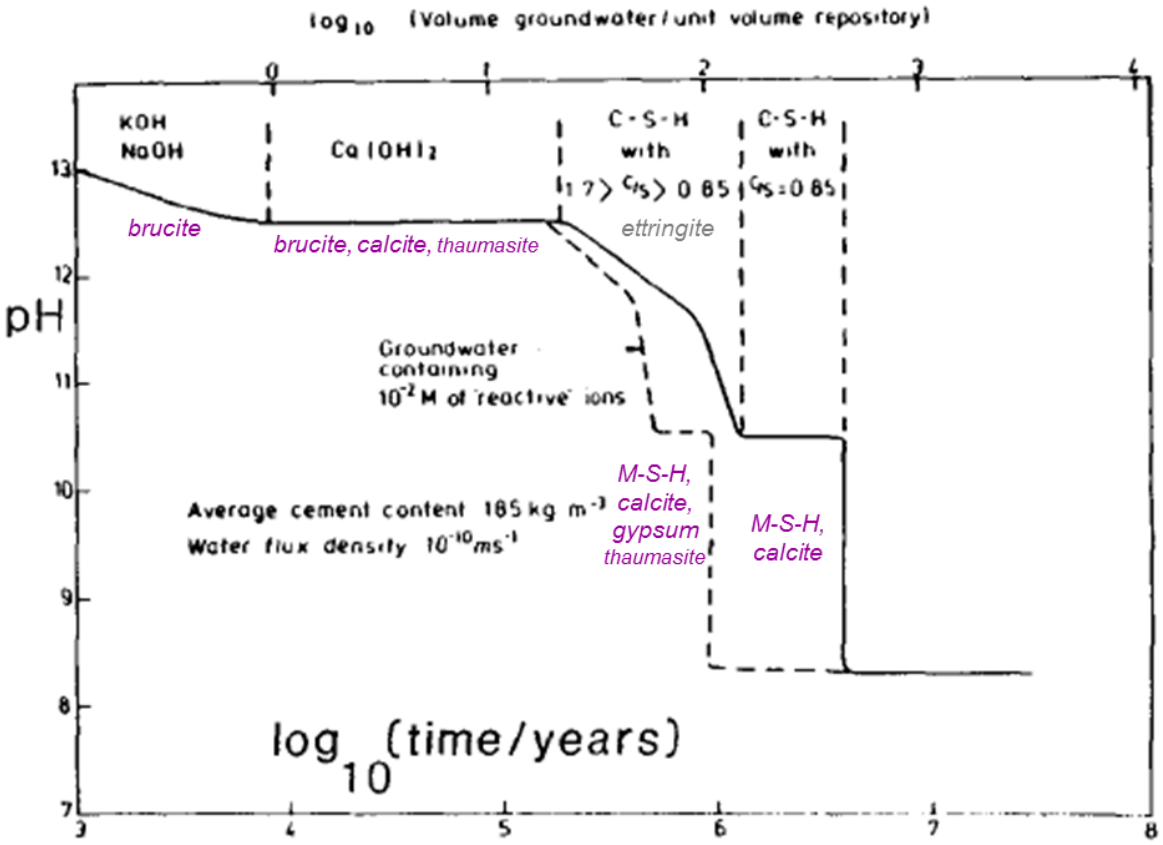

Figure 2-20: The estimated time dependence of pH within a repository of radius 20 m. The phases which control the pH are indicated. The broken curve is for pore water containing 0.01 M of reactive species e.g. Mg^{2+} (Atkinson et al., 1985) and added precipitated and additional dissolved compounds in italics.

In this calculation, the reduction in pH is averaged over the whole repository. A more space dependent calculation also with a ground water flux density of 10^{-10} m/s without reactive species such as Mg^{2+} estimated a progression of a pH=10.5 front of 1 metre for each 15,000 years (Atkinson et al., 1985). These calculations are made with a relatively low cement content of 185 kg/m^{-3}. The concrete buffer has a cement content of 350 kg/m^{-3} (Van Humbeeck et al., 2007) and concrete segments have a cement content of about 400 kg/m^3 (Verhoef et al., 2014). A twice as large cement content would reduce the

progression of the pH front in this calculation by half, i.e. 0.5 metre for each 15,000 years. The biggest game changer might however be the lower ground water flux density of which the value of 10^{-10} m/s was considered an upper limit (Atkinson et al., 1985). The water flux density (hydraulic conductivity in section 2.1.3.2 and 2.1.3.3) is two orders in magnitude smaller. More representative values for the physical transport have been used in Cebama. The progression front of brucite has been calculated to be less than 20 cm after 100,000 years for concrete interfacing indurated clay Callovo-Oxfordian clay (Idiart et al., 2019). After 100,000 years, vitrified HLW has become less radiotoxic than uranium ore (see Figure 1-2).

2.3.1.3 Fracture of the carbon steel overpack

The bentonite buffers for HLW disposal cells in granitic and indurated clay host rocks are continuously compressed by the lithostatic pressure. An ice age can increase the load on these buffers as a function of the thickness of an ice sheet above the geological disposal facility. Further deformation of the bentonite buffers is restricted by the mechanical strength of the carbon steel overpack. This strength decreases by reduction in thickness of non-corroded carbon steel by chemical corrosion. The left carbon steel preferentially cracks in areas where there is empty volume. The 5 mm thickness of the stainless steel canister is too small to accommodate the lithostatic load and will fracture just below the mushroom that was used to lift the canister. Finally at fracture, bentonite in Figure 2-21 has one type of alteration size, i.e. the zone affected by iron corrosion.

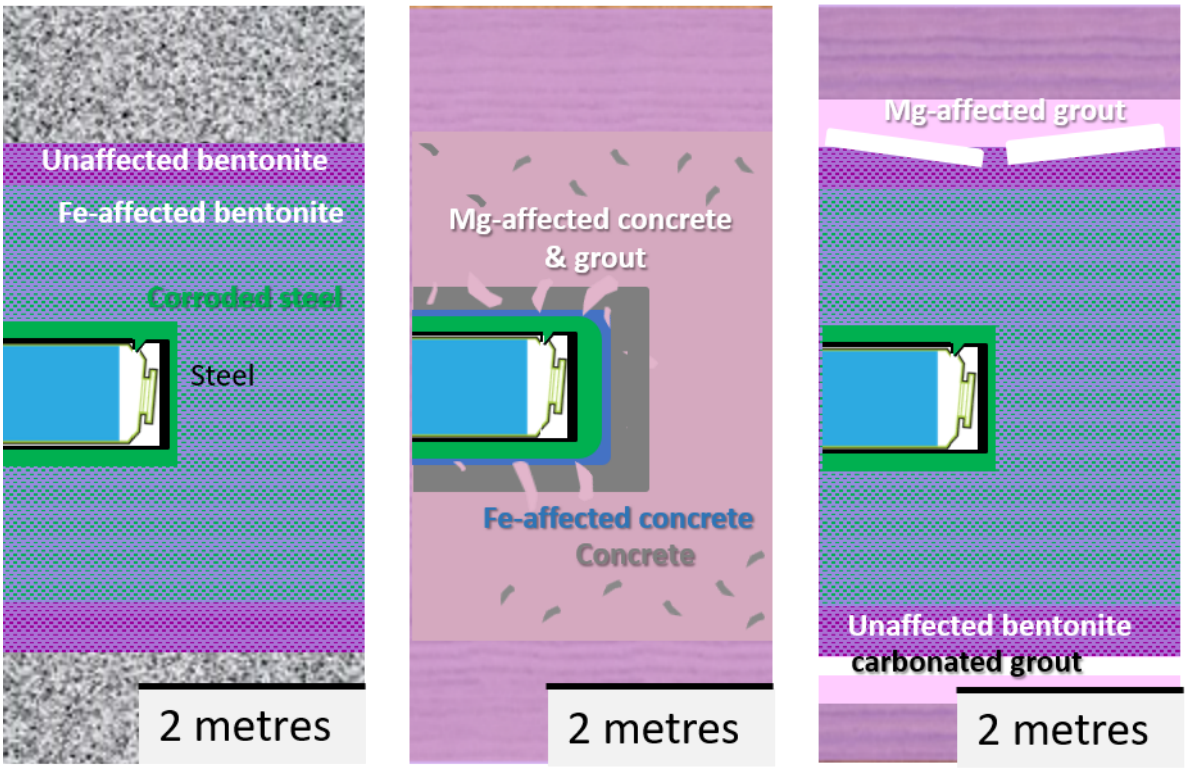

Figure 2-21: Chemically evolved disposal cells after about 10,000s years till 100,000s of years or more containing vitrified HLW for the host rocks: granite, poorly indurated clay and indurated clay. Blue = vitrified HLW, black = left metallic substrate of steel overpack, green = corroded part of steel overpack, unaffected bentonite (purple), Fe-affected bentonite (blueish purple), carbonated grout (white), Fe-affected concrete (blue), unaffected concrete (grey), Mg-affected concrete and grout (pink).

Shotcrete interfacing indurated clay slowly lost its strength by ingress of magnesium from the clay host rock. Gaseous carbonation can increase the strength of concrete, but the carbonated thickness of

shotcrete in the operational phase is considered here to be too thin to prevent fracturing in the post-closure phase. The concrete buffer has two alteration zones: an iron corrosion affected zone, and a zone that has lost its strength by the ingress of magnesium from the clay pore water. Like the bentonite buffer, also the concrete buffer is continuously compressed by the lithostatic pressure of the host rock, but this buffer has its own mechanical strength to prevent deformation. The outer parts of the concrete buffer have lost their strength due to the ingress of dissolved species from the clay pore water. The inner parts of the concrete buffer may still have a high pH, but the iron affected part is assumed to have lost its strength. Only the chemically unaffected concrete part has strength but may be too thin to accommodate the lithostatic load. Consequently, fracture of the carbon steel overpack will be a combination of the reduction in thickness of the carbon steel overpack by chemical corrosion as well as reduction in thickness of the concrete buffer that still has compressive strength. Also, similarly as the carbon steel overpack that was encapsulated in the bentonite buffer, fracture is envisaged at the empty volume between the mushroom and vitrified waste form.

2.3.1.4 After fracture of the stainless steel canister

2.3.1.4.1 Stainless steel

Stainless steel is a high alloy steel that can form different corrosion products than low alloy steel, e.g. carbon steel. Contact between pore water and the stainless steel canister is thermodynamically predicted to generate another spinel corrosion product than magnetite, i.e. chromite ($FeCr_2O_4$). At a similarly low concentration of dissolved iron species as in Figure 2-15, the pH stability region of chromite is larger than that of magnetite, i.e. this spinel phase is thermodynamically stable at neutral pH and the environment needs to be less reducing (Figure 2-22).

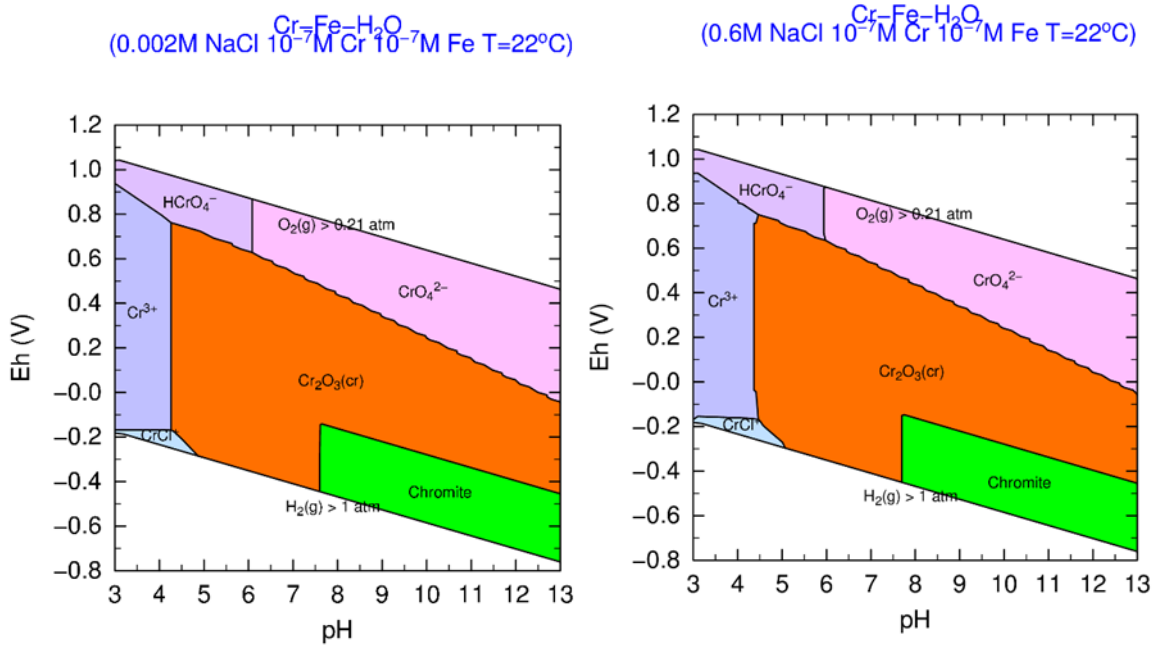

Figure 2-22: Pourbaix diagrams for the system Cr-Fe-H_2O with an activity of dissolved species of 10^{-7} M; 0.002 M NaCl is a reasonable concentration for tap water, 0.6 M NaCl is suitable chlorine concentration for seawater. Chromite (green) is $FeCr_2O_4$(s)[10].

[10] These figures have been made with Phreeplot (Kinniburg and Cooper 2018), a free available software programme that makes geochemical plots using Phreeqc (Parkhurst and Appelo 2013). The SIT database has been used as input for these calculations. This database corresponds to the PHREEQCi version of the ThermoChimie V.7.b, developed by Amphos 21, BRGM and HydAsa for ANDRA, the French National Radioactive Waste Management Agency.

Appendix B shows that chlorine is present in clay and granitic pore water[11]. Chlorine is frequently associated with an increase in the corrosion rate. Chromium-chlorine complexes are already formed at very small dissolved chlorine concentrations but the concentrations for iron need to be much larger than chlorine concentrations for tap water in order to be visible in the Pourbaix diagrams. These chlorine complexes may however not influence the chemical evolution since their presence is in the more acidic regime, even in environments as saline as seawater. Consequently, the small corrosion rates for stainless steel measured in CAST with a maximum of 0.01 µm per year (Mibus et al., 2018) are also assumed at fracture.

2.3.1.4.2 Vitrified waste form

The general picture of the formation on an alteration layer induced by the interaction between glass and water is described in section 2.2.1. Figure 2-23 shows the sequence of layers in this alteration layer[12]. The diffusion and gel layer acts a diffusion barrier. This diffusion barrier is a hydration zone containing silicon. The behaviour of other elements initially contained in vitrified waste highly depends on their solubility. Boron and with some reservations lithium, sodium and molybdenum are highly soluble and most of these elements will be dissipated towards the evolved pore water in the buffer. A reaction layer or alteration layer contains the precipitated products for the elements that form insoluble hydroxides, e.g. iron, aluminium, zinc, titanium or magnesium. The precipitated phases are clay minerals and, in some cases, also zeolites (Conradt et al., 1986). The clay minerals can be smectite clay minerals.

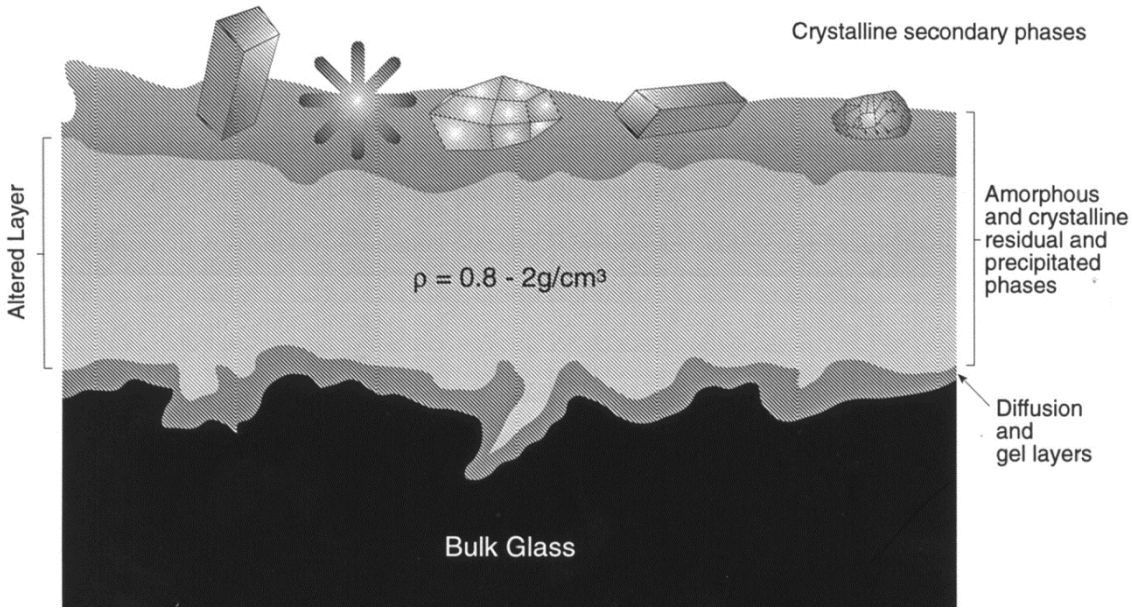

Figure 2-23: Schematic representation of glass alteration with 3 layers that form as glass dissolved in water, from Lutz and Ewing (Havlova et al., 2007) (Milodowski et al., 2015).

[11] Dissolved chlorine does not react with portlandite and C-S-H-phases but the phases containing aluminium such as hydrogarnet. These cement minerals are replaced by Friedel's salt. Friedel salt precipitation is accompanied by a reduction in porosity (Höglund, 2014). This reaction process is not considered harmful for concrete and therefore not discussed in section 2.3.1.2.

[12] Outer / inner reaction layer is the term first used for the observed rims at reacted glass surfaces for experiments performed with leachants (Conrad et al., 1986). Alteration layer is the term used for this rim in EURAD ACED Deliverable 2.5 (Deissmann et al., 2021). The diffusion and gel layers are the hydration zone in (Conradt et al., 1986)

Section 2.1.1.1 explained the presence of cracks in the bulk of the glass after fabrication of the vitrified waste form due to the stress induced by the cooling rate. Closure of these fractures takes place by precipitation of phases. Also, smectite clay further diminishes the ingress of reactive species into the diffusion and gel layers.

There is also a lot of dissolved iron present from the corroding stainless steel canister. The dissolved iron species is positively charged (see Figure 2-15) and can be preferentially sorbed on negatively charged clay minerals, similarly as explained in previous paragraphs for the chemical interaction between bentonite and carbon steel. Figure 2-22 shows that dissolved chromium is present as a negatively charged dissolved complex and is therefore expected to have a less detrimental effect on the alteration layer than dissolved iron complexes, if this alteration layer is mainly made from smectite. Also, the potential high alteration rate is only relevant for the vitrified waste form in the vicinity of steel and not for the bulk.

The dominant Si bearing species in a solution is usually H_2SiO_3 but changes at a pH higher than 10 into $HSiO_3^-$ (Conradt et al., 1986), and the solubility of SiO_2 is then increased. The 4th framework programme indicated that this silicic acid dissociation starts at a pH > 9 (Vernaz et al., 1996). In the 5th framework programme, it has been elucidated that the dissolved silica concentration at saturation exponentially increases from a pH beyond 9, but that the measured dissolved silica concentrations at saturation are smaller than the calculated ones (Ribet et al., 2007). In section 2.3.1.1, it was explained that the iron corrosion process of carbon steel can locally increase the pH up to 10, due to insufficient dissipation of the formed hydroxyl-ions. The vitrified waste form is interfacing stainless steel. The long-term corrosion rate of stainless steel can be ten times smaller than the corrosion rate of carbon steel and is therefore envisaged to induce a smaller increase in the local pH.

There may also be contact between pore water with a pH higher than 10 and the vitrified waste form for the disposal cells containing initially cementitious materials, provided that the chemically evolved concrete has sufficiently lost its mechanical strength. An alteration layer that limits further dissolution of the vitrified waste form is always generated whatever pH the vitrified waste form is exposed to. However, these layers are more effective at neutral pH than at high pH. Chemisorption of iron occurs by the generated clay minerals in the vicinity of corrosion products[13]. Ion exchange reactions are proposed as the rate controlling processes. The presence of solid clay in the leachant is therefore known to enhance the dissolution rate since the sorption of the less soluble elements aluminium, iron and zirconium takes place. Corrosion products have the same influence (Vernaz et al., 1996; Van Iseghem et al., 1992). Corrosion products such as chromite (Souza et al., 2012) and magnetite (Kim et al. 2001 in Eisele et al., 2005) are also negatively charged at pH conditions representative for disposal and therefore also preferentially sorb these less soluble elements.

The glass alteration process requires water; the influx of water into the fractured stainless steel is restricted by diffusion for the disposal cells in clay host rocks. The influx of water in these canisters for disposal cells in granitic host rocks depends on the properties of the altered bentonite buffer; e.g. cracks are expected to be present due to chemical interaction with dissolved iron.

[13] Recently, a Nature paper has been published in which a self-accelerating corrosion process of stainless steel canister with vitrified waste is described (Guo, et al., 2020). The oxidizing conditions and 90°C are not considered representative for the geological disposal conditions considered in Europe in which reducing conditions in host rocks are frequently used as a siting criterion in order to have a small solubility of released radionuclides and the waste has cooled down till the disposal depth temperatures upon fracture of the stainless steel canister. Mechanical fracture in section 2.3.1.3 instead of pitting corrosion in this Nature paper is therefore considered as a mechanism for fracture of the stainless steel canister with which contact between pore water and vitrified waste form has been established. For ACED, the potential entrapped oxygen between the stainless steel canister and carbon steel overpack due to the fabrication of these containments is assumed to have a negligible role on the chemical evolution.

2.3.1.4.2.1 Impact of alteration of glass on the mechanism for radionuclide release

The radionuclide release from the vitrified waste form is not studied in ACED but some basic rules can be suggested. For the radionuclides that are still left, the altered glass contains clays and zeolites that can also sorb dissolved cationic complexes. These cationic complexes are expected to be sorbed and very limitedly leave the fractured corroding evolving stainless steel canister. The glass alteration has therefore a very small impact on the potential radionuclide release, if the radionuclides are dissolved as cationic complexes. The released amount of plutonium, americium and radioactive caesium in solutions is only a fraction of the initially contained amount as has been measured in the 3rd framework programme (Van Iseghem et al., 1992).

Dissolved anionic complexes are not expected to be contained by the reaction layer. An example of a radionuclide that can be present in the vitrified waste form and becomes present as a dissolved anionic complex is ^{79}Se. The amount of ^{79}Se left at fracture of the stainless steel canister may also be limited due to the required period for fracture and a half-life of 327,000 years (IAEA, 2020). The pore water in the bentonite buffer as well as the evolved concrete buffer are saturated with silica. Alteration rates of basaltic glass, the natural analogue for a borosilicate waste form, have estimated to be 0.1 µm per 1000 years in these saturated environments (Lutze et al., 1987). Consequently, most of the left ^{79}Se is expected to decay within the vitrified waste form and not released to the surroundings.

2.3.2 ILW disposal cells

The radiological content in ILW packages is orders in magnitude smaller than in HLW packages. For example, the radionuclides contributing most to the radioactivity for CSD-c are, like CSD-v, also ^{137}Cs and ^{90}Sr. The guaranteed maxima are 65 TBq for ^{137}Cs and 115 for ^{90}Sr (COGEMA, 2001), i.e. about two orders in magnitude smaller than CSD-v that had 6600 TBq for ^{137}Cs (see section 2.3.1). For vitrified HLW, radiation enhanced corrosion in water can be excluded after a cooling period of 90 years, i.e. an ^{137}Cs activity of about 800 TBq. Consequently, radiation enhanced corrosion of metallic ILW is excluded to have an impact on the chemical evolution of an ILW disposal cell,since the required radiation dose rate for radiation enhanced corrosion are lowest for steel exposed to water. The radiological content of organic ILW such as spent ion exchange resins is smaller than CSD-c, for example two orders in magnitude (Verhoef et al., 2016). The most common form of resins, polystyrene divinylbenzene, is radiation resistant. Radiation enhanced degradation of these resins is therefore also excluded to have an impact on the chemical evolution of disposal cells.

Cementitious processing of metallic and organic ILW reduces the likelihood of microbial activity due to its high pH as explained in Chapter 2. Limiting microbial activity by space restriction within the cementitious matrices depends initially on the fabricated porosity. The waste package mortar can be manufactured with a similar cement content, additives and similar grading in aggregates as the concrete buffer. In those cases, microbial activity is also limited in waste package mortar. The fabricated porosity is larger in cementitious materials without aggregates or a lower content of aggregates with more limited grading in aggregates. The connecting pore throats in these cementitious materials may be too large to limit microbial activity. This activity can also be positive for example for the precipitation of biogenic calcite, which can make concrete stronger. For now, it is assumed that ingress of bicarbonate and magnesium into the liner made of shotcrete in granitic rocks (see Figure 2-8), which started in the operational phase, continues in the post-closure phase. The liner is expected to fracture after the start of the post-closure phase, due to continued replacement of calcium-binding phases by magnesium phases, by which the zones in which the strength of concrete is lost have progressively grown as explained in section 2.3.1.2.

The EDZ generated in granitic rock in the construction phase had generated sufficient fractured material to eliminate the initial gap between shotcrete and crushed rock by creep. The crushed rock is soon saturated with granitic pore water through fractures in granitic rock and shotcrete. The advective water flow of granitic pore water within crushed rock generates a continued refreshing of granitic pore water at the caissons. This preferential flow path of granitic pore water also makes that cement leachates are removed from the disposal facility. These leachates can react with the siliceous phases and secondary mineral precipitation in the fractures of the rock takes place that might even lead to clogging within fractures (see section 2.2.6). Figure 2-24 shows the chemically evolved disposal cells.

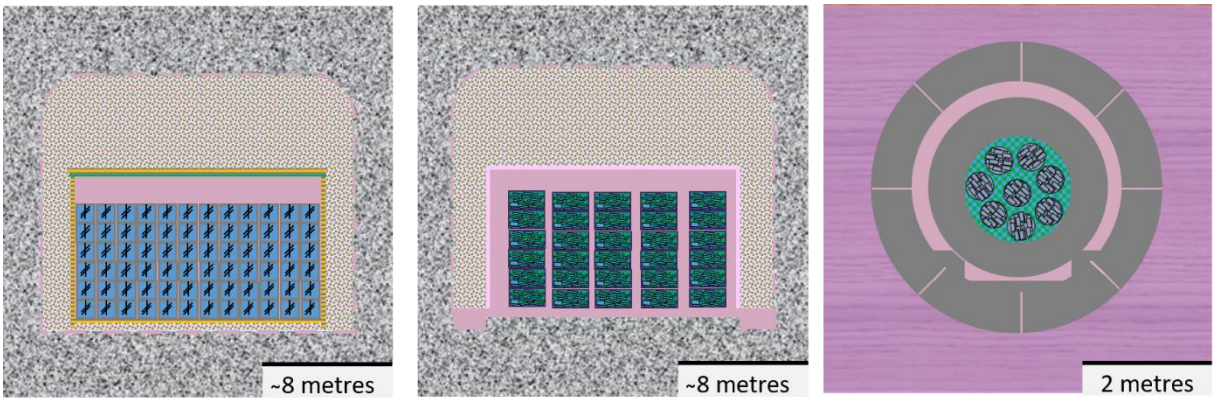

Figure 2-24: Chemically evolved disposal cells after about 10s of years till 1,000s of years containing cemented ILW considered in Europe for the host rocks: granite and poorly indurated clay. Blue = ILW or cemented ILW, black = steel, green & pink = crushed rock with granitic pore water, pink = Mg-affected grout, green = Fe-affected grout and corrosion products, unaffected concrete (grey).

For the reinforcement in caissons, it depends on the depth of the disposal facility how much oxygen is present in the granitic pore water. In case of anaerobic granitic pore water, anaerobic corrosion of the reinforcement bars is assumed. The initial pathway of granitic pore water within the caissons is assumed to be at the lid. The ingress of magnesium and bicarbonate in the caisson replaces the cementitious minerals by calcite, brucite and M-S-H phases. This continued replacement of calcium-binding phases by magnesium phases by which the zones in which the strength of concrete is lost has progressively grown as explained in section 2.3.1.2. The loss in strength is accompanied by a permeability increase that also favour the ingress of dissolved species from host rock pore water into concrete.

Chemical corrosion of the metallic materials in metallic ILW results into an alteration layer of corrosion products. The thickness of this layer hardly changes in case of anaerobic corrosion, since the corrosion process is controlled by the dissolution of the alteration layer. The dissolved metallic compounds are sorbed by cement minerals, by which an alteration zone within the grout is formed. Similarly, as explained earlier for HLW disposal cells, this Fe-affected zone is assumed to have a smaller strength than fabricated concrete.

The left image in Figure 2-24 shows the evolved ILW disposal cell containing spent ion exchange resins. Diffusional flow of water into the waste containers is envisaged along interfaces. The oxygen trapped during fabrication is consumed by chemical corrosion of the stirrer or traces of pyrite present in the cementitious matrix; microbial activity is limited due to the high pH. The porosity of the cementitious matrix is considered to be too high to obtain a local reduction of oxygen at the corroding stirrer. After oxygen consumption, anaerobic corrosion may have started in the operational phase since the saturation degree of water in the cementitious matrix after processing of 90% is sufficiently high for corrosion of steel. The corrosion process can stopduring the operational phase, if the consumption of water by the corrosion of the stirrer is not sufficiently supplemented by inflow of water into the container. Anaerobic corrosion of the steel container and sacrificial stirrer for the spent ion exchange resins processed with a cementitious matrix continues in the post-closure phase. The cementitious matrix is considered to be sufficiently porous in order to have the evolved hydrogen gas to be dissipated by diffusion. The same processes as described in sections 2.2.2 and 2.3.1.1 and shown in Figure 2-16 for the concrete-steel interface will take place.

2.3.2.1 Organic ILW

Organic materials in organic waste can act as food for the growth of microbes. These organic materials are altered into another form when used as food. This alteration can have an impact on the potential radionuclide release. The MIND project classified the organic waste into two groups (Abrahamsen et al., 2015):

1) addition polymers that are resistant to biodegradation for example polystyrene, polyethylene and polyvinylchloride;
2) condensation polymers that are susceptible to biodegradation for example cellulose.

Resins are polystyrene polymers as explained in section 2.1.2.1. There is no energy for microbes to be obtained upon their degradation of these resins (Abrahamsen et al., 2015). Consequently, microbial degradation of resins is excluded. Organic ILW was mainly specified as spent ion exchange resins, except in the French programme (Neeft et al, 2019).

Wood, clothing and paper is made of condensation polymers such as cellulose. Contaminated tissues and clothing are usually contact-handled waste and can rather be characterised as LLW. The formation of iso-saccharinic acid (ISA) during cellulose chemical degradation at alkaline conditions is important for the potential radionuclide migration as it forms soluble complexes with radionuclides. The hazard potential of LLW is however smaller than ILW.

Cemented resins have been investigated in CAST (Norris and Capouet, 2018) and are to be studied in the EURAD WP Cement Organic Radionuclide Interaction (CORI) (Altmaier et al., 2021). Chemical degradation of polymers is initiated by a nucleophilic attack of OH^- ions on a carbon atom with a positive

partial charge. Such carbon atoms are generally not present in addition polymers (Van Loon and Hummel, 1995). The chemical resistance of resins is high. A degradation rate of resins representative for the disposal conditions is therefore not yet available. Chemical degradation of resins can therefore be excluded as a factor for release of radionuclides such as carbon-14 (Capouet et al., 2018). Resins are like clays exchangers and any radionuclide release is expected to require sufficient ingress of anions and cations that have a stronger affinity than the sorbed anionic or cationic radionuclides (Neeft, 2018). For example, sulphate has a very strong affinity (IAEA, 2002) and sufficient ingress of sulphate at these resins will cause an exchange of sorbed anionic radionuclides.

2.3.2.2 Metallic ILW

2.3.2.2.1 Steel

The middle image in Figure 2-24 shows the stacking of containers with metallic waste made of steel. The entrapped oxygen is expected to be consumed at a very fast rate. There is insufficient inflow of water into the container for anaerobic corrosion of all steel surfaces in the operational phase, and therefore microbial as well as chemical corrosion is expected to be stopped. In the post-closure phase, there can be sufficient inflow of water in ILW disposal cells in granitic host rocks for anaerobic corrosion of this waste. The interaction between neutron irradiated Zircaloy and neutron irradiated steel and cementitious pore water have been investigated in the CAST project from the FP7 programme (Williams and Scourse, 2015; Norris and Capouet 2018). The speciation of radionuclides released from these waste forms can be studied in cementitious pore water while it is more complicated to study this speciation for metallic material interfacing concrete. Special care has been taken to simulate cementitious pore water, i.e. calcium saturated solutions have been used (e.g. Necib et al., 2018;Cvetković et al. 2018). The calcium-iron spinel type was thermodynamically more stable than magnetite in pore solutions containing calcium as shown in Figure 2-15 with which it is assumed that the dissolved calcium is crucial for the corrosion process of carbon steel. The spinel-type chromite calculated in Figure 2-22 is, however, also in calcium-saturated solutions of 0.02 M Ca^{2+} thermodynamically more stable than $CaFe_2O_4$. It is therefore expected that, unlike carbon steel, the dissolved amount of calcium in the pore solution has a negligible influence on the corrosion process of stainless steel. Another benefit of the performance of corrosion experiments with cementitious pore water is that the measurement of the hydrogen release from steel can be used to determine the anaerobic corrosion rate. In CAST, these corrosion rates measured in cementitious pore water had a maximum of 0.01 µm per year (Mibus et al., 2018). The hydrogen generation rate depends on the surface area of metallic waste that can be in direct contact with the pore water and corrosion rate. However, the long-term hydrogen generation rate cannot be larger than the consumption rate of water. Transport of water in the ILW disposal cells is therefore essential to determine long-term hydrogen generation rates.

2.3.2.2.1.1 Impact of alteration of steel on the mechanism for radionuclide release

There can be radionuclides present in steel waste as a result of contamination as well as neutron activated radionuclides . Most short-lived radionuclides have disappeared due to decay. The remaining radionuclides as a result of contamination diffuse through the concrete in the moment corrosion has started. The remaining neutron activated radionuclides have a similar release pattern as described for the vitrified waste form (see section 2.3.1.4); the radionuclides that become present in a cationic dissolved form in the corrosion process will be sorbed by corrosion products in the altered or reaction layer. The radionuclides that become present in anionic dissolved form in the corrosion process can be sorbed by cement minerals, if the pH of the concrete pore water is higher than 11.8, since the zeta potential is positive at these pH values (see section 2.3.1.2). These dissolved anionic complexes, however, compete with sorption of the metallic-dissolved complexes in equilibrium with the corrosion products.

2.3.2.2.2 Zircaloy

For the disposal cell in poorly indurated clay, e.g. the right image in Figure 2-24, the preferential flow of clay pore water into the cell is through the joints between concrete segments. The ingress of magnesium and bicarbonate into the cementitious materials in the disposal cell is expected to take place at a very small speed, but initially faster than in the HLW disposal cells, since there is no heat source desaturating these materials. The reaction fronts are similar as described in 2.3.1.2 and Figure 2-20. The consumption of entrapped oxygen by chemical corrosion of the canister or traces of pyrite present in the mortar may have been completed in the operational phase and the porosity of the mortar may be too large to generate a local reduction of oxygen at the corroding canister surfaces. If the mortar has a too large porosity to render microbial activity through space restriction, microbial activity within the mortar is still limited due to the high pH. Anaerobic corrosion may have started in the operational phase since the saturation degree of water in the mortar after processing of about 90% is sufficiently high for the corrosion of any metal. The corrosion process can stop during the operational phase, if the consumption of water by metal corrosion is not sufficiently supplemented by inflow of water into the container. This anaerobic metal corrosion continues in the post-closure phase due to diffusional flow of water from the grout backfill into the concrete container. The preferential pathway is at the top of container, e.g. at interfaces with a lid. There are two possibilities to have contact with pore water and the metallic waste inside the stainless steel canister:

- Uniform corrosion of the canister walls has been completed. Mechanical support against lithostatic load is provided by a sufficient thickness of the concrete container that has ample strength;
- Non-completed uniform corrosion combined with mechanical failure of the stainless steel canisters since the thickness of concrete with sufficient strength became too small to provide sufficient mechanical support against the lithostatic load.

With a maximum of 0.01 µm per year as measured in CAST (Mibus et al., 2018), it would take thousands of years for a complete uniform corrosion of the 5 mm stainless steel wall. The second possibility requires a zonal progression of reaction fronts and the knowledge about the mechanical strength of concrete in each zone. The Cebama modelling results showed a progression front of brucite of less than 20 cm after 100,000 years for concrete interfacing indurated clay Callovo-Oxfordian clay (Idiart et al., 2019). Assuming loss in strength of concrete with this progression front, the second possibility is more likely, i.e. non-complete uniform corrosion combined with mechanical failure of stainless steel for clay pore waters with a high magnesium content such as in France, Switzerland and Netherlands (see Appendix B). Belgium has however, a far smaller magnesium content; then the first possibility would be more probable, i.e. complete uniform corrosion of the canister walls.

Contact between pore water and compacted hulls will cause anaerobic corrosion of Zircaloy. The surface charge of the resulting corrosion product is unknown and therefore a credit to sorption of the radionuclides contained by Zircaloy cannot be provided. The corrosion rates are however very small, i.e. below 1 nm per year (Necib et al., 2018). These very small corrosion rates can also be understood from thermodynamic data. Figure 2-25 shows that the solution is supersaturated at Zr concentrations of 10^{-7} M. At these concentrations of 10^{-7} M, a pH dependent stability field for magnetite for carbon steel (see Figure 2-15) or chromite for stainless steel (see Figure 2-22) could be seen. The dissolved Zr complexes are not visible despite a larger range in pH from 1 to 13 for the Zr speciation instead of 3 to 13 used for the Fe and Cr speciation. Calculation of a pH dependent stability field for the alteration layer of Zircaloy requires far smaller concentration than carbon steel and stainless steel.

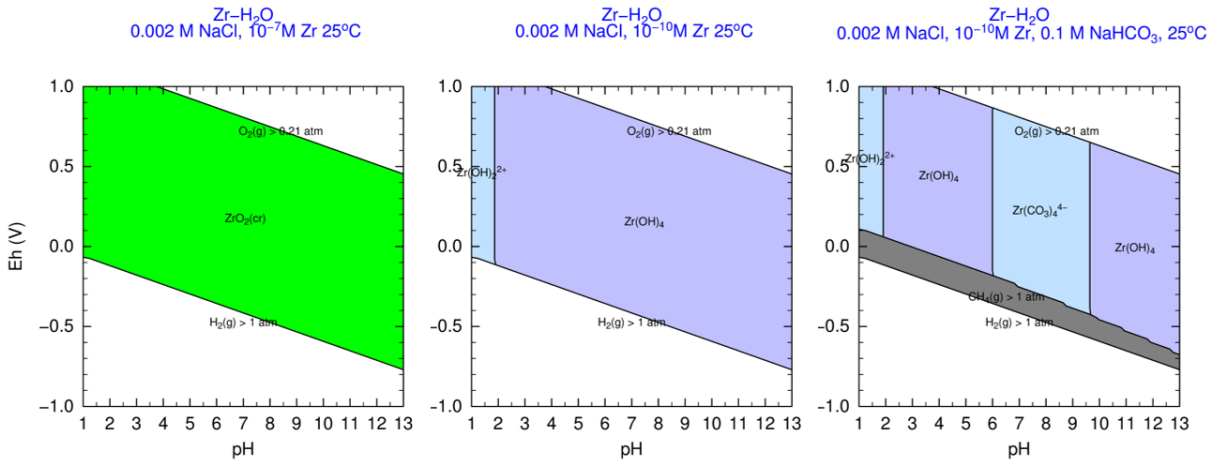

Figure 2-25: Pourbaix diagrams for the system Zr-H_2O with an activity of dissolved species of 10^{-7} M; 10^{-10} M, 0.002 M NaCl is a reasonable concentration for tap water and 0.1 M $NaHCO_3$ is an assumption for clay pore water (see Appendix B). $Zr(OH)_4$ (light purple) is $ZrO_2 \cdot H_2O$ in Gras (2014)[14].

The ingress of bicarbonate from the clay pore water has an impact on the stability of the alteration layer and active corrosion would be present at concentrations of 10^{-10} M at a pH < 10 (see Figure 2-25, right image). The predominant dissolved carbonate species changes from HCO_3^- to CO_2 at a pH of about 6.4. Dissolved zirconium-carbonate complexes cannot be made with CO_2. Consequently, the impact of bicarbonate on the Zircaloy corrosion rate becomes negligible at a pH < 6.4.

Like steel as calculated in Figure 2-15, calcium has also been noted to have an effect. However, in this case it is a negative effect since the presence of dissolved calcium reduces the stability of the passivation layer of zircaloy (Gras, 2014), by which the corrosion rate increases. The required calcium concentrations of at least 0.05 M to have an effect on this stability may, however, not occur. Cementitious pore water usually have a smaller calcium concentration than host rock pore water and the host rock pore waters do not exceed this required concentration of 0.05 M (see Appendix B).

2.3.2.2.2.1 Impact of alteration of Zircaloy on the mechanism for radionuclide release

The small corrosion rates below 1 nm per year as found in CAST for cementitious pore water (Necib et al., 2018), would make that most radionuclides generated by neutron activation will decay within the cladding and are not released to the surroundings. These corrosion rates would initially be representative for disposal in a clay host rock with a minor concentration of magnesium such as the Belgian case, since the concrete surrounding the canister can limit the ingress of bicarbonate from the clay pore water towards Zircaloy claddings. Higher corrosion rates are foreseen when the bicarbonate concentration at the Zircaloy claddings become larger. The radionuclides, however, may also be absent at that time.

Unlike steel, the generated hydrogen has no impact on the radionuclide release since most of the generated hydrogen is not released but picked-up. The Japanese studies measured a hydrogen pick-up of at least 90% at 30 °C, when Zircaloy is exposed to alkaline water as well as pure water. The hydrogen pick-up decreases with increasing temperature (Sakuragi, 2017). Unlike steel, a hydrogen measurement from an experiment of Zircaloy in (cementitious) pore water will underestimate the corrosion rate since uptake of hydrogen takes place. The possibility of hydride formation in any type of

[14] These figures have been made with Phreeplot (Kinniburg and Cooper, 2018), a free available software programme that makes geochemical plots using Phreeqc (Parkhurst and Appelo 2013). The SIT database has been used as input for these calculations. This database corresponds to the PHREEQCi version of the ThermoChimie V.7.b, developed by Amphos 21, BRGM and HydAsa for ANDRA, the French National Radioactive Waste Management Agency.

metal has been known for many decades (Lacher, 1937). For iron, hydride formation is not expected. It has been found that tritium diffuses through stainless steel in a reactor environment at a high rate, the rate being significantly higher than tritium diffusion through zirconium alloys (IAEA, 2004). High diffusion rates can be attributed to an insignificant hydride formation.

3 How to gain information on the chemical evolution

The conceptualisations of the chemical evolution of disposal cells have been extracted from understanding the experimental results from a geological disposal perspective. Measurements can be performed on materials in contact with geological disposal representative environments. Determination of the representativeness of these environments requires quantification of the radiological, chemical, physical properties of these materials as well as their environments. There is a lot of literature available with experimental results in which this quantification, for example, radiological quantification, has not been performed. This lack in quantification makes the use of these literature sources for the conceptualisation of the chemical evolution of disposal cells purely hypothetical. It may be very likely that the described processes do not occur. For example, a too high radiation dose rate had been used, or the concentration in dissolved chemical species to which materials have been exposed are too low (for example distilled water, lack in dissolved silica) or too high. Also, many measurements have been performed under unrealistic physical conditions from a geological disposal perspective, for example, polished surfaces of metals. Polishing of metallic ILW is never done before disposal, there is usually an existing oxide layer on these metals that limits the corrosion rate. Research time is then devoted into generation of this oxide layer that already exists. The experimental results obtained in this period may not be representative for disposal of waste. The experimental period may be too small to observe the processes relevant for disposal. Archaeological or natural analogues give experimental evidence over time scales (much) longer than is typically available in laboratory or in-situ experiments and therefore described first in this Chapter in gaining information on the chemical evolution.

3.1 Archaeological and natural analogues

The information that can be gained from analogues highly depends on the amount of activities that are performed in this area. A natural analogue working group was working in the 3rd and 4th framework programme and most studies were focussing on representative studies for radionuclide migration. NaNET in the 5th framework programme included more work on the durability of materials. They had made an analogue matrix for the near-field with analogues for each barrier, and such a matrix for the far-field with analogues for radionuclide migration in different types of host rocks. The analogue matrix for the near-field contained a specific section of the degradation of the engineered barriers (Nanet, 2006). Currently, the natural analogue working group operates without funding by the European Commission. Their website (www.natural-analogues.com) aims to contain all the available information on analogues.

The archaeological and natural analogues described in this report are limited to the alteration mechanisms of engineered materials used in the disposal cells and types of waste discussed in this report. The described analogue studies can be used for the description of a conceptual model for their alteration mechanism in the chemical evolution of the disposal cells. The alteration rate during disposal can in some cases also be determined from natural analogues, provided that the key components for their alteration are understood and are representative for disposal. Frequently, however, the initial and boundary conditions are not known in sufficient detail to determine this rate. Analogue studies can be used to verify the mathematical models that are used to assess the chemical evolution on the long-term, i.e. are the processes sufficiently understood.

3.1.1 Vitrified waste form

Of all natural volcanic glasses, basaltic glass has a similar SiO_2 content as the vitrified waste form (e.g. (Lutze et al., 1987; Laciok, 2004; Havlova et al., 2007). The alteration mechanism of basaltic glass is the same as expected for the vitrified waste form, except that the alteration product is named differently, i.e. palagonite, which is a mixture of clay minerals and zeolites. Palagonite occurs as rims of varying thickness around glass fragments. Fe-rich smectites are abundant for basaltic glass interfacing

sediments (Fe-Mg saponites being the most common) and zeolites are common in both fresh water and sea water altered basaltic glass. These rims are representative for the glass passivation layer that is formed when vitrified waste is exposed to pore water. The alteration rate depends on dissolved silica concentration. Clay pore water is saturated in dissolved silica (see Appendix B) and then alteration rates of 0.1 µm per 1000 years are representative. The rate of palagonitization highly depends on temperature, doubling for every 12 °C increase, which is similar to the 'palagonitization' of borosilicate glass, in which a doubling for the alteration rate of 10 °C has been found. The measured rate at 100 °C was 3 µm per year (Lutze et al., 1987).

There are also two main differences between natural glass and vitrified waste forms: there is no natural glass that has the same high boron content or radionuclide content as the vitrified waste form. These differences may however have no influences on the alteration mechanism since:

1) The release of boron from vitrified waste form does not give a representative glass dissolution rate, since boron is not contained in the glass passivation layer (Conradt et al., 1986). Consequently, boron does not take part in a representative glass degradation mechanism;
2) Glass is a metastable solid with no clear crystalline structure in which atoms can be displaced from their lattice position to weaken its strength. As explained in section 2.1.1.1, the temperature of glass at disposal is too high to have remnants of radiation damage that are detrimental to the physical resistance of glass. Radiation rather works as a network modifier. The high radionuclide content is only a chemical additional feature and that is also present in natural glass. Radioactive and nonradioactive glasses have the same corrosion time- and temperature dependence (Vernaz et al., 1996).

The alteration rates measured for natural basaltic glasses are also more representative for disposal than archaeological glasses, since the exposure environments of archaeological glasses are more near the surface and less representative for deep disposal with, for example, a higher water circulation and oxygenated conditions (Laciok and Dalton, 2005).

3.1.2 Steel

There are mainly archaeological analogues for steel, since native iron rarely occurs, e.g. upon precipitation from a Fe-rich magma that has been isolated from groundwater, it is usually incorporated into various oxides and silicate compounds. An exception is Disko Island (Greenland) in which native iron has been coated by micrometer sized magnetite and goethite layers (Ahonen, 2004a). The most famous archaeological analogues are the 2000 year old iron nails from Inchtuhil (Scotland) that clearly provided the evidence for the difference in corrosion rates at oxidising and reducing conditions (Hooker, 2003c). There are also many other examples that elucidated this feature including the impact of cementation and the presence of sulphides (Crossland, 2005; Dillmann et al., 2014). The corrosion behaviour of carbon steel has the same behaviour as iron, there are just more slag inclusions in iron than in steel.

The understanding of the corrosion process for carbon steel and interaction with the relevant surrounding media clay and concrete that are described in paragraphs sections 2.2.2, 2.2.3 and 2.3.1.1 could not have been made without the described archaeological analogues (Neff et al., 2004; Chitty et al., 2005). The determination of corrosion rates may, however, not be as exact as can be determined from laboratory experiments, since the corrosion rates are determined with the amount of measured iron near the interface, but the clay and cementitious material can also contain iron, i.e. may not be corroded iron, and the dimensions of the iron specimens are not always known. In addition, the initial corrosion process can have a corrosion rate that is three orders in magnitude larger than the steady state corrosion process. The long-term corrosion rate can then be easily overestimated if the total corroded amount is attributed to the whole period.

Stainless steel has a higher corrosion resistance than carbon steel due to the alloying of iron with chromium, nickel and molybdenum. It is a new material for which any archaeological analogue would

not be as old as previously described for carbon steel. The corrosion product, chromite, is however frequently found, e.g. in mafic and ultramafic rocks (Ahonen, 2004b). Research on such naturally occurring compounds revealed that solid solutions of these spinel types frequently exist and that these types are hard to distinguish with Raman spectroscopy; additional chemical analysis is necessary to identify the chemical compositions of spinel (Wang et al., 2004). These natural analogue studies put the laboratory studies performed in the eighties on carbon steel in a slightly different perspective (Naish et al., 1991), since only Raman spectroscopy was used to identify the corrosion product but its chemical composition can be slightly different from pure magnetite that also have a spinel type structure e.g. magnetite containing traces of calcium or perhaps even $CaFe_2O_4$.

3.1.3 Bentonite

Bentonite is an abundant material usually formed by hydrothermal alteration of lavas; there are bentonite mines to explore this material. For disposal, bentonite is compressed in order to achieve a sufficient high density to limit microbial activity (see section 2.1.1.3), water saturated, in a chemical reducing environment. In the early post-closure phase, there is also a thermal transient and associated dehydration. In NaNET, characteristics of a few deposits have been identified (Nanet 2006):

1. deposits which have been intruded by small igneous bodies to generate a thermal peak approximating the thermal transient from the waste;
2. deposits in contact with deep, reducing groundwaters, where groundwater bentonite interactions can be studied;
3. naturally compressed bentonite, where its long-term hydraulic properties may be investigated; and
4. deposits, where bentonite is in contact with other materials, which are analogues to components of the engineered barrier system to investigate possible interactions.

The thermal effect found in natural analogues in Isle of Skye (Scotland) (Wouters and Verheyen, 2004), Col du Perthus (France) (Trotignon et al., 2004), Busachi (Italy) (Wouters et al., 2005a) and Kinnekulle (Sweden) is the transformation of montmorillonite into illite (Wouters et al., 2005b). The understanding of this transformation indicated that a sufficient supply of potassium is needed for this transformation. Appendix B shows that granitic and clay pore waters are deficient in potassium, but cementitious pore waters are not. The inflow of granitic pore water into bentonite is limited due to desaturation of the buffer by the heating power of the waste. The mineralogical transformation is therefore negligible for HLW disposal cells in granitic host rocks (Hedin et al., 1999) but this transformation could be relevant for the bentonite-shotcrete interface for HLW disposal cells in indurated clay host rocks and concrete-poorly indurated clay interfaces.

Concerning the second aspect, all poorly indurated clay formations at disposal depth are considered suitable analogues such as the Boom Clay and Ypresian Clay formation, since the main clay mineral in poorly indurated clays is smectite and no mineral transformation is induced by the reducing conditions.

The analogue for the third aspect is the Dunarobbe Forest (Italy). This analogue is a collection of more than 2 million year old trees that had been preserved in compacted clay, due to the prevailing anaerobic conditions, limited nutrient supply and diffusion dominant transport regime. The trees were protected against microbial degradation and had therefore cellulose contents similar to present-day wood (Lombardi and Valentini 1996; De Putter, et al. 1997; Hooker, 2003a).

The analogues to investigate the possible interactions between bentonite and other components of the engineered barrier system are for the investigated disposal cells limited to carbon steel and concrete. The interaction between soil and iron (Neff et al., 2004) could be suitable analogues, but the focus was mainly on the iron and less on the clay minerals in the soils. Interaction with concrete is described in the next paragraph.

3.1.4 Concrete

3.1.4.1 Durability

The natural analogue for Ordinary Portland cement (OPC), which is the main component for CEM-I based cement, is the generation of lime (CaO) by limestone or chalk and a thermal source, i.e. metamorphism, and that this lime came in contact with groundwater. The Maqarin (Jordan) natural analogue project provided the evidence of three concrete leaching stages as identified earlier (see Figure 2-11 and Figure 2-20: a high pH Na/KOH leachates, $Ca(OH)_2$ buffered and silicate-dominated leachates. This analogue also shows the formation of thaumasite (Kamei et al., 2010) except that thaumasite was here a fracture filling mineral (Milodowski et al., 2015) rather than a mineral that deteriorates concrete by its expansive crystallisation volume as modelled for geological disposal facilities (Höglund, 2014). When the limestone contains silicates such as flint nodules or chert, the metamorphism can result into calcium-silicates such as larnite (β-Ca_2SiO_4) that upon hydration form C-S-H gels. Scawt Hill (Northern Ireland) is such a location in which C-S-H gels have been formed about 58 million years ago. This analogue also showed that precipitated calcite as a result of carbonation may surround C-S-H gels by which these poorly-crystalline gels are protected from further carbonation (Knight, 2003).

The past Roman Empire has left a lot of archaeological concrete in Europe. One of the most famous concrete structures showing the durability of concrete is the Pantheon in Rome (see Figure 3-1). Although exposed to ordinary air for almost 1900 years, it clearly shows that carbonation of concrete may not impact its performance if well engineered. The inside of the dome is a perfect analogue for the operational phase of the disposal facility in which the performance of the lining in the disposal facility can be hardly affected by carbonation.

Figure 3-1: Unreinforced concrete dome of the Pantheon in Rome was built in about 120 AD and retains its structural load-bearing integrity 1900 years later. Source: Neil Chapman.

The outside of the dome is exposed to weathering waters; the resulting leaching process is representative for disposal, if the dissolved calcium concentration in host rock pore water is smaller than this dissolved concertation in concrete pore water. This case is present for some countries (see Appendix B).

3.1.4.1.1 Cement

The durability of Roman concrete has been attributed to rigid quality control, low water to cement ratio, expert placement and compaction and the type of cement. Many Roman concrete is made of cement in which a part of the lime (CaO) has been replaced by natural pozzolans (Rassineux et al., 1989). Natural pozzolans are siliceous and/or aluminous earth materials: volcanic glass, zeolite minerals, opaline chert, and diatomaceous earths. They form part of a broader class of supplemental cementitious materials (SCM) such as fly ash and blast furnace slag. These SCMs can be considered as natural pozzolans. Concrete made with blended cements such as CEM II and CEM III are therefore more representative to Roman concrete than CEM I based concrete. The water in the concrete recipe in old Roman maritime concretes was seawater and the formation of Al-tobermite, a C-A-S-H mineral in the cementitious matrix has been attributed to its durability (Jackson et al., 2017). Also mortars to bind stone blocks in Hadrian's wall have C-S-H phases (Mallison and Davies, 1987), but these phases were mostly derived from the calcination of siliceous limestones during the production of the lime and, to a lesser extent, by reaction of fine-grained reactive silicate aggregate (Jull and Lees, 1990; Hooker, 2003b). The aggregate was chert (Mallison and Davies, 1987) that has a very high reactive surface area. It can be similar to silica fume that is used as an addition to make concrete, e.g. in plugs (Vehmas et al., 2019). It becomes clear from the investigations on historical and current concrete that cement containing lime (CaO) and pozzolan (very fine-grained reactive SiO_2 such as slag) results into C-S-H phases with a refined pore structure. This pore structure minimizes the rate of ingress of species that could alter the chemistry of concrete and therefore contribute to its durability.

Stone blocks are held together by a cementitious mortar in Hadrian's wall from the Roman empire (Hooker, 2003b). This wall contains in parts mortars that are still hard and sampling need to be performed by coring (Jull and Lees, 1999) ,but also parts that are softer (Mallison and Davies, 1987). These parts as well as younger structures, e.g. almost thousand year-old churches such as Reading Abbey, are soft and crumble and the concrete structures would not survive the lithostatic load in the underground. Apart from carbonation, these cementitious materials are also exposed to weathering waters that enhances leaching (Rassineux et al., 1989), since the calcium concentration in, for example, rain water is smaller than in concrete pore water.

The old cements used to manufacture concrete and mortars have larger grains size than modern cements (Mallison and Davies, 1987). There were therefore more non-hydrated phases present just after manufacturing than modern concrete, which leaves the possibility for fracture sealing.

Many types of the examination of historical concrete show calcite precipitation by atmospheric carbonation, e.g. Hadrian's wall. The empirical laws for carbonation found in historical concrete can be relevant for the operational phase of the disposal facility, e.g. shotcrete. Hardened concrete segments and the outside of concrete containers are polished to facilitate their lifting with vacuum techniques for their emplacement. The polishing effect for the long-term has been listed for historical concrete by the formation of closely knitted carbonation products that reduced the permeability and therefore enhances the durability of concrete (Mallison and Davies, 1987).

Many natural (e.g. Scawt Hill and Maqarin) and archaeological (e.g. Pantheon in Rome) studies, are available with a chemical composition for concrete that are used or intend to be used in geological disposal facilities but their exposure conditions are usually without ingress of dissolved magnesium and chlorine (Milodowski et al., 2015), which is expected for disposal cells in granitic and many clay host rocks (see Appendix B, host rock pore water). The exception is the Roman marine infrastructure but that type of concrete has been made with seawater and not tap water.

Portland cements were first manufactured in the middle of the 19th century (Rassineux et al., 1989) around 1840's (Steadman, 1986). The oldest available materials that can be compared with concrete made with modern cements such as CEM I are therefore less than 200 years old.

3.1.4.1.2 Aggregates

Aggregates are used for all cementitious materials used in the disposal cells, except sometimes for the waste form. The strength of concrete is determined by the strength of the aggregates and the bonding between the cementitious phase and these aggregates. Aggregates of limestone are used in the concrete buffer (Van Humbeeck et al., 2007). These limestones can contribute in buffering the pH between 8.5 and 10.5. Aggregates of quartz are used in concrete segments and backfill (Verhoef,et al. , 2014). Examined historical concrete contained basalt, granite or feldspars as aggregates by which the knowledge on the long-term behaviour of quartz aggregates in a cementitious matrix is scarce. An exception is the flint gravel that together with limestone, was used as aggregates for Reading Abbey; a church in England built in 1121. Like some of the dressed stones for building Hadrian's wall, the cementitious phase of Reading Abbey has become crumbly and washed away, leaving the appearance of these flint aggregates. But also, quartz grains have been flown within the cement mixture to make concrete, e.g. Camiros concrete 500 BC (Mallison and Davies 1987). The surface of the grain reacted with the cementitious matrix, i.e. 'was eaten away'. A rim of reacted material is visible since the reaction proceeded not further. Such reaction rims have also been observed in Roman concrete with aggregates of pumice and feldspars. The idea is that these reaction rims are generated during hardening until thickening of a reaction rim of hydrates covers the external surface; the reaction is then slowed down considerably and proceeds through a diffusion controlled process (Jackson et al., 2017). The reactive surface area of quartz aggregates is insignificant compared to the reactive surface area of fly ash or blast furnace slag used in blended cements, so these slags can react completely, while there are only rims visible for the aggregates. Again, from Reading Abbey, when the reactive surface area is large as in chert, 3 different types of reactions with lime have been identified (Mallison and Davies 1987):

1) densified carbonate, which may have originally been C-S-H, with a thickness of about 1 mm thick;
2) a porous amorphous rim;
3) affecting smaller flints, causing internal cracking and leaving the residual material very porous.

Aggregates of silica and feldspars in cementitious matrices usually have a very low porosity and examined rims at these dense aggregates have been attributed to reactions taking place during hardening (Jackson et al., 2017) (Mallison and Davies, 1987). These reacted rims may provide the necessary bonding between aggregates and cementitious phase for the strength of concrete but are also hardly noticed in the investigations of concrete. Also limestone, basalt and granitic rock have been used as aggregates. Extensive cracking of historical concrete has been attributed to cement shrinkage by drying (dehydration) and carbonation leaving voids between aggregates and the cementitious phase initially made of pure lime. Aggregates remain mainly unaffected (Mallison and Davies, 1987).

3.1.4.2 Effect of high-pH leachates on clay host rock and granitic host rocks

Clay host rocks and granitic host rocks are both alumina-silicate bearing rocks. Detailed investigation and understanding of the processes taking place in Maqarin (Jordan) elucidated the potential sequence of secondary mineral formation by interaction with alkaline fluids and alumina-silicate bearing rocks: C-S-H phases, low in Ca C-S-H phases, C-A-S-H, low Si/Al zeolite and high Si/Al zeolite as a function of pH (Milodowksi et al., 1998; Savage, 1998). This description in Figure 3-2 is similar to the identified concrete-bentonite interaction and concrete-granite interaction (see Figure 2-10 and Figure 2-12).

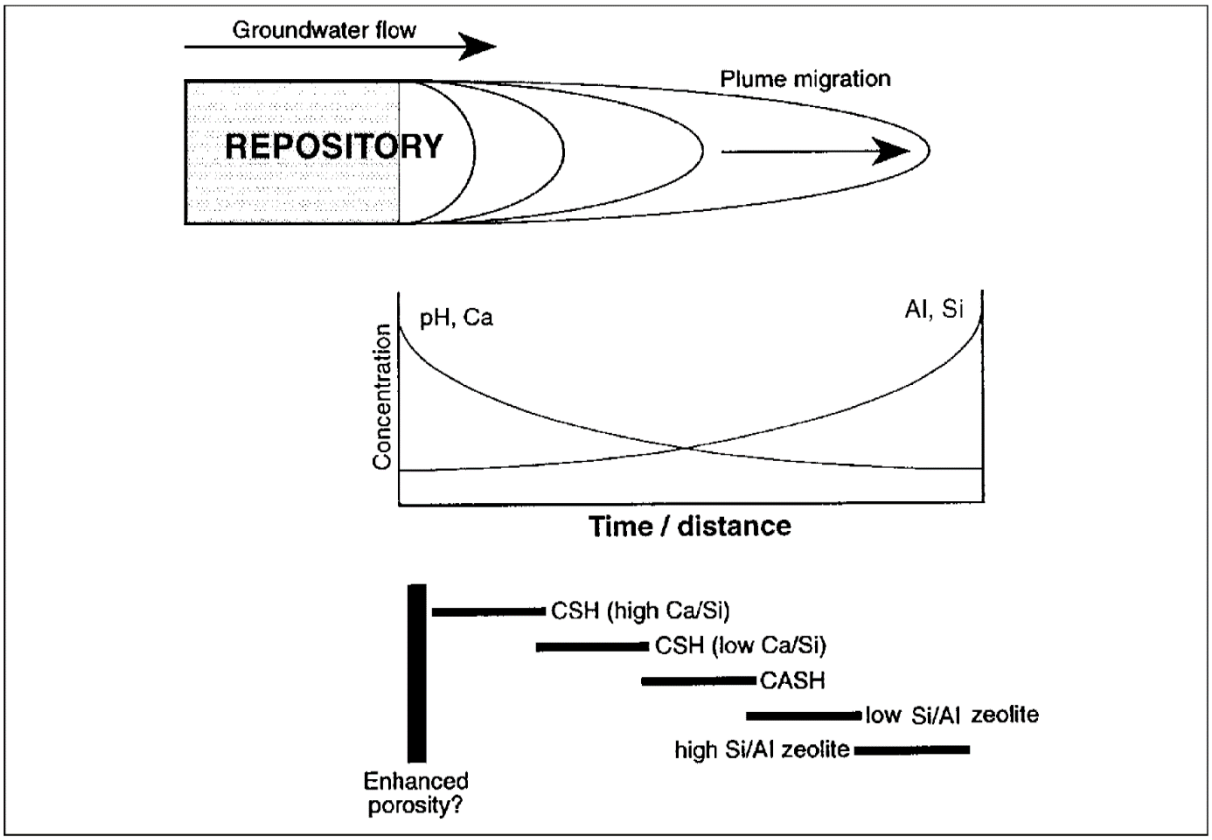

Figure 3-2: Schematic diagram of hyperalkaline plume migration from a cementitious repository for radioactive wastes, showing hypothesised variation in fluid composition and alteration mineralogy in space and time (Savage, 1998).

The sedimentary rock through which the hyperalkaline waters in the Maqarin analogue was more porous than the envisaged clay host rocks and the clay mineralogy in this sedimentary rock was dominated by illite and kaolinite. These clay minerals are also the dominating ones in indurated clays (see Appendix C). The chemical processes are therefore considered to be similar but the speed of the processes is significantly smaller, due to the low diffusion values in indurated clays as well as in concrete. Also the precipitation of calcite within concrete by ingress of bicarbonate from clay pore water would reduce the alkaline leachates. This analogue also revealed the reactivity of different mineralogical components. For example, quartz, K-feldspar and plagioclase are present in granitic host rocks (see Appendix C) but quartz and K-feldspar react more with hyperalkaline waters than plagioclase. The reactive surface area has a high impact on the observed alteration, e.g. chert clasts are composed of fine-grained or cryptocrystalline quartz and have reacted into C-S-H gels (Milodowksi et al., 1998). The natural analogues in Cyprus and Philippines in which hyperalkaline waters were passing clay deposits, similar to bentonite, showed minimal mineralogical alteration in a period of 10^5-10^6 years due to the low permeability of these clay deposits (Milodowski et al., 2015).

3.1.5 Organic waste

Organic matter can be considered as a potential food source for microbes, if the usable energy to breakdown the organic molecules provide sufficient energy. Microbial degradation of organic waste can therefore be a primary process for the potential release of radionuclides. As explained in section 2.3.2.1, a division is made between addition polymers and condensation polymers to distinguish the potential microbial degradation.

An example of an addition polymer that is also a predominant organic ILW-type is spent ion exchange resin. Natural resins are solidified products of higher plants with a great resistance to chemical attack and resins can also withstand decomposition by microbes. There is however not an analogue for cemented resins.

An example of a condensation polymer is cellulose (e.g. wood, paper). This type of organic waste is in exceptional cases ILW (see Chapter 2, Figure 2-1). The Dunarobbe forest analogue, previously described in paragraph section 3.1.3, described the good preservation of wood by lack of fluid flow and anaerobic conditions. These two features can also be provided by the conditioning grout for organic waste; the chemical corrosion of the steel drums can generate the required reducing conditions, if the cement did not contain traces of pyrite. There is the potential alteration of vegetable debris, i.e. condensation polymers, into polysaccharides by migrating alkaline fluids in Khushaym Matruk (Jordan) (Källström and Lindgren, 2014). Such alkaline migration is expected to take place for ILW disposal cells in granite, in which the conditioning grout had been extensively fractured due to the lithostatic load and mechanical degradation by the ingress of dissolved species that had reacted with the cementitious matrix.

3.2 Laboratory experiments / in-situ experiments

3.2.1 In-situ experiments

Natural and archaeological analogues are in-situ experiments that last a time frame relevant for the long-term in geological disposal of radioactive waste. Features that are important on the long-term such as the transformed medium or alteration zone in clay or concrete when exposed to steel can be observed (Chitty et al., 2005; Neff et al., 2004; Dillmann et al., 2014). Also the understanding of processes of materials interfacing concrete, granite (see section 2.2.5) and clay (see section 2.2.6) have been deduced primarily from the investigations on the Maqarin natural analogue. But not every old material or site can be an analogue. Quantitative knowledge on the chemical and physical properties of the engineered barriers and host rock are needed to justify the research on the materials and site. The investigation of sites with natural and archaeological analogues requires an understanding of the relevant processes during the implementation of geological disposal of radioactive waste and in the phase when the disposal facility is closed. The main disadvantage of analogues is the lack of information about the initial conditions, which makes it difficult to extract quantitative information for the performance assessment of the disposal of waste.

Transport properties within the host rock and engineered barriers are a key issue in the chemical evolution of disposal cells since it has a high impact on how there can be contact between the pore water and the waste form and when. The ‘how’ determines the chemical and physical conditions for the alteration mechanism of the waste form. The ‘when’ determines the radionuclides that are left and consequently the potential radionuclide release rate. The quantification of the transport properties can depend on the sample size since the heterogeneities on a large scale can have a high impact on these properties. In-situ experiments can therefore provide the most reliable determination of the (initial) transport properties for the chemical evolution of the disposal cells and its consequences on the radionuclide release rate from the waste forms as well the as the radionuclide migration rate through the engineered and natural barriers.

3.2.2 Laboratory experiments

There have been many experimental results obtained on a laboratory scale. The initial and boundary conditions in a laboratory set-up are usually known, which allows a robust interpretation of the monitored parameters. The main disadvantage of laboratory experiments is the small period in time. Extremes in radiological, chemical, physical and microbiological conditions are often used in order to observe

'something' within a few days, months or years. These conditions may not be representative for the quantification of processes during geological disposal of radioactive waste. The set-up conditions for a laboratory experiment with the purpose to provide a quantification of a process, e.g. the corrosion rate of steel, requires quantitative knowledge on the radiological, chemical and physical properties of the waste and the chemical and physical properties of the engineered barriers and host rock. An assessment of the potential of microbial activity needs to be made for each set-up and also whether microbial activity would be relevant for geological disposal of waste and why. Quantification in properties has sometimes been made for example (Smart et al, 2017),but frequently this quantification has not been made. An example is the refereed literature for the effect of γ radiation on the bentonite properties in section 2.2.3 of more than 10-20 Gy h^{-1} or 2.98 kGy h^{-1}. Such high radiation fields may not be relevant for disposal of waste (see section 2.3.1; Figure 2-13). Section 2.3.1 also explained why processes such as radiation enhanced corrosion of steel are not likely to occur, i.e. the required radiation fields and access to water are not present during disposal of waste.

Laboratory tests require the understanding of the relevant processes in order to structure an experimental set-up in which representative results for geological disposal can be generated. Monitoring variables need to be carefully selected in order to investigate the phenomena that are relevant. Some illustrative examples with an impact on the determination on the radionuclide release rate for vitrified waste and the assumed durability for carbon steel overpack are described.

3.2.2.1 Vitrified waste form

Almost all laboratory studies investigating the interaction of porous media with the vitrified waste form are leaching experiments in liquids. The understanding of the alteration mechanism of natural analogue studies on basaltic glasses highlighted the importance of silica saturation. All host rock and engineered pore waters are saturated in silica and therefore leaching experiments of samples in glass in distilled water would overestimate the alteration rate, especially if the leachate solution would be stirred. The dissolved concentrations of silicon, sodium, aluminium, iron and calcium in representative blank solution are usually too large to monitor a change in their concentrations and therefore the dissolved boron concentration is monitored to determine the glass dissolution rate (Van Iseghem et al., 1992). However, the dissolved boron does not represent the behaviour of glass dissolution, since the boron is not incorporated in the altered glass layers (Conradt et al, 1986). The alteration rate of vitrified waste can be determined with rising boron concentration, but this information provides limited knowledge on the potential radionuclide release, since the majority of the radionuclides that are dissolved as cationic species is sorbed by the alteration layer. The long-term boron release rate measured from vitrified waste forms exposed to silicon saturated solutions can therefore only be representative for the radionuclide release rate of anionic dissolved species if a reactive solid phase is absent. It requires some time to build up the alteration layer by which the early measured boron release rate are too large to be representative on the long-term in the post-closure phase.

These leaching experiments lack solid phases. These phases such as steel and corrosion products are present in a HLW disposal cell and their influence may result in larger alteration rates of vitrified waste form, due to enhanced sorption of dissolved cationic complexes that can no longer be used for building the alteration layer. The glass dissolution rates that are determined without these solid phases may initially therefore be too optimistic for geological disposal, if the diffusion of water is not the rate-limiting step, since access of water is required for the alteration. The interfacial area between the vitrified waste form and steel is, however, limited in the disposal cell. After complete coverage of the corroded steel surfaces with dissolved cationic complexes from the vitrified waste form, the glass alteration rate is envisaged to decline till the long-term boron release rate.

3.2.2.2 Steel

3.2.2.2.1 Sample preparation and its impact on the corrosion rate

Most laboratory experiments with steel start with polished surfaces (Swanton et al., 2015) in order to have a well-defined initial condition of the sample. This polishing removes the iron oxide-layer that was generated by atmospheric dry oxidation before its use, for example to make well-engineered reinforced concrete with ribbed carbon steel bars or iron-oxide layers that are formed on stainless steel after neutron irradiation in a nuclear plant. These layers can be passivation films that were present prior to disposal. The corrosion rate of steel can be several orders in magnitude larger without these films. It can take 4-6 months before a constant corrosion rate is observed (Johnson and King, 2008), if no dissolved calcium is present in the leachate (Kreis, 1991). This period to obtain a steady state can be more than 4 years for compacted clay (Johnson and King, 2008). This period in time is necessary to make the passivation film to obtain the long-term corrosion rate that is representative for disposal.

Another frequently used sample preparation methodology is acid etching. Rinsing with a 10% HCl-methanol solution is used to remove the iron oxide layer (King et al., 1973) that is naturally present. The weight loss from these samples in solutions containing iron sulphides becomes negligible after 30 days, probably because steel became passivated during the corrosion process. The impact of such type of research is that concrete made with a cement blended with Blast Furnace Slag (BFS) has not been accepted for disposal of waste, because iron sulphides within the cement have been observed to depolarise the water reduction reaction and thereby accelerate corrosion by absorbing hydrogen (Marsh et al., 1986). In reality, the rest potential of carbon steel has been measured to be achieved immediately for steel embedded in a grout mixture made with a BFS-blended cement. For carbon steel that is surrounded by mixtures of OPC/Pulverized Fly Ash (PFA) and OPC/Lime, it may take some time before entrapped oxygen is sufficiently consumed to obtain the rest potential of steel at anaerobic, alkaline conditions. Moreover, the iron oxide magnetite is expected for anaerobic, alkaline conditions (Figure 2-15) and is actually measured by Raman spectroscopy on the surface of carbon steel embedded in BFS-blended cement, but not on surfaces of steel that have been embedded in the mixtures OPC/PFA and OPC/Lime within the same experimental period (Naish et al., 1991).

3.2.2.2.2 Liquid phase versus solid phase

The solid phase restricts the access of species that may react with steel. There can be aerobic corrosion of steel in the operational phase and also for a small period in the post-closure phase of the chemical evolution of disposal cells. This corrosion process can be rendered due to insufficient access of oxygen towards steel with which for example the pits in carbon steel are larger for surfaces exposed to solutions than to bentonite; after two years exposure the depth of these pits was 3.7 mm for solutions and 0.5 mm for bentonite (Marsh et al., 1991). This insufficient access of oxygen towards the steel surface can be caused by the slow diffusion of oxygen in water-saturated bentonite as well as traces of pyrite present within bentonite that reacted with oxygen.

The benefit of the performance of the corrosion experiments performed in liquids is that the actual corrosion rate can be monitored with the measured hydrogen gas release with negligible loss in time by diffusion of hydrogen to the measurement device. The disadvantage of using only liquids is that the solid phases can increase the corrosion rate by sorption of dissolved iron if these solid phases contain charged minerals such as clay and concrete and if the diffusion of water required for the corrosion process is not the rate-limiting step.

3.2.2.2.3 Monitoring variable for the quantification of the corrosion rate

Long-term corrosion rates for carbon steel exposed to alkaline, anaerobic solutions are smaller than 0.1 µm per year using hydrogen evolution measurements. Corrosion rates for carbon steel exposed to concrete are limited to weight loss and electrochemical measurements (Swanton et al, 2015).

Electrochemical measurements overestimate the actual corrosion rate, especially when the corrosion rates are smaller than 1 µm per year. Corrosion rates that have achieved steady state have a total corrosion rate smaller than 0.57 µm per year using weight loss (Naish et al., 1991). These corrosion rates include the initial active corrosion phase in which the corrosion rate has been measured to be 3 orders in magnitude larger than the steady state corrosion rate. The measured corrosion rates by weight loss can at least be one order in magnitude larger than the measured corrosion rate by hydrogen release (Kaneko et al., 2004; Kursten and Druyts, 2015). Determination of the corrosion rate with a hydrogen evolution measurement has been performed for carbon steel in concrete for a period of 500 days (Kaneko et al., 2004) but not for carbon steel in clay. The hydrogen generation rate was extremely small despite the fact that accuracy was high, i.e. 0.001 µm per year. Delay in the arrival of hydrogen by the measurement device makes it hard to measure the corrosion rate.

3.3 Integration in modelling tools

Reactive transport models couple transport processes (advection, hydrodynamic dispersion, diffusion) with geochemical processes (thermodynamic equilibrium, kinetic processes). Such models are emerging for about 40 years and have found applications in many environmental and engineering application including geological disposal of radioactive waste. Some recent publications give an overview of the background, methods and available codes of reactive transport codes (Steefel et al., 2015a) and an overview of applications in the field of disposal of radioactive waste (Bildstein et al., 2019; Claret et al., 2018; De Windt and Spycher, 2019). Overall, during the last 10 years, coupled reactive transport with a large flexibility to include several equilibrium and kinetic processes are applied for many engineered systems at different spatial and temporal scales including applications relevant to geological disposal of radioactive waste. For background on the mathematical and numerical models, the reader is also referred to Anderson and Crerar (1993), Lichtner (1996), Steefel and MacQuarrie (1996) and Leal et al. (2017) for the basic mathematical and numerical formulations of geochemical and reactive transport equations.

As described in the previous sections, the chemical evolution in a disposal cell is not only governed by transport and geochemical processes, but also by water flow and absorption, multiphase flow phenomena and heat transfer. An overview of the key mathematical formulations of these processes is given in section 3.3.1. Section 3.3.2.1 describes some selected codes that have been used in the context of geological disposal of radioactive waste or to describe relevant processes at interface, waste package and disposal cell scales.

3.3.1 Governing equations for simulating water flow, heat transport, solute transport and geochemistry

The key processes in the conceptual model of the chemical evolution at an interface, of waste packages (under disposal conditions), or of disposal cells are transport of water (fluid flow), advective and diffuse transport of dissolved species (solutes) between the interfacing materials and reactions between these dissolved species and minerals within these materials.

Other processes, such as fluid flow but also sorption determine the speed in which the materials can be altered. For HLW, also the impact of temperature on these key processes needs to be assessed. The release mechanism and rate of radionuclides from the waste forms are determined by the chemical evolution of materials in the vicinity of the waste form in the disposal cell.

3.3.1.1 Continuum models

The scope of the reactive transport models described in this report is limited to continuum-scale models. In such approach, the micro-heterogeneities between different phases (e.g., aqueous phase, solids or even different minerals) are not represented in an explicit way by geometries and boundaries, but are averaged over a representative volume such that the porous medium properties vary continuously in space. These averaging can be orientation dependent, i.e. anisotropy of the porous media properties can be included to continuum-scale models.

On the other hand, there are pore-scale models in which pores and solids are represented explicitly, which currently are also coupled with geochemical solvers to simulate reactive transport at the pore scale (e.g., Molins et al., 2017; Patel et al., 2018; Seigneur et al., 2017). The codes then uses also different constitutive equations for flow (Navier-Stokes versus Darcy's Law) or transport (molecular diffusion in liquid phase versus effective diffusion in a porous medium). Obviously, this approach cannot be applied to a large scale due to the current computational power and the necessity to achieve calculational results within hours, days of perhaps weeks. Computational power will increase by which pore-scale models may be used in the future at disposal cell scale.

3.3.1.2 Fluid flow

This section describes equation for single-phase flow in porous media and through fractures. The mathematical formulation of a multiphase model is not covered; the mathematical model for single-phase flow of water is given for fully and partially water-saturated porous media.

3.3.1.2.1 Variably-saturated single-phase flow

When assuming a passive air phase and neglecting hysteresis, the mass conservation equation combined by the Darcy-Buckingham equation results in the Richards equation for variably saturated water flow in porous media:

$$\begin{aligned}\frac{\partial \theta_{\mathrm{w}}}{\partial t} &= \nabla \cdot \mathbf{q}_{\mathrm{w}} - Q_{\mathrm{w}} \\ &= \nabla \cdot \left[\mathbf{K} \left(\nabla h + \mathbf{e}_{\mathrm{z}} \right) \right] - Q_{\mathrm{w}}\end{aligned} \qquad 3.1$$

where θ_{w} is the water content ($m^3\ m^{-3}$), t is time (s), $\boldsymbol{q}_{\mathbf{w}}$ is the vector with the volumetric water flux density ($m^3\ kg^{-2}\ s$), Q_{w} is the sink/source term ($m^3\ m^{-3}\ s^{-1}$), $\mathbf{K}$ is the hydraulic conductivity ($m\ s^{-1}$) tensor, h is the pressure head (negative for unsaturated conditions) (m), and $\mathbf{e}_{\mathrm{z}}$ is a unit vector in the vertical direction. The water content is sometimes expressed as:

$$\theta_{\mathrm{w}} = \eta S_{\mathrm{w}} \qquad 3.2$$

where η is the porosity (m^3(void) m^{-3}(system)) and S_{w} is the degree of water saturation (m^3(water)m^{-3}(void)). To solve Eq. 3.1, material properties expressing the relation between the water content and pressure head (or capillary pressure, ψ Pa), for negative values of pressure head), called the moisture retention curve or the (aqueous) saturation function and the relation between the hydraulic conductivity and the pressure head / capillary pressure. These relations are mostly defined as closed-form formulations with a number of material-specific parameters. For the saturation curves ($S_{\mathrm{w}}(h)$ or $S_{\mathrm{w}}(\psi)$), many different functional forms exists; some of them are implemented in reactive transport codes, e.g. the formalism of van Genuchten, (1980) or (Brooks and Corey, 1964). The hydraulic conductivity curve requires typically the saturated hydraulic conductivity K_s (L m Ts-1) and a functional form of the relative conductivity, i.e. the change of hydraulic conductivity with pressure head. The standard method is to use a pore-size distribution models that calculates the relative hydraulic conductivity from the moisture retention model (e.g., Mualem, 1976; Burdine, 1953, see also van Genuchten et al., 1991).

3.3.1.2.2 Liquid flow in fully and variably saturated fractured media

Micro and macro cracks or fractures can develop or are present in engineered (e.g. concrete) and geological formations as a result of interactive physical, chemical and mechanical processes. As the existence of fracture networks forms preferential pathways for water flow and/or contaminant/constituent leaching, such networks are of particular concern for the long-term performance and chemical evolution of disposal facilities.

The effect of fracture networks on the release of contaminant fluxes is not univocal and depends on interplay between fracture network characteristics, matrix properties, regional hydraulic conditions and location of encapsulated wastes. Different flow patterns develop for different rates of water infiltration. If the water flux is low relative to the saturated hydraulic conductivity of the fracture, the fracture will not act as a preferential pathway: the fracture will be unsaturated with very low unsaturated hydraulic conductivity (only film or corner flow, Or and Tuller (2000), Tuller and Or (2001)). The unsaturated hydraulic conductivity of the fracture can be lower than the (un)saturated hydraulic conductivity of the matrix and flow might be primarily through the matrix domain (hydraulic conductivity might be very low, and transport is then mainly via diffusion). On the other hand, a water flux high enough to saturate the fractures might result in fractures becoming effective pathways for rapid advective-dominated migration of radionuclides (at least, if saturated hydraulic conductivity of fractures higher is than that of the matrix). The relative importance of fracture flow versus matrix in the light of their saturation properties has been studied in Cey et al. (2006), Or et al. (2005) or Perko et al. (2017). Under water-saturated conditions, the condition to be expected in a geological disposal, flow and transport is mainly in the fractures (when saturated hydraulic conductivity of the fractures is larger, see Cey et al. (2006), Or et al. (2005) or Perko et al. (2017)). However, under unsaturated conditions, the main flow and transport path can be in the matrix domain as well, depending on fracture properties (e.g. roughness), matrix hydraulic properties and pressures.

Several modelling approaches have been proposed to model flow and transport through fractured porous media. The hydrogeological mathematical models for flow and transport through fractured porous media fall into one of three broad classes: (a) equivalent (or single) continuum models and derivatives as dual-porosity and dual-permeability (or multiple) continuum models (e.g. Šimůnek and van Genuchten, 2008), (b) discrete network simulation models either as single fracture or fracture network models (e.g. Sudicky and Mclaren, 1992), and (c) hybrid models (e.g. Oda, 1985). The equivalent continuum models require volume-averaged hydraulic properties that reflect the large-scale average effects of fractures whilst the discrete models need mainly information about the geometric characteristics of fractures. The hybrid models need both sets of information.

Explicit modelling of saturated single phase flow in fractured systems

As an example, governing equations for the explicit representation of flow in fractures and surrounding rock matrix are given here. The fractures are assumed to be always saturated although in reality this may be unlikely. The saturated hydraulic conductivity of macro fractures with widths of the order of hundreds of µm is typically several orders of magnitude larger than that of a porous matrix. This means that larger fractures will drain out water quicker than the porous matrix, which holds water by suction.

The governing equation for the flow is based on Darcy's law in both the matrix (Eq. (3.3)) and in fractures (Eq. (3.4)) (Seetharam et al., 2014). The flow through fractures is modelled using tangential derivatives which define the flow along the interior boundaries representing fractures within a porous matrix. Eq. (3.6) is essentially an averaging of conservation equation across the fracture thickness (see Martin et al. (2005), for derivation).

$$\rho_l S \frac{\partial p}{\partial t} = -\nabla \cdot \rho_l \mathbf{u} \quad 3.3$$

$$\mathbf{u} = -\frac{K_s}{\rho_l g} \nabla p \quad 3.4$$

$$\rho_l S d_f \frac{\partial p}{\partial t} = -\nabla_T \cdot \rho_l \mathbf{u_T} \quad 3.5$$

$$\mathbf{u}_T = -d_f \frac{K_f}{\rho_l g} \nabla_T p \quad 3.6$$

$$K_f = \frac{\rho_l g d_f^2}{24\mu} \quad 3.7$$

where p is the total pressure (Pa) which is the dependent variable, ρ_l is the density of water (kg m^{-3}), S is the storage coefficient (Pa^{-1}), $\mathbf{u}$ is the Darcy's velocity vector (m s^{-1}) in the matrix as defined in Eq. **Erreur ! Source du renvoi introuvable.**, K_s is the saturated hydraulic conductivity of the concrete matrix (m s^{-1}), g is gravitational acceleration (m s^{-2}), d_f is the fracture width (m), K_f (m s^{-1}) is the hydraulic conductivity of a single fracture obtained from Eq. **Erreur ! Source du renvoi introuvable.** for planar fractures (Walton and Seitz, 1991), μ is the dynamic viscosity of water (kgm^{-1}s^{-1}), $\mathbf{u_T}$ is the tangential velocity vector and ∇_T denotes the gradient operator restricted to the fracture's tangential plane. The dependent variable, p, is same in both the matrix and fractures. The storage coefficient S is put to a very low number representing water compressibility. The state-of-the-art report of WP DONUT (Ahusborde et al., 2021) gives also an overview on treatment of fractures.

3.3.1.3 Heat transfer

Taking into account the main heat transport processes (conduction in the solid matrix, transport by the fluid phase, conduction in the fluid phase) and assuming a single temperature between the different phases, the heat transport equation can be written as:

$$\frac{\partial c_p \rho_p T}{\partial t} = \nabla \cdot \left(\boldsymbol{\lambda} \nabla T - c_w \rho_w \mathbf{q} T \right) \quad 3.8$$

where T is temperature [K], c_p is the specific heat capacity of the porous media [J kg^{-1} K^{-1}], ρ_p is the mass per unit volume [kg m^{-3}], c_w is the specific heat capacity of water [J kg^{-1} K^{-1}], ρ_w is the mass of water per unit volume [kg m^{-3}], λ is the thermal conductivity tensor [W m^{-1} K^{-1}] and θ is the water content. Please note that this heat equation can only be solved by taking into account fluid flow. Excluding the fluid flow and solving this equation solely with properties for saturated and non-saturated porous media provides a range in temperatures of materials as a function of time. A too low temperature will be calculated for properties with saturated media. A too high temperature will be calculated for properties with not-saturated media. The range in temperatures in too low and too high temperature can be acceptably small enough considering other uncertainties. This is a more simple calculation and less time consuming than including fluid flow. In unsaturated porous media, in addition to transport of heat by conduction, heat can be transport in the air phase via vapour transport and may become an important component of heat transport in unsaturated low permeable media (e.g. Collin et al., 2002). Note that this transport process is not included in Eq. 3.8.

3.3.1.4 Solute transport

In most reactive transport codes, transport is defined in terms of total concentration instead of transport of each individual aqueous species. The number of transport equations then equals the number of

primary species or components. This number is equal to the total number of aqueous species, N_a, minus the number of linearly independent reaction equations between species in chemical equilibrium (see section 3.3.1.5). As such, the total number of aqueous species, N_a, is divided between N_p primary species and $N_a - N_p = N_x$ secondary species. The total concentration $C_{w,i}$ of the ith primary species is then defined as:

$$C_{wi} = c_{wi} + \sum_{j=1}^{N_x} \nu_{ji} c_{wj} \qquad 3.9$$

where ν_{ji} is the stoichiometric coefficient (*i.e.* the number of moles of the ith primary species in the jth secondary species).

The general solute transport equation for transport of mobile components for a single phase system (liquid phase) can be written as:

$$\frac{\partial \theta_w C_{w,i}}{\partial t} = L(C_{w,i}) + R_i \qquad 3.10$$

where $L()$ is the linear transport operator, and R (mol m^{-3} s^{-1})is a sink/source term for geochemical reactions (section 3.3.1.5**Erreur ! Source du renvoi introuvable.**). These reactions can change the microstructure e.g. a local change in porosity.

The transport operator for the aqueous phase consists of a hydrodynamic dispersion and an advective component:

$$L() = \nabla \cdot \left(\theta_w \mathbf{D}_{hd} \nabla \cdot C_{wi}\right) - \nabla \cdot \left(\mathbf{q} C_{wi}\right) \qquad 3.11$$

where $\mathbf{D}_{hd}$ is the hydrodynamic dispersion tensor (m^2 s^{-1}), and the other symbols as defined before.

The hydrodynamic dispersion includes molecular diffusion in the aqueous phase, corrected for the tortuosity of the porous media and mechanical dispersion due to small scale variations in fluid velocities and travel paths.

Tortuosity multiplied with the molecular diffusion coefficient of the aqueous phase is often indicated by the term pore diffusion coefficient D_p or diffusion coefficients in porous media. This parameter is crucial for the assessment of chemical evolution of disposal cells in a geological disposal system as diffusion is often the most important transport process. Water flow and thus advective transport are usually of minor importance for geological disposal systems in clay systems due to the absence of strong hydraulic gradients and the low permeable host-rock and engineered barriers; advective flow could be relevant for granite host rocks when fractures are present.

This simpliffied transport operator assumes that individual diffusion coefficients of charged (ions) and uncharged complexes in water can be replaced by one average molecular diffusion coefficient for all primary species in order to ensure charge neutral transport. Instead of using the phenomenological Fick's law, the Nernst-Planck equations can be used that consider specific diffusion coefficients for each ion/complex and achieve charge neutrality of transport by calculation of cross-diffusion coefficients for charged species (Samson and Marchand, 2007, Liu et al., 2011; Steefel et al., 2015a). In addition, the gradient in the chemical potential gradient instead of the concentration (Steefel et al., 2015a). The diffusive term in Eq. (3.11) contains, beside the Fickian diffusion term, a term related to the gradient in electrostatic potential (related to Nernst-Planck) and a term related to the gradient in activity coefficients (Appelo, 2017; Samson and Marchand, 2007). A recent example of using the Nernst-Planck equation (only electrochemical effects, no chemical activity gradient) for geochemical changes over a cement-clay interface was presented by Idiart et al. (2020). The effect of electrochemical effects was clearly visible for non-reactive ions such as the mobility of Cl. When the ions concentrations are controlled by mineral phases, the effect of including electrochemical effects is limited.

3.3.1.4.1 Microstructure and diffusivity

Pore diffusion coefficients can be obtained by experimental in- or through diffusion experiments but these measurements are only valid for the microstructure of the porous media during the experiment. There exist different models to predict the tortuosity from continuum properties of the porous media. For saturated media, variants of Archies law (Archie, 1942) using an exponential relation on porosity are available in many reactive transport models. Models proposed by Milington and Quirk (Millington and Quirk, 1961) or Moldrup (Moldrup et al., 2000; Moldrup et al., 1997) account for water saturation degree of the porous media. It is important to note that these models or their parameters are mainly empirical in nature and using them predictive outside their calibration or measurement region (other materials or other range of porosity) is highly uncertain.

For cement-based materials, there exist alternative models adapted to the specificities of the material, see e.g. Patel et al. (2016) for an overview of models for diffusivity in saturated Portlandite cement and concrete. Some models are fitted on numerical (pore-scale models) such as Garboczi and Bentz (1992) or based on effective media theory, accounting possible accounting for different characteristics as different types of porosity, phases and aggregates (e.g., Bejaoui and Bary, 2007; Oh and Jang, 2004; Stora et al., 2009a). In general, such models are not always implemented in the numerical codes.

Geochemical reactions can cause a local change in the microstructure; specifically solid phase dissolution/precipitation/transformation reactions (see sections 3.3.1.5.2 and 3.3.1.5.6.1) can locally change e.g. the pore size distribution and porosity and thus solute migration can locally decrease or increase. The influence on solute diffusion is via the total porosity (area available for diffusion) and the tortuosity coefficient (see section 4.1.1.2).

3.3.1.4.2 Mechanical dispersion

Mechanical dispersion is calculated from the average velocity in the principal direction multiplied by the longitudinal or transversal dispersivity, α_L or α_T [L] respectively (Bear, 1972). The components of the dispersion tensor, D_{ij}, are given by

$$D_{ij} = \alpha_T v \delta_{ij} + \left(\alpha_L - \alpha_T\right)\frac{v_j v_i}{v} + \tau_w D_w \delta_{ij} \qquad 3.12$$

where v, v_i and v_j are the average velocity, and the velocity in the i and j direction, respectively, τ_w is the aqueous tortuosity factor which depends on microstructure but also on water content, D_w is the molecular diffusion coefficient in the aqueous phase, and δ_{ij} is the Kronecker delta.

3.3.1.5 Geochemical processes

The geochemical reaction term in Eq. 3.10 **Erreur ! Source du renvoi introuvable.**, R_i, accounts for heterogeneous equilibrium or kinetic geochemical reactions or homogeneous kinetic reactions. Homogeneous (aqueous) equilibrium reactions do not change the concentration of the primary species and therefore, there is no need to include them in a sink/source term in transport equation 3.10 for master species. Typical heterogeneous reactions taken into account in reactive transport models are (Steefel et al., 2015a) ion exchange, surface complexation, aqueous-gas exchange, mineral dynamics, and solid-solutions; most of them treated both in equilibrium or kinetically-controlled. Typical homogeneous kinetic reactions are radioactive decay and (microbiologically-mediated) kinetic degradation of, e.g. organics, or oxidation-reduction reactions.

In what followed, we give an overview of the most important geochemical reactions that are typically being accounted for in reactive transport models. We choose here to define express equilibrium in terms of the law of mass-action equations.

3.3.1.5.1 Aqueous reactions

The activity of aqueous species is crucial for many other geochemical processes. Several theories and models are published to calculate activity correction coefficients of aqueous species such as based on Debye-Hückel theory, specific ion interaction (SIT) model or Pitzer equations. Most basic handbooks on aquatic chemistry and geochemistry contain information of the different low and high ionic strength activity correction models for aqueous species (Anderson and Crerar, 1993; Appelo and Postma, 2005). Thermodynamic equilibrium between the aqueous and the solid phase or kinetic reactions is for example expressed in terms of activities rather than component concentration or species concentrations. Aqueous equilibrium reactions are written as:

$$A_j = \sum_{i=1}^{N_p} \nu_{ji} A_i \qquad 3.13$$

where A_i and A_j are the chemical formulae of the primary and secondary species, respectively. When thermodynamic equilibrium is obtained (*i.e.* at the minimum of the Gibbs free energy of the system), the concentration of the secondary species are obtained via the law of mass-action equation as:

$$c_j = \frac{\prod_{i=1}^{N_p} (\gamma_i c_i)^{\nu_{ji}}}{K_j \gamma_j} \qquad 3.14$$

where K_j is the equilibrium constant for the reaction and γ_i and γ_j are the activity correction coefficients for the primary and secondary species, respectively[2]. Activity correction coefficients relates the concentration of the species to the activities which are used in the definition of the equilibrium constant (activity $a_i = \gamma_i c_i$).

3.3.1.5.2 Mineral precipitation and dissolution

The composition and amount of the solid phase assemblage and its evolution are important variables for flow and transport parameters (as the amount and distribution of solid phases determine the microstructure) and for the sorption of aqueous speciation (capacity for sorption is defined by the type of minerals and their properties).

The general equation for a mineral dissolution and precipitation reaction is written as:

$$M_l = \sum_{k=1}^{N_l} \nu_{kl} A_k \qquad 3.15$$

where M represents the chemical formula of the mineral and N_l is the number of aqueous species in the reaction equation. The equilibrium constant is again expressed as the ratio of the activity product of the reactants (right hand-side) and the product (the mineral at the left hand side). The activity of a pure phase is assumed to be equal to 1, thus at equilibrium, following law of mass-action equation is satisfied:

$$K_l = \prod_{k=1}^{N_l} (\gamma_k c_k)^{\nu_{kl}} \qquad 3.16$$

A solid-solution is a solid phase consisting of variable mixing of pure end-member minerals. The activity of an end-member in a solid solution is different from 1 and is related to the mole fraction in the solid-solution:

$$a_i = \gamma_i X_i / X_i^0 \qquad 3.17$$

where a_i is the activity of the end member in solid-solution, X_i is the mole fraction and X_i^0 is the mole fraction at standard state (assumed to be 1). In an ideal solid solution, the activity correction factor γ_i equals 1 and thus the activity equals the mole fraction of the end member. For a non-ideal solution, the activity correction factor is related to the excess free-energy of mixing due to non-ideality. The non-ideality is described with semi-empirical models for binary, ternary, symmetric and asymmetric systems. One of the most often used models to calculate the activity correction factors for a binary non-ideal solid solution is based on Guggenheim series expansion (Glynn, 1991) but other models are also included in reactive transport models (e.g. via GEM3K (Kulik et al., 2013) and the TSolMod library (Wagner et al., 2012)). One particularity of non-ideal solid solutions is that the mechanical mixture of the end members is sometimes more stable than the one-phase solid solution leading to an immiscibility or a phase separation.

Mineral precipitation and dissolution reactions can alter the microstructure and local porosity and have an influence on material properties including permeability and solute transport parameters (see section 4.1.1) or even heat transport parameters.

Beside the equilibrium assumption discussed in this section, dissolution or precipitation rates are often slow compared to envisaged time scales (e.g. during transport calculations), meaning that time is required to reach equilibrium. In that case, a kinetic formulation is required which is discussed in section 3.3.1.5.6.1 The need to implement kinetic rather than equilibrium reactions depends on many factors including the time and spatial scale (experimental studies, ~months to year) at the interface scale may need rather a kinetic than equilibrium implementation), minerals involved (fast kinetics such as calcite compared to slow kinetics for e.g. clay minerals), and the overall goals/endpoints of a particular assessment. The dimensionless Damköhler number expresses the ratio of the transport (advective-dispersive) time over the reaction time; if this ratio is large, local equilibrium can be assumed (Sanchez-Vila et al., 2007). Note that small-scale heterogeneity can also contribute to a need to incorporate (heterogeneous) kinetics, specifically when mixing in the complete pore space is long compared to reaction time (diffusive time over reaction rate, Dentz et al. (2011)).

3.3.1.5.3 Ion exchange

The ion exchange process is a charge-neutral exchange of ions between the aqueous phase and exchange sites at the surface of solid phases. The site capacity of a surface is thus always occupied with species of the opposite charge such that the surface is charge neutral. Although this process includes also the exchange of anions with a positively charged surface, the cation exchange process (exchange of cations with a negatively charged surface of e.g. a clay mineral) is more common. In general form, the exchange reaction can be written as:

$$\nu_{A_j} A_k X_{\nu_{A_k}} + \nu_{A_k} A_j \rightleftharpoons \nu_{A_k} A_j X_{\nu_{A_j}} + \nu_{A_j} A_k \qquad 3.18$$

where X denotes the ion exchanger (with unit charge), A_k and A_j denote aqueous species with opposite charge than that of the exchanger, and ν_{Aj} and ν_{Ak} are the stoichiometry coefficients. The equilibrium constant is written as:

$$K = \frac{\left(\mathrm{A}_j \mathrm{X}_{\nu_{\mathrm{A}_j}}\right)^{\nu_{\mathrm{A}_k}} \left(\mathrm{A}_k\right)^{\nu_{\mathrm{A}_j}}}{\left(\mathrm{A}_k \mathrm{X}_{\nu_{\mathrm{A}_k}}\right)^{\nu_{\mathrm{A}_j}} \left(\mathrm{A}_j\right)^{\nu_{\mathrm{A}_k}}} \qquad 3.19$$

where () denotes activity. There are different conventions for calculating the activity correction coefficients for the exchange coefficients called Gaines-Thomas, Gapon or Vanselow conventions (see Appelo and Postma (2005) or Sposito (1981)). The Rothmund-Kornfeld model accounts for changing selectivity with site occupancy (Bloom and Mansell, 2001; Bond, 1995). Alternatively, different exchange

sites can be defined, each with different selectivity coefficients. At low concentrations, the high selective sites are first filled up; less selective sites are filled up at higher concentrations. The three-site exchange model for Cs sorption on illite of Bradbury and Baeyens (2000) is often applied to describe Cs in clay host formations (e.g. Maes et al., 2008).

Exchange reactions can be treated kinetically as well, although it is generally assumed that these reactions are fast enough to treat as equilibrium reactions. However, in a continuum approach, for heterogeneous media, time for mixing of the solutes in the complete pore space might be too long.

3.3.1.5.4 Surface complexation

Surface complexation is an important process as it describes sorption of major and trace elements as a function of the prevailing geochemical conditions near the solid phase surface. A major difference with exchange processes is that protons, cations and anions are released without compensation by other ions in equivalent properties (as opposed to exchange processes, Appelo and Postma (2005)). The surfaces can be positively or negatively charged (variable charged solid) depending on the pH of the soil solution. Such variable charged solids exist for both natural and engineered materials. Variable charged solids for natural subsurface systems are clays, oxides and organic matter. Also most materials for the technical barriers in an underground surface systems contains such variable charged solids such as cement (Missana et al., 2019; Olmeda et al., 2019).

In surface reactions, aqueous species binds to functional groups on the surface; as an example an equation of a metal sorbing on a surface hydroxyl site (≡OH):

$$\equiv XOH + M^z \leftrightarrow \equiv XOM^{z-1} + H^+ \qquad 3.20$$

Similar to aqueous complexes, the degree of surface complexation depends on the chemical affinity between the aqueous species and the surface functional group and on the electrostatic effects near the solid surface due to the surface charges. These two factors are represented in surface complexation models via following mass action analogue:

$$K_a = \frac{\left(\equiv XOM^{z-1}\right)\left(H^+\right)}{\left(\equiv XOH\right)\left(M^z\right)} e^{-\frac{zF\psi_0}{RT}} = K_{\text{int}} K_{coel} \qquad 3.21$$

where K_a is the apparent equilibrium constant, K_{int} is the intrinsic equilibrium constant, and K_{coel} represents the electrostatic component. Note that the adsorption reaction can also be written in terms of Gibbs free energy. The key point is to relate the charge distribution near the solid surface to the potential in order to calculate equilibrium. This gives rise to surface complexation models that differ in the way the division is made between charged surface and bulk solutions and the charge/potential relations that are used. The four most common models are the constant-capacitance model (CCM), the diffuse double layer model (DDL), the triple layer model (TLM) and the CD-MUSIC model (Goldberg et al., 2007).

In one layer models, all adsorbed ions are located on a single plane and the surface charge density at that single plane is used to calculate the surface potential by assuming a constant capacitance (CCM) or a variable capacitance calculated with the potential-charge relationship given by the Gouy-Chapman theory that depends on the ionic strength. It represents the diffuse layer of ions balancing the charge of the surface. Other models account for sorption directly to the surface (inner complexes, typically for H+ and OH-) and one or two additional planes (outer complexes). The Basic Stern Model (BSM) has one additional plane (inner plane) with a constant capacitance between the surface and inner planes and

neglect any potential change between the inner plane and the outer plane where the diffuse layer starts[15]. The TLM assumes a second capacity between the inner and outer layer. The CD-MUSIC model (Hiemstra and Van Riemsdijk, 2006; Hiemstra and Van Riemsdijk, 1996) distributed the charge of an adsorbed ion between different planes.

Most reactive transport models include one or more of these models to calculate K_{coel}. However, note that surface complexation models are also often implemented neglecting the electrostatic forces (i.e. K_{coel} = 1) or diffuse layer calculations.

Surface complexation reactions can be treated kinetically as well, although it is generally assumed that these reactions are fast enough to treat as equilibrium reactions. However, in a continuum approach, for heterogeneous media, time for mixing of the solutes in the complete pore space might be too long. One possible way is for example by a multi-rate multi-transport type of model as illustrated in Greskowiak et al. (2015) for U sorption.

3.3.1.5.5 Gas reactions

When a gaseous phase is present, exchange between a component G_i in the gaseous phase and a component A_i in the aqueous phase:

$$G_i \leftrightarrow A_i \qquad 3.22$$

is in most cases treated as equilibrium condition. Equilibrium is obtained when the ratio of the activities of the aqueous species in the reaction equation over the ratio of the fugacities of the gaseous species equals 1. Under the assumption of a mixture of ideal gases, the fugacity coefficient is 1 and the fugacity of a gas equals the partial pressure of the gas. For total gas pressures below 10 atm, the fugacity coefficient will be close to 1 (Appelo et al., 2014). For larger total gas pressures, fugacity correction factors can be calculated with the Peng and Robinson equation of state (Peng and Robinson, 1976).

Gaseous components are typically generated or consumed by kinetic reactions such as corrosion or degradation of organics acting for example as electron acceptors (see sections 3.3.1.5.6.2 and 3.3.1.5.6.3).

3.3.1.5.6 Kinetic processes

3.3.1.5.6.1 Kinetic dissolution/precipitation of solid phases (minerals)

Dissolution of minerals in porous media is often treated as a kinetic process. The dissolution kinetics are controlled by the reactions taken place at the surface of the minerals – surface-controlled reactions – and diffusion processes through different layers covering the reactive minerals – transport-controlled reactions (Mayer et al., 2002). Micro-scale transport processes may occur across a stagnant water layer or through surface coatings or alteration rims (Murphy et al., 1989). The reader is referred to several general textbooks (Brantley et al., 2008; Lasaga, 1998; Rimstidt, 2013) for more details on geochemical kinetics in general, and mineral kinetics specifically, and to Cama and Ganor (2015) for details on clay minerals. A general form of a surface-controlled kinetic reaction accounting for effect of reactive surface areas, temperature, different reaction mechanisms and dependence on solution saturation state is (Lasaga, 1998):

[15] Terminology indicates also, beside the surface plane, the Inner Helmholtz Plane (IHP) for sorption of the hydrated ions and an Outer Helmholtz Plane (OHP) that is the beginning of the diffuse layer.

$$r = S\left(\sum_j A_j e^{-E_{a,j}/\ RT} \prod_i a_i^{n_{i,j}} f(\Omega)\right) \quad 3.23$$

where r is the dissolution/precipitation rate [M T^{-1} L^{-3}], and the factors at the right hand side are:

- *S* – the reactive surface area [L^2 L^{-3}] which can be treated as an constant term, or a changing value (for spherical particles with uniform dissolution, the value change according to (m/m_0)^(2/3)
- Temperature dependence described by Arrhenius equation where parameter A_j is the Arrhenius pre-exponential factor [mol L^{-2} T^{-1}], $E_{a,j}$ is the apparent activation energy [J mol^{-1}], *R* is the universal gas constant [J mol^{-1} K^{-1}] and *T* is temperature [K]
- One or more terms representing different mechanisms (e.g., different catalyst for dissolution) where *a* is the activity of a given species, and $n_{i,j}$ is an empirical constant.
- A factor that represents the effect of the saturation state of the solution via saturation ratio Ω.

The reaction rate for many minerals depends on the pH. Palandri and Kharaka (2004), for example, defined 3 terms in Eq. (3.23) related to H^+, H_2O and OH^- promoting reactions for which the coefficients $n_{i,j}$ are obtained by a piecewise linear regression on measured reaction rates.

One of the most commonly used expressions of f() is (Brantley et al., 2008; Oelkers et al., 1994):

$$f(\Omega) = \left(1 - \Omega^p\right)^q \quad 3.24$$

where *p* and *q* are empirical constants, often assumed to be equal to 1. When an aqueous phase is in equilibrium with a mineral, Eq. 3.24equals zero and there reaction rate is zero. The sign of Eq. 3.24 is positive or negative in case of, respectively, over- or undersaturation enabling to simulate precipitation or dissolution. Note that Eq. 3.24limits the dissolution rate to a constant value when far from equilibrium, whereas the precipitation rate will increase with deviation from equilibrium.

3.3.1.5.6.2 Degradation of organics

The fate of organics present in the waste can be described by kinetic rate equations including Monod terms for electron donor and acceptor concentrations (Small and Abrahamsen-Mills, 2018). A general from of such equation is:

$$R = Q_{max} B \frac{[E_D]}{K_D + [E_D]} \frac{[E_A]}{K_A + [E_A]} I_B \prod(I_X) f_T \quad 3.25$$

where *R* is the degradation rate [M T^{-1} L^{-3}], Q_{max} is the maximum rate [M $M_B^{-1}T^{-1}$], *B* is the biomass [M_B L^{-3}], [E_D] and [E_A] are the concentrations of the electron donor and acceptor [M L^{-3}], K_D and K_A are the half-saturation constants for the electron donor and acceptor [M L^{-3}], the factor I_B accounts for rate reduction when the microbial biomass is too large due to e.g. pore restrictions (see e.g. Brovelli et al. (2009), Pham (2018), or Ben Moshe et al., (2021) for different functional forms). I_X are inhibition factors, typically in the form of (K_X / (K_X+[X]) with K_X the half saturation constant) which can control a redox sequence to suppress reactions when higher energy-yielding terminal electron acceptors are still present (e.g., de Blanc et al., 1996, Bhanja et al., 2019 or Small and Abrahamsen-Mills 2018), but may also include terms related to toxicity or pH (e.g Maia et al. 2016) or Small and Abrahamsen-Mills (2018)). Control of the rate by the pore water composition can be done as well by including a thermodynamic potential factor into the equation taking into account the Gibbs free energy of the electron transfer reaction and energy required for ATP synthesis (Jin and Bethke, 2003, 2005; Jin and Bethke, 2007). The last factor f_T accounts for temperature effects and is typically described by Arrhenius law. Note also that many variants exist for this particular equation, ranging from first-order definition to competitive effects (de Blanc et al., 1996). Or et al. (2007) reviews factors that are related to these reactions in

unsaturated porous media. Mathematically, a yield factor links the growth of biomass to the rate of degradation.

3.3.1.5.6.3 Dissolution of non-porous materials (Steel)

Metallic iron in low carbon or weakly alloyed steels is never under equilibrium in contact with aqueous solutions, both under oxic and anoxic redox conditions. It will be subjected to corrosion such as generalized or pitting corrosion processes. This disequilibrium also requires a kinetic treatment of these type of materials. The challenge is the representation of a non-porous material in a reactive transport model at the continuum scale.

Corrosion of metallic alloys in oxic and anoxic conditions under repository conditions are often simplified to (Bildstein et al., 2019):

- $$4Fe_{(s)}+6H_2O+3O_{2(aq)} \rightarrow 4Fe^{3+}+12OH^- \quad (3.26)$$

$$Fe_{(s)}+2H_2O \rightarrow Fe^{2+}+2OH^-+H_{2(aq)} \quad (3.27)$$

Often, steel corrosion in reactive transport models is described with a zero-order constant rate model, although some studies also investigated rates depending on solution composition (Wilson et al., 2015) or diffusion through the corrosion layer (Peña et al., 2008). The corrosion products are then simulated by either assuming equilibrium or kinetic precipitation reactions. In addition, in reactive transport models, it is conceptualized as a porous medium to enable transfer from Fe from the solid to the aqueous phase and diffusion into the neighbouring cells. Also the movement of the steel interface is a complex and challenging aspect not often taken into account in numerical studies on steel-bentonite, steel-clay, steel-cement and steel-glass. A step forward can be expected when electrochemical corrosion models (Bataillon et al., 2010; Macdonald et al., 2011) are introduced into reactive transport models (see also state-of-the-art report of WP DONUT, Ahusborde et al. (2021)).

3.3.2 Tools and databases

3.3.2.1 Codes

The overview is limited to codes that are expected to be used in ACED. An overview of the processes included in these codes is given in Table 3-1.

Table 3-1: Overview of processes discussed in section 3.3.1 and feedback between geochemistry and transport properties (see further, section 4.1.1) that are included in the different reactive transport codes used in ACED.

Process	CORE2D V5	Crunchflow	HPx	HYTEC	INVERSE-FADES-CORE2D V2	OPENGEOSYS	PFLOTRAN	PHREEQC-3
Fluid flow	Yes	Yes	Yes	Yes	Yes	Yes	Yes	No
Heat transfer	Yes	Yes	Yes	Yes	Yes	Yes	Yes	Yes
Solute transport	Yes	Yes	Yes	Yes	Yes	Yes	Yes	Yes
Aqueous reactions	Yes	Yes	Yes	Yes	Yes	Yes	Yes	Yes
Minerals	Yes	Yes	Yes	Yes	Yes	Yes	Yes	Yes
Solid solutions	No	Yes	Yes	No	No	Yes	No	Yes
Ion exchange	Yes	Yes	Yes	Yes	Yes	Yes	Yes	Yes
Surface complexation	Yes	Yes	Yes	Yes	Yes	Yes	Yes	Yes
Gas	Yes	Yes	Yes	Yes	Yes	Yes	Yes	Yes
Kinetics	Yes	Yes	Yes	Yes	Yes	Yes	Yes	Yes
Porosity change	Yes	Yes	Yes	Yes	Yes	Yes	Yes	No
Tortuosity change	Yes	Yes	Yes	Yes	Yes	Yes	Yes	No
Permeability change	Yes	Yes	Yes	Yes	Yes	Yes	Yes	No

3.3.2.1.1 Core^{2D} V5

CORE^{2D} V5 (Fernández, 2017) is a code for transient saturated and unsaturated water flow, heat transport and multicomponent reactive solute transport under both local chemical equilibrium and kinetic conditions in heterogeneous and anisotropic media. The flow and transport equations are solved with Galerkin finite elements and an Euler scheme for time discretization. The solute transport equation accounts for advection, molecular diffusion and mechanical dispersion. The chemical formulation is based on the ion association theory and uses an extended version of the Debye-Hückel equation (B-dot) for the activity coefficients of aqueous species. The following chemical reactions are considered: aqueous complexation, acid-base, redox, mineral dissolution/precipitation, cation exchange, surface complexation and gas dissolution/exsolution. CORE^{2D} V5 relies on the "com" thermodynamic database of EQ3/6 (Wollery, 1992). The code also allows the use of other thermodynamic databases. CORE^{2D} V5 is based on the sequential iteration approach to solve for chemical reactive solute transport. Iterations are repeated until some prescribed convergence criteria are attained (Samper et al., 2009). The concentrations of secondary species are computed from the concentrations of primary species through appropriate mass action laws (Xu et al., 1999). The concentrations of precipitated, exchanged and adsorbed species are computed using similar equations. The Gaines-Thomas convention is used for cation exchange. Surface complexation is modelled by using three types of protonation/deprotonation sites, S^{S}-OH, S^{W1}-OH and S^{W2}-OH, as proposed by (Bradbury and Baeyens, 1997). A detailed description of calculations of chemical reactions can be found in Xu et al. (1999). CORE^{2D} V5 takes into account the changes in porosity due to mineral dissolution/precipitation reactions and their feedback effect on the flow and transport parameters under isothermal and nonisothermal conditions (Águila et al., 2020; Fernández, 2017).

The code has been extensively verified against analytical solutions and other reactive transport codes. In addition, the code has been widely used to model laboratory and in situ experiments (Dai et al., 2008; Samper et al., 2008b; Samper et al., 2008c; Yang et al., 2008; Zhang et al., 2008), the interactions of corrosion products and bentonite (Lu et al., 2011; Samper et al., 2008a), to evaluate the long-term geochemical evolution of repositories in granite and clay (Mon et al., 2017; Samper et al., 2016; Yang et al., 2008), and model the impact of CO_2(g) leakage on groundwater quality (Yang et al., 2015; Yang et al., 2013).

Fernández (2017) updated and improved the THCM conceptual and numerical models and the flow and reactive transport codes of the CORE series developed at the University of A Coruña. These activities included: (1) Improvements in the code CORE^{2D}V5 dealing with porosity changes due to mineral dissolution/precipitation and the feedback effect on flow, transport and chemical parameters; (2) Update of CORE^{2D}V5 to use available public-domain post-processing tools; (3) Improve the convergence criteria to solve flow in variably saturated porous media in CORE^{2D}V5; and (4) Update of INVERSE-CORE2D to estimate large sets of variables. Particularly noteworthy were the improvements implemented by Fernández (2017) in CORE^{2D}V5 dealing with porosity changes and its verification. The reactive transport code was extended to take into account the porosity changes due to mineral dissolution/precipitation and their feedback effect on transport properties. The changes of the porosity in a porous medium due to mineral alteration processes, and the associated change of transport parameters are important processes which influence the evolution of the engineered barrier systems. If porosity increases substantially, preferential fluid migration pathways may be developed, accelerating solute transport. On the other hand, a significant porosity decrease may inhibit fluid and solute transport. Clogging occurs when the porosity is close to zero and the aqueous phase may completely vanish. The updated version of the code CORE^{2D}V5 has been extensively verified against analytical solutions and by benchmarking with other reactive transport codes.

3.3.2.1.2 Crunchflow

CrunchFlow[16] is a multidimensional reactive transport code in porous media developed by C. Steefel and coworkers at LBL (Steefel et al., 2015b). It allows for the simulation of advective, dispersive, and diffusive transport in 1D and 2D with a global implicit method and up to 3D using the "operator splitting" mode. Of particular interest in the project, diffusive transport and reactions can be treated in non-isothermal conditions including exchanges at equilibrium between the gas and aqueous phases (simulations with partially saturated flow requires a separate software).

The chemical processes taken into account in Crunchflow include:

- multicomponent aqueous complexation and redox reactions,
- ion exchange on multiple sites,
- surface complexation on multiple sites with or without electrostatic correction based on the double layer model (site densities may be linked to mineral amounts),
- kinetically controlled precipitation and dissolution of minerals based on the Transition State Theory, and microbially mediated reactions based on the Monod type formulation,
- kinetic isotope fractionation associated with mineral reactions.

For the diffusive transport, the user can also provide different diffusion coefficient for each aqueous species. The diffusive flux is then calculated accounting for the electrochemical migration of the ions and corrected for electroneutrality using the Nernst-Planck equation. Feedback induced by reactions on porosity, permeability, and diffusion can also be treated. Porosity is updated using the volume balance of dissolved and precipitated minerals. Diffusion coefficients can be updated using Archie's law with a user defined formation factor or cementation coefficient.

Crunchflow has been extensively used in a variety of contexts (Steefel et al., 2015b) and, in particular, in studies concerning the physicochemical evolution of disposal cells in deep geological repositories (e.g. Bildstein et al., 2016; Bildstein et al., 2006; Marty et al., 2015a; Wersin and Birgersson, 2014; Wersin et al., 2008). Two specific features of the code may be exploited in the EURAD/ACED program depending on the experimental data available. The first one is the capability of the code to treat the alteration of glass with a specific kinetic model, where the dissolution rate is controlled by the diffusion of water and ions in a passivating layer (the GRAAL model, Frugier et al. (2018)). The second one is the coupling of the code with the electrochemical corrosion model Calipso (Bataillon et al., 2010).

3.3.2.1.3 HPx

HPx (Jacques et al., 2018; Jacques et al., 2008) couples the flow and transport codes HYDRUS-1D[17] and HYDRUS(2D/3D)[18] (Šimůnek et al., 2016) with PHREEQC (Parkhurst and Appelo, 2013) using a sequential non-iterative coupling approach as described in Jacques et al. (2006). The HYDRUS-codes act as the transport solver solving equations for variable-saturated water flow, advective-dispersive transport of solutes, diffusive transport in the gas phase and heat transport. The current version includes the latest PHREEQC version (version 3.6.2, see paragraph 3.3.2.1.8). The coupling between HYDRUS and PHREEQC is done using hard-coupling and HPx is fully integrated in the graphical user interfaces of HYDRUS (see https://www.pc-progress.com/en/default.aspx). Geochemical calculations are calculated in parallel using the OpenMP (www.openmp.org) shared memory approach.

Using the flow and transport capabilities of HYDRUS, flow and transport can be simulated for both large scale (different materials) and small scale heterogeneity (spatial-variable hydraulic parameters, mobile-immobile transport models, dual porosity models) (Šimůnek and van Genuchten, 2008). From a geochemical point of view, virtually all geochemical models from PHREEQC can be used within HPx. The possibility to have scripts in the input file (similar to PHREEQC) increases the flexibility of the code

[16] https://bitbucket.org/crunchflow/crunchtope-dev/wiki/Home
[17] https://www.pc-progress.com/en/Default.aspx?h1d-hp1
[18] https://www.pc-progress.com/en/Default.aspx?h3d2-hp2

to handle kinetic rate equations. This functionality is enhanced in HPx by introducing a more flexible variant of BASIC scripting (https://github.com/paladin-t/my_basic) or more recently including python (version 3.7) as a scripting language. Scripts within an input file can be defined with different functionalities for preprocessing and initialization, specific calculations during the transport simulation or post-processing.

HPx allows for to dynamically altering flow and transport properties during the transport simulation. The functional form of e.g. the relation between permeability and porosity is not hard-coded but the user supply the relations between the geochemical state variables and the transport properties. To model the spatial-temporal evolution of flow parameters, the concept of linear scaling of hydraulic properties (Vogel et al., 1991) is used. The user thus defines the values of the scaling factors for the porosity, pressure head or hydraulic conductivity for each node at each time step using any model ranging from e.g. the Kozeny-Carman relation to models given in e.g. Wissmeier and Barry (2009) or Freedman et al. (2004). A similar flexibility exists for tortuosity in the aqueous or gaseous phase, dispersivity and parameters related to the heat transport equations.

3.3.2.1.4 HYTEC

The reactive transport code HYTEC (van der Lee et al., 2003) accounts for many commonly encountered chemical processes, including interface reactions (surface complexation with electrostatic correction and cation exchange), precipitation and dissolution of solid phases (minerals and colloids), organic complexation, and redox and microbial reactions. All reactions can be modelled using a full equilibrium or a mixed equilibrium–kinetic approach. Thermodynamic data are taken from international databases, such as Thermoddem and ThermoChimie.

The hydrodynamic module of HYTEC is adapted for hydrodynamic conditions commonly encountered in the laboratory or in the field. The code allows for dual porosity, saturated, unsaturated or two-phase flow, variable boundary conditions, sinks, and sources. HYTEC searches for an accurate solution to the multicomponent transport problem using an iterative, sequential, so-called strong coupling scheme. Strong coupling permits variable hydrodynamic parameters as a function of the local chemistry. For example, the porosity of a porous medium decreases after massive precipitation of newly formed mineral phases, which modifies the water flow paths and transport parameters, e.g., diffusion coefficients.

HYTEC solves this interdependency accurately, which makes the tool particularly useful for, e.g., cement alteration at long timescales. Heat-transfer by conduction and convection can also be modelled, with chemical and flow/transport parameters that are temperature-dependent. HYTEC has been widely used for the long-term safety assessment of nuclear waste disposal, from the waste form and engineered barrier to the host-rock (De Windt and Spycher, 2019).

3.3.2.1.5 INVERSE-FADES-CORE-V2

INVERSE-FADES-CORE V2 (Mon, 2017) is a finite element code for modelling non-isothermal multiphase flow, heat transport and multicomponent reactive solute transport under both chemical equilibrium and kinetic conditions in deformable media. The code takes into account the mass balance of water, air, solid and enthalpy; the transport of solids and the mechanical equilibrium. The solute transport equation accounts for advection, molecular diffusion and mechanical dispersion.

INVERSE-FADES-CORE V2 solves both forward and inverse multiphase flow and multicomponent reactive transport problems in 1-, 2- and 3-D axisymmetric porous and fractured media. The code is the result of integrating the capabilities of the THM code FADES (Navarro, 1997); the reactive transport code CORE^{2D} (Samper et al., 2011), the THMC code FADES-CORE (ENRESA, 2000) and the inverse methodology of INVERSE-CORE (Dai and Samper, 2004). The state variables of the forward model include the liquid and the gas pressures and temperature, which are solved with a Newton-Raphson method. Similar to CORE^{2D} V5, the concentrations of secondary species are computed from the

concentrations of primary species. The Gaines-Thomas convention is used for cation exchange. Surface complexation is modelled by using three types of protonation/deprotonation sites, S^{S}-OH, S^{W1}-OH and S^{W2}-OH. INVERSE-FADES-CORE V2 uses also a sequential iteration approach.

The equilibrium constants for aqueous complexes and minerals change with temperature under non-isothermal conditions. They are calculated with an analytical expression, which is valid for temperatures ranging from 0 to 300 ºC. The "com" thermodynamic database of EQ3/6 (Wollery, 1992)(Wolery, 1992) is used for aqueous complexes and minerals. INVERSE-FADES-CORE V2 also allows the use of other thermodynamic databases.

The inverse problem is solved by minimizing a generalized least-squares criterion with a Gauss-Newton-Levenberg-Marquardt method (Dai and Samper, 2004). The forward routines of INVERSE-FADES-CORE have been widely verified with analytical solutions and other reactive transport codes. The main applications of INVERSE-FADES-CORE include: the THC and THCM models of the FEBEX in situ test (Samper et al., 2008a; 2018a; Zheng et al., 2008a; 2011); the THCM model of the FEBEX mock up test (Zheng and Samper, 2008); the THCM model of a heating and hydration lab experiment performed on compacted FEBEX bentonite (Zheng et al., 2010; Samper et al., 2018b); and the THC model of the Ventilation Experiment on the Opalinus Clay (Zheng et al., 2008b).

Mon (2017) implemented the reactive gas transport in the reactive transport code INVERSE-FADES-CORE V2 by including additional mass balance equations for the reactive gaseous species in the gaseous phase. The mass balance equation for a given gas accounts for: a) Advection; b) Molecular diffusion; c) Mechanical dispersion; and d) Exchange with the liquid phase. The implementation of the reactive gas transport was verified by comparing the numerical results of INVERSE-FADES-CORE V2 with the results computed with TOUGHREACT (Xu et al., 2008) with four test cases. In addition, INVERSE-FADES-CORE V2 was benchmarked with other codes for the following two benchmarking problems: 1) Modeling the chemical interactions of the concrete liner with the compacted bentonite of the engineered barrier and the host clay rock; and 2) Modelling the carbonation of concrete in unsaturated conditions during the operational period of a repository.

3.3.2.1.6 OPENGEOSYS

OpenGeoSys[19] (OGS) is a scientific open-source initiative for the numerical simulation of thermo-hydro-mechanical-chemical (THMC) processes in porous and fractured media. The basic concept of OGS consists of providing a flexible numerical framework, using primarily the Finite Element Method (FEM) for solving multi-field coupled processes with application in different scientific and technical disciplines. For example, OGS has been successfully applied in the fields of regional, contaminant and coastal hydrology (Nixdorf et al. 2017; Walther et al. 2017; Jing et al. 2018, 2019), fundamental and geothermal energy systems (Chen et al., 2019; Parisio et al., 2019a; 2019b; Meng et al., 2018; Hein et al., 2016), geotechnical engineering (Zhu et al., 2020), energy storage (Miao et al., 2019; Lehmann et al., 2019; Böttcher et al., 2017; Nagel et al., 2017; Pfeiffer et al., 2016), CO_2 sequestration/storage(Liu et al., 2019; Li et al., 2014; Beyer et al., 2012) and nuclear waste management and disposal (Shao et al., 2019a, 2019b).

Since the mid-eighties (Kolditz, 1990;, Wollrath, 1990; Kroehn, 1991; Helmig, 1993) OpenGeoSys is in continuous development evolving through Fortran, C, and C++ implementation with the current released version being OpenGeoSys 6.2.2 (Naumov et al., 2020). OpenGeoSys-6 (Naumov et al., 2018; Bilke et al. 2019) is a complete re-implementation of OpenGeoSys 5 (Kolditz et al., 2004; Wang and Kolditz, 2006; Kolditz et al., 2012) which uses advanced methods in software engineering and architecture with focus on code quality, modularity, performance and comprehensive documentation. Till the present moment, particular emphasis has been placed on the implementation of advanced numerical methods for simulating propagation of discontinuities, such as enriched finite element function spaces (Watanabe

[19] https://www.opengeosys.org/

et al., 2012), non-local formulations (Parisio et al., 2018) and phase-field models (Yoshioka et al., 2019). As in the previous version, OGS-6 is taking advantage of High Performance Computing (HPC) platforms on both MPI and OpenMP concepts to analyze realistic complex geosystems (Fischer et al., 2019; Wang et al., 2015, 2017).

Regarding reactive transport processes, different approximations have been implemented in OGS along its development in order to consider multicomponent mass transport and bio/geochemical reactions (Chen et al., 2020; Boog et al., 2019a, 2019b; Yapparova et al., 2019). For example, Ballarini et al. (2014) used an internal OGS library to simulate kinetically controlled biogeochemical reactions. In other cases, OGS has been coupled in a sequential non-iterative approach with well-known external geochemical solvers (i.e. PHREEQC, GEMS, BRNS and ChemApp). The coupling of these codes are referred as OGS-PHREEQC (Xie et al., 2006; He et al., 2015), OGS-GEM (Kosakowski and Watanabe, 2014), OGS-BRNS (Centler et al., 2010) and OGS-ChemApp (Beyer et al., 2012; Li et al., 2014). Very recently, an alternative coupling solution of reactive transport has been developed and implemented by approximating the complex chemical reactions into a quickly calculating look-up table (Aguila et al., 2020; Huang et al., 2018). The novel implementation provides fast and efficient simulations, a feature especially relevant for long-term simulations. Reactive transport calculations referred above have been mainly performed with OGS-5, although OGS-6-iPHREEQC version is already released (Naumov et al., 2020). This new version includes a new implementation with direct memory access which allows efficient computational simulations. Application of OGS on reactive transport modelling in the framework of nuclear waste disposal includes long term cementitious materials/clay interactions (Idiart et al., 2020; Kosakowski et al., 2014; Kosakowski and Berner, 2013; Berner et al., 2013; Shao et al. 2013), laboratory scale precipitation/dissolution processes in combination with density driven flow and clogging effects (Poonoosamy et al., 2020, 2018, 2015) and with mechanical processes (Lu et al., 2018), concrete degradation due to reactive aggregates in combination with multi-phase transport of CO_2 (Huang et al., 2018) and radionuclide migration in clays (Aguila et al., 2020). Recently, the look up table approach has also been applied to model gas and humidity transport in combination with concrete/ organic matter degradation and corrosion of metals in a waste package during 100 years of intermediate storage (Huang, et al. 2019).

Finally, OpenGeoSys is participating in several international model development, validation and benchmarking initiatives, e.g., DEVOVALEX (with applications mainly in the assessment of nuclear waste repositories (Birkholzer et al., 2018), CO2BENCH (Kolditz et al,. 2012b), SeS Bench (Steefel et al., 2015) and HM-Intercomp (Maxwell et al., 2015), providing ongoing series of benchmark books (Lehmann et al., 2018) and tutorials (Jang et al., 2017). For more information please refer to the OpenGeoSys webpage (www.opengeosys.org).

3.3.2.1.7 PFLOTRAN

PFLOTRAN[20] (Hammond et al., 2014)is an open source, state-of-the-art massively parallel subsurface flow and reactive transport code. PFLOTRAN solves a system of generally nonlinear partial differential equations describing multiphase, multicomponent and multiscale reactive flow and transport in porous materials. The code is designed to run on massively parallel computing architectures as well as workstations and laptops. Parallelization is achieved through domain decomposition using the PETSc (Portable Extensible Toolkit for Scientific Computation) libraries. PFLOTRAN has been developed from the ground up for parallel scalability and has been run on up to 2^{18} processor cores with problem sizes up to 2 billion degrees of freedom. PFLOTRAN is written in object oriented, free formatted Fortran 2003. The choice of Fortran over C/C++ was based primarily on the need to enlist and preserve tight collaboration with experienced domain scientists, without which PFLOTRAN's sophisticated process

[20] https://www.pflotran.org/

models would not exist. The reactive transport equations can be solved using either a fully implicit Newton-Raphson algorithm or the less robust operator splitting method.

3.3.2.1.8 PHREEQC-3

PHREEQC-3[21] (Parkhurst and Appelo, 2013) is able to perform aqueous geochemical calculations including all typical processes relevant for subsurface reactive transport. It includes several options for (i) aqueous activity correction calculations (Davies, Debye-Hückel association models, Pitzer and specific-ion interaction theory), (ii) exchange models, (iii) surface complexation (diffuse double layer model, constant capacitance model, CD-MUSIC model), and (iv) solid solutions (ideal, binary non-ideal model). The code allows for calculating temperature and pressure dependence of equilibrium constants (Appelo et al., 2014). PHREEQC-3 handles full equilibrium or mixed kinetic-equilibrium reaction networks with kinetic homogeneous and heterogeneous rate equations of arbitrary rate equations defined via the embedded BASIC interpreter.

The native transport possibility of PHREEQC-3 allows for one dimensional advection-dispersive transport, multi-dimensional diffusion calculation (Appelo and Wersin, 2007; Weetjens et al., 2009) or diffusion according the Nerst-Planck equation (Appelo, 2017; Appelo and Wersin, 2007). However, PHREEQC-3 is frequently used as the geochemical solver coupled to flow and transport solvers either directly via the source code (e.g. HPx, Jacques et al. (2018)), or via the modules IPhreeqc (Charlton and Parkhurst, 2011) and PhreeqcRM (Parkhurst and Wissmeier, 2015). Examples of the latter are coupling with OPENGEOSYS (He et al., 2015) or with COMSOL (Nardi et al., 2014; Perko et al., 2015; Wissmeier and Barry, 2011).

3.3.2.2 Databases

The engineered materials are not in equilibrium with the host rock. The chemical evolution for the disposal cell is slowly progressing towards an equilibrium between the engineered materials and host rock. The expected geochemical reactions can be derived by calculating the stability of the evolved mineral as a function of pH, redox potential, concentration of dissolved solutes, temperature and pressure. There are several thermodynamic databases that have thermodynamic data to calculate the stabilities of the minerals. Geochemical models use these thermodynamic data to calculate the concentration of solutes in equilibrium with the mineral. Deviation of these concentration of solids will result in either a dissolution or precipitation of a mineral. Thermodynamic databases are therefore the cornerstone for reaction transport models and the establishment of consistent databases contributed significantly to geochemistry and is of uttermost importance for incorporation into reactive transport modelling (Oelkers et al., 2009). In many of the above mentioned codes, some available databases are derived from the SUPCRT92 thermodynamic database (Johnson et al., 1992) or one of the later versions of it (Zimmer et al., 2016). SUPCRT92 or later versions are also available in codes based on minimization of Gibbs free energy as GEMS[22] (Kulik et al., 2013; Wagner et al., 2012) and Reaktoro (Leal et al., 2017). Zhang et al. (2020) provides a software to convert SUPCRTBL (Zimmer et al., 2016) to PHREEQC-readable databases in the requested P-T range[23] .

The aim here is not to give an overview of all available database, but just to list a few databases that are frequently used in the framework of geological disposal:

- Thermoddem[24]: The database is developed by BRGM (Blanc et al., 2012) and contains reactions and thermodynamic data for a temperature range up to 300 °C. Phases for cement materials, clay minerals and zeolites are included. The database is also extended with information on

[21] https://www.usgs.gov/software/phreeqc-version-3
[22] http://gems.web.psi.ch/
[23] https://models.earth.indiana.edu/superphreeqc.php
[24] https://thermoddem.brgm.fr/

surface complexation and cation exchange reactions. The database is available in the formats for PHREEQC, Crunchflow, ToughReact[25] (Xu et al., 2006; Xu et al., 2011), Chess(van der Lee, 1998), and The Geochemist's Workbench[26] .

- ThermoChimie[27] : The database is initiated by Andra in 1995, but also RWM and Ondraf/Niras joined the "Thermochimie consortium". The ThermoChimie databased is specifically developed for conditions relevant within radioactive waste repositories, i.e., applied over a pH range between 6 to 14, temperatures below 80°C and Eh in the range of -0.5 to +0.5 V (Giffaut et al., 2014). It includes information on host-rock mineral phases, bentonites, cements and their evolving secondary phases (e.g. Blanc et al., 2015), and on radionuclides (Grivé et al., 2015). The current version (v10a[28]) is available for several geochemical codes including PHREEQC, Crunchflow, ToughReact, Chess and The Geochemist's Workbench.
- PSI/Nagra Chemical Thermodynamic Data Base[29] : This database is developed in the framework of ongoing safety assessments for planned LLW, ILW and HLW repositories in Switzerland (Hummel et al., 2002; Thoenen et al., 2014). The database is available in PHREEQC and GEMS format. The latest version of the PSI/Nagra chemical thermodynamic database 2020 includes an extended list of rock-forming minerals, specifically clays and zeolites, imported from Thermoddem TDB.
- CEMDATA18.1: This database is specifically for hydrated solid phases in Portland cement systems (Lothenbach et al., 2019). It contains thermodynamic data for C-S-H, AFm and AFt phases, hydrogarnet, hydrotalcite, zeolites, and M-S-H in a temperature range between 0 and 100°C. Several solid-solution models are implemented to represent these phases. The database is available in GEMS, PHREEQC and Geochemist's Workbench format. At 25°C, it is fully consistent with PSI/Nagra Chemical Thermodynamic Data Base.These databases are recently also supplemented by new databases for zeolites[30] (Ma and Lothenbach, 2020a,b, 2021).
- THERADA[31] (Thermodynamic Reference Database): This is a joint effort to build an internally consistent reference database that could be used in geochemical and reactive transport codes for processes in the near and far field of different host rock types envisaged as potential sites for final repositories in Germany, including high concentration conditions (Moog et al., 2015). It is available in PHREEQC, Geochemist's Workbench and ToughReact format.
- NEA TDB (Nuclear Energy Agency Thermodynamic DataBase): This is a joint effort between different countries (nowadays 12) in which thermodynamic data with a sufficient quality are included in a database. The elements and compounds that need to be investigated are determined by the different countries. The selection of data is performed by a group of experts with a high track record in relevant scientific publications. The data have recently been put in a Phreeqc-formatted file (Martinez et al., 2019). The database is not complete for a safety assessment of geological disposal of radioactive waste, but databases such as Thermochimie and PSI/Nagra Chemical Thermodynamic Data Base have included these NEA TDB data due to the high quality assurance of the NEA TDB data.

Some focussed studies compiled thermodynamic information for some specific applications. De Windt et al. (2015) compiled data for complexation of short-chained organics in a cementitious system (simplified CEM I).

For chemical kinetics, we mention here two relevant compilations:

- A compilation by Marty et al. (2015b) for minerals relevant to clay rich rocks and cements. Parameters were provided for both the linear regression model and the regression curve model. The kinetic parameters are consistent with the ThermoChemie database and are available in three different formats (for PHREEQC, CrunchFlow and ToughReact).
- A compilation for more than 100 minerals provided in PHREEQC format[32] by Zhang et al. (2019) based on the work of Palandri and Kharaka (2004), mostly based on the kinetic rate equation Eq. (3.23).

[25] https://tough.lbl.gov/software/toughreact/
[26] https://www.gwb.com/
[27] https://www.thermochimie-tdb.com/
[28] June 2021
[29] https://www.psi.ch/en/les/database
[30] https://www empa.ch/web/s308/zeolite
[31] https://www.thereda.de/en/
[32] https://github.com/HydrogeoIU/PHREEQC-Kinetic-Library

For kinetics of dissolution of the C-S-H phase in cement, the study of Trapote-Barreira et al. (2014) provides information on rate parameters as function of the Ca/Si ratio of the C-S-H phase.

3.3.3 Modelling the geochemical evolution of materials

In this section, we discuss shortly some of the approaches for geochemical modelling of relevant materials in radioactive waste disposal context.

3.3.3.1 Vitrified glass

Dissolution of the glass matrix is modelled with relatively simple models using an apparent Si equilibrium concentration together with a simple diffusion-based model (Liu et al., 2019; Liu et al., 2015; Mann et al., 2019). From a numerical point of view, such a diffusion-based dissolution model only needs one first order ordinary differential equation which can be solved, e.g., with Runge-Kutta methods implemented as kinetic reaction in PHREEQC. Thus this model can be easily combined into reactive transport models based on PHREEQC coupling. On the other hand, GRAAL model (Frugier et al., 2008) includes more dissolution mechanisms especially for early dissolution stages. This model assumes that glass dissolution is controlled by the affinity of a passivating reactive interface (PRI). This model has been successfully integrated into the reactive transport code HYTEC (Frugier et al., 2018) and potentially can be integrated into other reactive transport codes as well (e.g. PHREEQC (Debure et al., 2018)). The study of Repina et al. (2020) includes fractures in the glass into HYTEC and the GRAAL dissolution model.

3.3.3.2 Cement-based materials

During the last decade, a solid basis for modelling cementitious system in the frame of radioactive waste disposal became available, specifically because of the development of consistent and complete databases (Lothenbach and Zajac, 2019). Originally, databases were for ordinary Portland cement systems, but advancements have been made to include phases relevant for other systems including M-S-H (Roosz et al., 2018), blended cements, C-(N)-A-S-H (Myers et al., 2013; Roosz et al., 2018), or high Na, Cl or nitrate concentrations (Balonis et al., 2010; Balonis et al., 2011; De Weerdt et al., 2019). More recently, a sub-lattice C-S-H model was proposed that also includes the uptake of alkalies (Kulik et al., 2022, Miron et al., 2022). Thermodynamic models are used to define the initial properties (phases, cementitious pore water composition, porosity) of the hardened cement paste based on clinker oxide composition, supplementary cementitious materials, water cement ratio etc. Lothenbach and Zajac (2019) and references therein shows ample of examples. As an alternative for calculating the equilibrium assemblage after full hydration, the kinetic hydration processes itself can be modelled as well. This is mainly based on empirical rate equations (e.g. Lothenbach and Winnefeld (2006)); some recent tools allow for user-friendly environments to calculate these initial conditions or the hydration process, e.g. the CemGEMS web app[33] (Kulik et al., 2021) or HYDCEM (Holmes et al., 2020). Please note that thermodynamic equilibrium may not have been achieved as experimental results of fabricated cement paste have shown. Especially the pH of cementitious pore water of fabricated concrete - made with so-called low pH formulations made with blended cements - can be higher than modelled.

Chemical evolution of the hydrated cementitious materials due to interaction with the environment is often assessed with reaction path type of models in which the evolution of the cement phases and pore water composition is expressed as a function of reaction progress such as amount of reacted CO_2 (mimicking carbonation), amount of water (leaching), or specific reactants (NaCl, sulphate)

[33] https://cemgems.org/

(Elakneswaran et al., 2018; Han et al., 2021; Jacques et al., 2010; Ke et al., 2020; von Greve-Dierfeld et al., 2020). Although transport processes are neglected in a reaction path model, it provides insight into some of the complex alterations that can occur during chemical ageing and alteration of cementitious materials. Evaluating the stability of cementitious phases with changing temperatures is assessed with a reaction path model where the path variable is temperature (Lothenbach et al., 2008).

Combination of these modelling approaches with a coupled reactive transport model is straightforward and has been used in many studies, either by considering the cementitious material only with some fixed boundary conditions, either interacting with its surrounding including materials relevant for waste disposal (see also sections 2.2.5 and section 3.3.3.4). Again, kinetic hydration processes can be combined with thermodynamic equilibrium for hydrated phases, as in Li et al. (2021).

3.3.3.3 Clay-systems

Porewater chemistry is often calculated based on equilibrium with the primary clay minerals, protonation and deprotonation at clay edges (e.g., Bradbury and Baeyens 2003) and cation exchange processes, the latter may strongly be coupled to the pore water chemistry as illustrated for Boom Clay (Frederickx et al., 2018). Pore water chemistry studies have been done for natural clay systems (see Tournassat et al. (2015) for a general overview and for specific clay-rocks COx (Gaucher et al., 2009), Boom Clay (De Craen et al., 2004), Opalinus Clay (Pearson et al., 2011), Tournemire (Tremosa et al., 2012)) and bentonite (e.g. FEBEX (Fernández et al., 2011)). Thermodynamic data is available in some of the databases mentioned in section 3.3.2.2. Additional information on thermodynamic and kinetic data is given in Jenni et al. (2019). Recently, Blanc et al., (2021) presented a tool to estimate thermodynamic properties of clay minerals, including interstratified illite/smectite minerals and illustrated it in a reactive transport model example.

Modelling evolution of clay systems is mainly based on kinetic dissolution and precipitation of the primary clay minerals, their alterations and secondary phase formation using an equation similar to Eq. (3.23) for surface controlled kinetics, or alternative forms accounting for diffusion-controlled kinetics (including the notion of a shrinking core model, see Mayer et al. (2002), Liu et al. (2014) or Ngo et al. (2015)). In addition, other processes are sometimes taken into account such as protonation and deprotonation processes at clay edge sites (e.g., Wang et al., 2010), Ostwald ripening processes (e.g., Savage et al. 2010) and the coupling between precipitation/dissolution and cation exchange (e.g., Benbow et al., 2019).

Most modelling work is related to assess the impact of cementitious pore water on the clay mineralogy (e.g., Bildstein and Claret, 2015; Marty et al., 2015a; Deissmann et al., 2021 and references therein), but also on the fate of Fe in the clay barrier resulting from steel corrosion (see section 3.3.3.4.3).

3.3.3.4 Modelling reactions at the material interfaces

A recent overview of modelling work on interfaces between different materials relevant for disposal cells was given in Deissmann et al. (2021).

3.3.3.4.1 Glass-steel interface

The key point in modelling the glass-steel interface is the uptake of Si by the corrosion products as this influences the glass dissolution models. Some models accounted for the sorption of Si on the corrosion products (De Windt et al., 2006; Grambow, 1987; Grambow et al., 1987; Jordan and Rammensee, 1998; Jordan et al., 2007; Mayant, 2009; Mayant et al., 2008; Philippini et al., 2006) which can capture typically the glass alteration rate up to a given point at which a certain saturation point is reached of the magnetite sites. After that, magnetite could be partially transformed in another iron oxide with larger sorption capacity or precipitation of Fe silicates (Godon et al., 2013; Rebiscoul et al., 2015). Including the later in the reaction network leaded indeed to better predictions of glass alteration rates (Godon et al., 2013).

3.3.3.4.2 Steel-concrete interface

Up to our best knowledge, no coupled reactive transport simulations for iron/steel corrosion in alkaline and anoxic conditions (i.e. for conditions relevant in a disposal cell) have been found in literature.

3.3.3.4.3 Steel-clay interface

Extensive experimental studies and numerical models of the steel/iron-bentonite interactions under typical HLW-EBS conditions and the effects of corrosion products on the bentonite have been performed in the last two decades (Bildstein et al., 2016; Bildstein et al., 2006; Lu et al., 2011; Marty et al., 2010; Montes-H et al., 2005; Ngo et al., 2015; Ngo et al., 2014; Savage et al., 2010; Wersin et al., 2008; Wilson et al., 2006) (Balmer et al., 2017; Cuevas et al., 2016; Fernández et al., 2018a; Kaufhold et al., 2018; Mon et al., 2017; Samper et al., 2016). Bildstein et al. (2019) presented a comprehensive review of the reactive transport modelling studied at the iron-clay interface at the lab scale and at the scale of the disposal cell for waste repositories. They conclude that: (1) The most abundant corrosion product predicted by the models in the long-term is magnetite, sometimes with Fe-carbonates (siderite) and Fe-silicates (greenalite), sometimes incorporating Al (berthierine, cronstedtite); (2) Primary minerals in clay are often destabilized in favour of Fe-phyllosilicates or zeolites if they are allowed to precipitate; (3) Numerical studies often differ on the precise nature of the main secondary minerals; (4) The transformation of clay minerals into Fe-chlorite, and the timing, very much depend on whether it is included as a secondary mineral (in which case it is the most stable phase and precipitates from the beginning of the simulation) or it results from a ripening process; (5) One of the most sensitive parameters is the corrosion rate; (6) The extent of the perturbation is always predicted to be limited to a few centimetres, up to 20 centimetres into the clay barrier; and (7) Porosity clogging is considered in some simulations under different assumptions. Bildstein et al. (2019) also pointed out that a complete inhibition of the corrosion process has never been observed in experiments, even if a dense corrosion product layer is often identified, and the ubiquity of magnetite in simulation results as the dominant corrosion product in the long-term is questioned by many experimental results and archaeological analogues. Section 5.3 in Deissmann et al. (2021) provides further details on different modelling studies for this kind of interface.

3.3.3.4.4 Steel-granite interface

As noted in section 2.2.4, there is not direct interface between steel and granite in repository concepts. Therefore, no further discussion on models that would include explicitly this interface is given here.

3.3.3.4.5 Cement(mortar)-clay interface

This interface has been included in many modelling studies using a continuum-scale approach both for laboratory experiments, in-situ studies and long-term predictions. A recent overview of these modelling studies was presented in Deissmann et al. (2021). For the concrete part, most studies were done for OPC-CEMI (high pH) for which today excellent databases (see section 3.3.2.2) exist, which now include also phases previously not considered in simulations (M-S-H phases, several C-A-S-H phases). In addition, numerical studies including a concrete/clay interface are available for different host rocks such as Boom Clay (Read et al., 2001; Wang et al., 2010), Opalinus Clay (Berner et al., 2013; Dauzeres et al., 2016; Jenni et al., 2017; Kosakowski and Berner, 2013; Trotignon et al., 2007), or Callovo-Oxfordian clay (Idiart et al., 2020; Marty et al., 2015a; Marty et al., 2014; Marty et al., 2009; Trotignon et al., 2007). When compared to experimental results, numerical studies are, in general, able to capture the mineralogical transformation pathways and the change in porosity (cf. Bildstein et al., 2019). With respect to the long-term predictions, although starting from different geometries and assumptions on

evolutionary paths, models predict consistently a limited thickness of the altered zone, type of mineralogical transformation and porosity changes.

3.3.3.4.6 Cement(mortar)-granite interface

As mentioned in section 3.3.2.2, modelling the geochemical alterations in cement-based materials are well-established because of the fast development of high-quality thermodynamic databases for cement phases (see section 3.3.2.2). Coupling them in a coupled reactive transport model enables prediction of the degradation fronts as was done in the study of Höglund (2014) for leaching with a granite type of water. Also several modelling studies have been performed for the effect of the alkaline plume on crystalline rocks (Soler et al., 2006; Watson et al., 2017). The choice of reactive minerals is crucial to assess the extent of the perturbation (Chen et al., 2015). However, simulations shown that the model for the evolution of an alkaline plume in a host rock is largely consistent with experimental observations.

4 How to use the gained knowledge from assessing the chemical evolution?

This section describes what we can learn from assessing the chemical evolution besides the chemical evolution as such. We focus on two topics: how chemical evolution is linked to material properties and how it is linked to RN mobility.

4.1 Impact on material properties

4.1.1 Physical and transport properties

The geochemical gradients between different materials in a disposal facility induce geochemical alterations with logically effects on different physical properties. More and more, reactive transport codes implement these coupled effects (Georget et al., 2017; Seigneur et al., 2019; Xie et al., 2015) and studies in the framework of radioactive waste disposal apply this in their modelling studies (e.g. (Águila et al., 2020) and references in section 3.3.2.1). Although the underlying pore-scale is the driver for these changes, the discussion focusses here on how it can be implemented in continuum-scale reactive transport models. For a recent in-depth discussion on parameterization of evolving porous media, we refer to Seigneur et al. (2019).

4.1.1.1 Porosity

Dissolution and precipitation of solid phases will lead to changes in the porosity of the porous medium. At every time and location, the porosity is calculated from:

$$\eta = 1 - \sum_{i}^{N_m} m_i V_i \qquad 4.1$$

where η is the total porosity [$L^3\ L^{-3}$], N_m the number of solid phases, m_i is the number of moles of a given solid phase per unit volume [$M\ L^{-3}$] and V_i is the molar volume of the solid phase [$L^3\ M^{-1}$]. When the continuum domain is split into different domains (dual porosity (Šimůnek and van Genuchten, 2008), multiple interacting continua (Pruess and Narasimhan, 1985), multi rate mass transfer framework (de Dreuzy et al., 2013; Haggerty and Gorelick, 1995)), a porosity for each domain can be calculated.

- The simple equation for porosity (Eq. (4.1)) needs some further refinement for some particular properties of a porous medium:
- For a multiscale material as concrete, different types of porosity are defined with gel porosity as the porosity that is within the C-S-H phases; one may also distinguish between the porosity in the bulk of the hardened cement paste, and a more open structure in the interfacial transition zone;
- Also fractures contribute to porosity, and have to be treated in a continuum model as separate domains (as referenced above), or as part of the equivalent continuum model;
- In swelling materials (clay), fracture opening and porosity depend also on the water saturation degree and the aqueous composition. Porosity changes due to bentonite swelling was taken into account via a state surface approach in Samper et al. (2020).

4.1.1.2 Diffusion coefficient

Diffusion coefficients in porous media may vary in time of space due to:

- Changes in temperature, typically described by an Arrhenius type of equation
- Changes in water saturation degree, typically described by Millington-Quirk
- Changes in microstructure and porosity, the former linked to tortuoisity.

Reminding the equation of the effective diffusion coefficient: θD^p:

$$\theta D^p = \theta \tau_s \tau_p D_w \quad 4.2$$

where τ_s is the factor accounting for saturation degree [-] and τ_p the factor for the pore structure. The most widely used formula to link τ_p to porosity η is Archie's law (Archie, 1942; Xie et al., 2015):

$$\tau_p = \eta^{\alpha_c} \quad 4.3$$

where α_c is the cementation factor which is an empirical factor. There exist a number of other relations as well; some examples are given in Seigneur et al. (2019). Some models use the concept of a critical porosity below which diffusion does not occur (e.g., Bentz and Garboczi (1991)).

Models for tortuosity for cement, mortar and concrete have been developed taking into account the multiscale nature of cement (gel pores in C-S-H, capillary porosity) and mortar or concrete (aggregates, interfacial transition zone) using so-called effective media theories (see Patel et al. (2016) for a review). These models have been evaluated for initial conditions (e.g. after 28 days of hardening), there applicability for evolving media is less validated. However, as information on the different mineralogical phases are available in reactive transport models, in theory, they can be used in these models as well (e.g. Perko et al., 2010).

Beside parameterization via experimental results, relations and models can be obtained via pore-scale or microscale modelling that represent explicitly the underlying microstructure (Matyka et al., 2008). Recent pore-scale models for ageing of cement explore the evolution of microstructure and transport parameters (Patel et al., 2021; Patel et al., 2018; Seigneur et al., 2017) and derive functional relations (Bentz and Garboczi, 1991; Seigneur et al., 2017) (see also state-of-the-art report of WP DONUT, Ahusborde et al. (2021)). A new route is to using deep learning techniques to relate tortuosity to porosity (Graczyk and Matyka, 2020).

4.1.1.3 Hydraulic conductivity

Similar to diffusivity, hydraulic conductivity depends also on different factors that may change in time and space:

- Changes in temperature and solution composition that effects e.g. viscosity
- Changes in water saturation degree, typically described by models based on statistical pore size distributions (Burdine, 1953; Mualem, 1976)
- Changes in microstructure and porosity

Focussing here on saturated hydraulic conductivity , K_s [L T^{-1}], and changes due to microstructural and porosity evolution, the change in K_s can be described by a scaling factor α_K:

$$\alpha_K = \frac{K_s(t)}{K_{s,0}} = \frac{f\left(\eta(t)\right)}{f\left(\eta_0(t)\right)} \quad 4.4$$

where the subscript 0 refers to the initial values. The most common models are based on total porosity, and the Kozeny-Carman relation one of the most often used:

$$\alpha_K = \frac{\eta(t)^3\left(1-\eta(t_0)\right)^2}{\eta(t_0)^3\left(1-\eta(t)\right)^2} \quad 4.5$$

However, many relations have been proposed in literature, and we refer to MacQuarrie and Mayer (2005) and Hommel et al. (2018) for an overview.

Another group of models uses the statistical pore-size distribution rather than the total porosity for updating hydraulic conductivity. Precipitation and dissolution will alter the statistical pore size distribution because of change in pore radii. Consequently, the saturated and unsaturated hydraulic conductivity (and moisture retention characteristic) change when calculated with for example the model of Mualem (Mualem, 1976) or Burdini (Burdine, 1953). This approach, introduced for saturated conditions by Taylor et al. (1990), has been extended for unsaturated conditions as well by Freedman et al. (2004) and Wissmeier and Barry (2009). The latter model, called the selective radius shift model, assumes that precipitation/dissolution only occurs in the water-saturated region of the pore size distribution, whereas the former did not made a distinction between the wet and dry regions. When applied to the van Genuchten pore size distribution model, Wissmeier and Barry (2009) predicted changes in K_s and the empirical α_{VG} and n parameter of the van Genuchten model (van Genuchten, 1980); however, the approach is complicated for unsaturated conditions as a refitting of these parameters is needed when the pore-size distribution is altered. For fully saturated conditions, closed-form equations are obtained (Wissmeier and Barry, 2010):

$$\alpha_{\mathrm{VG}} = \alpha_{\mathrm{VG},0}\left(\frac{(\eta-\theta_r)}{(\eta_0-\theta_r)}\right)^{1/3} \quad 4.6$$

and

$$K_s = K_{s,0}\frac{\sqrt{\eta}\alpha_{\mathrm{VG}}^2(\eta-\theta_r)^2}{\sqrt{\eta_0}\alpha_{\mathrm{VG},0}^2(\eta_0-\theta_r)^2} \quad 4.7$$

where 0 denotes the initial values, and θ_r is the residual water content. This has been implemented to simulate leaching from cementitious materials in Perko et al. (2010). A recent application for cementitious materials for leaching and carbonation is given in Michel et al. (2021).

Liquid configuration-based models (Tuller and Or, 2001, 2002) that are based on statistical distributions of geometrically objects to represent the pores potentially offer also a basis for recalculating hydraulic properties during material alterations, but no applications have been found at this stage in the literature.

For saturated fractures, a local cubic law for rough fractures (i.e. fractures with spatially variable apertures) is used to predict the saturated hydraulic conductivity (Oron and Berkowitz, 1998). Liquid configuration-based models offer a physical based approach for estimating unsaturated hydraulic properties of a single fracture or a fracture network (Or and Tuller, 2000; Tuller and Or, 2002). We refer to Deng and Spycher (2019) for an overview of integrating fracture and geochemical fracture evolution into reactive transport models and consequences for the hydraulic (and other) properties.

4.1.2 Mechanical consequences

It is well acknowledged that the mechanical behaviour of cementitious materials is intimately linked to their micro, meso and macrostructural characteristics. These structural characteristics in turn depend on the chemical stability of the material. Therefore, any chemical perturbation will have an effect on the mechanical behaviour of the material such as strength, stiffness, etc. Moreover, it is the nature of the chemical perturbation (e.g. decalcification, sulphate attack) that governs the mechanical behaviour and hence the knowledge of evolution of field variables such as chemical concentrations in the liquid or solid phase is a pre-requisite. The manner in which the chemical field variables predicted by geochemical models (simplified or detailed) are used by some mechanical models are herein demonstrated for two degradation processes relevant to geological disposal: (i) decalcification, and (ii) sulphate attack. The principle in general remains the same for any other degradation processes such as alkali-aggregate reaction, etc.

4.1.2.1 Decalcification

Decalcification is characterized by a decrease in Young's modulus, compressive strength, cohesion, failure stress, plastic yield stress in deviatoric shearing and pore collapse yield stress (Carde et al., 1996; Gerard et al., 1996; Heukamp et al., 2003; Heukamp et al., 2001; Huang and Qian, 2011; Ulm et al., 1999; Xie et al., 2008), including decalcification shrinkage (Phung, 2015; Rougelot et al., 2010).

From an empirical point of view, Walton et al. (Walton et al., 1990) assumed that the concrete loses half of its strength when 33% of portlandite (CH) is depleted.

There are a number of models that estimate specific mechanical properties (e.g. Young's modulus) as a function of leached calcium, which are then used in coupled chemo-mechanical models to study mechanical stability of a specimen or a structure. For instance, Gerard et al. (Gerard et al., 1996) proposed the following relationship between overall Young's modulus with the initial Young's modulus of the material and a chemical damage function d_{ch}.

$$E = E_0\left(1 - d_{\mathrm{ch}}\right) \tag{4.8}$$

$(1 - d_{\mathrm{ch}})$ vs. liquid Ca^{2+} is obtained using micro-hardness experiments on leached cement paste samples. Similarly, Ulm et al. (Ulm et al., 1999) considered chemical damage and chemical shrinkage by considering loss of stiffness as a function of solid Ca concentration using the rule of mixtures and homogenization rule as follows:

$$E = VE^{\mathrm{p}} + \left(1 - V\right)E^{\mathrm{s}}\left(1 - \eta\right)^3 \tag{4.9}$$

where E is the overall modulus, E^{p} is the modulus of the portlandite, V is the portlandite volume ratio and $(1 - \eta)$ is the volume ratio occupied by the solid part of modulus E^s. They were also the first to propose a link between the solid Ca and irreversible damage of the material referred to as chemical softening, within the framework of chemo-plasticity. The latter simply means that the yield function is not only a function of stresses (as in typical elasto-plastic approach) but also on solid Ca that can be obtained from a geochemical model.

Stora et al. (2009b) used interaction direct derivation estimate to estimate bulk, shear and Young's modulus of leached concrete, which essentially uses the time dependent volume fractions of CH, unhydrated clinkers, capillary pores, AFt, C_4AH_{13}, hydrogarnet, AFm and CSH, in combination with measured properties of Young's modulus of the material. These moduli form inputs to a constitutive law (effective stress-strain relationship) in the standard mechanical equilibrium equation.

4.1.2.2 Sulphate attack

Sulphate attack occurs if the C_3A concentration has not been limited for the use of concrete in a sulphate rich environment (see section 2.1.1.3.2). The formation of ettringite, gypsum or thaumasite will result in expansive forces (Bensted et al., 2007). Thus, a key input to all mechanical models of sulphate attack is the amount of ettringite formed. Tixier and Mobasher (Tixier and Mobasher, 2003) used the following expression to compute volumetric strain, ε_v, due to external sulphate attack.

$$\varepsilon_{\mathrm{v}}\left(x,t\right)=\left(C_{\mathrm{a}}-C_{\mathrm{a0}}\sum_{P}\left(\frac{\Delta V}{V}\right)_{P}\right) \quad 4.10$$

$$\left(\frac{\Delta V}{V}\right)_{P}=\frac{\dfrac{1}{m_{\mathrm{v,ettringite}}}}{\dfrac{1}{m_{\mathrm{v},P}}+\dfrac{a}{m_{\mathrm{v,gypsum}}}}-1 \quad 4.11$$

where m_{v} represents the molar volume, *P* is the specific aluminate phase (C_4ASH_{12}, C_3A, C_4AH_{13}, C_3AH_6), ''*a*'' is the stoichiometric proportion of the calcium aluminates and gypsum, C_{a0} is the initial calcium aluminates, and C_{a} is the current calcium aluminates – all of which are outputs from a geochemical model. The volumetric strain can then be used in the standard mechanical equilibrium equation (not shown) to estimate the impact on stresses and cracking.

Whist the model of Tixier and Mobasher takes into account changes in molar volume of ettringite and gypsum, Sarkar et al. (Sarkar et al., 2010) consider the change in molar volume of all solid phases (Table 2 in (Sarkar et al., 2010)) in the hardened cement paste and hence their contribution to the overall volumetric strain as follows:

$$\varepsilon_{\mathrm{v}}=\frac{\left[\left\{\sum_{m=1}^{M}\left(V_m-V_m^{\mathrm{init}}\right)\right\}-b\varnothing V\right]}{V} \quad 4.12$$

where *M* is the number of solid phases, *V* is the representative volume element (total volume), V_m^{init} and V_m are the initial and current volume of the m^{th} solid phase, *b* is a calibration parameter and ∅ is the capillary porosity. If the parameter *b*=1, the newly formed solid phases do not contribute to the overall expansion until all the capillary pores are filled with them. Sarkar et al. (Sarkar et al., 2010) used the volumetric strain to determine the loss of stiffness of the material, which was then used in the standard mechanical equilibrium equation to study damage initiation/growth.

Bary (Bary, 2008) proposed a combined leaching and external sulphate attack model, which couples simplified leaching and sulphate attack reactions with a mechanical model based on combined damage and poroelasticity approach. Leaching problem is solved using dissolved Ca^{2+} as the primary variable (e.g. Mainguy et al., 2000) and sulphate attack problem is solved using dissolved SO_4^{2-} as the primary variable. Unlike the approaches discussed above, the model here is based on the concept of crystallization pressure resulting from interaction between growing AFm crystals and the surrounding C-S-H matrix, which is hypothesized to generate macroscopic swelling. They use the crystallization pressure expressed by Correns's equation involving the ratio between the activity product Q_{reac} and the equilibrium constant of the considered chemical reaction K_{reac} (Eq. 6 and 7 in (Bary, 2008)).

$$p_{\mathrm{c}}=\frac{RT}{V_{\mathrm{crys}}}\ln\left(\frac{Q_{\mathrm{reac}}}{K_{\mathrm{reac}}}\right) \quad 4.13$$

where $V_{\mathrm{crys}}$the molar volume of the growing crystal, *R* and *T* is are the gas constant and temperature, respectively. The crystallization pressure is substituted in the following effective stress equation based on poroelasticity.

$$\sigma=\left(1-D\right)\left(\mathbf{K}:\boldsymbol{\varepsilon}-\alpha_{\mathrm{AFm}}p_{\mathrm{c}}\mathbf{1}\right) \quad 4.14$$

where *D* is a scalar damage parameter linked to the elastic constants, **K** is the standard 4th order stiffness tensor, **ε** is the standard 2nd order strain tensor, α_{AFm} is the interaction coefficient of the AFm phase, which is essentially a function of the volume fraction of the AFm phase and the microstructure of

the hardened cement paste. In conclusion, their model not only requires mass action equations for the secondary phases ettringite and gypsum, but also the volume fractions of ettringite.

4.1.2.3 Concluding perspective

Using the decalcification and sulphate attack mechanisms as examples, this section clearly brought out the link between geochemical models (simplified or detailed) and mechanical models proposed by various researchers. Note however, that in disposal cells, either other processes might occur as well or that they occur simultaneously (e.g. decalcification together with carbonation). Also, by good choice of the cement type, some processes are of less importance in some circumstances (e.g. sulphate attack). In general, the evolution of liquid concentrations of primary chemical variables, solid phase concentrations of the reaction products, molar volumes of solid phases and volume fractions of various phases are seen to form minimum inputs to any mechanical model. Although not discussed, many of the fully coupled chemo-mechanical models are capable of considering mechanical response on the flow and transport behaviour. In such models, either the crack density or the actual crack width forms an input to permeability and diffusivity.

4.2 Impact on waste form and RN mobility

The impact on the fate and mobility of radionuclide in a disposal system is depending on the following important aspects:

- The change in transport properties due to microstructural alterations (see previous section) including the physical/mechanical properties of the waste forms themselves
- The change in speciation of radionuclides due to changes in the aqueous composition
- The change in amount of sorption sites due to dissolution and precipitation of minerals.
- Gas generation and transport that may influence transport at the cell disposal scale and in the host rock.

It is not within the scope of this report to summarize these effects for different radionuclides. The main message is that, based on a quantification of the above mentioned changes, the effects on radionuclide fate and mobility can be assessed in a quantitative way using the same or similar model concepts and tools as discussed in section 3.3. Similar to modelling the geochemical evolution of materials, process understanding, models, parameters and thermodynamic data are crucial. This has been or is still an important research subject.

Without being exhaustive, we guide the reader to the following information:

- Cementitious system: information on speciation of radionuclides during different ageing stages of concrete, together with processes regarding the sorption or immobilization processes, is summarized in Ochs et al. (2016). Results of the CEBAMA project are summarized in Grambow et al., (2020). The state-of-the-art report of WP CORI (Altmaier et al., 2021) provides additional references including the interaction with organics as well.
- Clay and Crystalline rocks: The theoretical background of sorption on clay minerals is given in many textbooks (Appelo and Postma, 2005); the reader is also referenced to Borisover and Davis (2015). The state-of-the-art report in the framework of the WP FUTURE (Maes et al., 2021) contains a large bibliographic review to many aspects of radionuclide fate and mobility.

5 Conclusion

There is a lot of literature available about the alteration processes of engineered barriers and host rocks when interfacing solutions and porous media with or without γ-radiation and microbial activity. Quantification of the radiological, chemical and physical properties of the engineered barriers and host rocks is necessary in order to deduce whether the described actors for the alteration processes are relevant for geological disposal of radioactive waste. From the quantification of the properties of the waste and engineered barriers, radiation enhanced alteration of engineered materials can be excluded to have an impact on the chemical evolution of HLW disposal cells. Radiation enhanced corrosion of metals in ILW disposal cells is also negligible compared to chemical corrosion. Natural and archaeological analogues can therefore be used to identify the relevant processes. This identification has been performed for the following interfaces: steel-concrete, steel-clay, concrete-clay and concrete-granite.

Clay host rocks and granitic host rocks are both alumina-silicate bearing rocks. Detailed investigation and understanding of the processes taking place in Maqarin (Jordan) elucidated the potential sequence of secondary mineral formation by interaction with alkaline fluids and alumina-silicate bearing rocks: C-S-H phases, low in Ca C-S-H phases, C-A-S-H, low Si/Al zeolite and high Si/Al zeolite as a function of pH. The low permeability in clay host rocks ensures that the mineralogical alteration is minimal in a period of 100,000 till 1 million years. The secondary mineral formation takes place within the fractures of granitic host rocks.

Formation of an alteration layer on the surface of steel takes place when steel is in contact with pore water. It takes some time to form this alteration layer and to achieve a constant alteration rate in a laboratory setup, especially if samples are prepared to obtain a well-defined initial condition for example polishing of steel and acid etching. In practice, there is always a metal-oxide layer present on steel before disposal.

An alteration layer is a passivating layer with the smallest possible alteration rate in that medium. Another word for alteration layer in the literature is ‘dense product layer’. A constant alteration rate is representative for the long-term. This alteration rate is a steady state between the dissolution of the alteration layer interfacing a porous medium and the formation of the alteration layer from the virgin material. The concentration of dissolved species is in equilibrium with the formed minerals in the alteration layer for example magnetite in case of steel. Dissolved species migrate away from the interface by diffusion in porous media to areas with a smaller concentration in these dissolved species. This migration from the interface can be enhanced by sorption of these dissolved species in porous media. Sorption by porous media can therefore result into larger alteration rates.

The sorbed iron species can alter the clay mineralogy in bentonite and the incorporated iron species are assumed to alter the cementitious minerals in concrete. The Fe-affected zone in bentonite and the Fe-affected zone in concrete are alteration zones. These zones can also be called ‘transformed media’ in literature. The available information for the Fe-affected zone in bentonite and its impact is abundant i.e. transformation from swelling clay minerals into non-swelling minerals. Its low permeability may be maintained in this transformation. For concrete, this information on the Fe-affected zone is limited to some chemical characterisations and a published observation of more than 30 years ago of concrete in the vicinity of steel being identified as ‘loosely bound material’.

The engineered materials in the HLW disposal cells are the waste form glass, steel, concrete and/or bentonite. Microbial induced corrosion is prevented on the short term by the thermal load and can also be excluded on the long term by design and quality assurance. In any disposal concept for vitrified HLW, a carbon steel overpack is used to prevent contact between the vitrified waste form and pore water until the heat emission of the waste has sufficiently been diminished. The period in time for a sufficient decay in heat depends on the disposal concept and can be 500 years or more than 1000 years.

The carbon steel overpack can be covered by a buffer made from bentonite or concrete. The long-term corrosion (alteration) rate of steel interfacing bentonite is about 100 times larger than this rate of steel interfacing concrete, i.e. below 10 µm per year and 0.1 µm per year, respectively. By design, the carbon steel overpack is therefore thicker in bentonite buffers than concrete buffers.

Mineralogical changes due to bentonite interfacing the host rocks are not envisaged i.e. the beneficial properties of bentonite remain on the long-term. The vitrified waste form comes into contact with pore water when the virgin carbon thickness in the bentonite buffer has become too small. This is different for concrete.

The pore water chemistry of the host rock pore water determines the chemical evolution of concrete. In well-engineered concrete, sulphate attack can be prevented and the ingress of magnesium from the host rock results into Mg-affected concrete with limited mechanical strength compared to fabricated concrete strength. The vitrified waste form comes into contact with pore water when the virgin carbon thickness has become too small and the Fe-affected zones and Mg-affected zones in the concrete buffer have become too large. The mechanical load of the host rock is transferred to the carbon steel overpack by the bentonite but the concrete buffer has its own fabricated strength. In this SOTA, it is assumed that the strength of the Fe-affected zone in concrete is negligible compared to its fabricated strength.

The bentonite, concrete and clay host rocks are materials with a low permeability. The chemical evolution of the disposal cells is determined by the exchange in dissolved species. The rate in exchange of dissolved species is small due to the low permeability. The excavation and drying of the indurated clay host rock further minimizes this rate in exchange. Quantification in transport properties and saturation degree in these low permeable materials are crucial in the determination when the carbon steel overpack has become too thin and the thickness of affected zones in concrete has become too large. The calculated periods to have material sufficiently altered in order to have contact between pore water and vitrified waste form can supersede the period in which vitrified HLW is more radiotoxic than uranium ore.

Like steel, formation of an alteration layer on the surfaces of glass takes place when glass is in contact with pore water, except that the alteration layer is composed of a diffusion gel layer and secondary mineral precipitates such as clay minerals and zeolites. Like steel, it may also take some time to form this alteration layer and to achieve a constant alteration rate in a laboratory setup. Relevant alteration rates have been obtained from natural analogues and depend on the silicon concentration in porous media. In a laboratory set-up, the liquids to which a simulant of the vitrified waste form is exposed can be chosen to be depleted in dissolved silicon. This set-up will not lead to an alteration rate that is representative for disposal since all porous media are saturated in silicon. After fracture of the carbon steel overpack, glass in the vicinity of steel can have higher alteration rates. The radionuclides dissolved as cationic complexes are, however, incorporated in the alteration layer of glass. Consequently, the containment of these radionuclides has been transformed from the engineered waste form into the naturally formed secondary mineral precipitates.

The vitrified waste form for HLW is well understood and characterised. Metallic ILW has been identified from the contributions provided by the information available from national programmes. The metals in cemented metallic ILW are steel (carbon steel and stainless steel) and Zircaloy. Like for carbon steel, also for stainless steel and Zircaloy, an alteration layer is formed with a mineral in equilibrium with a dissolved metal-complex concentration. The stability of these alteration layers depends on the pH and the concentration of dissolved species. The stability is largest at high pH for carbon steel (low alloy steel) and stainless steel (high alloy steel). Thermodynamic modelling and experimental studies show that dissolved calcium at representative disposal concentrations enhances the formation of this alteration layer for carbon steel. This calcium effect has not yet been included in the modelling of the chemical evolution at the interface between concrete and steel. Dissolved calcium can hinder the formation of the alteration layer for Zircaloy, but the required dissolved calcium concentrations are too high to be

representative for disposal. Also for stainless steel, no effect is envisaged with the dissolved calcium concentrations in the engineered materials or host rocks.

Stainless steel and Zircaloy are used in nuclear power reactors due to their high corrosion resistance. The envisaged radionuclide release mechanism is the alteration/corrosion rate. The envisaged corrosion rates are so small that many radionuclides decay within these neutron irradiated metals. The transport of water through the cementitious material from the host rocks can also limit the corrosion process since the envisaged anaerobic corrosion process consumes water.

Organic ILW has also been identified from the contributions provided by the information available from national programmes. Organic waste can be considered as a potential food source for microbes if the usable energy to breakdown the organic molecules provide sufficient energy. Microbial degradation of organic waste can therefore be a primary process for the potential release of radionuclides. Spent ion exchange resins are ILW that are processed with cementitious materials. These resins do not provide sufficient energy to be broken down and microbial enhanced degradation can therefore be neglected. These resins are used to clean nuclear reactor contaminated waters due to their high radiation and chemical resistance. The mechanism for radionuclide release may not be relevant with an alteration of the resins. Resins are like clays, exchangers. Any radionuclide release can therefore also be envisaged to require sufficient ingress of anions and cations that have a stronger affinity than the sorbed anionic or cationic radionuclide. Cellulosic waste such as paper and clothing are in exceptional cases also characterised as ILW. Microbial degradation of this waste can be a primary process for the potential release of radionuclides, provided that the high pH of cementitious materials does not minimize this activity. The chemical degradation can be stimulated by the high pH and reduced by the lack of fluid flow and anaerobic conditions in geologically disposed of cemented waste packages. The dominant processes for the chemical evolution of disposal cells with cellulosic waste are to be identified.

Appendix A. Thermal characteristics CSD-v and vitrified waste form

Figure A-5-1 shows the heat generating power per waste canister as a function of time. Decay of many short-lived radionuclides takes place in the period smaller than 30 years. Their contribution to the thermal power is assumed not be included in Figure A-5-1.

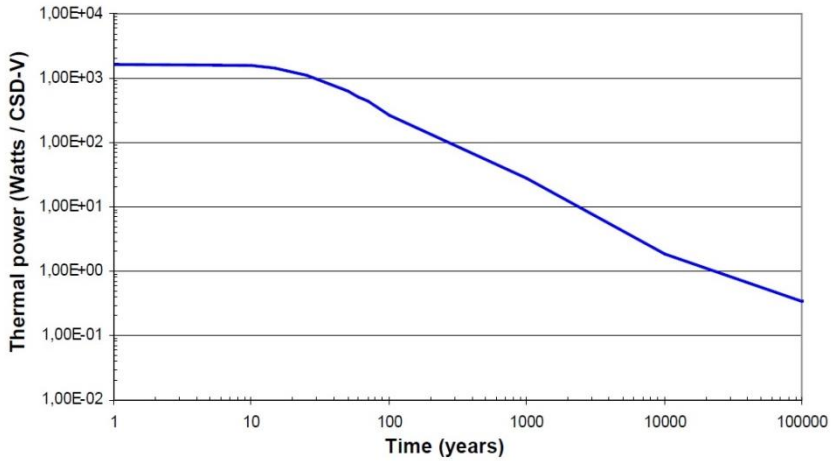

Figure A-5-1: Evolution of the thermal power of a typical residue UOX: 44000 MWd/tU initial enrichment 3.8% ^{235}U and mixed with MOX: 45.000 MWd/tU initial enrichment (AREVA, 2007).

A polynomial needs to be made for the implementation of the thermal power into a calculation. The thermal power is a sum of exponentials:

$$Q(t) = \sum_i A_i e^{\alpha_i [t + t_{storage}]}$$

The coefficients obtained with a fit by the eye are shown in Table A-1 for a storage period, $t_{storage}$, of 0 years. A larger storage period of canister results in a smaller thermal power at start of disposal. National programmes may have a maximum heat output of a canister, e.g. < 500 W is the acceptance criteria for disposal in France that considers clay host rock (ANDRA, 2018), i.e. a storage period between 65 and 70 years using these coefficients.

Table A-1: Coefficients to use in a sum exponentials for thermal power of CSD-v as a function of time; A_i in Watts/CSD-v and α in year^{-1}.

	A1	A2	A3	α_1	α_2	α_3
[Watt/canister]	1637	200	15	-0.025	-0.0025	-0.00025

This waste product was named UC-V in the 6th framework programme RED-IMPACT (Greneche et al., 2007). The thermal power beyond 100 years is larger in the specifications in this CSD-v (AREVA, 2007) than investigated in RED-IMPACT (see Figure A-5-2).

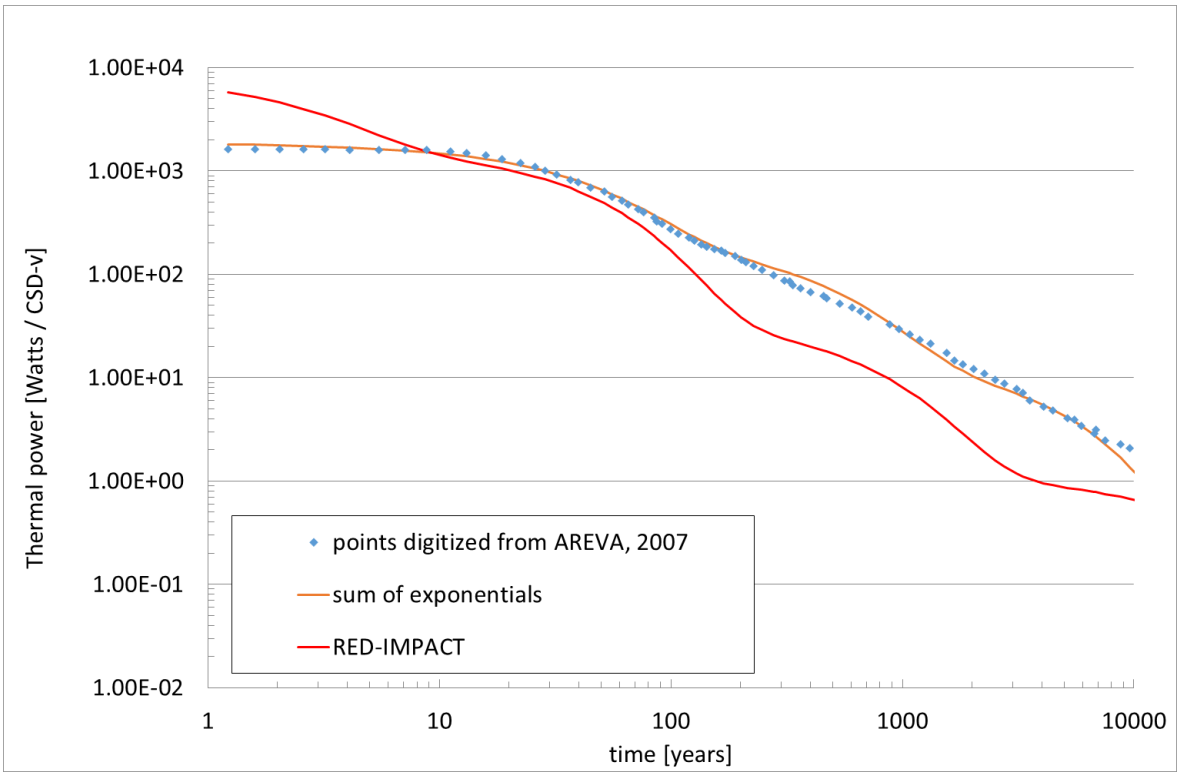

Figure A-5-2: Evolution of thermal powers in 6th framework programme compared to the more recent specifications from the waste product supplier.

The glass density is around 2800 kg m^{-3}. Table A-2 shows the thermal properties as supplied by AREVA, nowadays ORANO.

Table A-2: Thermal properties of glass (AREVA, 2007)

T (°C)	100	200	300	400	500	530 < T < 600
Thermal conductivity [W m^{-1} K^{-1}]	1.02	1.13	1.22	1.25	1.25	-
Specific heat [J g^{-1} K^{-1}]	0.88	0.97	1.02	1.04	1.14	1.52

Table A-3 shows the chemical content for vitrified waste forms. The minimum sum in the wt% of SiO_2, Al_2O_3 and B_2O_3 is 60 (AREVA, 2007). For convenience, the French inactive borosilicate reference glass SON 68 is also included (Conradt et al., 1986). A more detailed composition of SON 68 is available (Van Iseghem et al., 1992). The R7T7 reference glass studied in the 4th framework programme (Vernaz et al., 1996) has a broader range in wt% than provided by AREVA and is therefore not listed.

Table A-3: Oxides and metal particles in vitrified waste form (AREVA, 2007) and (Conradt, et al., 1986)

Component	Range in wt% of vitrified waste form	SON 68 wt%
SiO_2	42.4 to 51.7	45.5
B_2O_3	12.4 to 16.5	14.2
Al_2O_3	3.6 to 6.6	4.9
Fission products and actinides as oxides, ZrO & ZrO_2 and metal particles	4.2 to 18.5	
Oxides with Nd, Zr, Mo, Ba and Cs		7.9
Na_2O	8.1 to 11	9.9
Fe_2O_3	0 to 4.5	2.9
NiO	0 to 0.5	
Cr_2O_3	0 to 0.6	
P_2O_5	0 to 1	
Li_2O	1.6 to 2.4	2.0
ZnO	2.2 to 2.8	2.5
CaO	3.5 to 4.8	4.0
RuO_2 + Rh (metal particle) + Pd (metal particles	0 to 3	
rest		6.2

Appendix B. Pore water compositions

Suggestions for the pore water chemistries of the clay and granitic host rocks, the bentonite buffer and concrete used for the buffer and other applications are listed here. As much as possible, primary references of the published pore water chemistries are used since it seems to be very important how the chemistry has been measured and/or modelled.

Clay host rocks

Measured pore water compositions for clay host rocks are influenced by experimental artefacts e.g. (De Craen et al., 2004; Gaucher et al., 2009):

- the partial pressure of CO_2 is larger at depth of the disposal facility and degassing of CO_2 takes place when the samples are taken. This degassing has an impact on the measured bicarbonate (HCO_3^-) content and pH in the pore water composition;
- redox potentials cannot be measured with a sufficient accuracy due to the introduction of oxygen during the installation of the measurement device; these potentials are therefore usually calculated from a thermodynamic equilibrium;
- the clay host rock in the deep underground has usually been depleted in oxygen for millions of years. Pieces of host rock can be sensitive to the oxidized conditions above ground, e.g. pyrite (FeS_2) can be oxidized and this oxidizing reaction acidifies the sample with which a too high concentration of sulphate (SO_4^{2-}) and cation concentrations are measured as a result of dissolution of carbonates. The carbonates buffer the decreasing pH.

Data of clay core samples, e.g. obtained by mechanical squeezing or aqueous leaching, can be used as input for the thermodynamic modelling. Table A-4 shows these chemistries for poorly indurated clay, i.e. Boom Clay in Belgium (De Craen et al., 2004) and the Netherlands (Griffioen et al., 2017), indurated clay, i.e. Callovo-Oxfordian clay (Gaucher et al., 2006; Gaucher et al., 2009), the reference host rock in France and Opalinus Clay (Mäder, 2009), the reference host rock in Switzerland.

Table A-4: Modelled pore water chemistries in clay host rocks

Parameter	Unit	Belgian	Dutch	French	Swiss (reference)	Swiss (sea case)
Temperature	ºC	16	26	25	25[34]	25
pH	-log(H^+)	8.5	6.9	7.28	7.203	7.009
pe	-log(e^-)	-4.7	-2.8	-2.64	-2.781	-2.563
pCO_2	log(bar)	-2.62	-1.5	-1.96	-2.2	-2.5
Na^+	mmol/kg	15.6	460.9	32.1	164.4	527.5
K^+	mmol/kg	0.2	9.8	7.10	2.604	1.77
Ca^{2+}	mmol/kg	0.05	13.2	15.0	12.51	49.71
Mg^{2+}	mmol/kg	0.06	56.1	14.2	9.625	37.55
Sr^{2+}	mmol/kg			1.12	0.2106	0.422
Fe^{2+}	mmol/kg	0.003	0.0000031	0.332	0.0524	0.246
Al^{3+}	mmol/kg	0.000024	0.000033	0.00000695		
SiO_2 (aq)	mmol/kg	0.1	0.3	0.0940	0.1779	0.172
Cl^-	mmol/kg	0.7	541.0	30.1	160.0	662.0
SO_4^{2-}	mmol/kg	0.02	28.4	33.9	24.72	21.06
HCO_3^-	mmol/kg	14.4	7.2	2.78	2.043	0.631

The concentration of all cations can depend on the measured occupancy and selectivity of the clay minerals, but the limiting concentration for the cations Ca^{2+}, Mg^{2+}, Fe^{2+} and Sr^{2+} can also be the

[34] The pore water chemistries have been calculated at 25°C since the temperature dependency of a lot of phases are unknown. The deviation is also expected to be sufficiently small if the temperature is within a range of 10 K from 25°C (Mäder 2009).

formation of carbonates, i.e. calcite ($CaCO_3$), dolomite ($CaMg(CO_3)_2$), siderite ($FeCO_3$) and strontianite ($SrCO_3$). The aluminium concentration is limited by the dissolution products of clay minerals, e.g. kaolinite or chlorite (Mäder, 2009) and the dissolved SiO_2 content by the quartz or chalcedony (De Craen et al., 2004) solubility. The partial pressure of CO_2 determines the bicarbonate concentration and can be controlled by the mineral assemblage, (Mäder, 2009), (Wang et al., 2010). The chlorine, Cl^-, and sulphate, SO_4^{2-}, concentrations can be fixed in the modelling but celestite ($SrSO_4$) may control the sulphate concentration (Gaucher et al., 2009; Mäder, 2009). Traces of sulphide are also present in clay pore water due to presence of pyrite in the clay mineralogy. The presence of pyrite is the clear indication that clay formations have reducing conditions and pyrite can be used in the modelling to determine the redox potential.

Granitic host rocks

For granitic host rocks, the water flowing in a borehole through fractures can be measured. Pumping rates are adjusted in order to obtain the representative groundwater samples. There were not always modelled pore water chemistries available for granitic rocks, the redox conditions may be controlled by microbial activity and the groundwater composition may be also determined by mixing of ground waters in these host rocks, i.e. thermodynamic modelling may not always result in representative pore water chemistries. Table A-5 shows the measured and modelled pore water chemistries in granitic host rocks for granitic rocks in the Czech Republic (Cervinka et al., 2018) in Spain (ENRESA, 2001), in Sweden (Laaksoharju et al., 2005; Auqué et al., 2006) and in Finland (Pitkänen et al., 1996) with a temperature between 10-11ºC around a depth of 400 metre (Sedighi et al., 2014).

Table A-5: Modelled and measured pore water chemistries in granitic host rocks

Parameter	Unit	Czech (600 m)	Czech (1000 m)	Spanish	Swedish (512 m)	Finnish (446.0-558.5 m)
Temperature	ºC	25	25	30	11.35	11
pH	-log(H^+)	8.2	9.4	7.9	7.2	7.9
pe	-log(e^-)	+4.00	+4.00	-2.907	-2.54	-4.33
Na^+	mmol/kg	0.865	3.81	4.350	89	122
K^+	mmol/kg	0.0537	0.0179	0.05371	0.9	0.35
Ca^{2+}	mmol/kg	0.864	0.0324	0.1522	23	41.2
Mg^{2+}	mmol/kg	0.342	0.00412	0.1604	9.3	2.35
Sr^{2+}	mmol/kg					0.171
Fe^{2+}	mmol/kg	0.00179	0.00179	0.8953	0.033	0.00013
Al^{3+}	mmol/kg	0.00371	0.00371			0.002
SiO_2 (aq)	mmol/kg	0.520	0.481	0.3761		0.072
Cl^-	mmol/kg	0.0931	0.528	0.3949	153	214
SO_4^{2-}	mmol/kg	0.219	0.109	0.01561	5.2	0.114
HCO_3^-	mmol/kg	2.77	2.68	5.048	2.2	

Bentonite

Bentonite buffers are usually ‘dry’ emplaced around a steel overpack. Dry can mean for bentonite buffers a water content of 17 wt% (e.g. Johannesson et al., 2020) or 10% (e.g. Atabek et al., 1991). The pore water chemistry of this engineered barrier is therefore determined by the inflow of granitic water and establishment of equilibria between dissolved species present in this host rock water and minerals present in the bentonite buffer, i.e. there is no initial pore water chemistry as in concrete buffers. Table A-6 shows the pore water composition of bentonite calculated in the Spanish programme with and without saturation with granitic host rock pore water (ENRESA, 2001). The comparison of these pore water compositions and the knowledge of the available soluble salts in bentonite (see Appendix C) clearly indicates that the bentonite pore water becomes more diluted during the chemical interaction

between bentonite and the Spanish granitic host rock water. A smaller dilution would be expected for the Swedish and Finnish granitic ground waters since these waters are more saline.

Table A-6: Modelled bentonite pore water compositions (ENRESA, 2001)

Parameter	Unit	As emplaced	After saturation
Temperature	ºC	RT	83.07
pH	-log(H^+)	7.75	6.6
pe	-log(e^-)	12.85	-0.197
Na^+	mmol/kg	145.5	93.42
K^+	mmol/kg	1.253	0.811
Ca^{2+}	mmol/kg	20.78	11.19
Mg^{2+}	mmol/kg	22.30	16.07
Sr^{2+}	mmol/kg		
Fe^{2+}	mmol/kg	1.612×10^{-3}	6.583×10^{-2}
Al^{3+}	mmol/kg		
SiO_2 (aq)	mmol/kg	0.2646	0.9913
Cl^-	mmol/kg	159.9	106.2
SO_4^{2-}	mmol/kg	36.59	20.94
HCO_3^-	mmol/kg	0.4361	1.714

Cementitious materials

The concrete pore water compositions may be solely determined by the cement minerals generated during hydration assuming that the aggregates have not reacted with cement. Table A-7 shows the measured pore water chemistries from cement pastes by which the pore solutions were gained by a high-pressure apparatus and the main element concentrations were measured using ICP-OES (Kempl and Copuroglu, 2015). The pore solutions obtained with a high-pressure apparatus seem to approximate best the pore water chemistries (Atkins et al., 1991) and therefore other techniques to obtain pore solutions such as crushing hardened cement paste and contacting the crushed paste with water are not considered. The modelled pore water chemistries for CEM-I (Wang, 2009), the French contribution in EURAD Deliverable 2.4 (Cochepin et al., 2019) and for CEM-III/B (Cloet et al., 2019).

Table A-7: Modelled and measured pore water chemistries in cements

Parameter	Unit	CEM-I			CEM-III/B	
		Measured	Modelled (Belgian)	Modelled (French)	Measured	Modelled*
Temperature	ºC	RT	25		RT	20
pH	-log(H^+)	13.1	13.5	13.26	13.0	12.4
pe	-log(e^-)	-	-	7.74	-	-10.3
Na^+	mmol/kg	99.0	141	90	70.9	800
K^+	mmol/kg	68.1	367	220	39.8	800
Ca^{2+}	mmol/kg	2.1	0.7	1.5	2.8	7
Mg^{2+}	mmol/kg	0.02	$\approx10^{-7}$	3.2×10^{-7}	0.02	6×10^{-5}
Sr^{2+}	mmol/kg	*		-	*	-
Fe^{2+}	mmol/kg	*		6.2×10^{-4}	*	-
Al^{3+}	mmol/kg	*	0.06	0.77	*	0.8
SiO_2 (aq)	mmol/kg	*	0.05/0.3	7.7×10^{-2}	*	0.1
Cl^-	mmol/kg			40		100
SO_4^{2-}	mmol/kg	0.5	2	0.32	1.7	500
CO_3^{2-}	mmol/kg		0.3			0.07

* Concentrations have been read from Fig. 4.13 in Cloet et al., (2019) assuming mol/m^3 to be equal to mol/kg. Note that the thermodynamic set-up did not consider alkali or aluminium uptake by CSH. The pH is almost 13 iIn other modelling pore water chemistries of CEM III/B e.g. (Lothenbach et al., 2012).

A measured pH of concrete pore water larger than 13 is also available for similar cement pastes and measured from pore solutions that were gained by a high-pressure apparatus cement pastes containing fly ash (e.g. Andersson et al., 1989) but it may be difficult to understand these pore water chemistries without X-ray diffraction. Therefore, reference has been made to a paper that contained both pore water chemistry as well as X-ray diffraction (Kempl and Copuroglu, 2015).

The calcium concentrations in Table A-7 are an order in magnitude smaller than the maximum modelled concentration of calcium in equilibrium with CSH-gels of 20 mmol/kg (Berner, 1992) and (Vehmas and Itälä, 2019) without alkalis since the pH is controlled by the alkali content at a pH > 12.5 (van Eijk and Brouwers, 2000). As the alkali content and pH is reduced upon leaching or carbonation, the calcium concentration will increase.

A comparison between the cement pore water chemistries and host rocks shows that the dissolved calcium concentration in cement pore water is smaller for the French, Swiss, and Dutch clay host rocks and Swedish and Finnish granitic host rocks. Egress of calcium from concrete, i.e. leaching is initially not expected until cement is depleted in dissolved alkalis. Alteration of concrete is initially envisaged by ingress of dissolved species from the host rocks. The Belgian clay host rock and Czech and Spanish host rocks have a smaller dissolved calcium concentration than the cement pore water. Leaching of calcium and consequent increase in porosity can be a process in the alteration of concrete from the start of the interaction between the concrete and host rock.

Another important aspect of the cement pore water chemistry for interaction with steel is the redox potential. Reducing, i.e. negative, redox potentials for cements were measured for cements containing blast furnace slag, otherwise oxidising i.e. positive, redox potentials had been measured (Andersson et al., 1989; Atkins et al., 1991). The initial redox potential in concrete strongly depends on the type of cement used for its manufacturing. For Ordinary Portland Cement (OPC), i.e. CEM I, CaO is made by baking carbonate in limestone without a specific control of the heating environment. Blast furnace slag (BFS) is made in reducing environments as a by-product of steel production. OPC concrete lacks electroactive species and is therefore largely unbuffered, being slightly oxidizing after fabrication. Concrete made with cement in which OPC is blended with BFS contains traces of pyrite, FeS_2, and has therefore a reducing environment after fabrication. An oxygen penetration front into the concrete is observed as a loss of the blueish colour in above ground civil infrastructure.

Appendix C. Mineralogy and porosity

Suggestions for the mineralogy of the clay, the bentonite buffer and concrete used for the buffer and other applications are listed here. As much as possible, primary references of the published mineralogy's and porosities are used.

Clay host rocks

Table A-8 shows the mineralogy of the clay host rocks for poorly indurated clay, i.e. Boom Clay in Belgium (Mol) (Honty and De Craen, 2012) and the Netherlands (Griffioen et al., 2017), indurated clay, i.e. Callovo-Oxfordian clay (Bure) (Wenk et al., 2008) the reference host rock in France, and Opalinus Clay (Traber and Blaser, 2013), the reference host rock in Switzerland. The porosities of the virgin host rock are 36-40 vol% for Boom Clay in Belgium at HADES at 223 metres depth (Mol) (De Craen et al., 2004), 31-35 vol% for Boom Clay in the Netherlands at around 500 metres depth (Verweij et al., 2016), 17 vol% for Callovo-Oxfordian clay (Gaucher et al., 2009), and 15 vol% for Opalinus Clay (Alcolea et al., 2014).

Table A-8: Average or reference mineralogical compositions of clay host rocks in wt%

Mineral	Chemical formula	Belgian	Dutch	French	Swiss
Muscovite	$KAl_2(AlSi_3O_{10})(F,OH)_2$				
Illite/Muscovite		18.8			
Illite	$K^aAl^b{}_3Si^c{}_3O_{10}(OH)_2$		10.9	33.9	24
Ill/Sm mixed layer		21.8		1.9	9
Smectite^{montmorrilonite}	$(Na,Ca)_{0.33}(Al,Mg)_2(Si_4O_{10})(OH)_2 \bullet nH_2O$		25.4		
Kaolinite	$Al_2Si_5O_5(OH)_4$	7.4	4.1	3.3	18
Chlorite	$(Mg,Fe)_3(Si,Al)_4O_{10}(OH)_2 \bullet (Mg,Fe)_3(OH)_6$	2.2	1.1	3.8	9
Chl/Sm mixed layer					0
Clinoptilolite/ Heulandite	$((Na,K,Ca)_{4\text{-}6}Al_6Si_{30}O_{72} \bullet 24H_2O$/ $((Na,Ca)_{4\text{-}6}Al_6Si_{30}O_{72} \bullet 24H_2O$		0.6		
Quartz	SiO_2	38.9	42.0	24.0	20
Calcite	$CaCO_3$	0.6	5.3	24.3	13
K-feldspar	$KAlSi_3O_8$	4.8	6.7		2
Albite	$NaAlSi_3O_8$	2.0	2.4		
Plagioclase	from $NaAlSi_3O_8$ till $CaAl_2Si_2O_8$			3.9	0.9
Anorthite	$CaAl_2Si_2O_8$				
Dolomite/ankerite	$CaMg(CO_3)_2$	0.3		3.5	0.4
Siderite	$FeCO_3$	0.1			4
Pyrite	FeS_2	2.1	1.4	1.4	1
Apatite	$Ca_5(PO_4)_3(F,Cl,OH)$	0.2			

[a] can also be H_3O, [b] can also be Mg or Fe, [c] can also be Al

Granitic host rocks

The mineralogy in granitic rocks may not be as relevant for the chemical interaction between the engineered barrier system and the host rock as the mineralogy of the fracture fillings. The granitic rock is practically impervious due to its porosities of less than 1 vol%; transport of dissolved species mainly takes place through fractures. Precipitation of calcite, chlorite and clay minerals can be fracture fillings (Drake et al., 2006). Table A-9 shows the mineralogy's of granitic host rocks for granite in Czech Republic with the main mineral components quartz, feldspars, mica and amphibole (Vondrovic, 2015), El Berrocal granite in Spain (Siitari-Kauppi, et al. 2007), granite (to granodiorite) at Forsmark with an average porosity of 0.43 vol% (Drake et al., 2006), and migmatitic gneiss, the dominant rock type at Olkiluoto in Finland (Kärki and Paulamäki, 2006).

Table A-9: Average mineralogical compositions of granitic host rocks in vol%

Mineral	Chemical formula	Czech	Spanish	Swedish	Finnish
Quartz	SiO_2	+	40	35.6	30.3
Plagioclase	from $NaAlSi_3O_8$ till $CaAl_2Si_2O_8$	+	30	35.6	17.0
K-feldspar	$KAlSi_3O_8$	+	20	22.5	8.6
Biotite	$K(Mg,Fe)_3AlSi_3O_{10}(OH)_2$	+	+	5.1	22.7
Muscovite	$KAl_2(Si_3Al)O_{10}(OH,F)_2$	+	+		0.9
Hornblende	$Ca_2(Mg,Fe,Al)_5(Al,Si)_8O_{22}\bullet(OH)_2$				0.1
Chlorite	$(Mg,Fe)_3(Si,Al)_4O_{10}(OH)_2\bullet(Mg,Fe)_3(OH)_6$	+	+	0.2	2.6
Corderite	$Mg_2Al_4Si_5O_{18}$				4.0
Pinite	Muscovite and clay minerals				5.9
Sillimanite	Al_2SiO_5				1.8
Epidote	$Ca_2Al_2Fe(SiO_4)(Si_2O_7)(O,OH)_2$			0.6	0.0
Apatite	$Ca_5(PO_4)_3(F,Cl,OH)$				0.1
Saussurite	Mixture with epidote and feldspars				3.7
Sericite	Usually muscovite, illite or paragonite with small crystals				0.8
Opaques	Mainly magnetite Fe_3O_4 and small content of FeS_2			0.3	1.0
Titianite / sphene	$CaTiSiO_5$			0.2	0.1
Allanite	$(Ca,Mn,Ce,La,Y,Th)_2(Fe,Ti)(Al,Fe)_2O\bullet OH[Si_2O_7][SiO_4]$			0.3	

Bentonite

The durability of the carbon steel overpack is determined by the mineralogy of the engineered buffers bentonite and concrete, their density, porosity and thickness. Bentonite buffers are compressed blocks with a high smectite content of which montmorillonite is the most famous species. The smectite content can be 88 wt% as used in the Czech programme in EURAD Deliverable 2.4 (Neeft et al., 2019) and 75 wt% in the Swiss programme, in which smectite is further specified as Na-montmorillonite in Wyoming MX-80 (Müller-Vonmoos and Kahr ,1983). Wyoming MX-80 bentonite is also used in the Swedish programme (Wanner et al, 1994). The structural formula for Na-montmorillonite is $(Si_{3.96}Al_{0.04})(Al_{1.55}Fe^{3+}_{0.20}Fe^{2+}_{0.01}Mg_{0.24})O_{10}(OH)_2Na_{0.30}$ (Müller-Vonmoos and Kahr 1983) that seems to be later refined into $(Si_{3.98}Al_{0.02})(Al_{1.55}Fe^{3+}_{0.09}Fe^{2+}_{0.08}Mg_{0.28})O_{10}(OH)_2Na_{0.38}$ (Bradbury et al., 2014). The second contributor to the mineralogical composition is quartz. The Wyoming MX-80 bentonite also contains feldspar. Carbonates are the third contributor to the mineralogical composition. Pyrite and soluble salts (NaCl, KCl, $CaSO_4$) are present in trace amounts in Wyoming MX-80 bentonite and bentonite used in the Spanish and Czech programmes. The Czech programme also has the soluble salts $Mg(NO_3)_2$ and $NaHCO_3$. The porosity, ε, of bentonite is determined by the dry density, ρ_{dry}, and specific density ρ_{sp} (Ochs and Talerico 2004):

$$\varepsilon = 1 - \frac{\rho_{dry}}{\rho_{sp}}$$

For example, a specific density of 2760 kg m^{-3} is made with a dry density of 1590 kg m^{-3} and the porosity becomes 0.43 (43 vol%). There is also a perfect correlation between the dry density and hydraulic conductivity, also for MX-80 bentonite, but the stress state is important for determination of the hydraulic conductivity (Atabek et al., 1991).

Cementitious materials

The mineralogy of concrete is determined by the calculated presence of cement minerals and aggregates. The calculated presence of cement minerals is determined by the compositions of oxides, amount of reacted phases with water and thermodynamic database. Table A-10 shows the compositions of oxides as reported by the cement industry, (CCB, 2016; HCM, 2006), the total amount may not

approach 100% due to rounding off. The groundwater compositions in clay host rocks and also the oxidation of pyrite can generate high sulphate contents. The content of tricalciumaluminate in these cements should therefore be small enough to prevent delayed ettringite formation, especially for CEM I cements an additional identification is assigned for this chemical resistance: Sulphate Resistance (SR), SR3, i.e. a tricalciumcontent smaller than 3 wt%. CEM II and III are blended cements containing a fraction of OPCt with either fly ash slag (V) or blast furnace slag to have a sufficient high pH to activate reaction of these slags. The amount of clinker in these cements are for CEM I 95-100 wt%, CEM II/B-V 65 79 wt%, CEM III/ A 35-64 wt% and CEM III/B 20-34 wt% according to this cement classification following the European standard EN-197-1. The maximum amount of other additions than slag is 5 wt%. The largest proportion is preserved for gypsum ($CaSO_4$•$2H_2O$) or anhydrite (Ca_2SO_4) that is added to cements and determines the SO_3 content. The alkalis are also present as readily soluble sulphates. Gypsum acts as a retarder but there is a limit of 4 wt% to limit ettringite formation. The alkali equivalents (LA) are small enough to prevent alkali-silica reactions if SiO_2 aggregates were to be used. The types of cement used for the waste packaging or building the disposal facility have the same ingredients but with a smaller range in proportions than specified in this European standard.

Table A-10: Average oxide compositions of different types of cement in wt%

Cement type	CaO	SiO_2	Al_2O_3	MgO	Fe_2O_3	SO_3	Na_2O	K_2O
CEM I 52.5 N SR3 LA	63.5	21.3	3.5	2.0	4.3	2.6	0.10	0.63
CEM II/B-V 42.5 N	53	27	6.8	1.2	5.8	2.9	0.30	0.30
CEM III/A 42.5 N	48	28	9.6	4.9	2.0	2.3	0.16	0.91
CEM III/B 42.5 N LH/SR LA	48	29	9.9	6.0	1.3	2.4	0.29	0.61

SR Sulphate resistance to prevent delayed ettringite formations, LA Low alkali to prevent alkali silica reaction

The numbers 52.5 and 42.5 refer to the compressive strength that is to be achieved after 28 days. One of those specified concretes is the Cebama reference mix that was designed for plugs for a disposal facility hosted in granitic rock. The CaO and SiO_2 in Cebama reference mix are 36.0 wt% and 50.7 wt% based on the specified contents of CEM I, silica fume and blast furnace slag (Vehmas et al., 2019). The Ca/Si ratio is significantly smaller than in the cements listed in Table A-10.

Hydration models e.g. (Parrot and Killoh, 1984; van Eijk and Brouwers, 2000) are used to model the composition of hydrated cement. The model by Parrot and Killoh is incorporated in GEMS by PSI in which CEMDATA18 has been used as a thermodynamic database[35]. It is a hydration model for OPC (CEM I) cementitious materials and requires input as tricalcium silicate (C_3S, alite, 3CaO SiO_2), dicalcium silicate (C_2S, belite, 2CaO SiO_2), tricalcium aluminate (C_3A, aluminate, 3CaO Al_2O_3) and tetra alumina ferrite (C_4AF, ferrite, 4CaO Al_2O_3 Fe_2O_3). By default, an amount of gypsum is included. Figure A-5-3 shows the calculated mineralogy in wt% C_3S (alite): 64.6, C_2S(belite): 9.3, C_3A(aluminate):7.4, and C_4AF(ferrite):7.8, w/c=0.5 and relative humidity 1 (default input) and right in wt% C_3S: 81.3, C_3A: 2.0, and C_4AF:4.4 to the oxide compositions for the sulphate resistant cement CEM I in Table A-10.

[35] https://digitaltwin.geoml.eu – PREDIS demo

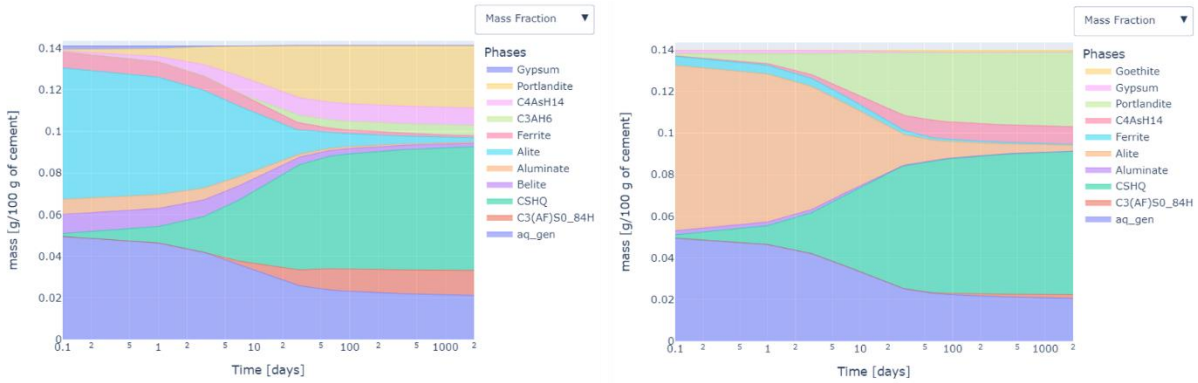

Figure A-5-3: OPC hydration model from digital twin; left standard input clinker composition, right in sulphate resistant cement CEM I [36]

Figure A-5-3 clearly shows that alite (C_3S) is mainly transformed into portlandite and CSH-phases (CSHQ). The CSHQ model is able to describe the entire range of Ca/Si ratios encountered, it is best used for high Ca/Si C-S-H, as it still lacks the ability to predict aluminium uptake, which is of less importance for Portland cements than for blended cements. C_4AsH_{14} is an AFm phase (monosulphate), C_3AH_6 is a hydrogarnet (Lothenbach et al., 2019). Ettringite is the most common AFt phase (trisulphate).

Blended cements such as CEM II and CEM III in Table A-10 are more difficult to calculate than OPC, i.e. CEM I cements. There are also experimental results to decipher the mineralogy. But X-ray diffraction results of hydrated cement and the following Rietveld analysis for CSH identification remains difficult, due to their poor crystallinity, complex solid solution formation with alkali elements, occurrence of polymorphs and varying water concentrations (Kempl and Copuroglu, 2015). Portlandite, ettringite and carbonate minerals can be well measured by X-ray. Portlandite and ettringite are shown in Table A-11 since calcium carbonate is only measured in carbonated cement samples, i.e. a cement mineral composition with calcite ($CaCO_3$) does not represent initial state, although it can be calculated from an hydration model (e.g. Höglund, 2014; Cloet et al., 2019). In examination of historical concrete, the presence of portlandite, ettringite and calcite are identified with their characteristic temperature peaks in the differential thermal analysis (Mallison and Davies, 1987).

Portlandite is measured in CEM I as well as CEM III/B, the amount is in CEM III/B three times less than CEM I (Kempl and Copuroglu, 2015). For the CSH-gels: a CSH-gel high in Ca and a gel low in Ca can be used (Neall, 1994). The CSH gels with a Ca/Si ratio of 1.8 (C1.8SH) and 1.1 (C1.1SH) (Höglund, 2001) in (Höglund, 2014) are used in Table A-11. C1.8SH could also be afwillite (Wang, 2009). Although afwillite and other well crystallised minerals are considered in the Rietveld analyses, these well crystallised CSH-phases are not measured (Kempl and Copuroglu, 2015; Atkins et al., 1991). The presence of portlandite in CEM III/B as measured has been calculated to be dependent on the amount of reacted slag. However, slags are relatively CaO-rich and the Ca/Si ratio of C-S-H can decrease in OPC-slag blends even in the presence of portlandite. Such a decrease in the Ca/Si ratio in the presence of portlandite cannot yet be incorporated in thermodynamic modelling (Lothenbach et al., 2012). The blended cements could only contain low Ca-CSH gel in order to have some amount portlandite as measured in cement pastes made with CEM III/B (Kempl and Copuroglu, 2015) and to be stoichiometric with the average oxide compositions in Table A-10.

Ettringite is controlled by the added amount of gypsum, hydrotalcite is controlled by the available magnesium (Neall, 1994) and the left-over for iron and aluminium control the amount of hydrogarnets. Monosulphate is the location for sulphate in hydration models e.g. (Höglund, 2014), (Berner, 1992) but

[36] A free available software programme from the PREDIS Demo that makes these hydration plots using GEMS (Gibbs Energy Minimization Software for geochemical modelling developed by PSI. The CEMDATA18 database (Lothenbach et al., 2019) has been used as input for these calculations.

only ettringite has been measured and therefore used as the location for sulphate in the mineralogical composition in Table A-11. This is also assumed in the Belgian programme (Wang, 2009). Monosulphate is however metastable with respect to ettringite but in some studies monosulphate instead of ettringite is measured with XRD (Atkins et al., 1991). All suggested mineralogical compositions in Table A-11 are stoichiometric with the average oxide compositions in Table A-10.

Table A-11: Educated guess of the mineralogical composition from average oxides in Table A-10

Mineral	Chemical formula	Molar weight [gram/mol]	Mineralogical composition in wt%			
			CEM I	CEM II/B-V	CEM III/A	CEM III/B
Portlandite	$Ca(OH)_2$	74.1	18	6	4	5
CSH-gel	C1.8SH1.8	193	55	1	1	0
Low Ca-CSH gel	C1.1SH1.8	154	0	53	55	56
Hydrotalcite	$Mg_4Al_2O_7•10H_2O$	443	4	3	10	13
Hydrogarnet	$(CaO)_3Al_2O_3•3H_2O$	378	5	16	18	16
Fe-hydrogarnet	$(CaO)_3Fe_2O_3•3H_2O$	436	9	12	4	3
Ettringite	$Ca_6Al_2(SO_3)_4(OH)_{12}•26H_2O$	1254	8	9	7	7
Pyrite	FeS_2	120	0	0	0.14	0.20

The porosity in the cementitious materials is controlled according to their application. Concrete buffers, concrete segments and plugs are made with aggregates that have a negligible porosity. The concentration of quartz aggregates ranges between 1700 and 2000 kgm^{-3}. The porosity is mainly located within the hydrated cementitious phase provided there is a good bonding between hydrated cement and aggregates. Otherwise, there also some additional porosity at the interface between hydrated cement and aggregates. Kerosine porosimetry seems to give the best reliable result and a porosity of 12.5% was measured for the concrete designed for plugs in the disposal facility for results to be obtained on a short time (Vehmas et al., 2019). Reliable porosity measurements can also be gravimetrically determined but require a long period in laboratory time.

Higher porosities are present for cementitious materials that are used as a backfill and shotcrete, e.g. between 25-35 vol% (NAGRA, 2008). The porosity of concrete made with blended cements is similar to concrete made with OPC based cement with the same factors such as cement content, water/cement ratio, curing conditions etc, but CEM I (i.e. OPC) based concrete has a relative open pore structure compared to blended cements containing slag. Concrete made with these blended cements are called low-permeability concretes due to the refined pore structure (Atkins et al., 1991; Atabek et al., 1991; Jackson et al., 2017).

Cemented metallic and organic waste is investigated for the ILW disposal cells that are studied in ACED. Conditioning grout for waste may have a similar concentration of aggregates as concrete and the porosity can then assumed to be equal to concrete. Aggregates are usually absent if a waste immobilization matrix is made with cementitious materials.

References

Abrahamsen, L., Arnold, T., Brinkmann, H., Leys, N., Merroun, M., Mijnendonckx, K., Moll, H., Polvika, P., Ševců, A., Small, J., Vikman, M. and Wouters, K. 2015 A review of anthropogenic organic wastes and their degradation behaviour - Deliverable 1.1 MIND

Adler, M., Mäder, U.K., Waber, H.N. (1999). High-pH alteration of argillaceous rocks: an experimental study. Schweizerische Mineralogische und Petrographische Mitteilungen 79, 445-454.

Adler, M. (2001). Interaction of claystone and hyperalkaline solutions at 30°C: A combined experimental and modelling study. Ph.D. thesis, University of Bern, Bern, Switzerland.

Águila, J. F., Samper, J., Mon, A., and Montenegro, L. (2020). Dynamic update of flow and transport parameters in reactive transport simulations of radioactive waste repositories. Applied Geochemistry 117.

Ahn, T.M., Soo, P. (1995). Corrosion of low-carbon cast steel in concentrated synthetic groundwater at 80 to 150 °C. Waste Management 15, 471-476.

Ahonen, L. (2004a) Disko Island (Greenland), http://www.natural-analogues.com/nawg-library/na-overviews/analogue review.

Ahonen, L. (2004b) Josephinite, http://www.natural-analogues.com/nawg-library/na-overviews/analogue review.

Ahusborde, E., Amaziane, B., Baksay, A., Bator, G., Becker, D., Bednar, A., Beres, M., Blaheta, R., Bohti, Z., Bracke, G., Brazda, L., Brendler, V., Brenner, K., Brezina, J., Cances, C., Chainais-Hillairet, C., Chave, F., Claret, F., Domesova, S., Havlova, V., Hokr, M., Horak, D., Jacques, D., Jankovsky, F., Kazymyrenko, C., Kolditz, O., Kodelka, T., Kovacs, T., Krejci, T., Kruis, J., Laloy, E., Landa, J., Lipping, T., Lukin, D., Masin, D., Masson, R., Meeussen, J. C. L., Mollaali, M., Mon, A., Montenegro, L., Montoya, V., Pepin, G., Poonoosamy, J., Prasianakis, N. I., Saadi, Z., Samper, J., Scaringi, G., Sochala, P., Tournassat, C., Yoshioka, K., and Yuankai, Y. (2021). "State Of the Art Report in the fields of numerical analysis and scientific computing. Final version as of 16/02/2020 of deliverable D4.1 of the HORIZON 2020 project EURAD. EC Grant agreement no: 847593.

Alcolea, A., Kuhlmann, U., Lanyon, G.W. and Marschall, P. (2014). Hydraulic conductance of the EDZ around underground structures of a geological repository for radioactive waste – A sensitivity study for the candidate host rocks in the proposed siting regions in Northern Switzerland, NAGRA Arbeitsbericht NAB 13-94.

Alexander, W.R. and McKinley, I.G. (1999). The chemical basis of near-field containment in the Swiss high-level radioactive waste disposal concept. Geological Society, Special publication 157(1), 47-69.

Alexander, R. (2012). The impact of a (hyper)alkaline plume on (fractured) crystalline rock. In: NEA, 2012. Cementitious materials in safety cases for geological repositories for radioactive waste: Role, evolution and interactions, NEA/RWM/R(2012)3/REV, 85-88.

Alexander, W.R., Smellie, J.A.T. (1998). Maqarin natural analogue project. ANDRA, CEA, NAGRA, Nirex and SKB synthesis report on Phases I, II and III. NAGRA Technical Report NTB 98-08.

Alexander, W.R., Milodowski, A.E. (eds.) (2011). Cyprus Natural Analogue Project (CNAP) Phase II Final Report. Posiva Working Report WR2011-08, Posiva, Eurajoki, Finland.

Alexander, W.R., Dayal, R., Eagleson, K., Eikenberg, J., Hamilton, E., Linklater, C.M., McKinley, I.G., Tweed, C.J. (1992). A natural analogue of high pH cement pore waters from the Maqarin area of northern Jordan. II: results of predictive geochemical calculations. Journal of Geochemical Exploration 46, 133-146.

Alexander, W.R., Arcilla, C.A., McKinley, I.G., Kawamura, H., Takahashi, Y., Aoki, K., Miyoshi, S. (2008). A new natural analogue study of the interaction of low-alkali cement leachates and the bentonite buffer of a radioactive waste repository. Materials Research Society Symposium Proceedings 1107, 493.

Allard, T., Balan, E., Calas, G., Fourdrin, C., Morichon, E., Sorieul, S. (2012). Radiation-induced defects in clay minerals: A review. Nuclear Instruments and Methods in Physics Research B 277, 112-120.

Alonso, M.C., García Calvo, J.L., Cuevas, J., Turrero, M.J., Fernández, R., Torres, E., Ruiz, A.I. (2017). Interaction processes at the concrete-bentonite interface after 13 years of FEBEX-Plug operation. Part I: Concrete alteration. Physics and Chemistry of the Earth, Parts A/B/C 99, 38-48.

Altmaier, M., Blin, V., García, D., Henocq, P., Missana, T., Ricard, D. and Vandenborre, J. (2021). SOTA on cement-organic-radionuclide interactions. Final version as of 19.05.2021 of deliverable D3.1 of the HORIZON 2020 project EURAD. EC Grant agreement no: 847593.

Andersson, K., Allard, B., Bengtsson, M. and Magnusson, B. (1989). Chemical composition of cement pore solutions. Cement and Concrete Research 19, 327-332.

Anderson, G. M., and Crerar, D. A. (1993). "Thermodynamics in geochemistry: The equilibrium model," Oxford University Press, Oxford, UK.

ANDRA (2018) Safety Options Report -Operating Part (DoS-Expl), CG-TE-D-NTE-AMOA-SR1-0000-15-0060.

Appelo, C. A. J. (2017). Solute transport solved with the Nernst-Planck equation for concrete pores with 'free' water and a double layer. Cement and Concrete Research 101, 102-113.

Appelo, C. A. J., Parkhurst, D. L., and Post, V. E. A. (2014). Equations for calculating hydrogeochemical reactions of minerals and gases such as CO2 at high pressures and temperatures. Geochimica et Cosmochimica Acta 125, 49-67.

Appelo, C. A. J., and Postma, D. (2005). "Geochemistry, groundwater and pollution, 2nd edition," A.A. Balkema Publishers, Amsterdam, The Netherlands.

Appelo, C. A. J., and Wersin, P. (2007). Multicomponent Diffusion Modeling in Clay Systems with Application to the Diffusion of Tritium, Iodide, and Sodium in Opalinus Clay. Environmental Science and Technology 41, 5002-5007.

Aréna, H., Godon, N., Rébiscoul, D., Podor, R., Garcès, E., Cabie, M., Mestre, J.-P. (2016). Impact of Zn, Mg, Ni and Co elements on glass alteration: additive effects. Journal of Nuclear Materials 470, 55-67.

AREVA (2007). Specification for standard vitrified waste residue (CSD-v) with high actinide content produced at la Hague AREVA (ed), p. 23, (Confidential document not published openly).

Archie, G. E. (1942). The electrical resistivity log as an aid in determining some reservoir characteristics. Trans. AIME 164, 54-67.

Argo, J. (1981). A qualitative test for iron corrosion products, Studies in Conservation 26, 140-142.

Atabek, R., Beziat, A., Coulon, H., Dardaine, M., Debrabant, P., Eglem, A., Farcy, C., Fontan, N., Gatabin, C., Gegout, P., Lajudie, A., Landoas, O., Lechelle, J., Plas, F., Proust, D., Raynal, J. and Revertegat, E. (1991). Nearfield behaviour of clay barriers and their interaction with concrete - Task 3 Characterization of radioactive waste forms A series of final reports (1985-1989) No 26, Nuclear Science and Technology, EUR 13877.

Atkins, M., Beckley, N., Carson, S., Cowie, J., Glasser, F.P., Kindness, A., Macphee, D., Pointer, C., Rahman, A., Jappy, J.G., Evans, P.A., McHugh, G., Natingley, N.J. and Wilding, C. (1991).

Medium-active waste form characterization: the performance of cementbased systems Task 3 Characterization of radioactive waste forms A series of final reports (1985-1989) No 1, Nuclear Science and technology, EUR 13452.

Atkinson, A., Goult, D.J. and Hearne, J.A. (1985). An assessment of the long-term durability of concrete in radioactive waste repositories. Mat. Res. Soc. Symp. Proc. 50.

Auqué, L.F., Gimeno, M.J., Gómez, J.B., Puigdomenech, I., Smellie, J.A.T. and Tullborg, E.-L. (2006). Groundwater chemistry around a repository for spent nuclear fuel over a glacial cycle Evaluation for SR-Can, p. 123, SKB Technical Report TR-06-31.

Azcárate, I., Insausti, M., Madina, V. (2004). Estudio de los productos de CORROsión de la cápsula y su interacción con la barrera arcillosa de BENtonita CORROBEN. ENRESA, Madrid, Spain

Baker, A.J., Bateman, K., Hyslop, E.K., Ilett, D.J., Linklater, C.M., Milodowski, A.E., Noy, D.J., Rochelle, C.A., Tweed, C.J. (2002). Research on the alkaline disturbed zone resulting from cement-water-rock reactions around a cementitious repository. UK Nirex Limited Report N/054, UK Nirex Ltd., Harwell, Didcot, United Kingdom.

Balmer, S., Kaufhold, S., Dohrmann, R. (2017). Cement-bentonite-iron interactions on small scale tests for testing performance of bentonites as a barrier in high-level radioactive waste repository concepts. Applied Clay Science 135, 427-436.

Balonis, M., Lothenbach, B., La Saout, G., and Glasser, F. P. (2010). Impact of chloride on the mineralogy of hydrated Portland cement systems. Cement and Concrete Research 40, 1009-1022.

Balonis, M., Mędala, M., and Glasser, F. P. (2011). Influence of calcium nitrate and nitrite on the constitution of AFm and AFt cement hydrates. Advances in Cement Research 23, 129-143.

Bamforth, P.B., Baston, G.M.N., Berry, J.A., Glasser, F.P., Heath, T.G., Jackson, C.P, Savage, D., Swanton, S.W. (2012). Cement materials for use as backfill, sealing and structural materials in geological disposal concepts. A review of current status. Serco Report SERCO/005125/001 Issue 3, Serco, Harwell, Didcot, United Kingdom.

Bart, G., Zwicky, H.U., Aerne, E.T., Graber, T.H., Z'Berg, D., Tokiwai, M. (1987). Borosilicate glass corrosion in the presence of steel corrosion products. Materials Research Society Symposium Proceedings 84, 459-470.

Bartier, D., Techer, I., Dauzères, A, Boulvais, P., Blanc-Valleron, M.-B., Cabrera, J. (2013). In situ investigations and reactive transport modelling of cement paste/argillite interactions in a saturated context and outside an excavated disturbed zone. Applied Geochemistry 31, 94-108.

Bary, B. (2008). Simplified coupled chemo-mechanical modeling of cement pastes behavior subjected to combined leaching and external sulfate attack. International Journal for Numerical and Analytical Methods in Geomechanics 32, 1791-1816.

Bataillon, C., Bouchon, F., Chainais-Hillairet, C., Desgranges, C., Hoarau, E., Martin, R., Perrin, S., Tupin, M., Talandier, J. (2010). Corrosion modelling of iron based alloy in nuclear waste repository. Electrochimica Acta 55, 4451-4467.

Bateman, K., Coombs, P., Noy, D.J., Pearce, J.M., Wetton, P., Haworth, A., Linklater, C. (1999). Experimental simulation of the alkaline disturbed zone around a cementitious radioactive waste repository: numerical modelling and column experiments. Geological Society of London, Special Publication 157, 183-194.

Baxter, S., Appleyard, P., Hartley, L., Hoek, J. and Williams, T. (2018). Exploring conditioned simulations of discrete fracture networks in support of hydraulic acceptance of deposition holes, Posiva SKB report 07.

Bear, J. (1972). Dynamics of Fluids in Porous Media. Elsevier.

Beattie, T.M., Williams, S.J. (2012). An overview of near-field evolution research in support of the UK geological disposal programme. Mineralogical Magazine 76, 2995-3001.

Bejaoui, S., and Bary, B. (2007). Modeling of the link between microstructure and effective diffusivity of cement pastes using a simplified composite model. Cement and Concrete Research 37, 469-480.

Bel, J.P., Wickham, S.M., Gens, R.M.F. (2006). Development of the supercontainer design for deep geological disposal of high-level heat emitting radioactive waste in Belgium. Materials Research Society Symposium Proceedings 932.

Ben Moshe, S., Weisbrod, N., and Furman, A. (2021). Optimization of soil aquifer treatment (SAT) operation using a reactive transport model. Vadose Zone Journal 20, e20095.

Benbow, S., Wilson, J., Metcalfe, R., and Lehikoinen, J. (2019). Avoiding unrealistic behaviour in coupled reactive-transport simulations of cation exchange and mineral kinetics in clays. Clay Minerals 54, 83-93.

Bensted, J., Rbrough, A., and Page, M. M. (2007). 4 - Chemical degradation of concrete. In "Durability of Concrete and Cement Composites" (C. L. Page and M. M. Page, eds.), pp. 86-135. Woodhead Publishing.

Bentz, D. P., and Garboczi, E. J. (1991). Percolation of phases in a three-dimensional cement paste microstructural model. Cem. Concr. Res. 21, 325–344.

Berner, U.R. (1992). Evolution of pore water chemistry during degradation of cement in a radioactive waste repository environment. Waste Management 12, 201-219.

Berner, U., Kulik, D.A., Kosakowski, G. (2013). Geochemical impact of a low-pH cement liner on the near field of a repository for spent fuel and high-level radioactive waste. Physics and Chemistry of the Earth Parts ABC 64, 46-56.

Bernier, F., Li, X.L., Bastiaens, W., Ortiz, L., Van Geet, M., Wouters, L., Frieg, B., Blümling, P., Desrues, J., Viaggiani, G., Coll, C., Chanchole, S., De Greef, V., Hamza, R., Malinsky, L., Vervoort, A., Vanbrabant, Y., Debecker, B., Verstraelen, J., Govaerts, A., Wevers, M., Labiouse, V., Escoffier, S., Mathier, J.-F., Gastaldo, L. and Bühler, C. (2007). Fractures and Self-healing within the Excavation Disturbed Zone in Clays (SELFRAC), Nuclear Science and Technology European Commission, EUR 22585.

Bertolini, L., Elsener, B., Pedeferri, P., Polder, R. (2004). Corrosion of steel in concrete: prevention, diagnosis, repair. Wiley-VCH Verlag.

Bhanja, S. N., Wang, J., Shrestha, N. K., and Zhang, X. (2019). Microbial kinetics and thermodynamic (MKT) processes for soil organic matter decomposition and dynamic oxidation-reduction potential: Model descriptions and applications to soil N2O emissions. Environmental Pollution, 812-823.

Bildstein, O., and Claret, F. (2015). Chapter 5 - Stability of Clay Barriers Under Chemical Perturbations. In "Developments in Clay Science" (C. Tournassat, C. I. Steefel, I. C. Bourg and F. Bergaya, eds.), Vol. 6, pp. 155-188. Elsevier.

Bildstein, O., Claret, F., and Frugier, P. (2019). RTM for Waste Repositories. Reviews in Mineralogy and Geochemistry 85, 419-457.

Bildstein, O., Lartigue, J., Pointeau, I., Cochepin, B., Munier, I., Michau, N. (2012). Chemical evolution in the near field of HLW cells: interactions between glass, steel and clay-stone in deep geological conditions. 5th ANDRA International Meeting, 22–25 Oct 2012, Montpellier, France.

Bildstein, O., Lartigue, J. E., Schlegel, M. L., Bataillon, C., Cochepin, B., Munier, I., and Michau, N. (2016). Gaining insight into corrosion processes from numerical simulations of an integrated iron-claystone experiment. Geol Soc, London Spec Publ 443, 253–267.

Bildstein, O., Trotignon, L., Perronnet, M., and Jullien, M. (2006). Modelling iron-clay interactions in deep geological disposal conditions. Physics and Chemistry of the Earth 31, 618-625.

Bildstein, O., Trotignon, L., Pozo, C., Jullien, M. (2007). Modelling glass alteration in an altered argillaceous environment. Journal of Nuclear Materials 362, 493-501.

Björner, I.K., Christensen, H., Hermansson, H.P., Tsukamo, M., Werme, L. (1989). Corrosion of radioactive, crushed waste glass. Materials Research Society Symposium Proceedings 127, 113-120.

Blackwood, D.J., Gould, L.J., Naish, C.C., Porter, F.M., Rance, A.P., Sharland, S.M., Smart, N.R., Thomas, M.I., Yates, T. (2002). The localised corrosion of carbon steel and stainless steel in simulated repository environments. Report AEAT/ERRA-0318, AEA Technology, Harwell, United Kingdom.

Blanc, P., Gherardi, F., Vieillard, P., Marty, N. C. M., Gailhanou, H., Gaboreau, S., Letat, B., Geloni, C., Gaucher, E. C., and Madé, B. (2021). Thermodynamics for clay minerals: Calculation tools and application to the case of illite/smectite interstratified minerals. Applied Geochemistry 130, 104986.

Blanc, P., Lassin, A., Piantone, P., Azaroual, M., Jacquemet, N., Fabbri, A., and Gaucher, E. C. (2012). Thermoddem: A geochemical database focused on low temperature water/rock interactions and waste materials. Applied Geochemistry 27, 2107-2116.

Blanc, P., Vieillard, P., Gailhanou, H., Gaboreau, S., Marty, N., Claret, F., Madé, B., and Giffaut, E. (2015). ThermoChimie database developments in the framework of cement/clay interactions. Applied Geochemistry 55, 95-107.

Bloom, S. A., and Mansell, R. S. (2001). An algorithm for generating cation exchange isotherms from binary selectivity coefficients. Soil Science Society of America Journal 65, 1426-1429.

Bond, W. J. (1995). On the Rothmund-Kornfeld description of cation exchange. Soil Science Society of America Journal 59, 436-443.

Borisover, M., and Davis, J. A. (2015). Chapter 2 - Adsorption of Inorganic and Organic Solutes by Clay Minerals. In "Developments in Clay Science" (C. Tournassat, C. I. Steefel, I. C. Bourg and F. Bergaya, eds.), Vol. 6, pp. 33-70. Elsevier.

Bradbury, M. H., and Baeyens, B. (1997). A mechanistic description of Ni and Zn sorption on Na-montmorillonite Part II: modelling. Journal of Contaminant Hydrology 27, 223-248.

Bradbury, M. H., and Baeyens, B. (2000). A generalised sorption model for the concentration dependent uptake of caesium by argillaceous rocks. Journal of Contaminant Hydrology 42, 141-163.

Bradbury, M. H., and Baeyens, B. (2003). Porewater chemistry in compacted re-saturated MX-80 bentonite. Journal of Contaminant Hydrology 61, 329-338.

Bradbury, M.H., Berner, U., Curti, E., Hummel, W., Kosakowski, G., Thoenen, T. (2014). The long term geochemical evolution of the nearfield of the HLW repository. NAGRA Technical Report NTB 12-01.

Brantley, S. L., Kubicki, J. D., and White, A. F. (2008). "Kinetics of Water-Rock Interaction," Springer, New York, NY.

Brooks, R. H., and Corey, A. (1964). Hydraulic properties of porous media. Hydrol. Paper No. 3, Colorado State Univ., Fort Collins, CO.

Broomfield, J.P. (2007). Corrosion of steel in concrete: Understanding, investigation and repair (2nd edition). Taylor & Francis.

Brooks, R. H., and Corey, A. (1964). Hydraulic properties of porous media. Hydrol. Paper No. 3, Colorado State Univ., Fort Collins, CO.

Brovelli, a., Malaguerra, F., and Barry, D. a. (2009). Bioclogging in porous media: Model development and sensitivity to initial conditions. Environmental Modelling & Software 24, 611-626.

Bruhn, D.F., Frank, S.M., Roberto, F.F., Pinhero, P.J. and Johnson, S.G. (2009). Microbial film growth on irradiated, spent nuclear fuel cladding. Journal of Nuclear Materials 384(2), 140-145.

Burdine, N. T. (1953). Relative permeability calculations from pore-size distribution data. Petrol. Trans., Am. Inst. Min. Eng. 198, 71-76.

Burger, E., Rébiscoul, D., Bruguier, F., Jublot, M., Lartigu, J.E., Gin, S. (2013). Impact of iron on nuclear glass alteration in geological repository conditions: A multiscale approach. Applied Geochemistry 31, 159-170.

Cama, J., and Ganor, J. (2015). Chapter 4 - Dissolution Kinetics of Clay Minerals. In "Developments in Clay Science" (C. Tournassat, C. I. Steefel, I. C. Bourg and F. Bergaya, eds.), Vol. 6, pp. 101-153. Elsevier.

Capouet, M., Necib, S., Schumacher, S., Mibus, J., Neeft, E.A.C., Norris, S., Nummi, O. and Rübel, A. (2018). CAST outcomes in the context of the safety case: WP6 Synthesis report D 6.4 of the EURATOM seventh framework project CAST grant agreement no. 604779.

Carde, C., François, R., and Torrenti, J.-M. (1996). Leaching of both calcium hydroxide and C-S-H from cement paste: Modeling the mechanical behavior. Cement and Concrete Research 26, 1257-1268.

Caré, S., Nguyen, Q.T., L'Hostis, V., Berthaud, Y. (2008). Mechanical properties of the rust layer induced by impressed current method in reinforced mortar. Cement and Concrete Research 38, 1079-1091.

Carlson, L., Karnland, O., Oversby, V.M., Rance, A., Smart, N., Snellman, M., Vähänen, M., Werme, L.O. (2007). Experimental studies of the interactions between anaerobically corroding iron and bentonite. Physics and Chemistry of the Earth 32, 334-345.

Carlson, L., Karnland, O., Rance, A. and Smart, N. (2008). Experimental studies on the interactions between anaerobically corroding iron and bentonite, SKB R-08-28.

Carlsson, A. and Christiansson, R. (2007). Construction experiences from underground works at Forsmark, SKB report R-07-10.

CCB (2016) CEM I 52,5 N SR LA (CIBELCOR)

Carpén, L., Rajala, P., Kinnunen, T. (2018). Real-time corrosion monitoring system under in situ conditions of crystalline groundwater. 114552. European Corrosion Congress, EUROCORR 2018, Krakow, Poland.

Cau Dit Coumes, C., Courtois, S., Nectoux, D., Leclercq, S., Bourbon, X. (2006). Formulating a low-alkalinity, high-resistance and low-heat concrete for radioactive waste repositories. Cement and Concrete Research 36, 2152-2163.

Černoušek, T., Kokinda, J., Vizelková, K., Shrestha, Ševců, A. (2019). Anaerobic microbial corrosion of canister material - Deliverable 2.13 MIND.

Cervinka, R., Klajmon, M., Zeman, J. and Vencelides, T. (2018). Geochemical calculations and reactive transport modelling, SURAO technical report 271/2018/ENG (data in Czech contribution in EURAD Deliverable 2.4 Treatment of the chemical evolution in National Programmes).

Cey, E., Rudolph, D., and Therrien, R. (2006). Simulation of groundwater recharge dynamics in partially saturated fractured soils incorporating spatially variable fracture apertures. Water Resources Research 42.

Chamssedine, F., Sauvage, T., Peuget, S., Fares, T. and Martin, G. (2010). Helium diffusion coefficient measurements in R7T7 nuclear glass by 3He(d,α)1H nuclear reaction analysis. Journal of Nuclear Materials 400, 175-181.

Chaparro, M.C., Saaltink, M.W., Soler, J.M. (2017). Reactive transport modelling of cement-groundwater-rock interaction at the Grimsel Test Site. Physics and Chemistry of the Earth 99, 64-76.

Chapman, N.A., Hooper A. (2012). The disposal of radioactive wastes underground, Proceedings fo the Geologists' Assocoation 123 (1), 46-63.

Charlet, L., Tournassat, C. (2005). Fe(II)-Na(I)-Ca(II) cation exchange on montmorillonite in chloride medium: evidence for preferential clay adsorption of chloride - metal ion pairs in seawater. Aquatic Geochemistry 11, 115-137.

Charlton, S. R., and Parkhurst, D. L. (2011). Modules based on the geochemical model PHREEQC for use in scripting and programming languages. Computers & Geosciences 37, 1653-1663.

Charpentier, D., Devineau, K., Mosser-Ruck, R., Cathelineau, M., Villiéras, F. (2006). Bentonite–iron interactions under alkaline condition: an experimental approach. Applied Clay Science 32, 1-13.

Chitty, W.-J., Dillmann, P., L'Hostis, V. and Lombard, C. (2005). Long-term corrosion resistance of metallic reinforcements in concrete—a study of corrosion mechanisms based on archaeological artefacts. Corrosion Science 47, 1555–1581.

Chomat, L., L'Hostis, V., Amblard, E., Bellot-Gurlot, L. (2014). Long term study of passive corrosion of steel rebars in Portland mortar in context of nuclear waste disposal. Corrosion Engineering, Science and Technology 49, 467-472.

Chomat, L., Amblard, E., Varlet, J., Blanc, C., Bourbon, X. (2017). Passive corrosion of steel reinforceement in blended cement-based material in the context of nuclear waste disposal. Corrosion Engineering, Science and Technology 52, 148-154.

Chen, X., Thornton, S. F., and Small, J. (2015). Influence of Hyper-Alkaline pH Leachate on Mineral and Porosity Evolution in the Chemically Disturbed Zone Developed in the Near-Field Host Rock for a Nuclear Waste Repository. Transport in Porous Media 107, 489-505.

Claret, F., Marty, N., and Tournassat, C. (2018). Modeling the long-term stability of multi-barrier systems for nuclear waste disposal in geological clay formations. In "Reactive Transport Modeling: Applications in Subsurface Energy and Environmental Problems" (X. Yitian, W. Fiona, X. Tianfu and C. Steefel, eds.), pp. 395-451. John Wiley & Sons Ltd.

Clarke, A.S., Scales, C., Patel, N., Roe, J., Banford, A.W. (2020). Active demonstration of the thermal treatment of surrogate sludge and surrogate drums using the GeoMeltTM In Container Vitrification (ICV) melter installed in NNL central laboratory. IOP Conference Series: Materials Science and Engineering 818, 012004.

Cloet, V., Lothenbach, B., Lura, P., Kosakowski, G., Curti, E., Wieland, E., Lanyon, G.W., Diomidis, N. and Leupin, O. (2019). Cementitious backfill for a high-level waste repository: impact of repository-induced effects - NAGRA Arbeitsbericht NAB 18-41 (not available at NAGRA's website).

Cochepin, B., Martin, C. and Munier, I. (2019). Chapter 10 France, E. Neeft, E. Weetjens, A. Vokal, M. Leivo, B. Cochepin, C. Martin, I. Munier, G. Deissmann, V. Montoya, P. Poskas, D. Grigaliuniene, A. Narkuniene, E. García, J. Samper, L. Montenegro, and A. Mon. 2019. "Treatment of chemical evolution in National Programmes. D 2.4 of the HORIZON 2020 project EURAD. EC Grant agreement no: 847593.

COGEMA (2001). Specification for compacted waste standard residue from light water reactor fuel, p. 22, COGEMA Technical document 300 AQ 055-03 (Confidential document not published openly).

Collin, F., Li, X.L., Radu, J.P., and Charlier, R. (2002). Thermo-hydro-mechanical coupling in clay barriers. Engineering Geology 64:179-193.

Conradt, R., Roggendorf, H. and Ostertag, R. (1986). The basic corrosion mechanisms of HLW glasses, Commission of the European Communities - Nuclear Science and Technology, EUR 10680.

Corkhill, C.L., Cassingham, N.J., Heath, P.G., Hyatt, N.C. (2013). Dissolution of UK High-level waste glass under simulated hyperalkaline conditions of a collocated geological disposal facility. International Journal of Applied Glass Science, 4, 341-356.

Crossland, I. (2005). Long-term corrosion of iron and copper, The 10th International Conference on Environmental Remediation and Radioactive Waste Management, Glasgow (Scotland), ICEM05-1272, ASME.

Crossland, I.C. (2006). Long-term properties of cement - Evidence from nature and archaeology. Crossland Report CCL/2006/01.

Cuevas, J., Villar, M.V., Martín, P.L., Cobeña, J., Leguey, S. (2002). Thermo-hydraulic gradients on bentonite: Distribution of soluble salts, microstructure and modification of the hydraulic and mechanical behavior. Applied Clay Science 22, 25-38.

Cuevas, J., Vigil de la Villa, R., Ramirez, S., Sanchez, L., Fernández, R., Leguey, S. (2006). The alkaline reaction of FEBEX bentonite: a contribution to the study of the performance of bentonite/concrete engineered barrier systems. Journal of Iberian Geology 32, 151-174.

Cuevas, J., Ruíz, A.I., Fernández, R., Torres, E., Escribano, A., Regadío, M., Turrero, M.J. (2016). Lime mortar-compacted bentonite-magnetite interfaces: An experimental study focused on the understanding of the EBS long-term performance for high-level nuclear waste isolation DGR concept. Applied Clay Science 124-125, 79-93.

Dai, Z., and Samper, J. (2004). Inverse problem of multicomponent reactive chemical transport in porous media: Formulation and applications. In "Water Resources Research", Vol. 40, pp. W07407-W07doi.

Dai, Z. X., Samper, J., Wolfsberg, A., and Levitt, D. (2008). Identification of relative conductivity models for water flow and solute transport in unsaturated bentonite. Physics and Chemistry of the Earth 33, S177-S185.

Dauzères, A. (2016). Geochemical and physical evolution of cementitious materials in an aggressive environment. In: Vehmas, T., Holt, E. (eds.) CEBAMA Deliverable D 1.03 - WP1 Experimental studies – State of the art literature review, 136-174.

Dauzères, A., Le Bescop, P., Sardini, P., Cau Dit Coumes, C. (2010). Physico-chemical investigation of clayey/cement-based materials interaction in the context of geological waste disposal: Experimental approach and results. Cement and Concrete Research 40, 1327-1340.

Dauzères, A., Le Bescop, P., Cau-Dit-Coumes, C., Brunet, F., Bourbon, X., Timonen, J., Voutilainen, M., Chomat, L., Sardini, P. (2014). On the physico-chemical evolution of low-pH and CEM I cement pastes interacting with Callovo-Oxfordian pore water under its in situ CO2 partial pressure. Cement and Concrete Research 58, 76-88.

Dauzeres, A., Achiedo, G., Nied, D., Bernard, E., Alahrache, S., and Lothenbach, B. (2016). Magnesium perturbation in low-pH concretes placed in clayey environment-solid characterizations and modeling. Cement and Concrete Research 79, 137-150.

Davis, J.R. (ed.) (2000). Corrosion: Understanding the basics. ASM International, Materials Park, Ohio, USA.

de Blanc, P. C., McKinney, D. C., and Speitel Jr., G. E. (1996). Chapter 1. Modelling subsurface biodegradation of non-aqueous phase liquids. In "Advances in Porous Media, Volume 3" (M. Y. Corapcioglu, ed.), pp. 1-82. Elsevier Science.

De Craen, M., Wang, L., Van Geet, M., and Moors, H. (2004). "Geochemistry of Boom Clay pore water at the Mol site," Rep. No. SCKCEN-BLG-990. SCK•CEN, Mol, Belgium, SCKCEN-BLG-990.

De Combarieu, G., Barboux, P., Minet, Y. (2007). Iron corrosion in Callovo-Oxfordian argilite: from experiments to thermodynamic/kinetic modeling. Physics and Chemistry of the Earth 32, 346-358.

De Combarieu, G., Schlegel, M., Neff, D., Foy, E., Vantelon, D., Barboux, P., Gin, S. (2011). Glass–iron–clay interactions in a radioactive waste geological disposal: an integrated laboratory scale experiment. Applied Geochemistry 26, 65-79.

de Dreuzy, J. R., Rapaport, A., Babey, T., and Harmand, J. (2013). Influence of porosity structures on mixing-induced reactivity at chemical equilibrium in mobile/immobile Multi-Rate Mass Transfer (MRMT) and Multiple INteracting Continua (MINC) models. Water Resources Research 49, 8511-8530.

De Echave, T., Tribet, M., Gin, S., Jégou, C. (2019). Influence of iron on the alteration of the SON68 nuclear glass in the Callovo-Oxfordian groundwater. Applied Geochemistry 100, 268-278.

De Putter, T., Grainger, P., Lombardi, S., Manfroy, P. and Valentini, G. (1997). Fourth European Conference on Management and Disposal of Radioactive waste, pp. 609-626, EUR 17543. Luxembourg.

De Weerdt, K., Lothenbach, B., and Geiker, M. R. (2019). Comparing chloride ingress from seawater and NaCl solution in Portland cement mortar. Cement and Concrete Research 115, 80-89.

De Windt, L., Bertron, A., Larreur-Cayol, S., and Escadeillas, G. (2015). Interactions between hydrated cement paste and organic acids: Thermodynamic data and speciation modeling. Cement and Concrete Research 69, 25-36.

De Windt, L., Leclercq, S., and van der Lee, J. (2006). Assessing the durability of nuclear glass with respect to silica controlling processes in a clayey underground disposal. Materials Research Society Symposium Proceedings 932, 313-320.

De Windt, L., and Spycher, N. F. (2019). Reactive Transport Modeling: A Key Performance Assessment Tool for the Geologic Disposal of Nuclear Waste. Elements 15, 99-102.

Debure, M., De Windt, L., Frugier, P., and Gin, S. (2018). Mechanisms involved in the increase of borosilicate glass alteration by interaction with the Callovian-Oxfordian clayey fraction. Applied Geochemistry 98, 206-220.

Deissmann, G., Ait Mouheb, N. (2021). Interface “cement/concrete – clay”. Chapter 4 in: Deissmann, G., Ait Mouheb, N., Martin, C., Turrero, M. J., Torres, E., Kursten, B., Weetjens, E., Jacques, D., Cuevas, J., Samper, J., Montenegro, H., Leivo, M., Somervuori, M., Carpen, L. (2021). Experiments and numerical model studies on interfaces. Final version as of 12.05.2021 of deliverable D2.5 of the HORIZON 2020 project EURAD. EC Grant agreement no: 847593.

Deissmann, G., Ait Mouheb, N., Martin, C., Turrero, M. J., Torres, E., Kursten, B., Weetjens, E., Jacques, D., Cuevas, J., Samper, J., Montenegro, H., Leivo, M., Somervuori, M., Carpen, L. (2021). Experiments and numerical model studies on interfaces. Final version as of 12.05.2021 of deliverable D2.5 of the HORIZON 2020 project EURAD. EC Grant agreement no: 847593.

Deng, H., and Spycher, N. (2019). Modeling Reactive Transport Processes in Fractures. Reactive Transport in Natural and Engineered Systems 85, 49-74.

Deshpande, P.G., Seddelmeyer, J.D., Wheat, H.G., Fowler, D.W., Jirsa, J.O. (2000). Corrosion performance of polymer-coated, metal-clad and other rebars as reinforcement in concrete. Report FHWA/TX-03/4904-2, Texas Department of Transportation (TxDOT), Austin, TX, USA.

Dillmann, P., Neff, D. and Féron, D. (2014). Archaeological analogues and corrosion prediction: from past to future. A review. Corrosion Engineering, Science and Technology 49(6), 567-576.

Dillmann, P., Gin, S., Neff, D., Gentaz, L., Rébiscoul, D. (2016). Effect of natural and synthetic iron corrosion products on silicate glass alteration processes. Geochimica Cosmochimica Acta 172, 287-305.

Dizier, A., Chen, G., Li, X.L. and Rypens, J. (2017). The PRACLAY Heater test after two years of the stationary phase, EURIDICE Report, ref. EUR_PH_ 17_043.

Drace, Z., Ojovan, M.I. (2013). A summary of IAEA coordinated research project on cementitious materials for radioactive waste management, in: Bart, F., Cau-dit-Coumes, C., Frizon, F., Lorente, S. (eds) Cement-based materials for nuclear waste storage, Springer, 3-11.

Drake, H., Sandström, B. and Tullborg, E.-L. (2006). Mineralogy and geochemistry of rocks and fracture fillings from Forsmark and Oskarshamn: Compilation of data for SR-Can, SKB Report R-06-109.

Druyts, F., Kursten, B., Van Iseghem, P. (2001). Corrosion evaluation of metallic materials for long-lived HLW/Spent Fuel disposal containers. Final report to EDF for the period 1996-1998. SCK.CEN report R-3533, SCK CEN, Mol, Belgium.

Eglinton, M. (1998). Resistance of concrete to destructive agencies. In: Hewlett, P.C. (Ed.): Lea's chemistry of cement and concrete. Arnold, London, 299-342.

Eisele, T.C., Kawatra, S.K. and Ripke, S.J. (2005). Water chemistry effects in iron ore concentrate agglomeration feed. Mineral Processing and Extractive Metallurgy Review 26(3-4), 295-305.

Elakneswaran, Y., Owaki, E., and Nawa, T. (2018). Modelling long-term durability performance of cementitious materials under sodium sulphate interaction. Applied Sciences 8, 2597.

ENRESA, (2000). FEBEX Project. Full-Scale Engineered Barriers Experiment for a Deep Geological Repository for High-Level Radioactive Waste in Crystalline Host Rock. Final Report. Publicación Técnica ENRESA 1/2000.

ENRESA (2001). Evolucíon del comportamiento y de las seguridad de un almacén geológico profundo de residuos radioactivos en arcilla, ENRESA-AGP 49-1PP-I-10-01 Rev. A, 2001, (in Spanish, English in Spanish contribution in EURAD Deliverable 2.4 Treatment of the chemical evolution in National Programmes).

Fernández, A. M., Cuevas, J., and Rivas, P. (2011). Pore Water Chemistry of the Febex Bentonite. MRS Online Proceedings Library 663, 573.

Fernández, R., Ruiz A.I., Cuevas, J. (2016). Formation of C-A-S-H phases from the interaction between concrete or cement and bentonite. Clay Minerals 51, 223-235.

Fernández, R., Torres, E., Ruiz, A.I., Cuevas, J., Alonso, M.C., García Calvo, J.L., Rodríguez, E., Turrero, M.J. (2017). Interaction processes at the concrete-bentonite interface after 13 years of FEBEX-Plug operation. Part II: Bentonite contact. Physics and Chemistry of the Earth, Parts A/B/C 99, 49-63.

Fernández, J. (2017). Reactive Transport Models of low Permeability Structured Porous and Fractured Media, Universidad de A Coruña, Spain.

Fernández, A. M., Kaufhold, S., Sánchez-Ledesma, D. M., Rey, J. J., Melón, A., Robredo, L. M., Fernández, S., Labajo, M. A., and Clavero, M. A. (2018). Evolution of the THC conditions in the FEBEX in situ test after 18 years of experiment: Smectite crystallochemical modifications after

interactions of the bentonite with a C-steel heater at 100 °C. Applied Geochemistry 98, 152-171.

Frederickx, L., Honty, M., de Craen, M., Dohrmann, R., and Elsen, J. (2018). Relating the Cation Exchange Properties of the Boom Clay (Belgium) to Mineralogy and Pore-Water Chemistry. Clays and Clay Minerals 66, 449-465.

Freedman, V. L., Bacon, D. H., Saripalli, K. P., and Meyer, P. D. (2004). A Film Depositional Model of Permeability for Mineral Reactions in Unsaturated Media. Vadose Zone J. 3, 1414-1424.

Frugier, P., Gin, S., Minet, Y., Chave, T., Bonin, B., Godon, N., Lartigue, J. E., Jollivet, P., Ayral, A., De Windt, L., and Santarini, G. (2008). SON68 nuclear glass dissolution kinetics: Current state of knowledge and basis of the new GRAAL model. Journal of Nuclear Materials 380, 8-21.

Frugier, P., Minet, Y., Rajmohan, N., Godon, N., and Gin, S. (2018). Modeling glass corrosion with GRAAL. npj Materials Degradation 2, 35.

Fujisawa, R., Cho, T., Sugahara, K., Takizawa, Y., Horikawa, Y., Shiomi, T., Hironaga, M. (1997). The corrosion behaviour of iron and aluminium under waste disposal conditions. Materials Research Society Symposium Proceedings 465, 675-684.

Fujisawa, R., Kurashige, T., Inagaki, Y., Senoo, M. (1999). Gas generation behaviour of transuranic waste under disposal conditions. Materials Research Society Symposium Proceedings 556, 1199-1206.

Fujiwara, A., Yasutomi, I., Fukudome, K., Tateishi, T., Fujiwara, K. (2001). Influence of oxygen concentration and alkalinity on the hydrogen gas generation by corrosion of carbon steel. Materials Research Society Symposium Proceedings 663, 497-505.

Fukushi, K., Sugiura, T., Morishita, T., Takahashi, Y., Hasebe, N., Ito, H. (2010). Iron-bentonite reactions in the Kawasaki bentonite deposit, Zao area, Japan. Applied Geochemistry 25, 1120-1132.

Furkas, F.E., Lothenbach, B., Burkan Isgur, O., Mundra, S., Zhang, Z., Angst, U.E. (2022). Solubility and speciation of iron in cementitious systems. Cement and Concrete Research 151, 106620.

Gaboreau, S., Pret, D., Tinseau, E., Claret, F., Pellegrini, D., Stammose, D. (2011). 15 years of in situ cement–argillite interaction from Tournemire URL: Characterisation of the multi-scale spatial heterogeneities of pore space evolution. Applied Geochemistry 26, 2159–2171.

Gaboreau, S., Lerouge, C., Dewonck, S., Linard, Y., Bourbon, X., Fialips, C.I., Mazurier, A., Prêt, D., Borschneck, D., Montouillout, V., Gaucher, E.C., Claret, F. (2012). In-situ interaction of cement paste and shotcrete with claystones in a deep disposal context. American Journal of Science, 312, 314–356.

Gaucher, E.C., Blanc, P. (2006). Cement/clay interactions - A review: Experiments, natural analogues, and modeling. Waste Management 26, 776-788.

Gaucher, E.C., Blanc, P., Bardot, F., Braibant, G., Buschaert, S., Crouzet, C., Gautier, A., Girard, J.-P., Jacquot, E., Lassin, A., Negrel, G., Tournassat, C., Vinsot, A. and Altmann, S. (2006). Modelling the porewater chemistry of the callovian-oxfordian formation at a regional scale. Comptes Rendus Géoscience 338, 917-930.

Gaucher, E. C., Tournassat, C., Pearson, F. J., Blanc, P., Crouzet, C., Lerouge, C., and Altmann, S. (2009). A robust model for pore-water chemistry of clayrock. Geochimica Et Cosmochimica Acta 73, 6470-6487.

Gdowski, G.E., Bullen, D.B. (1988). Survey of degradation modes of candidate materials for high-level radioactive waste disposal containers. Oxidation and corrosion. LLNL Report UCID-21362, Vol. 2., Lawrence Livermore National Laboratory, Livermore, CA, USA.

Géhin, A., Grenèche, J.-M., Tournassat, C., Brendlé, J., Rancourt, D.G., Charlet, L. (2007). Reversible surface sorption induced electron transfer oxidation of Fe(II) at reactive sites on a synthetic clay minera, Geochimica Cosmochimica Acta 71, 863-876.

Georget, F., Prévost, J. H., and Huet, B. (2017). A reactive transport simulator for variable porosity problems. Computational Geosciences 21, 95-116.

Gerard, B., Didry, O., Marchand, J., Gerard, B., Breysse, D., and Hornain, H. (1996). "Modelling the long-term durability of concrete barriers for radioactive waste disposals," France.

Giffaut, E., Grive, M., Blanc, P., Vieillard, P., Colas, E., Gailhanou, H., Gaboreau, S., Marty, N., Made, B., and Duro, L. (2014). Andra thermodynamic database for performance assessment: ThermoChimie. Applied Geochemistry 49, 225-236.

Gin, S. (2014). Open scientific questions about glass corrosion. Procedia Materials Sciences 7,163-171.

Gin, S., Beaudoux, X., Angéli, F., Jégou, C., Godon, N. (2012). Effect of composition on the short-term and long-term dissolution rates of ten borosilicate glasses of increasing complexity from 3 to 30 oxides. Journal of Non-Crystalline Solids 358, 2559-2570.

Gin, S., Abdelouas, A., Criscenti, L.J., Ebert, W.L., Ferrand, K., Geisler, T., Harrison, M.T., Inagaki, Y., Mitsui, S., Mueller, K.T., Marra, J.C., Pantano, C.G., Pierce, E.M., Ryan, J.V., Schofield, J.M., Steefel, C.I., Vienna, J.D. (2013). An international initiative on long-term behaviour of high-level nuclear waste glass. Materials Today 16, 243-248.

Gin, S., Jollivet, P., Fournier, M., Angéli, F., Frugier, P., Charpentier, T. (2015). Origin and consequences of silicate glass passivation by surface layers. Nature Communication 6.

Glasser, F.P., Marchand, J., Samson, E. (2008). Durability of concrete - Degradation phenomena involving detrimental chemical reactions. Cement and Concrete Research 38, 226-246.

Glasser, F.P. (2011). Application of inorganic cements to the conditioning and immobilisation of radioactive wastes. In: Ojovan, M.I. (ed.) Handbook of advanced radioactive waste conditioning technologies, Woodhead, 67-135.

Glynn, P. D. (1991). MBSSAS : A code for the computation of Margules parameters and equilibrium relation in binary solid-solution aqueous-solution systems, Computers & Geosciences 17, 907-966.

Godon, N., Gin, S., Rebiscoul, D., and Frugier, P. (2013). SON68 glass alteration enhanced by magnetite. Proceedings of the Fourteenth International Symposium on Water-Rock Interaction, Wri 14 7, 300-303.

Goldberg, S., Criscenti, L. J., Turner, D. R., Davis, J. A., and Cantrell, K. J. (2007). Adsorption - Desorption processes in subsurface reactive transport modeling. Vadose Zone Journal 6, 407-435.

Goñi, S., Andrade, C. (1990). Synthetic concrete pore solution chemistry and rebar corrosion rate in the presence of chlorides. Cement and Concrete Research 20, 525-539.

Graczyk, K. M., and Matyka, M. (2020). Predicting porosity, permeability, and tortuosity of porous media from images by deep learning. Scientific Reports 10.

Grambow, B. (1987). Nuclear waste glass dissolution: Mechanism, model and experiment. Report to JSS Project Phase IV. Report No. JSS-87-02.

Grambow, B., Zwicky, H.U., Bart, G., Björner, I.K., Werme, L.O. (1987). Modeling the effect of iron corrosion products on nuclear glass performance. Materials Research Society Symposium Proceedings 84, 471-481.

Grambow, B., López-García, M., Olmeda, J., Grivé, M., Marty, N.C.M., Grangeon, S., Claret, F., Lange, S., Deissmann, G., Klinkenberg, M., Bosbach, D., Bucur, C., I., F., R., D., Isaacs, M., Read, D., Kittnerová, J., Drtinová, B., Vopálka, D., Cevirim-Papaioannou, N., Ait-Mouheb, N., Gaona, X., Altmaier, M., Nedyalkova, L., Lothenbach, B., Tits, J., Landesman, C., Rasamimanana, S. and Ribet, S. (2019). Retention of radionuclides on cementitious systems: main outcome of the CEBAMA project, Deliverable 2.6 Manuscript for peer review of the results generated in WP2 of the CEBAMA project.

Grambow, B., López-García, M., Olmeda, J., Grivé, M., Marty, N. C. M., Grangeon, S., Claret, F., Lange, S., Deissmann, G., Klinkenberg, M., Bosbach, D., Bucur, C., Florea, I., Dobrin, R., Isaacs, M., Read, D., Kittnerová, J., Drtinová, B., Vopálka, D., Cevirim-Papaioannou, N., Ait-Mouheb, N., Gaona, X., Altmaier, M., Nedyalkova, L., Lothenbach, B., Tits, J., Landesman, C., Rasamimanana, S., and Ribet, S. (2020). Retention and diffusion of radioactive and toxic species on cementitious systems: Main outcome of the CEBAMA project. Applied Geochemistry 112, 104480.

Grauer (1988). The corrosion behaviour of carbon steel in portland cement, NAGRA Technical report 88-02 E.

Greneche, D., Quiniou, B., Boucher, L., Delpech, M., Gonzalez, E., Alvarez, F., Cunado, M.A., Serrano, G., Cormnezana, J.L., Kuckshinrichs, W., Odoj, R., von Lensa, W., Wallenius, J., Westlén, D., Zimmerman, C. and Marivoet, J. (2007) RED-IMPACT Impact of Partitioning, Transmutation and Waste Reduction Technologies on the Final Nuclear Waste Disposal - Synthesis report, Schriften des Forschungszentrums Jülich - Reihe Energie & Umwelt / Energy & Environment Band - Band / Volume 15.

Greskowiak, J., Gwo, J., Jacques, D., Yin, J., and Mayer, K. U. (2015). A benchmark for multi-rate surface complexation and 1D dual-domain multi-component reactive transport of U(VI). Computational Geosciences 19, 585-597.

Griffioen, J., Koenen, M., Meeussen, H., Cornelissen, P., Peters, L. and Jansen, S. (2017). Geochemical interactions and groundwater transport in the Rupel Clay. A generic model analysis. OPERA-PU-TNO522.

Grivé, M. and Olmeda, J. (2015). Molybdenum behaviour in cementitious materials. in Cebama project Deliverable 2.03 WP2: State of the Art Report (initial), pp. 32-66.

Grivé, M., Duro, L., Colas, E., and Giffaut, E. (2015). Thermodynamic data selection applied to radionuclides and chemotoxic elements: An overview of the ThermoChimie-TDB. Applied Geochemistry 55, 85-94.

Guillaume, D., Neaman, A., Cathelineau, M., Mosser-Ruck, R., Peiffert, C., Abdelmoula, M., Dubessy, J., Villiéras, F., Baronnet, A., Michau, N. (2003). Experimental synthesis of chlorite from smectite at 300 °C in the presence of metallic Fe. Clay Minerals 38, 281-302.

Guillaume, D., Neaman, A., Cathelineau, M., Mosser-Ruck, R., Peiffert, C., Abdelmoula, M., Dubessy, J., Villiéras, F., Michau, N. (2004). Experimental study of the transformation of smectite at 80 and 300 °C in the presence of Fe oxides. Clay Minerals 39, 17-34.

Guo, X., Gin, S., Lei, P., Yao, T., Liu, H., Schreiber, D.K., Ngo, D., Viswanathan, G., Li, T., Kim, S.H., Vienna, J.D., Ryan, J.V., Du, J., Lian, J., Frankel, G.S. (2020). Self-accelerated corrosion of nuclear waste forms at material interfaces. Nature Materials 19, 310-316.

Hadi, J., Wersin, P., Serneels, V., Greneche, J.M. (2019). Eighteen years of steel–bentonite interaction in the FEBEX in situ test at the Grimsel Test Site in Switzerland. Clays and Clay Minerals 67, 111-131.

Haggerty, R., and Gorelick, S. M. (1995). Multiple-rate mass transfer for modeling diffusion and surface reactions in media with pore-scale heterogeneity. Water Resources Research 31, 2383-2400.

Hammond, G. E., Lichtner, P. C., and Mills, R. T. (2014). Evaluating the performance of parallel subsurface simulators: An illustrative example with PFLOTRAN. Water Resources Research 50, 208-228.

Havlova, V., Knight, L., Laciok, A., Cervinka, R. and Vokal, A. (2007). Analogue evidence relevant to UK HLW glass waste forms p. 37, NIREX 509009 made by Nuclear Research Institute Řež; natural-analogues.com/nawg-library.

Han, S.-C., Jo, Y., and Yun, J.-I. (2021). Chemical degradation of fly ash blended concrete with the seasonal variation of rainwater in a radioactive waste repository: A thermodynamic modeling approach. Cement and Concrete Research 141, 106326.

HCM (2006). HCM Cement productinformatie Hoogovencement / product information cement blend with blast furnace slag CEM III/B 42.5 N -LH/SR LA, CEM III/A 42.5 N and fly ash CEM II/B-V 42.5 N.

He, W., Beyer, C., Fleckenstein, J. H., Jang, E., Kolditz, O., Naumov, D., and Kalbacher, T. (2015). A parallelization scheme to simulate reactive transport in the subsurface environment with OGS#IPhreeqc 5.5.7-3.1.2. Geosci. Model Dev. 8, 3333-3348.

Hermansson, H.-P. (2004). The Stability of Magnetite and its Significance as a Passivating Film in the Repository Environment, SKI Report 2004:07.

Heukamp, F. H., Ulm, F.-J., and Germaine, J. T. (2003). Poroplastic properties of calcium-leached cement-based materials. Cement and Concrete Research 33, 1155-1173.

Heukamp, F. H., Ulm, F. J., and Germaine, J. T. (2001). Mechanical properties of calcium-leached cement pastes: Triaxial stress states and the influence of the pore pressures. Cement and Concrete Research 31, 767-774.

Hewlett, P.C. (ed.) (1998). Lea's chemistry of cement and concrete. Arnold, London

Hiemstra, T., and Van Riemsdijk, W. H. (2006). On the relationship between charge distribution, surface hydration, and the structure of the interface of metal hydroxides. Journal of Colloid and Interface Science 301, 1-18.

Hiemstra, T., and Van Riemsdijk, W. H. (1996). A surface structural approach to ion adsorption: The charge distribution (CD) model. Journal of Colloid and Interface Science 179, 488-508.

Hoch, A.R., Baston, G.M.N., Glasser, F.P., Hunter, F.M.I., Smith, V. (2012). Modelling evolution in the near field of a cementitious repository. Mineralogical Magazine. 76, 3055-3069.

Höglund L.O. (2014). The impact of concrete degradation on the BMA barrier functions. SKB Report R-13-40.

Holmboe, M., Jonsson, M., Wold, S. (2012). Influence of γ-radiation on the reactivity of montmorillonite towards H2O2. Radiation Physics and Chemistry 81, 190-194.

Holmes, N., Kelliher, D., and Tyrer, M. (2020). Simulating cement hydration using HYDCEM. Construction and Building Materials 239.

Hommel, J., Coltman, E., and Class, H. (2018). Porosity–Permeability Relations for Evolving Pore Space: A Review with a Focus on (Bio-)geochemically Altered Porous Media. Transport in Porous Media 124, 589-629.

Honda, A., Teshima, T., Tsurudome, K., Ishikawa, H., Yusa, Y., Sasaki, N. (1991). Effect of compacted bentonite on the corrosion behavior of carbon steel as geological isolation overpack material. Materials Research Society Symposium Proceedings 212, 287-294.

Honty, M. and De Craen, M. (2012). Boom Clay mineralogy – qualitative and quantitative aspects - SCK•CEN contract: CO-90-08-2214-00 NIRAS/ONDRAF contract: CCHO 2009-0940000 Research Plan Geosynthesis, External report SCK•CEN-ER-194.

Hooker, P. (2003a). Dunarobba, http://www.natural-analogues.com/nawg-library/na-overviews/analogue review.

Hooker, P. (2003b). Hadrian's wall, http://www.natural-analogues.com/nawg-library/na-overviews/analogue review.

Hooker, P. (2003c). Inchtuthil Roman Fort (Scotland), http://www.natural-analogues.com/nawg-library/na-overviews/analogue review.

Huang, B., and Qian, C. (2011). Experiment study of chemo-mechanical coupling behavior of leached concrete. Construction and Building Materials 25, 2649-2654.

Huang Y., Shao, H., Wieland E., Kolditz, O., and Kosakowski, G. (2018). A new approach to coupled two-phase reactive transport simulation for long-term degradation of concrete. Construction and Building Materials 190, 805–829.

Huang, Y., Shao, H., Wieland, E., Kolditz, O., and Kosakowski, G. (2021). Two-phase transport in a cemented waste package considering spatio-temporal evolution of chemical conditions. npj Materials Degradation 5:4.

Hummel, W., Berner, U., Curti, E., Pearson, F. J., and Thoenen, T. (2002). "Nagra/PSI chemical thermodynamic data base 01/01," Rep. No. also published as Nagra Technical Report NTB 02-16, Wettingen, Switzeland. Universal Publishers/uPUBLISH.com, USA, USA.

Hunter, F.M.I., Bate, F., Heath, T.G., Hoch, A.R. (2007). Geochemical investigation of iron transport into bentonite as steel corrodes. SKB Technical Report TR-07-09.

Hussain, S.E., Rasheeduzzafar (1993). Effect of temperature on pore solution composition in plain cements. Cement and Concrete Research 23, 1357-1368.

Hussain, S.E., Al-Gahtani, A.S., Rasheeduzzafar (1996). Chloride threshold for corrosion of reinforcement in concrete. ACI Materials Journal 94, 534-538.

IAEA (2002). Application of Ion Exchange Processes for the Treatment of Radioactive Waste and Management of Spent Ion Exchangers, IAEA Technical Reports Series no. 408.

IAEA (2004). International Atomic Energy Agency, Management of waste containing tritium and carbon-14, IAEA Technical Report Series 421.

IAEA (2009). Classification of radioactive waste, IAEA Safety standards General Safety Guide No. GSG-1.

IAEA (2022). IAEA Isotope Browser, IAEA Nuclear Data Section, accessed 2022.

Idiart, A., Laviña, M., Kosakowski, G., Cochepin, B., Munier, I., Meeussen, J.C.L., Samper, J., Mon, A., Montenegro, L., Montoya, V., Deissmann, G., Rohmen, S. and Poonoosamy, J. (2019). Manuscript for peer-reviewed publication of Work Package 3: Benchmark of reactive transport modelling of a low-pH concrete / clay interface, CEBAMA Deliverable 3.08.

Idiart, A., Lavina, M., Kosakowski, G., Cochepin, B., Meeussen, J. C. L., Samper, J., Mon, A., Montoya, V., Munier, I., Poonoosamy, J., Montenegro, L., Deissmann, G., Rohmen, S., Damiani, L. H., Coene, E., and Naves, A. (2020). Reactive transport modelling of a low-pH concrete / clay interface. Applied Geochemistry 115.

Jackson, M.D., Mulcahy, S.R., Chen, H., Li, Y., Li, Q., Cappelletti, P. and Wenk, H.-R. (2017). Philipsite and Al-tobermite mineral cements produced through low-temperature water-rock reactions in Roman marine concrete. American Mineralogist 102(7), 1435-1450.

Jacques, D., Simunek, J., Mallants, D., and van Genuchten, M. T. (2018). The HPx software for multicomponent reactive transport during variably-saturated flow: Recent developments and applications. Journal of Hydrology and hydromechanics 66, 211-226.

Jacques, D., Šimůnek, J., Mallants, D., and van Genuchten, M. T. (2006). Operator-splitting errors in coupled reactive transport codes for transient variably saturated flow and contaminant transport in layered soil profiles. Journal of Contaminant Hydrology 88, 197-218.

Jacques, D., Šimůnek, J., Mallants, D., and van Genuchten, M. T. (2008). Modeling Coupled Hydrologic and Chemical Processes: Long-Term Uranium Transport following Phosphorus Fertilization. Vadose Zone Journal 7, 698-711.

Jacques, D., Wang, L., Martens, E., and Mallants, D. (2010). Modelling chemical degradation of concrete during leaching with rain and soil water types. Cement and Concrete Research 40, 1306-1313.

Jefferies, N.L., Tweed, C.J., Wisbey, S. (1988). The effects of changes in pH within a clay surrounding a cementitious repository. Materials Research Societey Symposium Proceedings 112, 43-52.

Jenni, A., Mäder, U., Lerouge, C., Gaboreau, S., Schwyn, B. (2014). In situ interaction between different concretes and Opalinus Clay. Physics and Chemistry of the Earth, Parts A/B/C 70, 71–83.

Jenni, A., Wersin, P., Thoenen, T., Baeyens, B. Ferrari, A., Gimmi, T., Mäder U.K., Hummerl, W., and Leupin, O.X. (2019). Bentonite backfill performance in a high-level waste repository: a geochemical perspective, Nagra Technical Report NTB 19-03.

Jin, Q., and Bethke, C. M. (2003). A New Rate Law Describing Microbial Respiration. 69, 2340-2348.

Jin, Q., and Bethke, C. M. (2005). Predicting the rate of microbial respiration in geochemical environments. Geochimica et Cosmochimica Acta 69, 1133-1143.

Jin, Q., and Bethke, C. M. (2007). The thermodynamics and kinetics of microbial metabolism. American Journal of Science 307, 643-677.

Jodin-Caumon, M.C., Mosser-Ruck, R., Randi, A., Pierron, O., Cathelineau, M., Michau, N. (2012). Mineralogical evolution of a claystone after reaction with iron under thermal gradient. Clays and Clay Minerals 60, 443-455.

Johannesson, L.-E., Hermansson, F., Kronberg, M. and Bladström, T. (2020). Manufacturing of large scale buffer blocks Uniaxial compaction of block – test made with three different bentonites, SKB Report R-19-28.

Johnson, L. and King, F. (2008). The effect of the evolution of environmental conditions on the corrosion evolutionary path in a repository for spent fuel and high-level waste in Opalinus Clay. Journal of Nuclear Materials 379, 9-15.

Johnson, J. W., Oelkers, E. H., and Helgeson, H. C. (1992). SUPCRT92: A software package for calculating the standadard molal thermodynamic properties of minerals, gases, aqueous species and reactions from 1 to 5000 bar and 0 to 1000>C. In "Computers and Geosciences", Vol. 18, pp. 899-947.

Jordan, G., and Rammensee, W. (1998). Dissolution Rates of Calcite (1014) Obtained by Scanning Force Microscopy: Microtopography-Based Dissolution Kinetics on Surfaces with Anisotropic Step Velocities. In "Geochimica et Cosmochimica Acta", Vol. 62, pp. 941-947.

Jordan, N., Marmier, N., Lomenech, C., Giffaut, E., and Ehrhardt, J. J. (2007). Sorption of silicates on goethite, hematite, and magnetite: Experiments and modelling. Journal of Colloid and Interface Science 312, 224-229.

Jull, S.P. and Lees, T.P. (1990). Studies of historic concrete, Commission of the European Communities - Nuclear Science and Technology EUR 12972.

Källström, K. and Lindgren, M. (2014). Waste form and packaging process report for the safety assessment SR-PSU, SKB Technical Report TR-14-03.

Kamei, G., Alexander, W.R., Clark, I.D., Degnan, P., Elie, M., Khoury, H., Milodowski, A.E., Pitty, A.F., Salameh, E. and Smellie, J.A.T. (2010). Natural analogues of cement: overview of the unique systems in Jordan, Tsukuba (Japan).

Kaneko, M., Miura, N., Fujiwara, A. and Yamamoto, M. (2004). Evaluation of Gas Generation Rate by Metal Corrosion in the Reducing Environment, RWMC Engineering Report RWMC-TRE-03003.

Kärki, A. and Paulamäki, S. (2006). Petrology of Olkiluoto, Posiva report 2006-02.

Kaufhold, S., Dohrmann, R., Ufer, K., and Kober, F. (2018). Interactions of bentonite with metal and concrete from the FEBEX experiment: mineralogical and geochemical investigations of selected sampling sites. Clay Minerals 53, 745-763.

Ke, X., Bernal, S. A., Provis, J. L., and Lothenbach, B. (2020). Thermodynamic modelling of phase evolution in alkali-activated slag cements exposed to carbon dioxide. Cement and Concrete Research 136, 106158.

Kempl, J. and Copuroglu, O. (2015). The interaction of pH, pore solution composition and solid phase composition of carbonated blast furnace slag cement paste activated with aqueous sodium monofluorophosphate, pp. 287-296, Delft, the Netherlands.

Kim, S.S., Lee, J.G., Choi, J.K., Lee, G.H., Chun, K.S. (1997). Effects of metals, metal oxides and metal hydroxide on the leaching of simulated nuclear waste glass. Radiochimica Acta 79, 199-205.

King, R.A., Miller, J.D.A. and Smith, J.S. (1973). Corrosion of Mild Steel by Iron Sulphides. British Corrosion Journal 8(3), 137-141.

King, F. (2008). Corrosion of carbon steel under anaerobic conditions in a repository for SF and HLW in Opalinus Clay. Nagra Technical Report NTB 08-12.

King, F. (2014). Durability of high level waste and spent fuel disposal containers – an overview of the combined effect of chemical and mechanical degradation mechanisms. Quintessa Report QRS-1589A-R1_AppB2, Quintessa, Henley-on-Thames, United Kingdom.

King, F., Kolar, M., Keech, P.G. (2014). Simulations of long-term anaerobic corrosion of carbon steel containers in Canadian deep geological repository. Corrosion Engineering Science and Technology 49, 455-459.

Kinniburg, D.G. and Cooper, D.M. (2018). (Phreeplot) Creating graphical output with PHREEQC; www.phreeplot.org.

Knight, L. (2003). Scwat Hill, http://www.natural-analogues.com/nawg-library/na-overviews/analogue review.

Kosakowski, G., and Berner, U. (2013). The evolution of clay rock/cement interfaces in a cementitious repository for low- and intermediate level radioactive waste. Physics and Chemistry of the Earth, Parts A/B/C 64, 65-86.

Kosakowski, G., and Watanabe, N. (2014). OpenGeoSys-Gem: A numerical tool for calculating geochemical and porosity changes in saturated and partially saturated media. Physics and Chemistry of the Earth 70-71, 138-149.

Kosakowski, G., Berner, U., Wieland, E., Glaus, M., Degueldre C (2014). Geochemical Evolution of the L/ILW Near-field, NAGRA Technical report 14-11.

Koskinen, K. (2014). Effects of cementitious leachates on the EBS. Posiva Report 2013-04, Posiva, Olkiluoto, Finland.

Kreis, P. (1991). Hydrogen evolution from corrosion of iron and steel in low/intermediate level waste repositories, NAGRA Technical Report 91-21.

Kulik, D. A., Wagner, T., Dmytrieva, S. V., Kosakowski, G., Hingerl, F. F., Chudnenko, K. V., and Berner, U. R. (2013). GEM-Selektor geochemical modeling package : Revised algorithm and GEMS3K numerical kernel for coupled simulation codes. Computational Geosciences 17, 1-24.

Kulik, D.A., Miron, D., and Lothenbach, B. (2022). A structurally-consistent CASH+ sublattice solid solution model for fully hydrated C-S-H phases: thermodynamic basis, methods, and Ca-Si-H2O core sub-model. Cement and Concrete Research, 151, 106585.

Kulik, D.A., Winnefeld, F., Kulik, A., Miron, D., and Lothenbach, B. (2021). CemGEMS – an easy-to-use web application for thermodynamic modelling of cementitious materials. RILEM Tech Lett 2021, 6, 36-52.

Kursten, B., Smailos, E., Azkarate, I., Werme, L., Smart, N.R., Santarini G. (2004a). COBECOMA, State-of-the-art document on the COrrosion BEhaviour of COntainer MAterials. European Commission, Contract N° FIKW-CT-20014-20138 Final Report.

Kursten, B., Smailos, E., Azkarate, I., Werme, L., Smart, N.R., Marx, G., Cuñado, M.A., Santarini, G. (2004b). Corrosion evaluation of metallic materials for long-lived HLW/Spent Fuel disposal containers: Review of 15-20 years of research. Euradwaste04, 6th EC Conference on the Management and Disposal of Radioactive Waste, 29 March – 1 April 2004, Luxembourg.

Kursten, B., Druyts, F., Macdonald, D., Smart, N., Gens, R., Wang, L., Weetjens, E., Govaerts, J. (2011). Review of corrosion studies of metallic barrier in geological disposal conditions with respect to Belgian Supercontainer concept. Corrosion Engineering, Science and Technology, 46, 91-97.

Kursten, B. and Druyts, F. (2015). Assessment of the uniform corrosion behaviour of carbon steel radioactive waste packages with respect to the disposal concept in the geological Dutch Boom Clay formation, OPERA-PU-SCK513.

Kursten, B., Weetjens, E., Jaques, D. (2021). Interface “steel/iron – concrete“. Chapter 6 in: Deissmann, G., Ait Mouheb, N., Martin, C., Turrero, M. J., Torres, E., Kursten, B., Weetjens, E., Jacques, D., Cuevas, J., Samper, J., Montenegro, H., Leivo, M., Somervuori, M., Carpen, L. (2021). Experiments and numerical model studies on interfaces. Final version as of 12.05.2021 of deliverable D2.5 of the HORIZON 2020 project EURAD. EC Grant agreement no: 847593.

Laaksoharju, M., Auqué, L., Gimeno, M., Gómez, J., Gurban, I., Hallbeck, L., Molinero, J., Raposo, J., Smellie, J.A.T. and Tullborg, E.-L. (2005). Hydrogeochemical evaluation Preliminary site description Forsmark area – version 1.2, SKB Rapport R-05-17.

Lacher, J.R. (1937). A theoretical formula for the solubility of hydrogen in palladium. Proceedings of the Royal Society of London A 161, 525-545.

Laciok, A. (2004). Glasses: natural, http://www.natural-analogues.com/nawg-library/na-overviews/analogue review.

Laciok, A. and Dalton, J. (2005). Glasses: archeological and historical http://www.natural-analogues.com/nawg-library/na-overviews/analogue review.

Lainé, M., Balan, E., Allard, T., Paineau, E., Jeunesse, P., Mostafavi, M., Robert, J.L., Le Caër, S. (2017). Reaction mechanisms in swelling clays under ionizing radiation: influence of the water amount and of the nature of the clay mineral. RSC Advances 7, 526-534.

Lalan, P., Dauzères, A., De Windt, L., Bartier, D., Sammaljärvi, J., Barnichon, J.-D., Techer, I., Detilleux, V. (2016). Impact of a 70 °C temperature on an ordinary Portland cement paste/claystone interface: An in situ experiment. Cement and Concrete Research 83, 164-178.

Landolt, D., Davenport, A., Payer, J., Shoesmith, D. (2009). A review of materials and corrosion issues regarding canisters for disposal of spent fuel and high-level waste in Opalinus Clay. Nagra Technical Report NTB 09-02, Nagra, Wettingen, Switzerland.

Lanson, B., Lantenois, S., van Aken, P.P., Bauer, A., Plançon, A. (2012). Experimental investigation of smectite interaction with metal iron at 80 °C: structural characterization of newly formed Fe-rich phyllosilicates. American Mineralogist 97, 864-871.

Lantenois, S., Lanson, B., Muller, F., Bauer, A., Jullien, M., Plançon, A. (2005). Experimental study of smectite interaction with metal Fe at low temperature: 1. Smectite destabilization. Clays and Clay Minerals 53, 597-612.

Lanyon, G.W. (2015). Modellers Summary of LCS Experiment 2 (F16) Tracer Testing. Nagra Aktennotiz AN 15-025-Rev.1. Nagra, Wettingen, Switzerland.

Lasaga, A. C. (1998). "Kinetic Theory in the Earth Sciences," Princeton University Press, Princeton, NJ

Leal, A. M. M., Kulik, D. A., Smith, W. R., and Saar, M. O. (2017). An overview of computational methods for chemical equilibrium and kinetic calculations for geochemical and reactive transport modeling. Pure and Applied Chemistry 89, 597-643.

Leivo, M. (2021). Interface “cement/mortar – granite”. Chapter 3 in: Deissmann, G., Ait Mouheb, N., Martin, C., Turrero, M. J., Torres, E., Kursten, B., Weetjens, E., Jacques, D., Cuevas, J., Samper, J., Montenegro, H., Leivo, M., Somervuori, M., Carpen, L. (2021). Experiments and numerical model studies on interfaces. Final version as of 12.05.2021 of deliverable D2.5 of the HORIZON 2020 project EURAD. EC Grant agreement no: 847593.

Lemmens, K. (2001). The effect of clay on the dissolution of nuclear waste glass. Journal of Nuclear Materials 298, 11-18.

Lerouge C., Gaboreau S., Grangeon S., Claret F., Warmont F., Jenni A, Cloet V, Mäder. (2017). In situ interactions between Opalinus Clay and Low Alkali Concrete. Physics and Chemistry of the Earth, Parts A/B/C 99, 3-21.

Leupin, O.X., Smith, P., Marschall, P., Johnson, L., Savage, D., Cloet, V., Schneider, J. and Senger, R. (2016). High-level waste repository-induced effects, NAGRA Technical Report 14-13.

Levasseur, S., Collin, F., Daniels, K., Dymitrowska, M., Harrington, J., Jacops, E., Kolditz, O., Marschall, P., Norris, S., Sillen, X., Talandier, J., Truche, L. and Wendling, J. (2021). Initial State of the Art on Gas Transport in Clayey Materials. Deliverable D6.1 of the HORIZON 2020 project EURAD, Work Package Gas. EC Grant agreement no: 847593.

L’Hostis, V., Amblard, E., Blanc, C., Miserque, F., Paris, C., Bellot-Gurlet, L. (2011). Passive corrosion of steel in concrete in context of nuclear waste disposal. In: Lyon, S., Kursten, B. and Druyts, F. (eds.) Proceedings of the Fourth International Workshop on Long-Term Prediction of Corrosion Damage in Nuclear Waste Systems, June 28 – July 2, 2010, Bruges, Belgium, Corrosion Engineering, Science and Technology 46, 177-181.

Li, L., Weetjens, E., Vietor, T. and Hart, J. (2010). Integration of TImoDaZ results within the safety case and recommendations for repository design. D 14 of the 6th EURATOM framework programme project TimoDaZ contract no. FI6W-CT-2007-0364449.

Li, D, Bauer, S., Benisch, K., Graupner, B. Beyer C. (2014). Opengeosys-chemapp: a coupled simulator for reactive transport in multiphase systems and application to CO2 storage formation in northern Germany. Acta Geotechnica, 9 (1), 67-79.

Li, X., Shui, Z., Gao, X., and Ling, G. (2021). Hydration implanted reactive transport modelling in saturated cement-based materials. Construction and Building Materials 275, 122185.

Lichtner, P. C. (1996). Continuum formulation of multicomponent-multiphase reactive transport. In "Reviews in Mineralogy and Geochemistry" (P. C. Lichtner, C. Steefel and E. H. Oelkers, eds.), Vol. 34, pp. 1-81.

Liu, C., Shang J., and Zachara, J.M. (2011). Multispecies diffusion models: A study of uranyl species diffusion. Water Resources Research, 47, W12514.

Liu, C., Wang, J., Zhang, Z., Han, E-H. (2017). Studies on corrosion behavior of low carbon steel canister with and without γ-irradiation in China's HLW disposal repository. Corrosion Engineering, Science and Technology 52, 136-140.

Liu, S. H., Ferrand, K., and Lemmens, K. (2015). Transport- and surface reaction-controlled SON68 glass dissolution at 30 degrees C and 70 degrees C and pH=13.7. Applied Geochemistry 61, 302-311.

Liu, S., Ferrand, K., Aertsens, M., Jacques, D., and Lemmens, K. (2019). Diffusion models for the early-stage SON68 glass dissolution in a hyper-alkaline solution. Applied Geochemistry 111.

Liu, S., Jacques, D., Govaerts, J., and Wang, L. (2014). Conceptual model analysis of interaction at a concrete-Boom Clay interface. Physics and Chemistry of the Earth 70-71, 150-159.

Lombardi, S. and Valentini, G. (1996). The Dunarobbe forest as natural analogue: analysis of the geoenvironmental factors controlling the wood preservation, pp. 127-133, Sixth EC Natural analogue working group meeting Proceedings of an international workshop held in Santa Fe, New Mexico, USA. EUR 16761.

Lothenbach, B., Kulik, D. A., Matschei, T., Balonis, M., Baquerizo, L., Dilnesa, B., Miron, G. D., and Myers, R. J. (2019). Cemdata18: A chemical thermodynamic database for hydrated Portland cements and alkali-activated materials. Cement and Concrete Research 115, 472-506.

Lothenbach, B., Le Saout, G., Ben Haha, M., Figi, R. and Wieland, E. (2012). Hydration of a low-alkali CEM III/B–SiO2 cement (LAC). Cement and Concrete Research 42, 410-423.

Lothenbach, B., Matschei, T., Möschner, G., and Glasser, F. P. (2008). Thermodynamic modelling of the effect of temperature on the hydration and porosity of Portland cement. Cement and Concrete Research 38, 1-18.

Lothenbach, B., and Winnefeld, F. (2006). Thermodynamic modelling of the hydration of Portland cement. Cement and Concrete Research 36, 209-226.

Lothenbach, B., and Zajac, M. (2019). Application of thermodynamic modelling to hydrated cements. Cement and Concrete Research 123, 105779.

Lu, C. H., Samper, J., Fritz, B., Clement, A., and Montenegro, L. (2011). Interactions of corrosion products and bentonite: An extended multicomponent reactive transport model. Physics and Chemistry of the Earth 36, 1661-1668.

Lutze, V., Grambow, B., Ewing, R.C. and Jercinovic, M.J. (1987). Natural analogues in radioactive waste disposal. Côme, B. and Chapman, N.A. (eds), Commission of the European Communities - Radioactive Waste Management Series EUR 11037.

Ma, B., Fernandez-Martinez, A., Madé, B., Findling, N., Markelova, E., Salas-Colera, E., Maffeis, T.G.G., Lewis, A.R., Tisserand, D., Bureau, S., Charlet, L. (2018) XANES-based determination of redox potentials imposed by steel corrosion products in cement-based media, Environmental Science and Technology 52, 11931−11940.

Ma, B., Lothenbach, B. (2020a). Thermodynamic study of cement/rock interactions using experimentally generated solubility data of zeolites. Cement and Concrete Research 135, 106149.

Ma, B., and Lothenbach, B. (2020b). Synthesis, characterization, and thermodynamic study of selected Na-based zeolites. Cement and Concrete Resarch 135, 106111.

Ma, B., Lothenbach, B. (2021). Synthesis, characterization, and thermodynamic study of selected K-based zeolites. Cement and Concrete Research 148, 106537.

Macdonald, D. D., Urquidi-Macdonald, M., Engelhardt, G. R., Azizi, O., Saleh, A., Almazooqi, A., and Rosas-Camacho, O. (2011). Some important issues in electrochemistry of carbon steel in

simulated concrete pore water Part 1-theoretical issues. Corrosion Engineering Science and Technology 46, 98-103.

MacQuarrie, K. T. B., and Mayer, K. U. (2005). Reactive transport modeling in fractured rock: A state-of-the-science review. In "Earth-science reviews", Vol. 72, pp. 189-227.

Mäder, U. (2009). Reference pore water for the Effingen Member (Standordtregion Südjura) for the provisional safety-analysis in the framework of the sectoral plan - interim results (SGT-ZE), p. 73, Arbeitsbericht NAB 09-13

Mäder, U.K., Fierz, T., Frieg, B., Eikenberg, J., Rüthi, M., Albinsson, Y., Möri, A., Ekberg, S., Stille, P. (2006). Interaction of hyperalkaline fluid with fractured rock: Field and laboratory experiments of the HPF project (Grimsel Test Site, Switzerland). Journal of Geochemical Exploration 90, 68-94.

Mäder, U., Jenni, A., Lerouge, C., Gaboreau, S., Miyoshi, S., Kimura, Y., Cloet, V., Fukaya, M., Claret, F., Otake, T., Shibata, M., Lothenbach B. (2017). 5-year chemico-physical evolution of concrete–claystone interfaces, Mont Terri rock laboratory (Switzerland). Swiss Journal of Geosciences, DOI 10.1007/s00015-016-0240-5.

Maes, N., Glaus, M. A., Baeyens, B., Marques Fernandes, M., Churakov, S., Dähn, R., Grangeon, S., Tournassat, C., Geckeis, H., Charlet, L., Brandt, F., Poonoosamy, J., Hoving, A., Havlova, V., Fisher, C., Scheinost, A. C., Noseck, U., Britz, S., Siitari-Kauppi, M., and Missana, T. (2021). "State-of-the-Art report on the understanding of radionuclide retention and transport in clay and crystalline rocks. Final version as of 30.04.2021 of deliverable D5.1 of the HORIZON 2020 project EURAD. EC Grant agreement no: 847593.."

Maes, N., Salah, S., Jacques, D., Aertsens, M., Vangompel, M., De Canniere, P., and Velitchkova, N. (2008). Retention of Cs in Boom Clay: Comparison of data from batch sorption tests and diffusion experiments on intact clay cores. Physics and Chemistry of the Earth, Parts A/B/C 33, S149-S155.

Maia, F., Puigdomènech, I., and Molinero, J. (2016). "Modelling rates of bacterial sulphide production using lactate and hydrogen as energy sources," Rep. No. SKB Technical Report TR-16-05. SKB.

Mainguy, M., Tognazzi, C., Torrenti, J.-M., and Adenot, F. (2000). Modelling of leaching in pure cement paste and mortar. Cement and Concrete Research 30, 83-90.

Majzlan, J., Grevel, K.-D., Navrotsky, A. (2003). Thermodynamics of Fe oxides: Part II. Enthalpies of formation and relative stability of goethite (α-FeOOH), lepidocrocite (□-FeOOH) and maghemite (□-Fe2O3). American Mineralogist 88, 855-859.

Mallinson, L.G. and Davies, I.L.I. (1987). A historical examination of concrete, Commission of the European Communities - Nuclear Science and Technology, EUR 10937.

Mann, C., Ferrand, K., Liu, S., Eskelsen, J. R., Pierce, E., Lemmens, K., and Corkhill, C. (2019). Influence of young cement water on the corrosion of the International Simple Glass. Npj Materials Degradation 3.

Marcos, N. (2003). Bentonite-iron interactions in natural occurrences and in laboratory - the effects of the interactions on the properties of bentonite: a literature survey. Posiva Working Report WR2003-55, Posiva Oy, Olkiluoto, Finland.

Marsh, G.P., Taylor, K.J., Sharland, S.M., Tasker, P.W. (1987). An approach for evaluation the general and localised corrosion of carbon-steel containers for nuclear waste disposal. Materials Research Society Symposium Proceedings 84, 227.

Marsh, G.P., Harker, A.H., Taylor, K.J. (1989). Corrosion of carbon steel nuclear waste containers in marine sediment. Corrosion 45, 579-589.

Marsh, G.P., Taylor, K.J., Sharland, S.M. and Diver, A.J. (1991). Corrosion of carbon steel overpacks for the geological disposal of radioactive waste Task 3 Characterization of radioactive waste forms A series of final reports (1985-89) No 29, Nuclear Science and technology Commission of the European Communities, EUR 13671

Martin, C. (2021). Interface “glass – steel”. Chapter 2 in: Deissmann, G., Ait Mouheb, N., Martin, C., Turrero, M. J., Torres, E., Kursten, B., Weetjens, E., Jacques, D., Cuevas, J., Samper, J., Montenegro, H., Leivo, M., Somervuori, M., Carpen, L. (2021). Experiments and numerical model studies on interfaces. Final version as of 12.05.2021 of deliverable D2.5 of the HORIZON 2020 project EURAD. EC Grant agreement no: 847593.

Martin, V., Jaffre, J., and Roberts, J. E. (2005). Modeling fractures and barriers as interfaces for flow in porous media. Siam Journal on Scientific Computing 26, 1667-1691.

Martinez, J. S., Santillan, E. F., Bossant, M., Costa, D., and Ragoussi, M. E. (2019). The new electronic database of the NEA Thermochemical Database Project. Applied Geochemistry 107, 159-170.

Marty, N. C. M., Bildstein, O., Blanc, P., Claret, F., Cochepin, B., Gaucher, E. C., Jacques, D., Lartigue, J.-E., Liu, S., Mayer, K. U., Meeussen, J. C. L., Munier, I., Pointeau, I., Su, D., and Steefel, C. (2015a). Benchmarks for multicomponent reactive transport across a cement/clay interface. Computational Geosciences 19, 635-653.

Marty, N. C. M., Claret, F., Lassin, A., Tremosa, J., Blanc, P., Madé, B., Giffaut, E., Cochepin, B., and Tournassat, C. (2015b). A database of dissolution and precipitation rates for clay-rocks minerals. Applied Geochemistry 55, 108-118.

Marty, N. C. M., Fritz, B., Clément, A., and Michau, N. (2010). Modelling the long term alteration of the engineered bentonite barrier in an underground radioactive waste repository. Applied Clay Science 47, 82-90.

Marty, N. C. M., Munier, I., Gaucher, E. C., Tournassat, C., Gaboreau, S., Vong, C. Q., Giffaut, E., Cochepin, B., and Claret, F. (2014). Simulation of Cement/Clay Interactions: Feedback on the Increasing Complexity of Modelling Strategies. Transport in Porous Media 104, 385-405.

Marty, N. C. M., Tournassat, C., Burnol, A., Giffaut, E., and Gaucher, E. C. (2009). Influence of reaction kinetics and mesh refinement on the numerical modelling of concrete/clay interactions. Journal of Hydrology 364, 58-72.

Maslehuddin, M. (1994). The influence of Arabian Gulf environment on mechanisms of reinforcement corrosion. Ph.D. Thesis, The University of Aston in Birmingham, United Kingdom.

Maslehuddin, M., Page, C.L., Rasheeduzzafar, Al Mana, A.I. (1996). Effect of temperature on pore solution chemistry and reinforcement corrosion in contaminated concrete. In: Page, C.L., Bamforth, P.B., Figg, J.W. (eds.) Corrosion of reinforcement in concrete construction, RSC Special Publications 183, 67-75.

Matyka, M., Khalili, A., and Koza, Z. (2008). Tortuosity-porosity relation in porous media flow. Physical Review E 78.

Mayant, C. (2009). Étude des propriétés de rétention et de transport de la magnétite dans un état compacté, Nantes, France.

Mayant, C., Grambow, B., Abdelouas, A., Ribet, S., and Ledercq, S. (2008). Surface site density, silicic acid retention and transport properties of compacted magnetite powder. Physics and Chemistry of the Earth 33, 991-999.

Mayer, K. U., Frind, E. O., and Blowes, D. W. (2002). Multicomponent reactive transport modeling in variably saturated porous media using a generalized formulation for kinetically controlled reactions. Water Resources Research 38, 1174, doi:10.1029/2001WR000862.

McCafferty, E. (2010). Introduction to Corrosion Science. Springer.

McVay, G.L., Buckwalter, C.Q. (1983). Effect of iron on waste-glass leaching. Journal of the American Ceramic Society 66, 170-174.

Metcalfe, R., Walker, C. (2004). Proceedings of the International Workshop on Bentonite-Cement Interaction in Repository Environments, Tokyo. Posiva Working Report WR2004-25, Posiva, Olkiluoto, Finland.

Mibus, J., Diomidis, N., Wieland, E. and Swanton, S. (2018). Final synthesis report on results from WP2 - D 2.18 from CArbon-14 Source Term project from the European Union's Seventh Framework Programme for research, technological development and demonstration under grant agreement no. 604779.

Michau, N. (2005). ECOCLAY II: Effects of cement on clay barrier performance. Andra Report C.RP.ASCM.04.0009, Andra, Paris, France.

Michel, A., Nygaard, P.V., Geiker, M.R. (2013). Experimental investigation on the short term impact of temperature and moisture on reinforcement corrosion. Corrosion Science 72, 26-34.

Michel, A., Marcos-Meson, V., Kunther, W., and Geiker, M. R. (2021). Microstructural changes and mass transport in cement-based materials: A modeling approach. Cement and Concrete Research 139, 106285.

Michelin, A., Burger, E., Leroy, E., Foy, E., Neff, D., Benzerara, K., Dillmann, P., Gin, S. (2013a). Effect of iron metal and siderite on the durability of simulated archeological glassy material. Corrosion Science 76, 403-414.

Michelin, A., Drouet, E., Foy, E., Dynes, J.J., Neff, D., Dillmann, P. (2013b). Investigation at the nanometre scale on the corrosion mechanisms of archaeological ferrous artefacts by STXM. Journal of Analytical Atomic Spectrometry 28, 59-66.

Michelin, A., Leroy, E., Neff, D., Dynes, J.J., Dillmann, P., Gin, S. (2015). Archaeological slag from Glinet: an example of silicate glass altered in an anoxic iron-rich environment. Chemical Geology 413, 28-43.

Mihara, M., Nishimura, T., Wada, R., Honda, A. (2002). Estimation on gas generation and corrosion rates of carbon steel, stainless steel and zircaloy in alkaline solutions under low oxygen condition. JNC Technical Review 15, 91-101 (in Japanese).

Mijnendonckx, K., Miroslav, H., Wang, L., Jacops, E., Provoost, A., Mysara, M., Wouters, K., De Craen, M. and Leys, N. (2019). An active microbial community in Boom Clay pore water collected from piezometers impedes validating predictive modelling of ongoing geochemical processes. Applied Geochemistry 106, 149-160.

Milodowski, A.E., Hyslop, E.K., Pearce, J.M., Wetton, P.D., Kemp, S.J., Longworth, G., Hodginson, E. and Hughes, C.R. (1998). Magarin natural analogue study: Phase III Volume I. Smellie, J.A.T. (ed), pp. 135-180, SKB Technical report TR-98-04.

Milodowski, A.E., Cave, M.R., Kemp, S.J., Taylor, H., Green, K., Williams, C.L., Shaw, R.A., Gowing, C.J.B., Eatherington, N.D. (2009). Mineralogical investigations of the interaction between iron corrosion products and bentonite from the NF-PRO experiments. SKB Technical Report TR-09-03, SKB, Stockholm, Sweden.

Milodowski, A.E., Alexander, W.R., West, J.M., Shaw, R.P., McEvoy, F.M., Scheidegger, J.M., Field, L.P. (2015). A catalogue of analogues for radioactive waste management. British Geological Survey Commissioned Report CR/15/106, British Geologcial Survey, Keyworth, Nottingham, United Kingdom.

Milodowski, A.E., Norris, S., Alexander, W.R. (2016). Minimal alteration of montmorillonite following long-term interaction with natural alkaline groundwater: Implications for geological disposal of radioactive waste. Applied Geochemistry 66, 184-197.

Millington, R. J., and Quirk, J. P. (1961). Permeability of porous solids. Transactions of the Faraday Society 57, 1200-1206.

Miron, D., Kulik, D.A., Yan, Y., Tits, J., and Lothenbach, B. (2022). Miron, G. D., Kulik, D. A., Yan, Y., Tits, J., & Lothenbach, B. (2022). Extensions of CASH+ thermodynamic solid solution model for the uptake of alkali metals and alkaline earth metals in C-S-H. Cement and Concrete Research, 152, 106667.

Missana, T., Garcia-Gutierrez, M., Mingarro, M., and Alonso, U. (2019). Selenite Retention and Cation Coadsorption Effects under Alkaline Conditions Generated by Cementitious Materials: The Case of C-S-H Phases. Acs Omega 4, 13418-13425.

Moldrup, P., Olesen, T., Gamst, J., Schjonning, P., Yamaguchi, T., and Rolston, D. E. (2000). Predicting the gas diffusion coefficient in repacked soil: Water-induced linear reduction model. Soil Science Society of America Journal 64, 1588-1594.

Moldrup, P., Olesen, T., Rolston, D. E., and Yamaguchi, T. (1997). Modeling diffusion and reaction in soils .7. Predicting gas and ion diffusivity in undisturbed and sieved soils. Soil Science 162, 632-640.

Molins, S., Trebotich, D., Miller, G. H., and Steefel, C. I. (2017). Mineralogical and transport controls on the evolution of porous media texture using direct numerical simulation. Water Resources Research 53, 3645-3661.

Mon, A. (2017). Coupled Thermo-Hydro-Chemical-Mechanical Models for the Bentonite Barrier in a Radioactive Waste Repository, Ph.D. Dissertation. University of A Coruña, Spain.

Mon, A., Samper, J., Montenegro, L., Naves, A., and Fernández, J. (2017). Long-term non-isothermal reactive transport model of compacted bentonite, concrete and corrosion products in a HLW repository in clay. Journal of Contaminant Hydrology 197, 1-16.

Moncouyoux, J., Aure, A. and Ladirat, C. (1991). Investigation of full-scale high-level waste containment glass blocks Task 3 Characterization of radioactive waste forms A series of final reports (1985-89) - No 24, Commission of the European Communities Nuclear science and Technology EUR 13612.

Montes, G.H., Fritz, B., Clement, J.A., Michau, N. (2005). Modeling of transport and reaction in an engineered barrier for radioactive waste confinement. Applied Clay Science 29, 155-171.

Moog, H. C., Bok, F., Marquardt, C. M., and Brendler, V. (2015). Disposal of nuclear waste in host rock formations featuring high-saline solutions – Implementation of a thermodynamic reference database (THEREDA). Applied Geochemistry 55, 72-84.

Mosser-Ruck, R., Cathelineau, M., Guillaume, D., Charpentier, D., Rousset, D., Barres, O., Michau, N. (2010). Effects of temperature, pH, and iron/clay and liquid/clay ratios on experimental conversion of dioctahedral smectite to berthierine, chlorite, vermiculite, or saponite. Clays and Clay Minerals 58, 280-291.

Moyce, E.B.A., Rochelle, C., Morris, K., Milodowski, A.E., Chen, X., Thornton, S., Small, J.S., Shaw, S. (2014). Rock alteration in alkaline cement waters over 15 years and its relevance to the geological disposal of nuclear waste. Applied Geochemistry 50, 91-105.

Mualem, Y. (1976). A new model for predicting the hydraulic conductivity of unsaturated porous media. Water Resources Research 12, 513-522.

Müller-Vonmoos, M. and Kahr, G. (1983). Mineralogische unterschungen von Wyoming Bentonit MX-80 und montigel, NAGRA Technischer bericht 83-12.

Murphy, W. M., Oelkers, E. H., and Lichtner, P. C. (1989). Surface-Reaction Versus Diffusion Control of Mineral Dissolution and Growth-Rates in Geochemical Processes. Chemical Geology 78, 357-380.

Myers, R. J., Bernal, S. A., San Nicolas, R., and Provis, J. L. (2013). Generalized structural description of calcium-sodium aluminosilicate hydrate gels: The cross-linked substituted tobermorite model. Langmuir 29, 5294-5306.

NAGRA (2002). Project Opalinus Clay. Models, codes and data for safety assessment. Demonstration of disposal feasibility for spent fuel, vitrified high-level waste and long-lived intermediate-level waste. NAGRA Technical Report 02–06.

NAGRA (2008). Effects of post-disposal gas generation in a repository for low- and intermediate-level waste sited in the Opalinus Clay of Northern Switzerland, NAGRA Technical report 08-07.

Naish, C.C., Balkwill, P.H., O'Brien, T.M., Taylor, K.J. and Marsh, G.P. (1991). The anaerobic corrosion of carbon steel in concrete, Task 3: Characterization of waste forms. A series of final reports (1985-1989) No 33, Nuclear Science and Technology Commission of the European Communities EUR13663.

NAnet (2006). Analogues for the near-field of a repository WP1 of the European Community under the 'Competitive and Sustainable Growth' Programme (1998-2002) EUR 21919.

Nardi, A., Idiart, A., Trinchero, P., De Vries, L. M., and Molinero, J. (2014). Interface COMSOL-PHREEQC (iCP), an efficient numerical framework for the solution of coupled multiphysics and geochemistry. Computers & Geosciences 69, 10–21.

Navarro, V. (1997). Modelo de comportamiento mecánico e hidráulico de suelos no saturados en condiciones no isotermas, Universidad Politécnica de Cataluña.

NDA (2016). Geological disposal - Geosphere status report. NDA Report no. DSSC/453/01, Nuclear Decommissioning Authority, Harwell, Didcot, United Kingdom.

NEA (2012). Cementitious Materials in Safety Cases for Geological Repositories for Radioactive Waste: Role, Evolution and Interactions. NEA/RWM/R(2012)3/REV.

Neall, F. (1994). Modelling of the near-field chemistry of the SMA repository at the Wellenberg site: application of the extended cement degradation model NAGRA Technical report 94-03.

Necib, S., Linard, Y., Crusset, D., Michau, N., Daumas, S., Burger, E., Romaine, A., Schlegel, M.L. (2016). Corrosion at the carbon steel–clay borehole water and gas interfaces at 85 °C under anoxic and transient acidic conditions. Corrosion Science 111, 242-258.

Necib, S., Linard, Y., Crusset, D., Schlegel, M., Daumas, S., Michau, N. (2017a). Corrosion processes of C-steel in long-term repository conditions. Corrosion Engineering, Science and Technology 52, 127-130.

Necib, S., Diomidis, N., Keech, P., Nakayama, M. (2017b). Corrosion of carbon steel in clay environments relevant to radioactive waste geological disposals, Mont Terri rock laboratory (Switzerland). Swiss Journal of Geosciences 110, 329-342.

Necib, S., Bucur, C., Caes, S., Cochin, F., Cvetković, B.Z., Fulger, M., Gras, M., Herm, M., Kasprzak, L., Legand, S., Metz, V., Perrin, S., Sakuragi, T. and Suzuki-Muresan, T. (2018). Overview of 14C release from irradiated Zircaloys in geological disposal conditions. Radiocarbon 60(6), 1757-1771.

Necib, S., Schlegel, M.L., Bataillon, C., Daumas, S., Diomidis, N., Keech, P., Crusset, D. (2019). Long-term corrosion behaviour of carbon steel and stainless steel in Opalinus clay: influence of stepwise temperature increase. Corrosion Engineering, Science and Technology 54, 516-528.

Neeft, E., Weetjens, E., Vokal, A., Leivo, M., Cochepin, B., Martin, C., Munier, I., Deissmann, G., Montoya, V., Poskas, P., Grigaliuniene, D., Narkuniene, A., García, E., Samper, J., Montenegro, L. and Mon, A. (2019). Treatment of chemical evolution in National Programmes. D 2.4 of the HORIZON 2020 project EURAD. EC Grant agreement no: 847593.

Neeft, E.A.C. (2018). 14C exposure from disposal of radioactive waste compared to 14C exposure from cosmogenic origin. Radiocarbon 60(6), 1911-1923.

Neff, D., Reguer, S., Bellot-Gurlet, L., Dillmann, P. and R., B. (2004). Structural characterisation of corrosion products on archaeological iron. An integrated analytical approach to establish corrosion forms. Journal of Raman Spectroscopy 35(8-9), 739-745.

Neff, D., Dillmann, P., Descostes, M., Beranger, G. (2006). Corrosion of iron archaeological artefacts in soil: Estimation of the average corrosion rates involving analytical techniques and thermodynamic calculations. Corrosion Science 48, 2947-2970.

Neff, D., Saheb, M., Perrin, S., Descostes, M., L'Hostis, V., Crusset, D., Millard, A., Dillmann, Ph. (2010). A review of the archaeological analogue approaches to predict the long-term corrosion behaviour of carbon steel overpack and reinforced concrete structures in the French disposal systems. Journal of Nuclear Materials 402, 196-205.

NF-PRO (2008). Understanding and Physical and Numerical Modelling of the Key Processes in the Near Field and their Coupling for Different Host Rocks and Repository Strategies (NF-PRO), European Commission Nuclear Science and Technology, EUR 23720.

Ngo, V. V., Clément, A., Michau, N., and Fritz, B. (2015). Kinetic modeling of interactions between iron, clay and water: Comparison with data from batch experiments. Applied Geochemistry 53, 13-26.

Ngo, V. V., Delalande, M., Clement, A., Michau, N., and Fritz, B. (2014). Coupled transport-reaction modeling of the long-term interaction between iron, bentonite and Callovo-Oxfordian claystone in radioactive waste confinement systems. Applied Clay Science 101, 430-443.

NIROND (2013). ONDRAF/NIRAS Research, Development and Demonstration (RD&D) Plan State-of-the-art report as of December 2012.

Norris, S. and Capouet, M. (2018). Overview of CAST project. Radiocarbon 60(6), 1649-1656.

Ochs, M. and Talerico, C. (2004). SR-Can Data and uncertainty assessment Migration parameters for the bentonite buffer in the KBS-3 concept, SKB Technical Report TR-04-18.

Ochs, M., Mallants, D., and Wang, L. (2016). "Radionuclide and Metal Sorption on Cement and Concrete," Springer.

Oda, M. (1985). Permeability Tensor for Discontinuous Rock Masses. Geotechnique 35, 483-495.

Oelkers, E. H., Benezeth, P., and Pokrovski, G. S. (2009). Thermodynamic Databases for Water-Rock Interaction. Rev Mineral Geochem 70, 1-46.

Oelkers, E. H., Schott, J., and Devidal, J.-L. (1994). The effect of aluminum, pH, and chemical affinity on the rates of aluminosilicate dissolution reactions. Geochimica et Cosmochimica Acta 58, 2011-2024.

Oh, B. H., and Jang, S. Y. (2004). Prediction of diffusivity of concrete based on simple analytic equations. Cement and Concrete Research 34, 463-480.

Olmeda, J., Missana, T., Grandia, F., Grive, M., Garcia-Gutierrez, M., Mingarro, M., Alonso, U., Colas, E., Henocq, P., Munier, I., and Robinet, J. C. (2019). Radium retention by blended cement pastes and pure phases (C-S-H and C-A-S-H gels): Experimental assessment and modelling exercises. Applied Geochemistry 105, 45-54.

Or, D., Smets, B. F., Wraith, J. M., Dechesne, A., and Friedman, S. P. (2007). Physical constraints affecting bacterial habitats and activity in unsaturated porous media – a review. Advances in Water Resources 30, 1505-1527.

Or, D., and Tuller, M. (2000). Flow in unsaturated fractured porous media: Hydraulic conductivity of rough surfaces. Water Resources Research 36, 1165-1177.

Or, D., Tuller, M., and Fedors, R. (2005). Seepage into drifts and tunnels in unsaturated fractured rock. Water Resources Research 41, W05022.

Oron, A. P., and Berkowitz, B. (1998). Flow in rock fractures: The local cubic law assumption reexamined. Water Resources Research 34, 2811-2825.

Padovani, C., King, F., Lilja, C., Féron, D., Necib, S., Crusset, D., Deydier, V., Diomidis, N., Gaggiano, R., Ahn, T., Keech, P.G., Macdonald, D.D., Asano, H., Smart, N., Hall, D.S., Hänninen, H., Engelberg, D., Noël, J.J., Shoesmith, D.W. (2017). The corrosion behaviour of candidate container materials for the disposal of high-level waste and spent fuel – a summary of the state of the art and opportunities for synergies in future R&D. Corrosion Engineering, Science and Technology, 52, 227-231.

Paine, K. A. (2019). 7 - Physicochemical and Mechanical Properties of Portland Cements☆. In "Lea's Chemistry of Cement and Concrete (Fifth Edition)" (P. C. Hewlett and M. Liska, eds.), pp. 285-339. Butterworth-Heinemann.

Palandri, J. L., and Kharaka, Y. K. (2004). "A Compilation of Rate Parameters of Water-Mineral Interaction Kinetics for Application to Geochemical Modeling," Rep. No. Open File Report 2004-1068.

Parkhurst, D. L., and Appelo, C. A. J. (2013). "Description of Input and Examples for PHREEQC Version 3 — A Computer Program for Speciation , Batch-Reaction , One-Dimensional Transport , and Inverse Geochemical Calculations ". U. S. Geological Survey.

Parkhurst, D. L., and Wissmeier, L. (2015). PhreeqcRM: A reaction module for transport simulators based on the geochemical model PHREEQC. Advances in Water Resources 83, 176-189.

Parrot, L.J. and Killoh, D.C. (1984). Prediction of cement hydration British Ceramic Society Proceedings 35, 41-54.

Pastina, B., Lehikoinen, J., Puigdomenech, I. (2012). Safety case approach for a KBS-3 type repository in crystalline rock. In: NEA, 2012. Cementitious materials in safety cases for geological repositories for radioactive waste: Role, evolution and interactions, NEA/RWM/R(2012)3/REV, 120-124.

Patel, R., Phung, Q. T., Seetharam, S. C., Perko, J., Jacques, D., Maes, N., De Schutter, G., Ye, G., and van Breugel, K. (2016). Diffusivity of saturated ordinary Portland cement- based materials: A critical review of experimental and analytical modelling approaches. Cement and Concrete Research 90, 52-72.

Patel, R. A., Churakov, S. V., and Prasianakis, N. I. (2021). A multi-level pore scale reactive transport model for the investigation of combined leaching and carbonation of cement paste. Cement and Concrete Composites 115.

Patel, R. A., Perko, J., Jacques, D., De Schutter, G., Ye, G., and Van Breugel, K. (2018). A three-dimensional lattice Boltzmann method based reactive transport model to simulate changes in cement paste microstructure due to calcium leaching. Construction and Building Materials 166, 158-170.

Paul, A. (1977). Chemical durability of glasses; a thermodynamic approach. Journal of Materials Science 12, 2246-2268.

Pearson, F. J., Tournassat, C., and Gaucher, E. C. (2011). Biogeochemical processes in a clay formation in situ experiment: Part E - Equilibrium controls on chemistry of pore water from the Opalinus Clay, Mont Terri Underground Research Laboratory, Switzerland. Applied Geochemistry 26, 990-1008.

Pelayo, M., García-Romero, E., Labajo, M.A., Pérez del Villar, L. (2011). Occurrence of Fe–Mg-rich smectites and corrensite in the Morrón de Mateo bentonite deposit (Cabo de Gata region,

Spain): A natural analogue of the bentonite barrier in a radwaste repository. Applied Geochemistry 26, 1153-1168.

Peña, J., Torres, E., Turrero, M. J., Escribano, A., and Martín, P. L. (2008). Kinetic modelling of the attenuation of carbon steel canister corrosion due to diffusive transport through corrosion product layers. Corrosion Science 50, 2197-2204.

Peng, D.-Y., and Robinson, D. B. (1976). A new two-constant equation of state. Industrial and Engineering Chemistry Fundamentals 15, 59-64.

Perko, J., Jacques, D., and Govaerts, J. (2017). "Water saturation and flow in a surface disposal facility - Numerical study for the Dessel repository," Rep. No. SCK•CEN ER-0355. SCK•CEN, Mol, Belgium.

Perko, J., Jacques, D., Seetharam, S. C., and Mallants, D. (2010). "Long-term evolution of the near surface disposal facility at Dessel," Rep. No. NIROND-TR 2010–04 E. ONDRAF/NIRAS.

Perko, J., Mayer, K. U., Kosakowski, G., De Windt, L., Govaerts, J., Jacques, D., Su, D., and Meeussen, J. C. L. (2015). Decalcification of cracked cement structures. Computational Geosciences 19, 673-693.

Pfingsten, W., Paris, B., Soler, J.M., Mäder, U.K. (2006). Tracer and reactive transport modelling of the interaction between high-pH fluid and fractured rock: field and laboratory experiments. Journal of Geochemical Exploration 90, 95-113.

Pham, H. L. (2018). Operation of biofilters: a numerical approach to some couplings between hydrodynamic and biofilm growth modeling, Université Grenoble Alpes.

Philippini, V., Naveau, A., Catalette, H., Leclercq, S. (2006). Sorption of silicon on magnetite and other corrosion products of iron. Journal of Nuclear Materials 348, 60-69.

Philippini, V., Naveau, A., Catalette, H., Leclercq, S. (2007). Erratum to “Sorption of silicon on magnetite and other corrosion products of iron”. Journal of Nuclear Materials 362, 139

Phung, Q. T. (2015). Effects of Carbonation and Calcium Leaching on Microstructure and Transport Properties of Cement Pastes. Doctoral thesis, UGent - Universiteit Gent.

Pitkänen, P., Snellman, M. and Vuorinen, U. (1996). On the origin and chemical evolution of groundwater at the Olkiluoto site, Posiva-96-04.

Pointeau, I., Coreau, N. and Reiller, P.E. (2008). Uptake of anionic radionuclides onto degraded cement pastes and competing effect of organic ligands. Radiochimica Acta 96(6), 367-374.

POSIVA (2012). Safety case for the disposal of spent nuclear fuel at Olkiluoto - Features, events and processes 2012. Posiva Report 2012-07, Posiva, Olkiluoto, Finland.

Poyet, S. (2006). The Belgian supercontainer concept: Study of the concrete buffer behaviour in service life. Journal de Physique IV Proceedings, EDP Sciences, Corrosion and Long Term Performance of Concrete in NPP and Waste Facilities, 136, 167-175.

Poyet, S. (2007). Design of the ONDRAF supercontainer concept for vitrified HLW diposal in Belgium: study of the thermo-hydric behaviour of the concrete buffer, p. 26, CEA RT DPC/SCCME/07-741-A (Confidential document, not published openly).

Pruess, K., and Narasimhan, T. N. (1985). A Practical Method for Modeling Fluid and Heat-Flow in Fractured Porous-Media. Society of Petroleum Engineers Journal 25, 14-26.

Qin, Z., Demko, B., Noël, J., Shoesmith, D., King, F., Worthingham, R., Keith, K. (2004). Localized dissolution of millscale-covered pipeline steel surfaces. Corrosion 60, 906-914.

Rajala, P. (2017). Microbially-induced corrosion of carbon steel in a geological repository environment. VTT Science 155; PhD Thesis. ISBN 978-951-38-8545-8.

Rajala, P., Carpén, L., Vepsäläinen, M., Raulio, M., Sohlberg, E., Bomberg, M. (2015). Microbially induced corrosion of carbon steel in deep groundwater environment. Frontiers in Microbiology 6, 647.

Rassineux, F., Petit, J.C. and Meunier, A. (1989). Ancient analogues of modern cement: calcium hydrosilicates in mortars and concretes from Gallo-Roman thermal baths of Western France J. Am. Ceram. Soc. 72(6), 1026-1032.

Read, D., Glasser, F.P., Ayora, C., Guardiola, M.T., Sneyers, A. (2001). Mineralogical and microstructural changes accompanying the interaction of Boom Clay with ordinary Portland cement. Advances in Cement Research 13, 175-183.

Rébiscoul, D., Tormos, V., Godon, N., Mestre, J.-P., Cabie, M., Amiard, G., Foy, E., Frugier, P., Gin, S. (2015). Reactive transport processes occurring during nuclear glass alteration in presence of magnetite. Applied Geochemistry 58, 26-37.

Reijonen, H.M., Alexander, W.R. (2015). Bentonite analogue research related to geological disposal of radioactive waste – current status and future outlook. Swiss Journal of Geosciences 108, 101-110.

Reimers, P. (1992). Quality assurance of radioactive waste packages by computerized tomography Task 3 Characterization of radioactive waste forms A series of final reports (1985-89) - No 37, Nuclear Science and Technology Commission of the European Communities, EUR13879.

Reiser, J., Neill, L., Weaver, J., Parruzot, B., Musa, C., Neeway, J., Ryan, J.V., Qafoku, N., Gin, S., Wall, N.A. (2015). Glass corrosion in the presence of iron-bearing materials and potential corrosion suppressors. Materials Research Society Symposium Proceedings 1744, 139-144.

Repina, M., Bouyer, F., and Lagneau, V. (2020). Reactive transport modeling of glass alteration in a fractured vitrified nuclear glass canister: From upscaling to experimental validation. Journal of Nuclear Materials 528, 151869.

Ribet, I., Bétrémieux, S., Gin, S., Angeli, F. and Jégu, C. (2009). Long-term behaviour of vitrified waste packages, Proceedings Global 2009, Paris.

Ribet, I., Gin, S., Godon, N., Jollivet, P., Minet, Y., Grambow, B., Abdelouas, A., Ferrand, K., Lemmens, K., Aertsens, M., Pirlet, V., Jacques, D., Crovisier, J.L., Clément, A., Fritz, B., Munier, I., Del Nero, M., Ozgümüs, A., Curti, E., Luckscheiter, B. and Schwyn, B. (2007). Long-term behaviour of glass: Improving the glass source term and substantiating the basic hypotheses (GLASTAB), European Commission - Nuclear Science and Technology.

Rimstidt, J. D. (2013). "Geochemical Rate Models: An Introduction to Geochemical Kinetics," Cambridge University Press, Cambridge, UK (2014).

Roadcap, G.S., Sanford, R.A., Jin, Q., Pardinas, J.R. and Bethke, C.M. (2006). Extremely alkaline (pH > 12) ground water hosts diverse microbial community. Ground Water 44(4), 511-517.

Roosz, C., Vieillard, P., Blanc, P., Gaboreau, S., Gailhanou, H., Braithwaite, D., Montouillout, V., Denoyel, R., Henocq, P., and Madé, B. (2018). Thermodynamic properties of C-S-H, C-A-S-H and M-S-H phases: Results from direct measurements and predictive modelling. Applied Geochemistry 92, 140-156.

Rougelot, T., Burlion, N., Bernard, D., and Skoczylas, F. (2010). About microcracking due to leaching in cementitious composites: X-ray microtomography description and numerical approach. Cement and Concrete Research 40, 271-283.

Sakuragi, T. (2017). Final Report on Zr alloys corrosion studies at RWMC D 3.19 of the EURATOM seventh framework project CAST grant agreement no. 604779.

Samper, J., Lu, C. H., and Montenegro, L. (2008a). Reactive transport model of interactions of corrosion products and bentonite. Physics and Chemistry of the Earth 33, S306-S316.

Samper, J., Mon, A., and Montenegro, L. (2020). A coupled THMC model of the geochemical interactions of concrete and bentonite after 13 years of FEBEX plug operation. Applied Geochemistry 121, 104687.

Samper, J., Naves, A., Montenegro, L., and Mon, A. (2016). Reactive transport modelling of the long-term interactions of corrosion products and compacted bentonite in a HLW repository in granite: Uncertainties and relevance for performance assessment. Applied Geochemistry 67, 42-51.

Samper, J., Xu, T., and Yang, C. (2009). A sequential partly iterative approach for multicomponent reactive transport with CORE2D. Computational Geosciences 13, 301-316.

Samper, J., Yang, C., Zhen, L., Montenegro, L., Xu, T., Dai, Z., Zhang, G., Lu, C., and Moreira, S. (2011). CORE2D V4: A code for water flow, heat and solute transport, geochemical reactions, and microbial processes. In "Groundwater Reactive Transport Models" (F. Zhang, G. T. Yeh, C. Parker and X. Shi, eds.), pp. 161-186. Bentham Science Publishers.

Samper, J., Zheng, L., Fernandez, A. M., and Montenegro, L. (2008b). Inverse modeling of multicomponent reactive transport through single and dual porosity media. Journal of Contaminant Hydrology 98, 115-127.

Samper, J., Zheng, L., Montenegro, L., Fernandez, A. M., and Rivas, P. (2008c). Coupled thermo-hydro-chemical models of compacted bentonite after FEBEX in situ test. Applied Geochemistry 23, 1186-1201.

Samson, E., and Marchand, J. (2007). Modeling the transport of ions in unsaturated cement-based materials. Computers & Structures 85, 1740-1756.

Sanchez-Vila, X., Dentz, M., and Donado, L. D. (2007). Transport-controlled reaction rates under local non-equilibrium conditions. Geophysical Research Letters 34.

Sarkar, S., Mahadevan, S., Meeussen, J. C. L., van der Sloot, H., and Kosson, D. S. (2010). Numerical simulation of cementitious materials degradation under external sulfate attack. Cement and Concrete Composites 32, 241-252.

Savage, D. (1998). Maqarin natural analogue study: Phase III. Smellie, J.A.T. (ed), pp. 281-316, SKB Technical report TR-98-04.

Savage, D. (2006). Analogue evidence relevant to the alkaline disturbed zone - Report prepared for United Kingdom Nirex Limited. Quintessa Report QRS-1300A-1, Quintessa, Henley-on-Thames, United Kingdom.

Savage, D. (2009). A review of experimental evidence for the development and properties of cement bentonite interfaces with implications for gas transport. Nagra Report NAB 09-30, Nagra, Wettingen, Switzerland.

Savage, D., Watson, C., Benbow, S., and Wilson, J. (2010). Modelling iron-bentonite interactions. Applied Clay Science 47, 91-98.

Savage, D. (2011). A review of analogues of alkaline alteration with regard to long-term barrier performance. Mineralogical Magazine 75, 2401-2418.

Savage, D. (2014). An assessment of the impact of the long term evolution of engineered structures on the safety-relevant functions of the bentonite buffer in a HLW repository. NAGRA Technical Report TR 13-02.

Savage, D., Benbow, S. (2007). Low pH cement. SKI Report 2007:32, Swedish Nuclear Power Inspectorate, Stockholm, Sweden.

Savage, D., Cloet, V. (2018). A review of cement-clay modelling. NAGRA Arbeitsbericht NAB 18-24.

Savage, D., Walker, C., Arthur, R.C., Rochelle, C.A., Oda, C., Takase, H. (2007). Alteration of bentonite by hyperalkaline fluids: a review of the role of secondary minerals. Physics and Chemistry of the Earth 32, 287-297.

Schlegel, M.L., Bataillon, C., Benhamida, K., Blanc, C., Menut, D., Lacour, J.L. (2008). Metal corrosion and argillite transformation at the water-saturated, high-temperature iron–clay interface: A microscopic-scale study. Applied Geochemistry 23, 2619-2633.

Schlegel, M.L., Bataillon, C., Brucker, F., Blanc, C. Prêt, D., Foy, E., Chorro, M. (2014). Corrosion of metal iron in contact with anoxic clay at 90°C:Characterization of the corrosion products after two years of interaction. Applied Geochemistry 51, 1-14.

Schlegel, M.L., Martin, C., Brucker, F., Bataillon, C., Blanc, C., Chorro, M., Jollivet, P. (2016). Alteration of nuclear glass in contact with iron and claystone at 90 °C under anoxic conditions: characterization of the alteration products after two years of interaction. Applied Geochemistry 70, 27-42.

Scourfield, S.J., Kent, J.E., Wickham, S.M., Nieminen, M., Clarke, S., Frasca, B. (2020). Thermal treatment for radioactive waste minimisation and hazard reduction: overview and summary of the EC THERAMIN project. IOP Conference Series: Materials Science and Engineering 818, 012001.

Sedighi, M., Bennett, D., Masum, S.A., Thomas, H.R. and Johansson, E. (2014). Analysis of Temperature Data at the Olkiluoto, Posiva Working Report 2013-58.

Seetharam, S. C., Perko, J., Jacques, D., and Mallants, D. (2014). Influence of fracture networks on radionuclide transport from solidified waste forms. Nuclear Engineering and Design 270, 162-175.

Seigneur, N., L'Hôpital, E., Dauzères, A., Sammaljärvi, J., Voutilainen, M., Labeau, P. E., Dubus, A., and Detilleux, V. (2017). Transport properties evolution of cement model system under degradation - Incorporation of a pore-scale approach into reactive transport modelling. Physics and Chemistry of the Earth, Parts A/B/C 99, 95-109.

Seigneur, N., Mayer, K. U., and Steefel, C. I. (2019). Reactive Transport in Evolving Porous Media. Reactive Transport in Natural and Engineered Systems 85, 197-238.

Sellin, P., Leupin O.X. (2013). The use of clay as an engineered barrier in radioactive waste management - a review. Clays and Clay Minerals 61, 477-498.

Siitari-Kauppi, M., Leskinen, A., Kelokaski, M., Togneri, L., Alonso, U., Missana, T., García - Gutiérrez, M. and Patelli, A. (2007). Physical Matrix Characterization: Studies of Crystalline Rocks and Consolidated Clays by PMMA Method and Electron Microscopy as a Support of Diffusion Analyses, Informes Técnicos Ciemat 1127.

Šimůnek, J., and van Genuchten, M. T. (2008). Modeling Nonequilibrium Flow and Transport Processes Using HYDRUS. Vadose Zone Journal 7, 782-797.

Šimůnek, J., van Genuchten, M. T., and Šejna, M. (2016). Recent Developments and Applications of the HYDRUS Computer Software Packages. Vadose Zone Journal 15.

Shade, J.W., Pederson, L.R., McVay, G.L. (1983). Waste glass-metal interactions in brines. In: Wicks, G.G., Ross, W.A. (eds.) Advances in Ceramics VIII, Nuclear Waste Management, American Ceramic Society, 358-367.

Shanggeng, L., Zhaoguang, W.U., Delu, L. (1995). Study of media effect on glass surface. Materials Research Society Symposium Proceedings 353, 63-71.

Sidborn, M., Marsic, N., Crawford, J., Joyce, S., Hartley, L., Idiart, A., de Vries, L.M., Maia, F., Molinero, J., Svensson, U., Vidstrand, P., Alexander, R. (2014). Potential alkaline conditions for

deposition holes of a repository in Forsmark as a consequence of OPC grouting. SKB Report R-12-17.

Small, J., Nykyri, M., Hovi, U., Sarlin, T., Itävaara, M. (2008). Experimental and modelling investigations of the biochemistry of gas production from low and intermediate level radioactive waste. Applied Geochemistry 23, 1383-1418.

Small, J. S., and Abrahamsen-Mills, L. (2018). "Modelling of microbial processes relevant to ILW disposal. Deliverable D1.8 in MIND project.."

Smart, N.R. (2009). The corrosion behaviour of carbon steel radioactive waste packages: A summary review of Swedish and U.K. research. Corrosion 65, 195-212.

Smart, N.R., Adams, R. (2006). Natural analogues for expansion due to the anaerobic corrosion of ferrous materials. SKB Technical Report TR-06-44, SKB, Stockholm, Sweden.

Smart, N.R., Blackwood, D. J., Werme, L. (2001). The anaerobic corrosion of carbon steel and cast iron in artificial groundwaters. SKB Technical Report TR-01-22, SKB, Stockholm, Sweden.

Smart, N.R., Blackwood, D.J., Marsh, G.P., Naish, C.C., O'Brien, T.M., Rance, A.P., Thomas, M.I. (2004). The anaerobic corrosion of carbon and stainless steels in simulated cementitious repository environments: a summary review of Nirex research. Report AEAT/ERRA-0313, AEA Technology, Harwell, Didcot, United Kingdom.

Smart, N.R., Carlson, L., Heath, T.G., Hoch, A.R., Hunter, F.M., Karnland, O., Kemp, S.J., Milodowski, A.E., Pritchard, A.M., Rance, A.P., Reddy, B., Werme L.O. (2008a). Interactions between iron corrosion products and bentonite. NF-PRO Final Report. Serco/TAS/MCRL/19801/C001 Issue 2.

Smart, N.R., Rancea, A.P. and Wermeb, L.O. (2008b). The effect of radiation on the anaerobic corrosion of steel. Journal of Nuclear Materials 379(1-3), 97-104.

Smart, N., Reddy, B., Rance, A.P., Nixon, D.J., Diomidis, N. (2017a). The anaerobic corrosion of carbon steel in saturated compacted bentonite in the Swiss repository concept. Corrosion Engineering, Science and Technology 52(S1), 113-126.

Smart, N., Reddy, B., Rance, A.P., Nixon, D.J., Frutschi, M., Bernier-Latmani, R., Diomidis, N. (2017b). The anaerobic corrosion of carbon steel in compacted bentonite exposed to natural Opalinus Clay porewater containing native microbial populations. Corrosion Engineering, Science and Technology 52(S1), 101-112.

Smart, N.R., Rance, A.P., Fennell, P.A.H., Reddy, B., Padovani, C. (2019). Experimental studies of radiation induced corrosion in support of the Belgian Supercontainer concept. Wood Reference 207022/01, Issue 1.

Smart, N.R., Rance, A.P., Nixon, D.J., Fennell, P.A.H., Reddy, B. and Kursten, B. (2017c). Summary of studies on the anaerobic corrosion of carbon steel in alkaline media in support of the Belgian supercontainer. Corrosion Engineering, Science and Technology 52, 217-226.

Snelman, M., Vieno, T. (2005). Long-term safety aspects of the use of cement in a repository for spent nuclear fuel. Proceedings 2nd Workshop R&D on low pH cement for a geological repository, 15-16 June 2005, Madrid, Spain, 27-40.

Soler, J.M. (2012). High-pH plume from low-alkali-cement fracture grouting: reactive transport modeling and comparison with pH monitoring at ONKALO (Finland). Applied Geochemistry 27, 2096-2106.

Soler, J.M., Mäder, U.K. (2007). Mineralogical alteration and associated permeability changes induced by a high-pH plume: modeling of a granite core infiltration experiment. Applied Geochemistry 22, 17-29.

Soler, J.M., Mäder, U.K. (2010). Cement-rock interaction: infiltration of a high-pH solution into a fractured granite core. Geol. Acta 8, 221–233.

Soler, J.M., Pfingsten, W., Paris, B., Mäder, U.K., Frieg, B., Neall, F., Källvenius, G., Yui, M., Yoshida, Y., Shi, P., Rochelle, C.H.A. (2006). HPF-Experiment: modelling report. NAGRA Technical Report NTB--05-01.

Soler, J.M., Vuorio, M., Hautojärvi, A. (2011). Reactive transport modeling of the interaction between water and a cementitious grout in a fractured rock. Application to ONKALO (Finland). Applied Geochemistry 26, 1115-1129.

Somervuori, M., Carpen, L. (2021). Interface “steel/iron – granite”. Chapter 7 in: Deissmann, G., Ait Mouheb, N., Martin, C., Turrero, M. J., Torres, E., Kursten, B., Weetjens, E., Jacques, D., Cuevas, J., Samper, J., Montenegro, H., Leivo, M., Somervuori, M., Carpen, L. (2021). Experiments and numerical model studies on interfaces. Final version as of 12.05.2021 of deliverable D2.5 of the HORIZON 2020 project EURAD. EC Grant agreement no: 847593.

Souza, R.F., Brandão, P.R.G. and Paulo, J.B.A. (2012). Effect of chemical composition on the ζ-potential of chromite. Minerals Engineering 36-38, 65-74.

Sposito, G. (1981). "The thermodynamics of soil solutions," Oxford University Press, Oxford.

Steadman, J.A. (1986). CEC Natural analogue working group second meeting Côme, B. and Chapman, N.A. (eds), pp. 165-170, Commission of the European Communities - Nuclear Science and Technology, EUR 10671.

Steefel, C., and MacQuarrie, K. T. B. (1996). Approaches to modeling of reactive transport in porous media. In "Reviews in Mineralogy and Geochemistry " (P. C. Lichtner, C. Steefel and E. H. Oelkers, eds.), Vol. 34, pp. 85-129.

Steefel, C. I., Appelo, C. A. J., Arora, B., Jacques, D., Kalbacher, T., Kolditz, O., Lagneau, V., Lichtner, P. C., Mayer, K. U., Meeussen, J. C. L., Molins, S., Moulton, D., Shao, H., Šimůnek, J., Spycher, N., Yabusaki, S. B., and Yeh, G. T. (2015a). Reactive transport codes for subsurface environmental simulation. Computational Geosciences 19, 445-478.

Steefel, C. I., Yabusaki, S. B., and Mayer, K. U. (2015b). Reactive transport benchmarks for subsurface environmental simulation. Computational Geosciences 19, 439-443.

Stein, M. (2014) Erläuterungen zur Verpackung radioaktiver Abfälle im Endlagerbehälter, NAGRA Arbeitsbericht NAB 14-04.

Stroes-Gascoyne, S., Hamon, C.J., Dixon, D.A., Kohle, C., Maak, P. (2007). The effects of dry density and porewater salinity on the physical and microbiological characteristics of highly compacted bentonite. Materials Research Society Symposium Proceedings 985, 0985-NN13-02.

Stroes-Gascoyne, S., Hamon, C.J., Maak, P., Russell, S. (2010). The effects of the physical properties of highly compacted smectitic clay (bentonite) on the culturability of indigenous microorganisms. Applied Clay Science 47, 155-162.

Stroes-Gascoyne, S., Hamon, C.J. and Maak, P. (2011). Limits to the use of highly compacted bentonite as a deterrent for microbiologically influenced corrosion in a nuclear fuel waste repository. Physics and Chemistry of the Earth, Parts A/B/C 36(17), 1630-1638.

Stroes-Gascoyne, S. and West, J.M. (1997). Microbial studies in the Canadian nuclear fuel waste management program. Federation of European Microbiological Societies. (FEMS) Microbiology reviews 20, 573-590.

Stora, E., Bary, B., He, Q. C., Deville, E., and Montarnal, P. (2009a). Modelling and simulations of the chemo-mechanical behaviour of leached cement-based materials: Leaching process and induced loss of stiffness. In "Cem. Concr. Res.", Vol. 39, pp. 763-772.

Stora, E., Bary, B., He, Q. C., Deville, E., and Montarnal, P. (2009b). Modelling and simulations of the chemo–mechanical behaviour of leached cement-based materials. Cement and Concrete Research 39, 763-772.

Sudicky, E. A., and Mclaren, R. G. (1992). The Laplace Transform Galerkin Technique for Large-Scale Simulation of Mass-Transport in Discretely Fractured Porous Formations. Water Resources Research 28, 499-514.

Swanson, J.S., Cherkouk, A., Arnold, T., Meleshyn, A. and Reed, D.T. (2018). Microbial Influence on the Performance of Subsurface, Salt-Based Radioactive Waste Repositories. An Evaluation Based on Microbial Ecology, Bioenergetics and Projected Repository Conditions., NEA No. 7387.

Swanton, S.W., Baston, G.M.N. and Smart, N.R. (2015). Rates of steel corrosion and carbon-14 release from irradiated steels – state of the art review D2.1 from CArbon-14 Source Term project from the European Union's Seventh Framework Programme for research, technological development and demonstration under grant agreement no. 604779.

Szabó-Krausz, Z., Aradi, L.E., Király, C., Kónya, P., Török, P., Szabó, C., Falus, G. (2021). Signs of in-situ geochemical interactions at the granite–concrete interface of a radioactive waste disposal. Applied Geochemistry 126, 104881.

Taniguchi, N., Kawasaki, M, Kawakami, S., Kubota, M. (2004). Corrosion behaviour of carbon steel in contact with bentonite under anaerobic condition. Proceedings of the 2nd International Workshop "Prediction of Long Term Corrosion Behaviour in Nuclear Waste Systems", Publication Andra, Science and Technology Series, ISBN 2-9510108-6-9.

Taylor, H.F.W. (1997). Cement chemistry (2nd edition). Thomas Telford Publishing, London.

Taylor, S. W., Milly, P. C. D., and Jaffe, P. R. (1990). Biofilm growth and the related changes in the physical-properties of a porous-medium. 2. Permeability. Water Resources Research 26, 2161-2169.

Techer, I., Bartier, D., Boulvais, P., Tinseau, E., Suchorski, K., Cabrera, J., Dauzères, A. (2012a). Tracing interactions between natural argillites and hyper-alkaline fluids from engineered cement paste and concrete: Chemical and isotopic monitoring of a 15-years old deep-disposal analogue. Applied Geochemistry 27, 1384-1402.

Techer, I., Michel. P., Bartier, D., Tinseau, E., Devol-Brown, I., Boulvais, P., Suchorski, K. (2012b). Engineered analogues of cement/clay interactions in the Tournemire experimental platform (France): A couple mineralogical and geochemical approach to track tiny disturbances. In: NEA, 2012. Cementitious materials in safety cases for geological repositories for radioactive waste: Role, evolution and interactions, NEA/RWM/R(2012)3/REV, 182-185.

Thoenen, T., Hummel, W., Berner, U., and Curti, E. (2014). "The PSI/Nagra Chemical Thermodynamic Database 12/07."

Tinseau, E., Bartier, D., Hassouta, L., Devol-Brown, I., Stammose, D. (2006). Mineralogical characterization of the Tournemire argillite after in situ reaction with concretes. Waste Management 26, 789-800.

Tixier, R., and Mobasher, B. (2003). Modeling of Damage in Cement-Based Materials Subjected to External Sulfate Attack. I: Formulation. 15, 305-313.

Torres, E. (2011). Geochemical processes at the C-steel / bentonite interface in a deep geological repository: experimental approach and modeling. Ph.D. thesis, Universidad Complutense de Madrid.

Torres, E., Turrero, M.J., Peña, J., Martín, P.L., Escribano, A., Alonso, U., Villar, M.V. (2007). Interaction iron-compacted bentonite: corrosion products and changes in the properties of the bentonite. Final Report NF-PRO_Deliverable D2.3.2 of Component 2.

Torres, E., Escribano, A., Baldonedo, J.L., Turrero, M.J., Martin, P.L., Peña, J., Villar, M.V. (2009). Evolution of the geochemical conditions in the bentonite barrier and its influence on the corrosion of the carbon steel canister. Materials Research Society Symposium Proceedings 1124, 301-306.

Torres, E., Turrero, M.J., Escribano, A., Martín, P.L. (2014). Formation of iron oxide and oxyhydroxides under different environmental conditions. Iron/bentonite interaction. PEBS Project, Deliverable D2.3-6-2.

Tournassat, C., Vinsot, A., Gaucher, E. C., and Altmann, S. (2015). Chapter 3 - Chemical Conditions in Clay-Rocks. In "Developments in Clay Science" (C. Tournassat, C. I. Steefel, I. C. Bourg and F. Bergaya, eds.), Vol. 6, pp. 71-100. Elsevier.

Traber, D. and Blaser, P. (2013). Gesteinsparameter der Wirtgesteine Opalinuston, 'Brauner Dogger', Effinger Schichten und Helvetische Mergel als Grundlage für die Sorptionsdatenbank, NAGRA Arbeitsbericht NAB 12-39.

Trapote-Barreira, A., Cama, J., and Soler, J. M. (2014). Dissolution kinetics of C-S-H gel: Flow-through experiments. Physics and Chemistry of the Earth 70-71, 17-31.

Tremosa, J., Arcos, D., Matray, J. M., Bensenouci, F., Gaucher, E. C., Tournassat, C., and Hadi, J. (2012). Geochemical characterization and modelling of the Toarcian/Domerian porewater at the Tournemire underground research laboratory. Applied Geochemistry 27, 1417-1431.

Trotignon, L., Techer, I. and Kohler, E. (2004). Col du Perthus, http://www.natural-analogues.com/nawg-library/na-overviews/analogue review.

Trotignon, L., Devallois, V., Peycelon, H., Tiffreau, C., and Bourbon, X. (2007). Predicting the long term durability of concrete engineered barriers in a geological repository for radioactive waste. Physics and Chemistry of the Earth 32, 259-274.

Tuller, M., and Or, D. (2001). Hydraulic conductivity of variably saturated porous media: Film and corner flow in angular pore space. Water Resources Research 37, 1257-1276.

Tuller, M., and Or, D. (2002). Unsaturated Hydraulic Conductivity of Structured Porous Media: A Review of Liquid Configuration–Based Models. Vadose Zone Journal 1, 14-37.

Tunturi, P.J. (1988). Korroosiokäsikirja, Suomen korroosioyhdistys, Hangon kirjapaino. ISBN 951.99916-7-0.

Turrero, M.J., Torres, E., Cuevas, J., Samper, J., Montenegro, L. (2021). Interface "steel/iron – bentonite". Chapter 5 in: Deissmann, G., Ait Mouheb, N., Martin, C., Turrero, M. J., Torres, E., Kursten, B., Weetjens, E., Jacques, D., Cuevas, J., Samper, J., Montenegro, H., Leivo, M., Somervuori, M., Carpen, L. (2021). Experiments and numerical model studies on interfaces. Final version as of 12.05.2021 of deliverable D2.5 of the HORIZON 2020 project EURAD. EC Grant agreement no: 847593.

Tuutti, K. (1982). Corrosion of steel in concrete. Report no. 4 82, Swedish Cement and Concrete Research Institute, Stockholm, Sweden.

Ulm, F.-J., Torrenti, J.-M., and Adenot, F. (1999). Chemoporoplasticity of Calcium Leaching in Concrete. Journal of Engineering Mechanics 125, 1200-1211.

Uras, S. (2021). State of the Art in packaging, storage, and monitoring of cemented wastes. D 7.1 of the HORIZON 2020 project. EC Grant agreement no: 945098.

Utton, C.A., Swanton, S.W., Schofield, J., Hand, R.J., Clacher, A., Hyatt, N.C. (2012). Chemical durability of vitrified wasteforms: effects of pH and solution composition. Mineralogical Magazine 76, 2919-2930.

Utton, C.A., Hand, R.J., Bingham, P.A., Hyatt, N.C., Swanton, S.W., Williams, S.J. (2013). Dissolution of vitrified wastes in a high-pH calcium-rich solution. Journal of Nuclear Materials 435, 112-122.

Vahlund, F. and Andersson, E. (2015). Safety analysis for SFR Long-term safety Main report for the safety assessment SR-PSU, SKB TR-14-01.

van der Lee, J. (1998). "Thermodynamic and mathematical concepts of CHESS."

van der Lee, J., De Windt, L., Lagneau, V., and Goblet, P. (2003). Module-oriented modeling of reactive transport with HYTEC. Computers & Geosciences 29, 265-275.

van Eijk, R.J. and Brouwers, H.J.H. (2000). Prediction of hydroxyl concentrations in cement pore water using a numerical cement hydration model. Cement and Concrete Research 30(11), 1801-1806.

van Genuchten, M. T. (1980). Closed-form Equation for Predicting the Hydraulic Conductivity of Unsaturated Soils. Soil Science Society America Journal 44, 892-898.

van Genuchten, M. T., Leij, F. J., and Yates, S. R. (1991). "The RETC Code for Quantifying the Hydraulic Functions of Unsaturated Soils, Version 1.0."

Van Humbeeck, H., De Bock, C. and Bastiaens, W. (2007). Demonstrating the construction and backfilling feasibility of the supercontainer design for HLW (2B.14), pp. 336-354, Reposafe, Braunschweig.

Van Iseghem, P., Berghman, K., Lemmens, K., Timmermans, W. and Wang, L. (1992). Laboratory and in-situ interaction between simulated waste glasses and clay Task 3 Characterization of radioactive waste forms A series of final reports (1985-89) No 21, Commission of the European Communities - Nuclear science and technology, EUR 13607.

Van Iseghem, P., Lemmens, K., Aertsens, M., Gin, S., Ribet, I., Grambow, B., Crovisier, J.L., Del Nero, M., Curti, E., Schwyn, B., Luckscheiter, B., McMenamin, T. (2006). Chemical durability of high-level waste glass in repository environment: main conclusions and remaining uncertainties from the GLASTAB and GLAMOR projects. Materials Research Society Symposium Proceedings 932, 293-304.

Van Loon, L.R. and Hummel, W. (1995). The Radiolytic and Chemical Degradation of Organic Ion Exchange Resins under Alkaline Conditions: Effect on Radionuclide Speciation, NAGRA Technical Report 95-08.

Vehmas, T. and Itälä, A. (2019). Compositional parameters for solid solution C-S-H and the applicability to thermodynamic modelling, pp. 293-300, KIT Scientific reports 7752 : Proceedings of the Second Workshop of the Horizon 2020 Cebama project.

Vehmas, T., Montoya, V., Cruz Alonso, M., Vašíček, R., Rastrick, E., Gaboreau, S., Večerník, P., Leivo, M., Holt, E., Ait Mouheb, N., Svoboda, J., Read, D., Červinka, R., Vasconcelos, R. and Corkhill, C. (2019). Low-pH Cementitious Materials containing Slag used in Underground Radioactive Waste Repositories - Manuscript for peer-reviewed publication on results generated in WP1 D 1.07 from Cebama project from Horizon 2020 framework programme.

Vehmas, T., Montoya, V., Alonso, M.C., Vašíček, R., Rastrick, E., Gaboreau, S., Večerník, P., Leivo, M., Holt, E., Fink, N., Ait Mouheb, N., Svoboda, J., Read, D., Červinka, R:, Vasconcelos, R., Corkhill, C. (2020). Characterization of Cebama low-pH reference concrete and assessment of its alteration with representative waters in radioactive waste repositories. Applied Geochemistry 121, 104703.

Verhoef, E.V., de Bruin, A.M.G., Wiegers, R.B., Neeft, E.A.C. and Deissmann, G. (2014). Cementitious materials in OPERA disposal concept, OPERA-PG-COV020.

Verhoef, E.V., Neeft, E.A.C., Deissmann, G., Filby, A., Wiegers, R.B. and Kers, D.A. (2016). Waste families in OPERA, OPERA-PU-COV023.

Vernaz, E., Grambow, B., Lutze, W., Lemmens, K. and Van Iseghem, P. (1996). Assessment of the long-term durability of radioactive waste glass. McMenamin, T. (ed), European Commission, EUR 17543, Luxembourg.

Verweij, J.M., Nelskamp, S. and Valstar, J. (2016). Definition of the present boundary conditions for the near-field model_1, p. 37, OPERA-PU-TNO421_1.

Vienna, J.D., Ryan, J.V. (2013). Current understanding and remaining challenges in modeling long-term degradation of borosilicate nuclear waste glasses. International Journal of Applied Glass Science 4, 283-294.

Vieno, T., Lehikoinen, J., Löfman, J., Nordman, H. and Mészáros, F. (2003) Assessment of Disturbances Caused by Construction and Operation of ONKALO, Posiva 2003-06.

Virpiranta, H., Taskila, S., Leiviskä, T., Rämö, J. and Tanskanen, J. (2019). Development of a process for microbial sulfate reduction in cold mining waters - Cold acclimation of bacterial consortia from an Anrtic mining district. Environmental pollution 252, 281-288.

Vogel, T., Cislerova, M., and Hopmans, J. W. (1991). Porous Media With Linearly Variable Hydraulic Properties. Water Resources Research 27, 2735-2741.

von Greve-Dierfeld, S., Lothenbach, B., Vollpracht, A., Wu, B., Huet, B., Andrade, C., Medina, C., Thiel, C., Gruyaert, E., Vanoutrive, H., Saéz del Bosque, I. F., Ignjatovic, I., Elsen, J., Provis, J. L., Scrivener, K., Thienel, K.-C., Sideris, K., Zajac, M., Alderete, N., Cizer, Ö., Van den Heede, P., Hooton, R. D., Kamali-Bernard, S., Bernal, S. A., Zhao, Z., Shi, Z., and De Belie, N. (2020). Understanding the carbonation of concrete with supplementary cementitious materials: a critical review by RILEM TC 281-CCC. Materials and Structures 53, 136.

Vondrovic, L. (2015). Czech siting programme, www.posiva.fi/files/4350/D3_7.1_Czech_siting_programme_Vondrovic_SURAO_2015.

Wagner, T., Kulik, D. A., Hingerl, F. F., and Dmytrieva, S. V. (2012). GEM-Selektor geochemical modeling package: TSolMod library and data interface for multicomponent phase models. Canadian Mineralogist 50, 1173-1195.

Walton, J. C., Plansky, L. E., and Smith, R. W. (1990). "Models for estimation of service life of concrete barriers in low-level radioactive waste disposal," United States.

Walton, J. C., and Seitz, R. R. (1991). Performance of Intact and Partially Degraded Concrete Barriers in Limiting Fluid Flow. Vol. NUREG/CR-5614, EGG-2614.

Wang, A., Kuebler, K.E., Jolliff, B.L. and Haskin, L.A. (2004). Raman spectroscopy of Fe-Ti-Cr-oxides, case study: Martian meteorite EETA79001. American Mineralogist 89, 665-680.

Wang, L. (2009). Near-field chemistry of a HLW/SF repository in Boom Clay - scoping calculations relevant to the supercontainer design, External Report SCK•CEN-ER-17.

Wang, L., Jacques, D. and De Cannière, P. (2010). Effects of an alkaline plume on the Boom Clay as a potential host formation for geological disposal of radioactive waste Report prepared by SCK•CEN in the framework of ONDRAF/NIRAS programme on geological disposal, under contract CCHO 2004-2470/00/00, External Report SCK•CEN-ER-28.

Wang W., Kolditz O (2006). Object oriented finite element analysis of thermohydromechanical (THM) problems in porous media. International Journal for Numerical Methods in Engineering, 69(1):162–201.

Wang, W., Fischer, T., Zehner, B., Böttcher N., Gürke, U.J, Kolditz, O (2015). A parallel finite element method for two-phase flow processes in porous media: Opengeosys with petsc. Environmental Earth Sciences, 73(5), 2269–2285.

Wang, W., Kolditz, O., Nagel, T. (2017). Parallel finite element modelling of multi-physical processes in thermochemical energy storage devices. Applied Energy, 185(P2):1954–1964.

Wanner, H., Albinsson, Y. and Wieland, E. (1994). Project Caesium–An ion exchange model for the prediction of distribution coefficients of caesium in bentonite, SKB Technical Report 94-10.

Watson, C., Savage, D., Wilson, J. (2017). Geochemical modelling of the LCS experiment. Quintessa Report QRS-1523D-2, Quintessa, Henley-on-Thames, United Kingdom.

Weetjens, E., Martens, E., and Jacques, D. (2009). Quantifying Conservatism of Performance Assessment Calculations by Sorption Model Reduction: Case Study on Near Field Cs Migration in Callovo-Oxfordian Clay. In "'Scientific basis for nuclear waste management XXXIII", Vol. Mater. Res. Soc. Symp. Proc, pp. 381-388.

Weetjens, E., Sillen, X. and Van Geet, M. (2006). NF-PRO Deliverable 5.1.2: Mass and Energy Balance Calculations: contribution from SCK•CEN under contract FI6W-CT-2003-02389.

Wenk, H.-R., Voltolini, M., Mazurek, M., Van Loon, L.R. and Vinsot, A. (2008). Preferrred orientations and anisotropy in shales: Callovo-Oxfordian shale (France) and Opalinus Clay (Switzerland). Clays and Clay Minerals 56(3), 285-306.

Werme, L., Björner, I.K., Bart, G., Zwicky, U., Grambow, B., Lutze, W., Ewing, R.C., Magrabi, C. (1990). Chemical corrosion of highly radioactive borosilicate nuclear waste glass under simulated repository conditions. Journal of Materials Research 5, 1130-1146.

Wersin, P., Johnson, L.H., Schwyn, B., Berner, U., Curti, E. (2003). Redox conditions in the near field of a repository for SF/HLW and ILW in Opalinus Clay. NAGRA Technical Report NTB 02-13.

Wersin, P., Kober, F. (2017). FEBEX-DP: Metal corrosion and iron-bentonite interaction studies. NAGRA Arbeitsbericht Report NAB 16-16.

Wersin, P., and Birgersson, M. (2014). Reactive transport modelling of iron-bentonite interaction within the KBS-3H disposal concept: the Olkiluoto site as a case study. Geol Soc London, Spec Publ 400, SP400.424.

Wersin, P., Birgersson, M., Karnland, O., and Snellman, M. (2008). "Impact of corrosion-derived iron on the bentonite buffer within the KBS-3H disposal concept. SKB report TR-08–34."

Williams, S.J. and Scourse, E.M. (2015). Carbon-14 Source term in geological disposal; The EC project CAST. Journal of nuclear research and development (10), 8-12.

Wilson, J.C. (2017). FEBEX-DP: Geochemical modelling of iron-bentonite interactions. Quintessa Report QRS-1713A-R3, Quitessa, Henley-on-Thames, United Kingdom.

Wilson, J., Cressey, G., Cressey, B., Cuadros, J., Ragnarsdottir, K.V., Savage, D., Shibata, M. (2006a). The effect of iron on montmorillonite stability. (II) Experimental investigation. Geochimica Cosmochimica Acta 70, 323-336.

Wilson, J., Savage, D., Cuadros, J., Shibata, M., Ragnarsdottir, K.V. (2006b). The effect of iron on montmorillonite stability. (I) Background and thermodynamic considerations. Geochimica Cosmochimica Acta 70, 306-322.

Wilson, J., Benbow, S., Sasamoto, H., Savage, D., Watson, C. (2015). Thermodynamic and fully-coupled reactive transport models of a steel–bentonite interface. Applied Geochemistry 61, 10-28.

Wissmeier, L., and Barry, D. a. (2009). Effect of mineral reactions on the hydraulic properties of unsaturated soils: Model development and application. Advances in Water Resources 32, 1241-1254.

Wissmeier, L., and Barry, D. a. (2010). Implementation of variably saturated flow into PHREEQC for the simulation of biogeochemical reactions in the vadose zone. Environmental Modelling & Software 25, 526-538.

Wissmeier, L., and Barry, D. a. (2011). Simulation tool for variably saturated flow with comprehensive geochemical reactions in two- and three-dimensional domains. Environmental Modelling & Software 26, 210-218.

Wollery, T. J. (1992). "EQ3/6. A software package for geochemical modeling of aqueous system: package overview and installation guide version 7.0. UCRL-MA-110662-PT-I." Lawrence Livermore National Laboratory, Livermore, California.

Wouters, K., Janssen, P., Moors, H. and Leys, N. (2016). Geochemical Performance of the EBS: Translation and Orientation of existing Knowledge towards the Boom Clay in the Netherlands (GePeTO), OPERA-PU-SCK515, www.covra.nl.

Wouters, K., Moors, H., Boven, B. and Leys, N. (2013). Evidence and characteristics of a diverse and metabolically active microbial community in deep subsurface clay borehole water. FEMS Microbiology Ecology 86.

Wouters, L. and Verheyen, A. (2004). Isle of Skye, http://www.natural-analogues.com/nawg-library/na-overviews/analogue review.

Wouters, L., Verheyen, A. and Dalton, J. (2005a). Busachi (Sardinia), http://www.natural-analogues.com/nawg-library/na-overviews/analogue review.

Wouters, L., Verheyen, A. and Dalton, J. (2005b). Kinnekulle, http://www.natural-analogues.com/nawg-library/na-overviews/analogue review.

Xie, M., Mayer, K. U., Claret, F., Alt-Epping, P., Jacques, D., Steefel, C., Chiaberge, C., and Šimůnek, J. (2015). Implementation and evaluation of permeability-porosity and tortuosity-porosity relationships linked to mineral dissolution-precipitation. Computational Geosciences 19, 655-671.

Xie, S. Y., Shao, J. F., and Burlion, N. (2008). Experimental study of mechanical behaviour of cement paste under compressive stress and chemical degradation. Cement and Concrete Research 38, 1416-1423.

Xie, M. L., Bauer, S., Kolditz, O., Nowak, T., and Shao, H.: Numerical simulation of reactive processes in an experiment with partially saturated bentonite, J. Contam. Hydrol., 83, 122–147, 2006.

Xu, T., Samper, J., Ayora, C., Manzano, M., and Custodio, E. (1999). Modeling of non-isothermal multi-component reactive transport in field scale porous media flow systems. Journal of Hydrology 214, 144-164.

Xu, T. F., Sonnenthal, E., Spycher, N., and Pruess, K. (2006). TOUGHREACT - A simulation program for non-isothermal multiphase reactive geochemical transport in variably saturated geologic media: Applications to geothermal injectivity and CO2 geological sequestration. Computers & Geosciences 32, 145-165.

Xu, T. F., Spycher, N., Sonnenthal, E., Zhang, G. X., Zheng, L. E., and Pruess, K. (2011). TOUGHREACT Version 2.0: A simulator for subsurface reactive transport under non-isothermal multiphase flow conditions. Computers & Geosciences 37, 763-774.

Yang, C., Hovorka, S. D., Treviño, R. H., and Delgado-Alonso, J. (2015). Integrated Framework for Assessing Impacts of CO2 Leakage on Groundwater Quality and Monitoring-Network

Efficiency: Case Study at a CO2 Enhanced Oil Recovery Site. Environmental Science and Technology 49, 8887-8898.

Yang, C. B., Romanak, K., Hovorka, S., and Triveno, R. (2013). Modeling CO2 Release Experiment in the Shallow Subsurface and Sensitivity Analysis. Environmental & Engineering Geoscience 19, 207-220.

Yang, C. B., Samper, J., and Montenegro, L. (2008). A coupled non-isothermal reactive transport model for long-term geochemical evolution of a HLW repository in clay. Environmental Geology 53, 1627-1638.

Yoshikawa, H., Gunji, E., Tokuda, M. (2008). Long term stability of iron for more than 1500 years indicated by archaeological samples from the Yamato 6th tumulus. Journal of Nuclear Materials 379, 112-117.

Zhang, G., Lu, P., Zhang, Y., Tu, K., and Zhu, C. (2020). SupPhreeqc: A program for generating customized Phreeqc thermodynamic datasets from Supcrtbl and extending calculations to elevated pressures and temperatures. Computers & Geosciences 143, 104560.

Zhang, G. X., Samper, J., and Montenegro, L. (2008). Coupled thermo-hydro-bio-geochemical reactive transport model of CERBERUS heating and radiation experiment in Boom clay. Applied Geochemistry 23, 932-949.

Zhang, J.Y., Qian, S.Y., Baldock, B. (2009). Laboratory study of corrosion performance of different reinforcing steels for use in concrete structures. Report IRC RR 284, National Research Council Canada (NRCC), Ottawa, Ontario, Canada.

Zhang, Y., Hu, B., Teng, Y., Tu, K., and Zhu, C. (2019). A library of BASIC scripts of reaction rates for geochemical modeling using phreeqc. Computers & Geosciences 133, 104316.

Zimmer, K., Zhang, Y., Lu, P., Chen, Y., Zhang, G., Dalkilic, M., and Zhu, C. (2016). SUPCRTBL: A revised and extended thermodynamic dataset and software package of SUPCRT92. Computers & Geosciences 90, 97-111.

Živica, V. (2002). Significance and influence of the ambient temperature as a rate factor of steel reinforcement corrosion. Bulletin Material Science 25, 375-379.